Synthesis of inorganic nanoparticles using microfluidic devices

Razwan Baber

A thesis submitted for the degree of

Doctor of Philosophy

From

University College London

Department of Chemical Engineering

Supervisors:

Prof. Asterios Gavriilidis

Prof. Nguyen TK Thanh

April 2017

Declaration of Authorship and Originality

I, Razwan Baber, confirm that the work presented in this thesis is my own. Where information has been derived from other sources, I confirm that this has been indicated in the thesis.

Signature: …….. **Date: April 2017**

Abstract

The well-known benefits of using micro-scale flow are associated with controlled mass transfer because of the reduced dimensions of microfluidic devices. The improved mass transfer characteristics make microfluidic devices an ideal candidate for synthesis of nanoparticles (NPs). In this study, mass transfer characteristics are investigated for microfluidic devices such as the coaxial flow reactor (CFR) and the impinging jet reactor (IJR), through the use of the interaction by exchange with the mean mixing model, Villermaux-Dushman reaction scheme, high speed camera images and flow visualization using dye and water. These reactors are contrasting in that the CFR has slower mixing because of its laminar flow profile whereas as the IJR has mixing time in the order of a few ms. The importance of mixing time as well as manipulation of hydrodynamics at the micro scale is shown through the use of these types of reactors for NP synthesis. Both types of reactors have beneficial properties for the synthesis of NPs. NPs were characterized using UV-Vis spectroscopy, DCS and TEM. Longer residence times and a higher consumption of reagents in the CFR led to reduction of size of silver NPs, leading to reductions in size from 9.3 ± 3 nm to 3.7 ± 0.8 nm. The IJR showed a reduction in NP size with increasing mixing efficiency, with a reduction in size from 7.9 ± 5.8 nm to 3.4 ± 1.4 nm using citrate as a ligand and from 5.4 ± 1.6 nm to 4.2 ± 1.1 nm using PVA as a ligand. A system to control nucleation and growth periods was developed by combining the CFR with a coiled flow inverter (CFI). Size control over gold NPs was achieved simply by changing the flow rate of reagents, with a reduction in size from 23.9 ± 4.7 nm to 17.9 ± 2.1 nm. Various hydrodynamics within the CFR were also tested. Vortex flow at higher Reynolds numbers did not give good control over NP size and dispersity, while reducing the inner tube internal diameter resulted in a decrease in NP size from 10.5 ± 4.0 nm to 4.7 ± 1.4 nm. Silver and gold NP synthesis was also performed in a batch reactor. Two different mixing configurations and variation in the order of reagent addition was investigated, and confirmed the importance of mass transfer conditions in determining size and dispersity. In both cases, fast and efficient mixing of the reducing agent to the precursor resulted in the smallest NPs. The range of sizes obtained were 6.7 ± 1.7 nm to 11.5 ± 2.4 nm and 13.1 ± 2.2 nm to 18.0 ± 4.8 nm for silver and gold NPs respectively. All these results show a strong link between mass transfer and NP size and dispersity for the systems tested, showing the need for well controlled and carefully considered mass transfer conditions.

Acknowledgements

I would like to express my deepest gratitude to my supervisors, Prof. Asterios Gavriilidis and Prof. Nguyen Thi Kim Thanh, whom without this work would not have been possible. Prof. Gavriilidis, has taught me a lot about research, but has also given me invaluable advice outside of work which really helped motivate me when the research was not going my way. Prof. Thanh was invaluable for her input, and along with her group at the Royal Institute of Great Britain, helped immeasurably with their expertise on nanoparticles. A special mention also goes to Dr. Luca Mazzei, who has been a mentor to me during this research. He taught me what it means to be critical when assessing any research, and to never stop being curious.

There are many people to thank from Prof. Gavriilidis' lab group. Special thanks to Enhong, who never ceases to amaze me with his flair for solving engineering problems. Thanks to Noor, Gaowei, Redza, Achilleas, Luigi, Damiano, Hendrik, Anand, Huang, Spyros, Conor, Chara and Valentina. You have all helped me in one way or another, whether it was taking the time to chat about a research problem or making me smile with a joke. Roxanne, Niall, Luke, Aans and Kuan, we went through many trials and tribulations together with the ever temperamental TEM through the years and I thank you for sharing.

Thanks to my good friends, Anayet and Akhbar. You are the funniest people I have met, each in your own way. You always lightened my mood when I was being too serious.

My parents, Mohammed and Chandni, my sincerest appreciation goes out to you. You always kept things in perspective for me, and reassured me when I was unsure. You always gave me motivation, when I was unmotivated, to keep going. Thank you for raising me, I hope I make you proud and continue to do so every day. To my brothers, Arshad, Asad and Imran, thank you for teaching me the lessons of life and looking out for me every step of the way. To my sister, Yasmin, thank you for teaching me how to be strong in adversity. To my sister, Rehksena, thank you for all the support and sacrifice you make every single day to make sure I am doing well.

Thank you to my best friend, for your love, support and understanding throughout this PhD. You helped to keep me going when I was ready to give up. You have perhaps made the biggest sacrifice of all for putting up with me. You are always in my mind and heart.

Thank you all for making this a pleasant and enjoyable journey.

Contents

List of figures

List of tables

List of abbreviations

CFD	Computational fluid dynamics
CFI	Coiled flow inverter
CFR	Coaxial flow reactor
DCS	Differential Centrifugal Sedimentation
ETFE	Ethylene tetrafluoroethylene
FWHM	Full width at half maximum
IJR	Impinging jet reactor
NP	Nanoparticle
PTFE	Polytetrafluoroethylene
PVA	Polyvinyl alcohol
RTD	Residence time distribution
SAR	Split and recombine
SAXS	Small angle x-ray scattering
TEM	Transmission electron microscopy
UV-Vis	Ultraviolet-visible

1 Introduction

1.1 Motivation

In recent years, nanoparticles (NPs) have become a widely researched area to investigate the many interesting properties arising from all manner of different materials, shapes and sizes. When considering the "bottom-up" chemical synthesis approach to making NPs, most studies employ the use of reactors consisting of a vessel which is mechanically stirred. In chemical engineering terms, these reactions are carried out in a "batch" reactor. The benefits of using such reactors suit the aim of discovering new methods involving different concentrations, temperatures and reagents in a relatively simple manner. More recently, microfluidic devices have been employed to synthesize NPs because of the various benefits offered by these types of reactors. These include improved heat and mass transfer, efficiency and safety.[1] It is believed because of these enhanced characteristics (in particular heat and mass transfer); improvements in the morphological characteristics of NPs synthesized using chemical methods can be made (i.e. narrow size distributions and control of size).

1.2 Nanoparticles

NPs are materials, with a size range from 1 to 100 nm, which differ from their bulk counterparts because they exhibit unique properties due to their high surface area to volume ratios and quantum effects.[2] Importantly, the properties of the NPs depend on the size, composition and shape, making them very different from their bulk counterparts which retain their properties irrespective of size. NPs exhibit a large surface area to volume ratio (a large percentage of their atoms are located on the surface), which changes significantly with increasing size in the scale between 1-100 nm, resulting in changing properties of the NPs. The most obvious example of this change in properties with size is quantum dots which exhibit different colours on exposure to ultraviolet light depending on the size of the NPs.[3, 4] Morphology controls the NP properties hence being able to control the size distribution and size of the synthesized NPs precisely is beneficial. Traditionally batch reactors have been used to explore new synthetic routes to obtain a variety of different NP shapes such as spheres,[5] plates,[6] disks,[7] rods,[8] flowers,[9] urchins,[10] octopods, [11] wires[12] and core shell structures.[13] Such a wide array of NP shapes have been the subject of interest because of the changing properties which a change in the shape of the NP would afford.

The main focus of the research presented herein has been on silver and gold NPs, the literature presented hereafter focuses on these materials. Silver NPs are used in many applications, such as sensors,[14-16] optics,[17-19] electronics,[20, 21] catalysis,[22 23, 24] biomedicine,[25-27] and surface enhanced Raman scattering.[28] Gold NPs can be used in biological/biomedical,[29, 30] electrochemical,[31] catalytic,[32] and optical applications.[19] With the vast amount of potential applications presented, even just considering gold and silver NPs, there is then a need to be able to control the size and dispersity of NPs for them to display suitable properties for any intended application. Besides this, it is also desirable to be able to produce NPs in suitable quantities in a reliable manner. Flow reactors have the advantage over traditionally used batch reactors for the synthesis of NPs, because they are less labour intensive and

more conducive to mass production of materials. Given that the size and dispersity of the NPs determines their properties and hence application, it is important to consider the advantages and disadvantages of the characterisation techniques for NP analysis used within this work.

1.3 Characterisation techniques to determine the morphology of nanoparticles

The following section contains a brief description along with the advantages and disadvantages of the characterisation techniques used in this work to determine the size and dispersity of the synthesised NPs. The characterisation techniques used were UV-Vis spectroscopy, DCS and TEM.

1.3.1 Ultraviolet-visible spectroscopy

UV-Vis spectroscopy allows the measure of the interaction of NPs with the visible and ultraviolet portions of the electromagnetic spectrum. This interaction is highly dependent on the material, size, shape and dispersity of the NPs being measured. Small changes in the size of the NPs can cause changes in their interaction with light waves.

1.3.2 Differential centrifugal sedimentation

DCS uses centrifugal force to separate particles of different size based on their density. Since NPs are very small, they do not settle in aqueous solutions very quickly and therefore a centrifugal force is applied using a spinning disc to allow smaller particles to sediment in a reasonable timeframe. Stokes' Law is used to determine the distribution of sizes in a nanoparticle population by determining the amount of time required for a given size of particle to settle in a solution of known viscosity and density. The operation of the DCS involves the injection of a sample of NPs into the centre of a spinning disk which contains a solution of sucrose in water with a density gradient. The size of the NP determines the speed at which it reaches the light source and detector. The intensity of the light is recorded over time and changes depending on the concentration of NPs passing through the light source and detector region. The time can be related to size using Stokes' Law and in this way the size distribution of the NPs can be determined.

1.3.3 Transmission electron microscopy

The TEM operation can briefly be described as follows. An electron gun generates electrons which travel through a vacuum generated within the microscope. The electrons pass through an electromagnetic lens which focuses the beam. This travels through the specimen (a thin carbon coated copper grid which the NP sample is placed on), where the NPs interact with the beam and electrons are absorbed or scattered. The beam travels through the specimen and through various lenses to reach a detector (such as a fluorescent film) where the sample is visualised. Areas where the electron beam interacted strongly with the sample and were absorbed and/or scattered appear dark, whereas areas where the electrons did not interact appear light. In this way, the NPs are visualised.

1.4 Microfluidics

Microfluidics is a branch of flow processes concerning flow reactors which have reaction channels with diameters in the micrometre range (<1mm). This has been an active area of research in recent years, uncovering many challenges and benefits that microfluidics present.[33]

In this study, various types of microfluidic devices have been employed to synthesize gold and silver NPs with the aim of investigating how different designs can be used to manipulate the resultant size and size distribution of the NPs. The size and dispersity of the NPs are largely controlled by a chemical reaction and subsequent nucleation and growth.[34] These are in turn controlled by parameters such as concentration of reagents, pH and temperature. Usually, a change in morphological parameters is brought about by changing one of the above parameters. Currently, many studies in the literature focus on doing exactly this. This approach enables a variety of shapes, sizes and compositions of NPs to be obtained in a relatively simple manner. On the other hand, mass transfer within the reactor has been the focus of much fewer studies. The mass transfer governs the concentrations at which the reactions take place, and microfluidic devices offer tighter control over mass transfer when compared to a larger volume flow or batch reactor. Another benefit of using microfluidic devices is the spatiotemporal separation of the various stages in the synthesis including reaction, nucleation and growth which allows for a greater control over size, shape, composition and size distribution of the NPs.[35-37] It also allows for an increased flexibility in analysing the mechanisms of each of these stages.[38-40]

As mentioned previously, the majority of research synthesising NPs has been carried out in batch processes, e.g. bringing the reactants together and allowing them to react to form product, followed by removal of the products after some reaction time. The main difference between a batch process and a flow process reaction is that product is continuously withdrawn as reactants are pumped in a flow process. Figure 1-1 shows a schematic of a batch reactor and Figure 1-2 shows a schematic of a flow reactor.

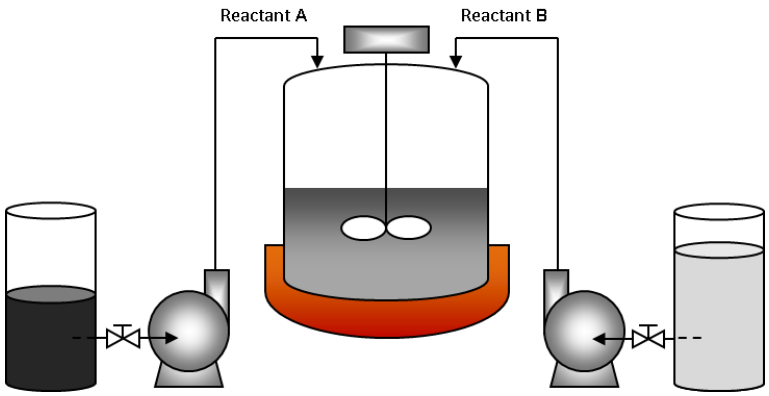

Figure 1-1: Schematic representation of a batch reactor

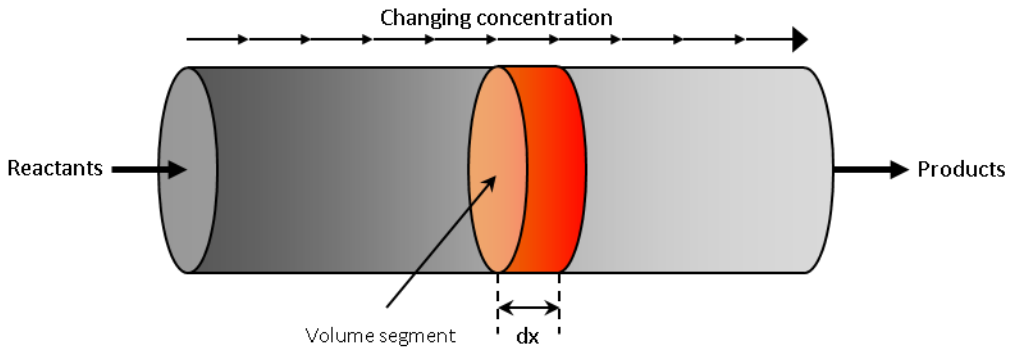

Figure 1-2: Schematic representation of a flow reactor

A key concept in mixing is the dimensionless Reynolds number, describing the ratio of inertial forces to viscous forces in a fluid:

$$\mathrm{Re} = \frac{\text{inertial forces}}{\text{viscous forces}} = \frac{\rho u d}{\mu}$$

where ρ is the density of the fluid, u is the velocity of the fluid, d is the diameter of the channel and μ is the viscosity of the fluid. This dimensionless number is useful in characterising the type of flow within the system. There are two distinct characteristic flows, laminar flow and turbulent flow. Laminar flows occur at low Reynolds numbers, typically at Re < 2000. Turbulent flow typically occurs at Re > 2000 (though in a microchannel, turbulence can occur at lower Reynolds numbers). There is a transitional phase between the two characteristic flows. In the laminar regime, mixing occurs through diffusion and the velocity profile is non-uniform across the channel (slower at the walls, faster in the centre). In the turbulent regime, non-uniform velocity profiles form resulting in a stretching and thinning of fluid lamellae. This improves the macromixing (time scale of bulk homogenisation) and also reduces the diffusion distance as fluid lamellae are stretched resulting in faster mixing on the microscale. A schematic representation of these types of flow within a channel is shown in Figure 1-3.

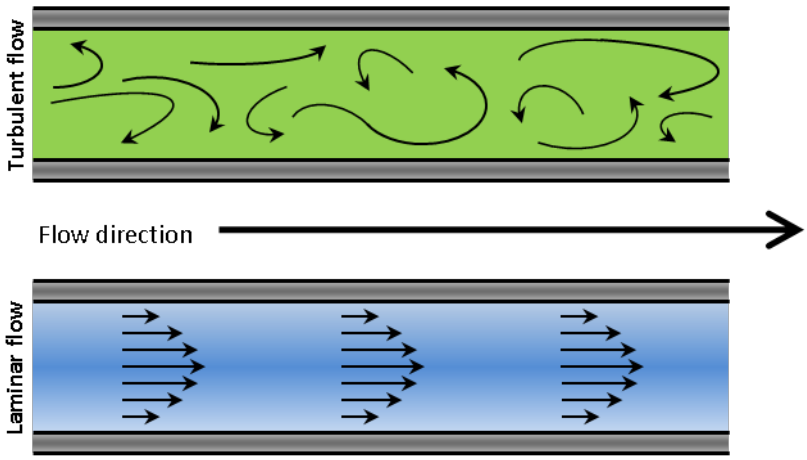

Figure 1-3: Schematic representation of turbulent flow and laminar flow

Within a microchannel, Reynolds numbers are usually very low (Re < 100) because of the small channel diameter the fluid flows through. This means that flow generally falls into the laminar regime so mixing primarily occurs through diffusion. The performance of a mixer can be measured by the amount of time it takes to mix reactants together (mixing time). Mixing time can be seen as the amount of time it takes for reactants to achieve a homogeneous concentration profile. Depending on the degree of turbulence in the microchannel, mixing will occur through a mixture of chaotic advection and diffusion. Diffusional transport is described by Fick's Law, and the characteristic mixing time can be deduced from this relationship as follows:

$$t \propto \frac{d_t^2}{D}$$

where t is the mixing time, d_t is the lamella width and D is the diffusion coefficient.[33] It can be seen from this relationship that mixing time is dependent on the distance across which a given species has to diffuse to mix with another species. Thus, to achieve quick mixing times it is necessary to efficiently reduce the diffusion distance between different species which are to be mixed. Ottino describes the striation thickness, s, as:

$$s = \frac{1}{2}(s_a + s_b)$$

where s_a and s_b are thicknesses of stream A and stream B respectively, as the simplest measure of the state of mechanical mixing.[41] This is linked to the mixing time being proportional to the lamella width as stated by Fick's Law. Mixing in microfluidic devices is generally focused on this reduction of striation thickness to improve mixing efficiency. Mixing efficiency is a key parameter when considering mass transfer. There are some other pertinent dimensionless numbers, besides the Reynolds number, when considering mixing within the microfluidic devices studied in the following chapters. The Peclet number is used to define the dominant mechanism of mass transport in a fluid and is a ratio of the timescales of diffusion and advection:

$$Pe = \frac{\text{diffusion time}}{\text{advection time}} = \frac{(\frac{L^2}{D})}{(\frac{u}{L})} = \frac{Lu}{D}$$

where L is the characteristic length, u is the flow velocity and D is the diffusion coefficient. A high Peclet number (>> 1) is indicative of an advection dominated mass transport mechanism whereas if the number is low (<< 1) it is an indicative of a diffusion dominated mass transport mechanism. Another important number is the Weber number, which is a ratio between the inertial forces and the surface tension forces in a fluid:

$$We = \frac{\rho u^2 d}{\sigma}$$

where ρ is the density of fluid, u is average velocity of fluid before impact, d is the diameter of the jet (taken as the tube internal diameter) and σ is the surface tension of the fluid. The Weber number is useful when describing the behaviour of impinging jets (chapter 4), as it is useful in characterising whether there is a continuous jet after impingement or there is droplet breakup away from the jet after impingement. This is an important consideration when looking at the mixing efficiency of impinging jets.

1.5 Mixing

Mixing occurs primarily through two mechanisms, advection and diffusion, which can be described in a more encompassing term, convection. Diffusion describes the movement of molecules from areas of high concentration to areas of low concentration and is relatively slow. When considering microfluidic devices, the primary mode of mass transport is through diffusion (because the flow is generally in the laminar regime). However, the distance across which diffusion of molecules occurs in a microfluidic device is small. Usually this distance is reduced further by manipulating the flow in the microfluidic devices to create thinner lamellae of fluid (different mixing designs are discussed in chapter 2). Laminar flow is a result of the viscous forces in moving fluid dominating the inertial forces (described by the Reynolds number), resulting in a smooth flow with straight streamlines along the direction of the flow. When the inertial forces begin to increase, either by increasing the fluid velocity or applying external force such as stirring of the fluid, the streamlines no longer maintain a smooth streamline in the direction of the flow. The movement of the fluid can then enhance the mixing through advection, where the fluid elements are stretched and folded, ultimately leading to faster mixing because diffusion can act over a shorter distance.

1.5.1 Diffusion

Fick's law of diffusion describes the flux of a species soluble in a fluid, where the species will travel within the fluid from an area of high concentration to an area of low concentration. Considering species a traveling through medium b in the y direction, the law can be stated as:

$$n_{ay} = -D_{ab}\frac{dC_a}{dy}$$

where n is the flux [mol/m^{2}s], D_{ab} is the molecular diffusivity of species a in medium b and C is the concentration [mol/m^3]. Diffusion describes the movement of material at the smallest scale, and is essentially how all mixing occurs. The speed at which this process occurs is dependent on the diffusivity of the material and the difference in concentration between the areas the material has to travel (as described by Fick's Law).

1.5.2 Advection

Advection of a fluid enhances the mass transfer through the motion of the bulk fluid, which can be described by its velocity profile. Velocity profiles within a fluid can be computed by using the Navier-Stokes Equations. This enhancement in mass transfer occurs when fluid moves in such a way to experience increased exposure to the surrounding bulk fluid. In laminar flow, each fluid element has limited interaction with the bulk fluid, because the velocity profile consists of straight streamlines which cause the fluid elements to stay on a linear path which cannot travel throughout the bulk fluid. When the flow transitions into a turbulent flow, the fluid elements follow more complex streamlines which allow them to interact with more fluid elements in the bulk fluid, as well as causing a stretching and thinning of these fluid elements to reduce diffusion distance, enhancing the mass transport through diffusion.

1.6 Objectives

Synthesis of NPs consists of reaction, nucleation and growth kinetics, also known as "reactive crystallization". Changes in size and dispersity of NPs can be achieved by changing reagent concentrations, thus affecting kinetics of the processes involved in reactive crystallization. This approach is often used from a chemistry perspective. The aim of this study is to investigate how changing mass transfer conditions affect NP size and dispersity from a chemical engineering perspective, hence considering flow hydrodynamics, mixing efficiency and concentration profiles within the microfluidic devices. This is achieved by using various characterization techniques on the microfluidic devices such as mixing time characterization using a competing parallel reaction scheme, high speed camera imaging and flow visualization using a microscope. This characterization enables an understanding of the mass transfer in each of the microfluidic devices used in this work. Synthesis of silver and gold NPs can then be performed under a variety of different mass transfer conditions afforded by the microfluidic devices used. This allows a connection to be made between the size and dispersity of NPs synthesized and the mass transfer conditions they were synthesized under.

1.7 Chapter overview

- Chapter 2 contains a literature review concerning microfluidic devices, silver NPs and gold NPs. Various designs of microfluidic devices used to achieve 'passive' mixing were reviewed ('active' mixers were not considered because of their increased complexity). Silver and gold NP synthesis in batch reactors, flow reactors and an overview of the mechanistic studies on nucleation and growth for each material are also covered.

- Chapter 3 contains a study on the synthesis of silver NPs using a coaxial flow reactor (CFR). Silver nitrate is reduced via sodium borohydride in the presence of trisodium citrate within the CFR. The effect of flow rate, precursor concentration and ligand concentration on NP size and dispersity are presented.

- Chapter 4 contains a study on the synthesis of silver NPs using an impinging jet reactor (IJR). The IJR is characterized using the Villermaux-Dushman reactions and high speed camera images. Details on the Villermaux-Dushman reactions and the interaction by exchange with the mean (IEM) mixing model are discussed. Silver NPs are synthesized by reduction of silver nitrate via sodium borohydride with either trisodium citrate or PVA used as a ligand. The effect of flow rate on silver NP size and dispersity using IJRs of two different jet diameters is presented.

- Chapter 5 contains a study on the synthesis of gold and silver NPs using a CFR in conjunction with other microfluidic devices (coiled flow inverter and split and recombine mixer) as well as using the CFR in isolation with different types of hydrodynamics (vortex flow and variation of stream thickness). Gold NPs are synthesized by reduction of tetrachloroauric acid via trisodium citrate at elevated temperatures, silver NPs are synthesized by reduction of silver nitrate via sodium borohydride in the presence of trisodium citrate. The effect of variations in mass transfer conditions and temperature on NP size and dispersity are presented.

- Chapter 6 contains a study on synthesis of gold and silver NPs using a batch reactor. Gold NPs are synthesized by reduction of tetrachloroauric acid via trisodium citrate at elevated temperatures, silver NPs are synthesized by reduction of silver nitrate via sodium borohydride in the presence of trisodium citrate. The effect of mixing efficiency and the order of reagent addition on NP size and dispersity are presented.

- Chapter 7 summarizes conclusions drawn from the work presented along with possible future directions.

2.1 Microfluidic devices for mass transfer

The following section gives an overview of microreactor technologies, in particular micromixers, currently in use. This is to aid in the understanding of how each technology works, the focus being on the method of mixing.

There exist a wide variety of micromixers reported in the literature. These are divided into two categories, passive and active micromixers.[42, 43] Active micromixers require the application of an external force to enhance the mixing performance, and are more complex to fabricate and package in general than passive micromixers. Passive micromixers rely on the geometrical manipulation of fluid elements within to achieve mixing.[44] This section focuses on passive micromixers, a simpler type of micromixer with many more studies reported in the literature.

2.1.1 Parallel lamination

T-mixers, [45-47] Y-mixers,[48] interdigitated streams[49] and hydrodynamic focusing fall[50] into this class of micromixing. The basic concept behind the mixing is to reduce the striation thickness between streams to be mixed, which in turn reduces diffusion distance and speeds up mixing. Figure 2-1 is an example of an interdigitated parallel lamination micromixer studied by Bessoth *et al.*[49]

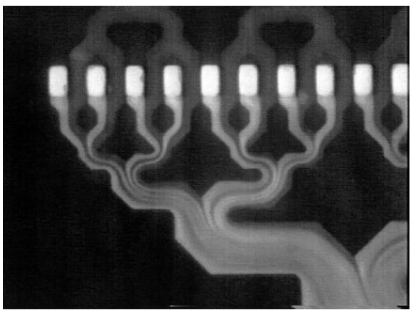

Figure 2-1: Example of a parallel lamination mixer.[49] Reproduced from Ref. 49 with permission of The Royal Society of Chemistry.

2.1.2 Serial lamination

This type of micromixer consists of a number of splitting and recombination (SAR) steps a stream consisting of two components to produce progressively thinner lamellae to decrease the diffusion path. This form consists of a number of elements which will perform successive SAR of the streams. The difference between parallel lamination and this type is that streams that are split, are recombined after one split. This is then repeated to produce progressively thinner lamellae. A characteristic advantage of this type of mixer is that the flowrate is not the main factor in determining mixing performance. Schonfeld *et al.*,[51] Kashid *et al.*,[52] Buchegger *et al.*[53] and Chen *et al.*[54] have all investigated serial laminators of different designs.

2.1.3 Segmented flow

This type of micromixer functions by splitting a continuous fluid flow into smaller discrete segments, similar to tiny individual reactors flowing through a larger flow reactor. These smaller segments are generally dispersed in a non-reacting medium which carry the smaller segments through the reactor. The movement of these segments creates an internal flow field,[42] thus mixing is generated within each segment. Waelchi and Von Rohr,[55] Kashid *et al.*,[56] Tanthapanichakoon *et al.*[57] have investigated segmented flow reactors. Figure 2-2 gives a visual depiction of the internal flow fields in slugs typically found in segmented flow.[57]

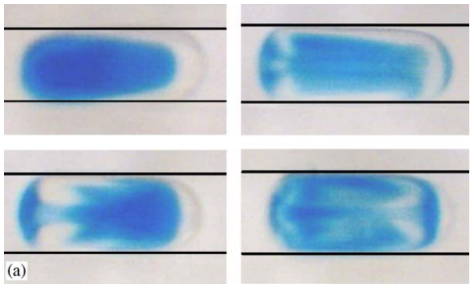

Figure 2-2: Slugs with a mixture of blue dye and water showing advection within. Reprinted from Ref. 57, Copyright (2006), with permission from Elsevier.

2.1.4 Injection micromixers

The basic mixing principle behind injection micromixers is one reagent is injected into another reagent stream through a number of small nozzles which reduce the striation thickness of the streams, resulting in quicker diffusion. Miyake *et al*.[58, 59] and Voldman *et al*.[60] have investigated injection micromixers.

2.1.5 Chaotic advection micromixers

Chaotic advection can be described as the movement of fluid in such a way that the interfacial area between reagents to be mixed is continuously increased, accompanied by a reduction in the diffusion length between reagents (striation thickness).[61] Usually some kind of internal structures within the microchannel are used to induce flow fields to increase the interfacial area between fluids to be mixed. Stroock *et al.*[62] and Kang and Kwon[63] have studied the staggered herringbone mixer (SHM), which is a type of chaotic advection micromixer.

2.2 Silver nanoparticles

This section presents silver NP synthesis studies using batch reactors, microfluidic devices and those that investigate mechanisms in silver NP formation. The main focus of the batch reactor section is silver NPs synthesized using sodium borohydride as a reducing agent given this is the system that has been studied in this work. A wider variety of systems have been reviewed for studies using microfluidic devices to highlight the possibilities of controlling size and dispersity of synthesized NPs. Studies that investigate the mechanisms of reaction, growth and nucleation of silver NPs are also reviewed.

2.2.1 Batch synthesis of silver nanoparticles via sodium borohydride reduction

A variety of reducing agents exist for reduction of silver precursors to form NPs. In this section, the focus is on sodium borohydride as a reducing agent given that this the reagent used in this work.

Creighton *et al*. used ice cold sodium borohydride to reduce silver nitrate to produce NPs in quite a wide range between 1-50 nm with some sols produced being in the range between 1-10 nm.[64] Interestingly, the sols were stable over a period of several weeks in the absence of any ligand.

Shirtcliffe *et al*. used silver nitrate, sodium borohydride and sodium hydroxide as reagents for the synthesis of silver NPs in the range between 15-77 nm.[65] They used Eppendorf pipettes to mix reagents within a cuvette at 2°C and found that the method and order of mixing had a significant effect. Addition of silver nitrate to a mixture of sodium borohydride and sodium hydroxide produced the narrowest and most reproducible peaks using UV-Vis analysis (though the TEM images showed quite large polydisperse NPs, possibly because of the lack of ligand used in the system).

Ryu *et al*. synthesized highly concentrated silver NP samples (up to 40 wt%) by reducing ice cold silver nitrate via slow addition of sodium borohydride and/or hydrazine monohydrate in the presence of polyelectrolytes in the MW range between 1200-30000.[66] NPs were in the range between 1-35 nm with the majority of conditions tested producing less than 10 nm NPs.

Song *et al*. produced silver NPs by adding silver nitrate to a solution of sodium borohydride and sodium dodecyl sulfate.[67] They observed that increased sodium borohydride resulted in less aggregation of the NPs, pointing to the hydrolysis of sodium borohydride causing aggregation but when a high molar ratio (sodium borohydride to precursor) was used, a thick layer of BH_4^- ions prevented boron hydroxide from attaching onto the surface and destabilizing the NPs. However another possibility is that the hydrolysis reaction causes an increase in pH which ultimately suppresses the hydrolysis reaction, preventing the switching point which results in a sudden shift to a higher size due to coalescence, because of the consumption of sodium borohydride.[68]

Pinto *et al*. synthesized silver NPs in the size range between 3-10 nm by addition of sodium borohydride to a mixture of silver nitrate and trisodium citrate.[69] On increasing sodium borohydride to silver nitrate molar ratios, the size of the NPs decreased and the concentration of NPs increased based on UV-Vis spectroscopy analysis. The standard deviation of the absorbance maximum increased with increasing sodium borohydride molar amount i.e. a lower reproducibility between experiments.

Thøgersen *et al*. synthesized silver NPs in the size range between 6-19 nm by addition of ice cold $AgNO_3$ slowly via drops to an ice cold solution of sodium borohydride.[70] They found an increasing size when the molar ratio of silver nitrate to sodium borohydride was increased.

Agnihotri *et al*. synthesized silver NPs in the range between 5-100 nm by adding silver nitrate to a heated solution of sodium borohydride and trisodium citrate (60°C), followed by further heating of the solution to 90°C.[5] They were able to synthesize monodispersed NPs and they suggested a two-step growth mechanism, where sodium borohydride produced small seeds through a coalescence of small silver clusters followed by a surface reduction type growth via citrate to grow the NPs into a more monodispersed sample. They were able to synthesize a wide range of sizes by varying the concentrations of the reagents used in the system. In general, altering the ratios of reducing agent to

precursor was the main method to achieve control of size of the NPs. This highlights the importance of concentration in the resultant NP size.

2.2.2 Microfluidic synthesis of silver nanoparticles

Wagner *et al.* have used split and recombine micromixers in series with residence loops in between to allow the growth of silver NPs.[71] They reduced silver nitrate using sodium borohydride. Synthesized silver NPs had a mean diameter of 15 nm. The study showed a dependency of the size distribution of the NPs on the flowrate, with an increased flowrate resulting in a narrower size distribution. A faster flowrate would result in better mixing, with a narrower size distribution pointing to a sharper distinction between nucleation and growth periods. This suggests mixing is extremely important in obtaining monodisperse NPs. Kohler *et al.* used a similar split and recombine mixer as well as a number of other configurations, which included the use of t-mixers and segmented flow techniques to synthesize composite gold and silver NPs.[72] Tetrachloroauric acid and silver nitrate were used as precursors, while ascorbic acid was used as a reducing agent.

Lin *et al.* mixed silver pentafluoropropionate in isomethyl ether in the presence of trioctylamine to form a single phase.[73] Silver NPs were formed through thermal decomposition using a simple tubular microchannel which was immersed in an oil bath held at temperature between 100-140°C. The experimental setup is shown in Figure 2-3.

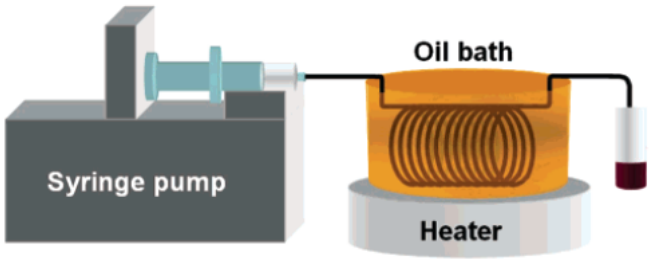

Figure 2-3: Experimental flow reactor setup of silver NP synthesis used by Lin *et al.* Reprinted with permission from Ref. 73. Copyright (2004) American Chemical Society.

Synthesized particles ranged from 7.4 to 8.7 nm in size with size variance ranging from 10% to 19%. The study showed an increase in flowrate resulted in a smaller average diameter of the NPs, though they were more polydisperse. The study suggests this is possibly down to wall effects playing a role, resulting in a parabolic velocity profile within the tube. Since this system is one phase (reagents are premixed), theoretically mixing should not be an issue (assuming they are well mixed beforehand). The activation of the reaction occurs through an increase in temperature. Therefore, to obtain monodisperse silver NPs the temperature profile must be uniform. Since microreactors have extremely high surface area to volume ratios, they excel at heat transfer. Assuming the temperature profile is uniform, the other possibility that leads to polydispersity is a broad residence time distribution (RTD).

Sonnichsen *et al.* used a simple setup involving a three way valve followed by a residence loop (tubing inner diameters of 0.75 mm for silver and 1mm for gold) shown in Figure 2-4.[74] They

synthesised both gold and silver nanorods based on the method by Jana *et al*.[75] Though reasonable results were obtained for gold nanorods, silver nanorods were more difficult. The results showed a wide range of different sizes and shapes in TEM images (Figure 2-4). They reported residence times with a spread of about 12 minutes when they injected a pulse of pre-made NPs into the reactor. This leads to poor size control of the NPs because residence times differ between different NPs flowing through the reactor. This would result in broader particle size distributions. Similar affects were seen in the work of Lin *et al*.[73]

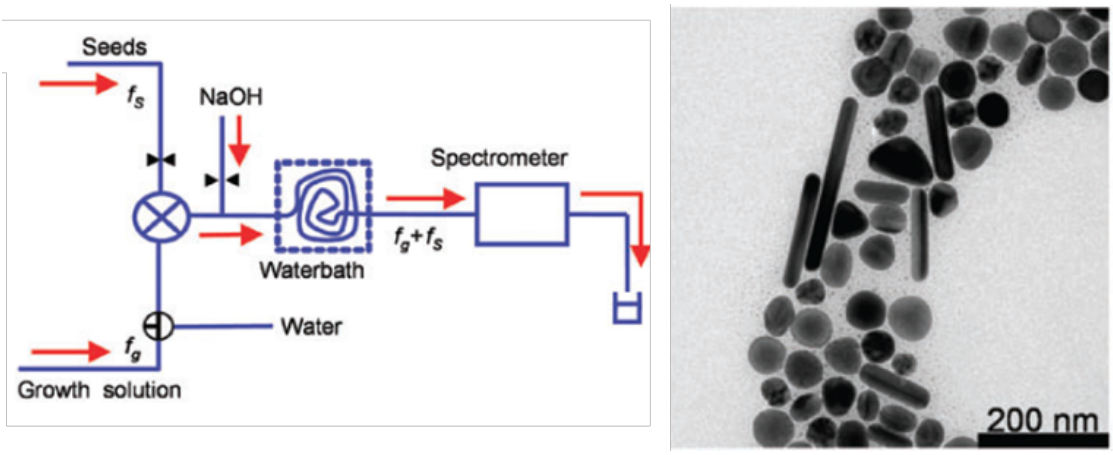

Figure 2-4: Micro flow setup to synthesise silver nanorods and TEM image of silver nanorods. Reproduced from Ref. 74 with permission of The Royal Society of Chemistry.

Knauer *et al.* employed a micro segmented flow technique within a microchannel to synthesise double shell NPs with a gold core which has a silver shell and a subsequent gold shell.[76] Tetrachloroauric acid and silver nitrate were reduced by ascorbic acid in the presence of cetyltrimethylammonium bromide. A narrower size distribution for the synthesized NPs was obtained in the case of the micro segmented flow reactor in comparison to the batch synthesis. This supports the idea of better control over size distributions with a better RTD. A narrow RTD is a characteristic of segmented flow techniques.[77]

Koehler *et al.* also synthesized Au/Ag composite NPs using a number of split and recombine mixers in series to bring the reactants together.[78] Tetrachloroauric acid and silver nitrate were reduced by ascorbic acid. The importance of mixing was highlighted in this study, indicated by the diverse range of different NP composites obtained by changing mixing orders, mixing times and flow rates (which also affects the rate of mixing).

Liu *et al.* studied the effects of various parameters on the size distribution of synthesized silver NPs.[79] The synthesis is a thermal reduction of silver nitrate using plant extract from C.Platycladi with addition of sodium hydroxide. The setup is shown in Figure 2-5.

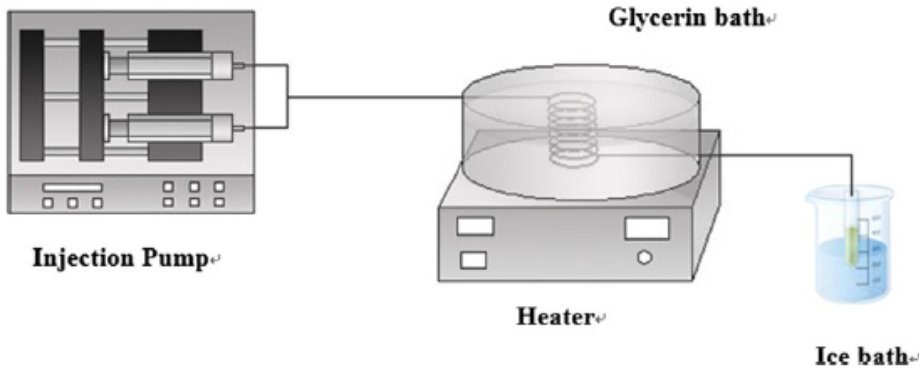

Figure 2-5: Experimental setup of microreactor used by Liu *et al.* Reprinted from Ref. 79, Copyright (2012), with permission from Elsevier.

Particle size increased when flow rate was increased from 0.2 ml/min to 0.4 ml/min (3.5 nm to 7.2 nm) and then decreased when the flow rate was further increased from 0.4 ml/min to 0.6 ml/min (7.2 nm to 3 nm). Increasing C.Platycladi concentration resulted in increasing particle size and dispersity (4.7 ± 1.9 nm to 15 ± 8.6 nm). The microreactor properties also played a key role. T-type mixers produced smaller and more narrowly distributed particles than that produced by Y-type mixers (4.7 ± 1.9 nm against 5.3 ± 2.9 nm respectively). Particles produced in PTFE reactors were smaller and more narrowly distributed than those produced in ETFE (4.2 ± 0.9 nm against 4.7 ± 1.9 nm respectively). Both reactors had a channel diameter of 0.8 mm. Smaller channel diameters (0.5 mm, 7.0 ± 1.9 nm) produced larger particles on average than larger channel sizes (0.8 mm, 4.7 ± 1.9 nm), however the flowrate was changed to produce similar residence times which may have also affected flow hydrodynamics.

Kumar *et al.* synthesised silver NPs in a spiral flow reactor using segmented flow techniques via inert liquid kerosene and inert gas air.[80] Stearic acid sophorolipid molecules were used as both a reducing and capping agent. Silver nitrate was reduced by these molecules at 90°C. Figure 2-6 shows the setup used in the study.

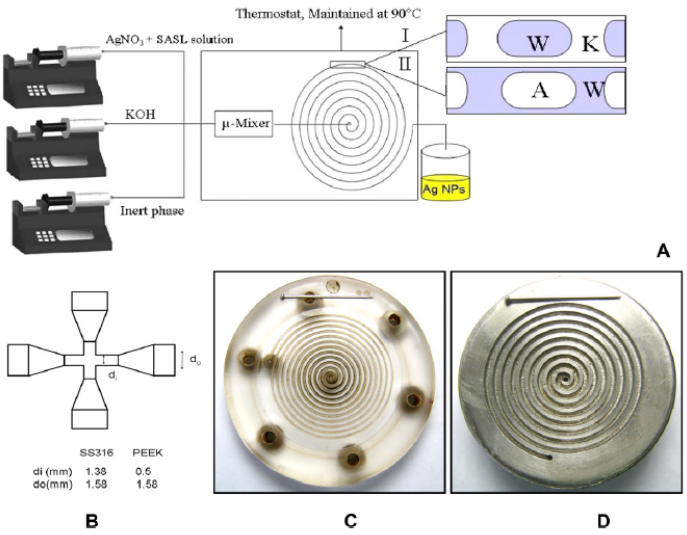

Figure 2-6: Spiral flow reactor used by Kumar *et al.*, [80] W represents reacting phase, K represents liquid kerosene inert phase, A represents gas air inert phase. B represents inlet micromixer (cross mixer) used to generate slugs, with PEEK and Stainless Steel being used (dimensions given). C and D are PMMA (0.5 mm ID) and Stainless Steel (1 mm ID) spiral reactors respectively. Reprinted from Ref. 80, Copyright (2012), with permission from Elsevier.

They studied the effects of variations in the slug flow (liquid-liquid, gas-liquid, size), flow rate, inlet micromixer diameter and flow rate ratios have on the size distribution of the formed silver NPs. Various effects were reported, the main one being that smaller and narrower size distributions were obtained when the reactive phase was continuous rather than in slug form. It is suggested that internal circulation (mixing), flow velocities and differences in material properties (liquid-liquid and gas-liquid) contribute to the particle size distribution. Flow rates used were 35 µl/min, 100 µl/min and 1 ml/min with ratios of inert phase to reacting phase being 0.5, 1 and 2. At lower flowrates, smaller and more narrowly distributed particles were formed, with air/water at 35 µl/min (2:1 air to water) performing the best in terms of narrow distribution with the smallest size.

Lazarus *et al*. studied the synthesis of silver and gold NPs using segmented droplet flow using ionic liquid.[81] Droplet formation of viscous BMIM-Tf_2N (1-butyl-3-methylimidazoliumbis-(trifluoromethylsulfonyl)imide) within a continuous fluorocarbon oil phase, polychlorotrifluoroethylene (PCTFE), was achieved by coating the PDMS microfluidic device with a fluoropolymer via initiated chemical vapour deposition (iCVD). This allows the carrier oil phase to coat the surface of the channel walls to prevent the ionic droplets from contacting the wall (improving the residence time because segmented flow is known to improve RTD, but further improvements would be obtained if wall effects are minimised as in this case). Droplet formation at a number of different flow rate ratios can be seen in Figure 2-7.

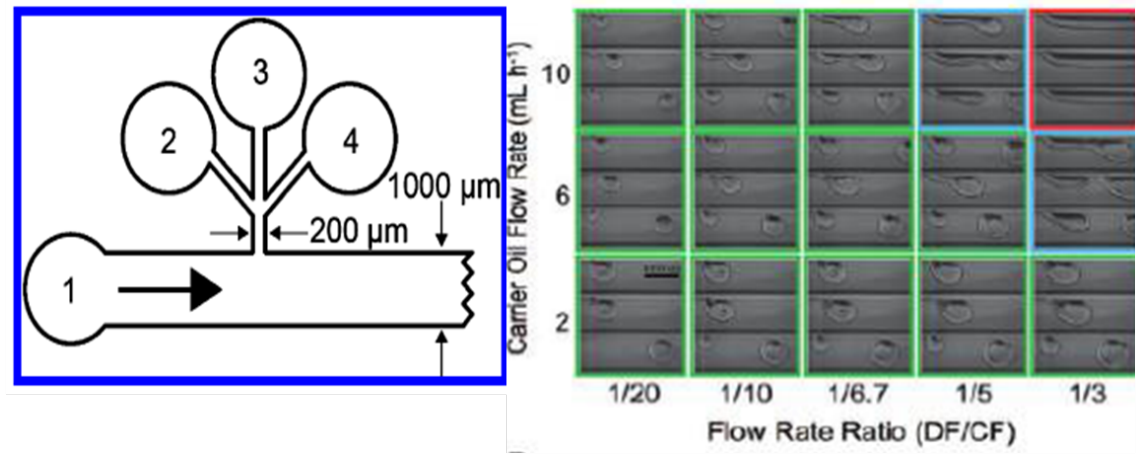

Figure 2-7: Configuration of microfludic device with four inlets: 1) Carrier fluid inlet, 2) Precursor solution inlet, 3) Solvent inlet, 4) Reducing agent inlet. Right hand side shows segmented flow of ionic liquid (BMIM-Tf_2N) within the oil carrier phase (PCTFE). At higher flowrates, jetting occurs further along the channel as the droplets pinch and form thin strand phases. Reprinted with permission from Ref. 81. Copyright (2012) American Chemical Society.

In the study, 1-butyl-3-methylimidazolium borohydride (BMIM-BH_4) is used as a reducing agent preferentially over sodium borohydride. 1-methylimidazole was used as a stabilising agent, because it binds to metal surfaces and serves as an acid scavenger which would prevent the destabilisation and agglomeration of NPs in the case of acid build-up. $AgBF_4$ was used as a precursor ($HAuCl_4$ was used for gold).

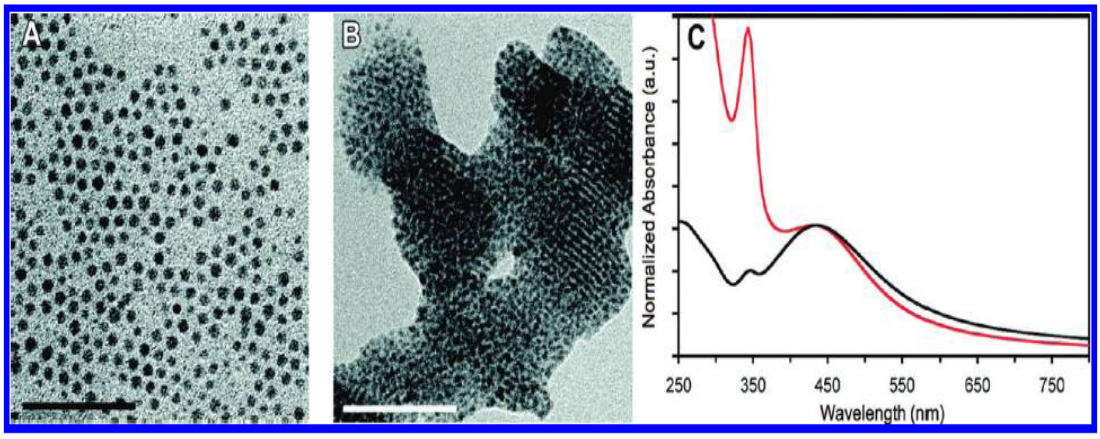

Figure 2-8: Silver NPs made using A) Microfluidic device, B) using a batch reactor, C) UV-Vis comparison of both (microfluidic device is black, batch is red). Reprinted with permission from Ref. 81. Copyright (2012) American Chemical Society.

Figure 2-8 shows the Ag NPs synthesised in the study with a marked difference between the two synthesis methods employed, batch reactor and microreactor. The mean size of the Ag NPs synthesised in the microfluidic device are 3.73 ± 0.77 nm whereas those in batch produced large coral like assemblies. The UV-Vis data presented suggests a high number of smaller Ag NPs of less than 10 atoms present in the batch synthesis.

Overall, a variety of different microfluidic devices have been used for the synthesis of silver NPs to showcase the potential benefits they present.

2.2.3 Mechanistic studies of silver nanoparticle synthesis

Polte *et al.* studied the mechanisms of silver NP synthesis using a continuous SAXS (small angle x-ray scattering) setup.[68] Silver perchlorate was used as a precursor, sodium borohydride as a reducing agent and PVP as a stabilising agent. System 1 used no stabilising agent and system 2 shows the synthesis with PVP as a stabiliser, showing similar trends but taking longer than system 1 in terms of the growth of silver NPs (Figure 2-9). It seems that surfactants may slow the kinetics down (PVP in this case). In both cases the growth mechanism is the same, however, the hydrolysis of $NaBH_4$ (which is supposedly sped up by the presence of metal NPs) slows down with the addition of PVP resulting in a longer time before the switching point. The switching point is the point at which particle stability decreases massively, resulting in particles coalescing from 2-3 nm up to 6-8 nm in size. The hydrolysis of sodium borohydride results in a change in the colloidal stability, resulting in an inevitable increase in the size of NPs due to coalescence coupled with a reduction in polydispersity. An illustration of the suggested mechanism is shown in Figure 2-9.

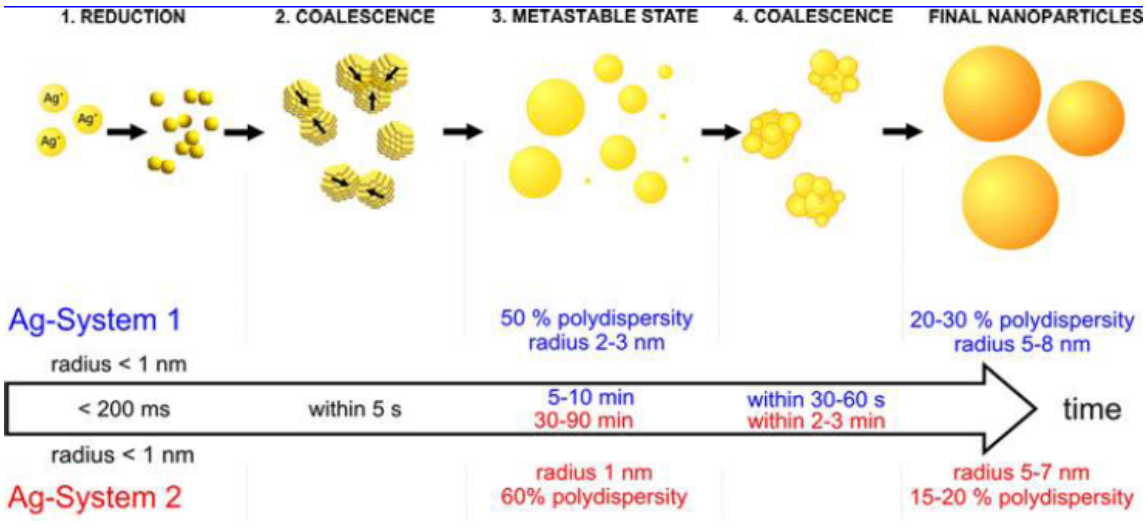

Figure 2-9: Suggested growth mechanism for silver NP synthesis. Reprinted with permission from Ref. 68. Copyright (2012) American Chemical Society.

Takesue *et al.* performed mechanistic studies on silver NP synthesis using silver nitrate as a precursor with citric acid as a stabiliser and tannic acid as a reducing agent.[82] SAXS was used to characterise the NPs online in a flow reactor setup (Y-mixer). The mole ratios of silver nitrate:citric acid:tannic acid was 1:5:0.02 with sodium hydroxide used to adjust the pH to 12. The main growth mechanism suggested by this study is that Ag_{13} clusters are formed which then coalesce and aggregate to form larger NPs. This is evidenced by an initial formation of seed particles which match the size of an Ag_{13} cluster, followed by gradual increase in the size of the NPs to a final average size of around 7 nm. Ag_{55} clusters were not formed in significant numbers because the size of this NP was only present in very small amounts. The proposed mechanism can be seen in Figure 2-10. The onset of nucleation becomes clear at 0.59 ms in

this synthesis. 0.71 nm Ag clusters form the majority between 0.59 and 0.79 ms, corresponding to Ag_{13} clusters, however some particles larger than 10 nm exist and the process of growth is essentially over at 3.93 ms. The author suggests the process of growth is dictated by Ag_{13} particles coalescing and growing to form larger particles.

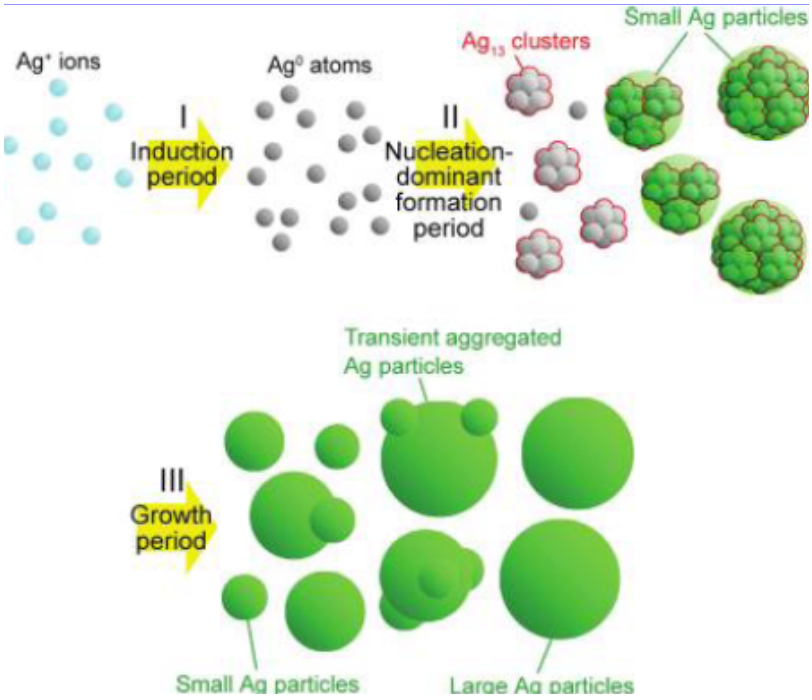

Figure 2-10: Mechanism of silver NP synthesis proposed by Takesue et al. [82] Silver nanoparticles are formed through (I) an induction period during which Ag+ ions are reduced to Ag0 atoms; (II) a nucleation-dominant formation period during which Ag13 clusters are nucleated and simultaneously consumed in silver nanoparticle formation; and (III) a growth period during which larger silver nanoparticles are formed by coalescence and aggregation of smaller silver nanoparticles. Reprinted with permission from Ref. 82. Copyright (2011) American Chemical Society.

Henglein and Giersig synthesised silver NPs using $AgClO_4$ solution as a precursor which also contains 2-propanol, N_2O and sodium citrate in various concentrations.[83] The reducing agent is the 1-hydroxyalkyl radical generated through radiolysis. The main findings of the paper is that at low citrate concentrations the NPs synthesised are partly agglomerated with many imperfections, at an intermediate concentration the particles are well formed and separated with narrow size distributions and at higher concentrations there is coalescence of particles due to the instability caused by the high ionic strength of the solution. The molar ratio of sodium citrate to precursor in the study ranges from 0.5 to 15. They propose two mechanisms of silver NP growth (Figure 2-11). Surface reduction growth which occurs via electron transfer, reducing Ag^+ ions onto the surface of the particles already present in the solution, or coalescence of smaller NPs to form larger NPs. The study suggests that if the citrate concentration is too low, the silver NPs are not sufficiently covered with stabilising citrate and coalescence occurs. At higher concentrations, the ionic strength of the solution destabilises particles. A very important growth experiment they carried out which involved taking a seed solution of silver NPs and adding further silver precursor and reducing electrons to check how the seed particles were affected. The experiment shows

a perfect surface reduction occurring as all the silver reduces to make existing particles bigger rather than produce new particles. This occurs by introducing 5 ml of seed particles to another 35 ml of solution, which after irradiation produces particles which have grown perfectly in size according to the amount of silver added. This is important because it shows the potential for tuning NP sizes but more importantly that the mechanism of surface reduction for growth of silver NPs does exist.

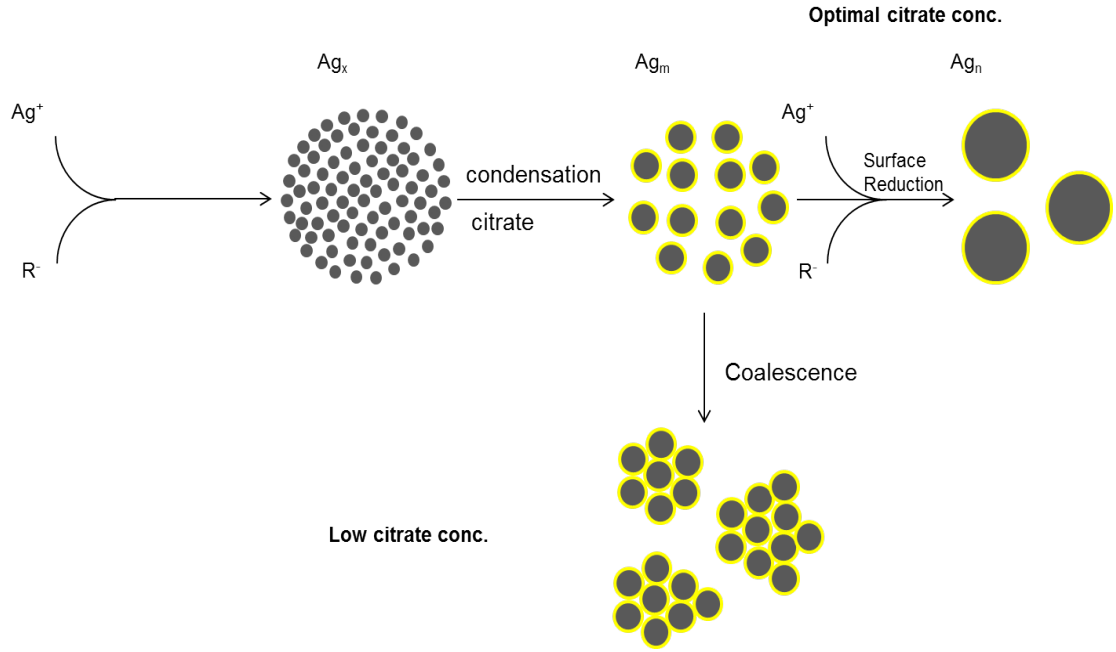

Figure 2-11: Growth mechanisms proposed by Henglein and Giersig at low and optimal citrate concentrations with two different mechanisms occurring. At optimal concentrations, it is suggested that a surface reduction of silver ions occurs on the surface of formed NPs owing to the reduction potential of the citrate adsorbed onto the surface. At low concentrations, coalescence of smaller silver NP clusters occurs.[34, 83] Ref. 34 published by The American Chemical Society.

Pillai and Kamat studied the role of the citrate ion in reducing silver ions as well as its stabilisation of silver NPs and the formation of complexes with silver ions.[84] They reduced silver nitrate using citrate at elevated temperatures as well as γ radiolysis. Using citrate as a reducing agent, a higher concentration allowed the reaction to proceed faster as well as resulting in increased absorbance at 420 nm wavelength on the UV-Vis peak. This is in agreement with a stronger reducing effect producing faster reactions, as well as producing a more concentrated sample at 420 nm, indicating more NPs in that size range were successfully formed and stabilised. In the case of using γ radiolysis, the author suggests the silver may not react at low citrate concentrations fully because of a lower peak absorbance. However, the peak absorbance may be lower because of the presence of aggregates; naturally the peak absorption will be lower if there is a higher concentration of aggregates which contribute absorbance to longer wavelengths (indicated by more prominent shoulder peaks). Citrate concentration in the case of γ radiolysis will affect the stabilisation of the NPs and as the concentration increases, the shoulder peak absorbance decreases indicating decreasing concentration of aggregates (Figure 2-12). Higher reducing power points to smaller average particle size from the difference in size between the two methods

(Turkevitch, 50-100 nm and γ radiolysis, 5-10nm), where the citrate has less reducing power than the radiolysis (resulting in a lower supersaturation). A growth dominated mechanism is favoured when the reducing power is relatively low (citrate) resulting in fewer nuclei which grow to larger sizes and vice versa for higher relative reducing power (γ radiolysis). The growth mechanism they suggest is shown in Figure 2-13.

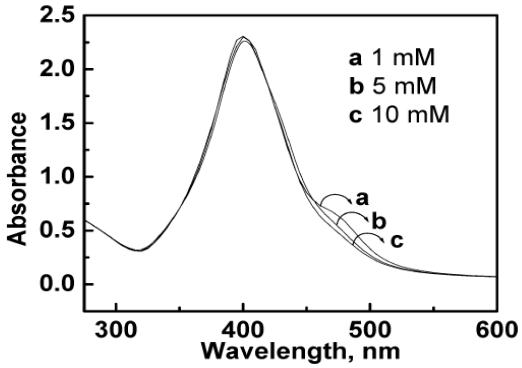

Figure 2-12: Absorption spectra of Ag colloids prepared by γ irradiation of an aqueous solution (N_2 purged) containing 1 mM $AgNO_3$, 1% methanol, and (a) 1mM, (b) 5mM, and (c) 10 mM sodium citrate as stabilizer.[84] Reprinted with permission from Ref. 84. Copyright (2003) American Chemical Society.

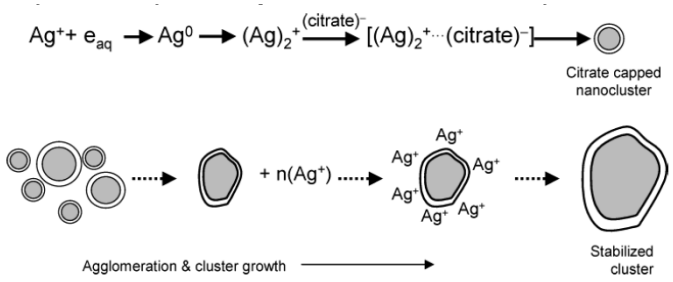

Figure 2-13: Growth mechanism through pulse radiolysis of a mixture of silver nitrate and trisodium citrate proposed by Pillai and Kamat: primary and secondary growth steps in the formation of silver nanocrystallites.[84] Reprinted with permission from Ref. 84. Copyright (2003) American Chemical Society.

Zhang *et al*. synthesised silver NPs and nanorods using silver nitrate as a precursor, sodium borohydride as a reducing agent and trisodium citrate as stabilizing agent.[85] Though this is not a specific mechanistic study, there is useful information regarding mechanisms of silver NP formation. To obtain different shapes of NPs, preferential growth is required in certain directions. The evidence in this study suggest that nanocrystals formed with little defects show a uniform coverage of citrate, whereas those with defects are more suitable for nanorod growth because of the preferential adsorption of citrate on different surfaces because of defects in the crystal structure. This has implications on monodispersity and shape control of NPs. Moreover, the difference in defects of NPs formed arises from a difference in the mixing of the reagents (all at once and dropwise).

Woehl et al. studied the effects of reducing power (i.e. number of electrons available for reduction) using in-situ TEM scanning on the nucleation and growth characteristics of silver NPs.[86] Reduction was achieved directly from electrons acquired from the TEM beam, which are transferred to the solution and reduce the silver nitrate. The authors use classical nucleation theory to explain the effects observed

pointing to a certain concentration of electrons (reducing power) needed to achieve the conditions which induce nucleation (supersaturation) and observed there was no nucleation below a certain threshold of electron concentration. They find at a dose rate much higher than this threshold, the growth of the NPs is diffusion limited and is controlled by how quickly silver atoms can find the surface of the crystals from the bulk of the solution. In this case the morphology of crystals was seen to be spherical. At an electron dosage closer to that of the threshold for inducing nucleation, growth is reaction limited in the sense that the surface reduction of silver atoms onto the NP is the slowest process resulting in NPs that grow into different shapes. These differences are attributed to diffusion limitations in the case of spherical particles, where there is an abundance of reduced silver ions which can attach onto the surface of formed nanocrystals, and reaction limited in the non-spherical case where there is a lack of electrons available near the surface of the particles leading to a surface reduction reaction limiting step. The summary of their investigation can be seen in Figure 2-14.

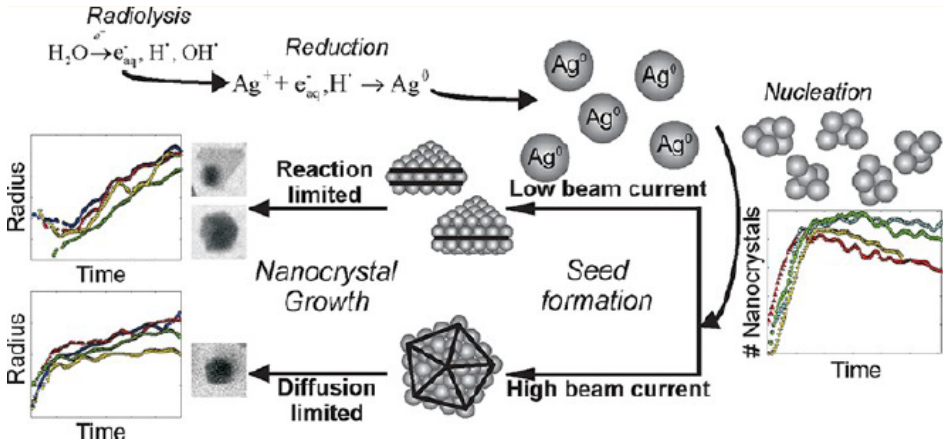

Figure 2-14: Mechanisms of silver NP growth using different beam currents under a TEM microscope.[86] Reprinted with permission from Ref. 86. Copyright (2012) American Chemical Society.

The various mechanistic studies in the literature have performed the silver NP synthesis using slightly different conditions (reaction vessels, chemicals, concentrations etc.), so must be considered when making comparisons. The studies by Polte *et al*. and Takesue *et al*. both use SAXS and achieved similar sized NPs. [68, 82] They are in agreement that the overarching mechanism of the silver NP formation is coalescence with no mention of surface reduction (surface reduction implied by the study by Henglein and Giersig).[83] However, because of the limited conditions at which the SAXS studies are carried out, it is possible that there may be different mechanisms depending on the conditions. Henglein and Giersig and Zhang *et al.* discuss the presence of defects in crystals, which is somewhat correlated in the studies to differences in shapes and size distributions.[83, 85] Different growth mechanisms depending on the defects present on the crystal surface have been highlighted by these studies. Lastly, Pillai and Kamat and Jiang *et al.* discuss the complexes formed between citrate and silver ions,[84, 87] which affect the kinetics of the growth, adding more complexity to the issue of controlling the size, distribution of size and shape of the silver NPs.

2.3 Gold nanoparticles

This section presents gold NP synthesis studies using batch reactors, microfluidic devices and those that investigate mechanisms in gold NP formation. The main focus of the batch reactor section is gold NPs synthesized using the Turkevich method. A wider variety of systems have been reviewed for studies using microfluidic devices to synthesize gold NPs. Finally, studies that investigate the mechanisms of reaction, growth and nucleation of gold NPs are reviewed.

2.3.1 Batch synthesis of gold nanoparticles

The most popular method for synthesis of gold NPs is known as the Turkevich method. Turkevich *et al*. tested a variety of different methods but found the sodium citrate method to be the most repeatable.[88] This famous method involves bringing a stirred aqueous solution of chloroauric acid to the boil before adding a sodium citrate solution to the precursor. Subsequently, the colour transitions through yellow, clear, grey-blue, purple and finally a wine red. The method produces NPs typically in the range between 15-20 nm. The popularity of this method is down to its ease and reliability in producing monodispersed gold NPs. The effect of temperature, sodium citrate concentration were studied by Turkevich *et al*. Decreasing temperature below 100°C resulted in slowing down the reaction, but a change in size was observed. The smallest NPs were seen at 80°C but increased slightly in size if synthesis temperature was set to 70°C. Reducing the sodium citrate concentration resulted in some marked changes such as the colour changes being more defined while the grey-blue was more blue with decreased concentration. The overall synthesis was more rapid at lower citrate concentrations while the average diameter of the NPs increased. The colour change of the solution, from the initial yellow of the chloroauric acid to the final wine red, gives an idea of the mechanisms taking place to form the NPs.

Frens worked further on this method and synthesis and synthesised NPs in the range of 12-150 nm by varying the amount of citrate which was injected into the boiling solution of tetrachlorauric acid.[89] The conclusion of the study was that the final size of the NPs was governed by the number of nuclei formed which was controlled by the amount of citrate added. Higher amounts of citrate led to smaller NPs, and Goodman *et al*. observed a similar trend with the same procedure when increasing citrate concentration with NP size from 21 to 80 nm.[90]

Chow and Zukoski synthesised gold NPs with sizes ranging between *ca*. 16-52 nm for unagglomerated particles (very large agglomerated NPs were seen in cases were the synthesis of gold NPs was not complete).[91] They varied temperature between 60-80°C and found that the final particle size tended to ca. 20 nm and it took longer to arrive at the final size with decreasing temperature.

Su *et al*. synthesised gold NPs by sonication of tetrachlorauric acid and trisodium citrate solutions at 4°C.[92] They varied the gold precursor to citrate molar ratio from 1:1 to 1:8 and found that non-stable large aggregates were formed at ratios at or below 1:3 and NPs in the size range between 17-22 nm were formed at or above ratios of 1:4.

Pei *et al*. synthesised gold nanowires with a modification on the standard method in which 200 ml of sodium tetrachloroaurate is brought up to 80°C in a temperature controlled bath followed by rapid addition of trisodium citrate in various controlled volumes to adjust the molar ratio of citrate to gold

from 0.1 to 2.7.[93] Nanowires were formed for ratios below 0.4, and particles were formed for ratios above 0.4. A blue colour was associated with wire formation which was observed at all ratios from 0.2 to 2.7, but this transitioned into a red colour for ratios at 0.4 or higher which is associated with spherical gold NPs.

Kimling *et al*. synthesised gold NPs using the Turkevich method, UV-assisted reduction with citrate and ascorbic acid reduction. The reaction volume for the Turkevich method was 100 ml, 2 ml in a cuvette for the UV-assisted reduction and 50 ml for ascorbic acid reduction.[94] They tested gold to citrate molar ratios of *ca*. 0.1-1.5 for all the syntheses. Using the Turkevich method they synthesised gold NPs between *ca*. 17-130 nm at concentrations of less than 0.8 mM, 1 mM and 1.2 mM tetrachlorauric acid. They found that the size increased when reducing the citrate concentration, attributed to the lack of stabilization of smaller NPs because of incomplete coverage of citrate. At concentrations less than 0.8 mM, the size of the NPs was independent of gold concentration and dependent on citrate concentration. When gold concentration was increased above 0.8 mM the size of the NPs almost doubled at lower citrate to gold molar ratios. In contrast the UV-assisted reduction showed a similar size correlation for gold concentrations of 1 and 1.6 mM with NPs in the *ca*. 17-117 nm range. The ascorbic acid reduction enabled synthesis of NPs between *ca*. 17-110 nm. This method showed an NP size increase when increasing the gold concentration from 0.5 mM to 1.6 mM similar to that in the Turkevich method, but when increasing the pH to 7, the size of the NPs was similar for both gold concentrations supposedly because of a reduction in instabilities caused by the acidity at the higher concentrations.

Ji *et al*. investigated the role of citrate in the standard method.[95] By varying the trisodium citrate concentration, they found a minimum size of *ca*. 15 nm to exist at a molar ratio of 3.5 to 1 trisodium citrate to tetrachloroauric acid, if the ratio was lower or higher than this there was increase in size of NPs. They found that at higher citrate ratios, the reaction took longer to proceed. Nanowire like structures were observed in the early stages of synthesis at citrate ratios in the lower range (< 3.5) while at higher ratios the NPs where spherical in all stages of the synthesis. The consumption of precursor was found to be in general more rapid at lower citrate ratios, in line with the idea that reactivity and hence nucleation rate is higher at lower pH. By tuning the pH but keeping the citrate to gold precursor molar ratio constant, the size was varied from small to large in the same way as increasing citrate concentration would but the dispersity was reduced and more constant through the pH variation method from 20-40 nm NP size.

Patungwasa and Hodak investigated the effect of pH on gold NPs.[96] They found that NP size decreased with increasing pH in the range between 4 and 6.5. This was suggested to be because of the charge on the citrate adsorbed onto the NP surface, at lower pH there is decreased charge on the citrate surface resulting in reduced stability whereas at higher pH the citrate has a higher charge which would explain why smaller and less polydisperse NPs are seen at higher pH. The system tends to higher average NP size at low pH.

Ojea-Jiménez *et al*. synthesised gold NPs using the standard method as well as a modification using deuterium oxide as a solvent instead of water.[97] They synthesised gold NPs by heating trisodium citrate in either 100% H_2O, 50% D_2O/H_2O or 100% D_2O to which they added tetrachloroauric acid and

subsequently let the solution boil for 3.5 min. The NP size was in the range of 5.3 ± 1.1 nm for pure D_2O and 9.0 ± 1.2 nm for pure H_2O. The reduction in size by using deuterium oxide was attributed to the increased reducing strength of the citrate (in D_2O).

Uppal *et al*. synthesised gold NPs from 11 to 15 nm with trisodium citrate added to boiling tetrachloroauric acid drop wise over a period of 6 min.[98] The solutions were removed from the temperature bath used to heat the solution when the colour of the sample went lilac and the samples were observed over a number of days. It was found that the peak wavelength decreased or blue-shifted from 540 nm to 522-523 nm regardless of whether the solution was stored in dark or light conditions. Uppal *et al*. also synthesised gold NPs with a number of different initiation methods.[99] This involved initiating the reaction between tetrachlorauric acid and trisodium citrate using thermal heating, sonolysis, microwaves and UV-light. These initiation methods were tested with premixed solutions of tetrachlorauric acid and trisodium citrate, where the trisodium citrate concentration was increased to vary the reducing agent/stabilising agent concentration. 11.0 to 11.9 nm NPs were formed using thermal initiation with little variance in size with increasing citrate concentration, 11-17 nm NPs were formed using microwaves with a decrease in size with increasing citrate concentration, 8 nm NPs were formed using UV-light initiation with an increase in the elliptical shape of the NPs with increasing citrate and 17 to 18 nm NPs were formed using sonolysis and size changed minimally with increasing citrate concentration.

Ojea-Jiménez *et al*. compared the standard method to an inverse method, which involves adding tetrachloroauric acid to hot sodium citrate.[100] They found that the NPs synthesised using the inverse method were smaller than those in the standard synthesis while NPs synthesized using the standard method at a sodium citrate to tetrachloroauric acid ratio of 13.6 were 36.6 nm while the inverse method gave NPs 9 nm in size, lowering the sodium citrate to tetrachloroauric acid ratio to 6.8 gave a smaller disparity in size between the methods: 17.8 nm and 14.9 nm for the standard and inverse method respectively. By using a mixture of sodium citrate and dicarboxyacetone (DCA) (90:10) they found that the surface plasmon resonance band of the solution developed quicker (from 11 min with no DCA, to 5 min with DCA) while there was a reduction from 21.2 to 17.7 nm in size when DCA was added to the citrate before addition to the hot tetrachloroauric acid. By using a 50:50 mixture of DCA and sodium citrate, it was found that the resultant NPs were larger and more polydisperse (25.9 nm) and using DCA only resulted in no NPs being formed. There was a possibility of changes in size when changing the sodium citrate DCA ratio because of changing pH, and pH is a parameter known to affect size of NPs.[95] To check whether DCA had a real effect on the NP size, the pH was modified using sodium hydroxide. A decrease in size was found when the pH was adjusted to similar values to that of experiments which do not use DCA, and the resultant NPs were found to be smaller suggesting that DCA does indeed play an important role in the synthesis of gold NPs. Ojea-Jiménez and Campanera synthesised gold NPs with a modification of pH by adding hydrochloric acid to the tetrachloroauric acid before addition of sodium citrate to the mixture at 90°C, with the pH of 6.5, 5.6 and 4.7 being tested.[101] The NP size decreased from 36.6 nm to 16.1 nm with decreasing pH value.

Sivaraman *et al*. synthesised gold NPs using the inverse method by adding tetrachloroauric acid to boiling trisodium citrate solution.[102] They found that at citrate to gold ratios of < 5, the mean size of the NP was not significantly affected (52 nm for inverse method, 56 nm for Turkevich method at a ratio of 1 to 1) whereas for ratios > 5, there was a significant reduction in the size of the NPs (10 and 16.1 nm at a 5.2 ratio, and 7.2 and 13.6 nm at a ratio of 20.8) when using the inverse method. They investigated the possibility of the oxidation of citrate to DCA by boiling citrate before addition to tetrachlorauric acid and comparing it to the standard method (citrate is not boiled before addition to boiling tetrachloroauric acid) and the inverse method. They found that the inverse method yielded smaller NPs as expected, but the first two methods yielded similar sizes suggesting that order of reactant addition is the cause for a change in NP size, rather than the oxidation of citrate to DCA.

Schulz *et al*. synthesized gold NPs of ~ 3.5 nm with a low dispersity of 5-6% using an inverse method.[103] The method was optimised by the use of sodium citrate/citric acid buffer to control pH. EDTA was used to remove potential trace contaminations of metals such as zinc or copper, it was suspected that these caused the formation of gold triangular plates since the metal ions can affect the growth of the Au NPs. It was found that the addition of EDTA reduced the formation of triangular particles to practically zero.

Wuithschick *et al*. synthesized gold NPs using the Turkevich method and investigated the effect of temperature, pH and variation of reactant concentrations and order of addition.[104] It was observed that there was a minimum size achieved of 12.2 nm when the synthesis was carried out 60°C and the synthesis time decreased with increasing temperature. By varying the initial pH of the tetrachloroauric acid, a pH window between 2.8 and 4 was found to produce the best dispersity of around 10% with the minimum size achieved of 10.8 nm. The citrate concentration supposedly had little effect as long as the concentration was enough to maintain a neutral pH after mixing, whereas increasing tetrachloroauric acid concentrations led to a decrease in the size of the NPs. Changing the order of reactant addition showed that adding tetrachloroauric acid to a larger volume of citrate gave smaller NPs than the standard method.

Piella *et al*. synthesised sub-10 nm gold NPs based on a modification on the inverse method, involving the use of tannic acid together with sodium citrate as a reducing agent.[105] Highly monodispersed 3.6 nm seeds were synthesised (505 nm peak wavelength) and were subsequently used in further growth steps to obtain a range of size in the sub-10 nm range. Parametric studies on optimal tannic acid to gold molar ratio, temperature and pH were conducted, and the optimal values were found to be 0.01, 70°C and pH 8 respectively for obtaining the smallest NPs. Sodium citrate and tannic acid were also tested in isolation where 10.9 ± 1.3 nm (518 nm peak wavelength) and 4-12 nm NPs (527 nm peak wavelength) were obtained respectively, suggesting there is a synergistic effect between the tannic acid and sodium citrate, although the resultant 4-12 nm NPs from using tannic acid alone may be because of insufficient stabilisation.

Kettemann *et al*. synthesised gold NPs using the standard method and a modification to improve reproducibility of the synthesis.[106] With the improved synthesis they were able to synthesise NPs in the 11-18 nm with less than 0.6 nm deviation in all cases. Similar to Schulz *et al*.,[103] in the improved

synthesis they used a buffer of sodium citrate and citric acid to achieve a pH between 5.5 and 6, which was found to be the area in which the synthesis is most reproducible because of the stability of the $HCit^{2-}$ species. This species was suggested as the form of the citrate which is responsible for the reduction of the gold precursor.

2.3.2 Microfluidic synthesis of gold nanoparticles

Weng *et al*. synthesized gold NPs using a Turkevich method in a novel microfluidic device (Figure 2-15).[40] Hexagonal NPs of around 35 nm were obtained at a temperature of 115°C with reaction time in the order of 2 to 5 min. They observed a coalescence of smaller NPs to form larger NPs by analyzing the sample at a reaction of 2 min. This mechanism was possibly due to the relatively quick mixing time obtained in the reactor (reaction volumes were ca. 30-40 µl) which may have led to the quick hydroxylation of the $AuCl_4^-$ species to $AuCl_xOH_{4-x}^-$ species, which is known to reduce the reactivity of the gold precursor, possibly leading to a lower nucleation rate and increased growth rate, particularly when the citrate to gold molar ratios are between ca. 4-9. The quicker mixing time (relative to a batch process) would have reduced the time for reaction while the $AuCl_4^-$ species exists in solution.

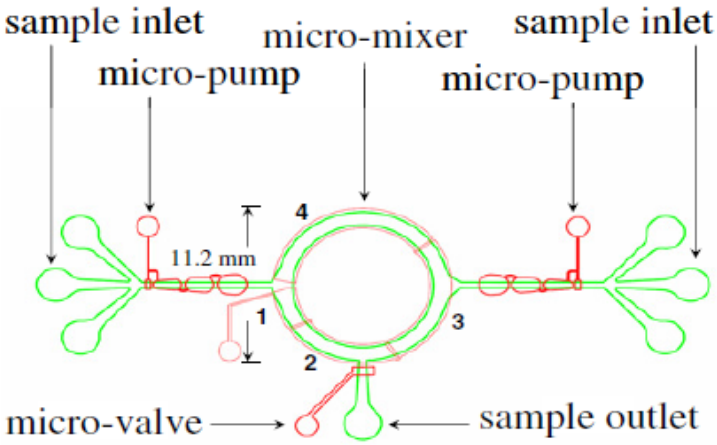

Figure 2-15: Microfluidic device used to synthesize hexagonal gold NPs.[40] Reprinted from Ref. 40 with permission from The Institute of Physics.

Ftouni *et al*. synthesized gold NPs with the Turkevich method using a fused silica capillary and a t-mixer to mix chloroauric acid to sodium citrate prior to introduction into the heated capillary (Figure 2-16).[107] In this case neither reagent was preheated before being mixed, and the residence times within the capillary were varied between 35 and 94 s. In this residence time range, they obtained NPs in the size range between 1.5 and 3 nm, with larger NPs being obtained at longer residence times. They further investigated the effect of sodium citrate to gold precursor molar ratio, and found a minimum at around 3.15. The explanation given is that at lower citrate ratios, there is an excess of gold precursor which is suggested to lead to an increased growth of NPs whereas at higher citrate ratios the size is suggested to increase because of an increased ionic strength in solution. No discussion on the balance between nucleation, growth and stabilization in terms of pH and reactivity of the respective reagents is made,

although this is likely to play a significant role in the final size of the NPs. Temperature effect was also investigated, and the size of the NPs decreased with increasing temperature in the range between 60 and 100°C.

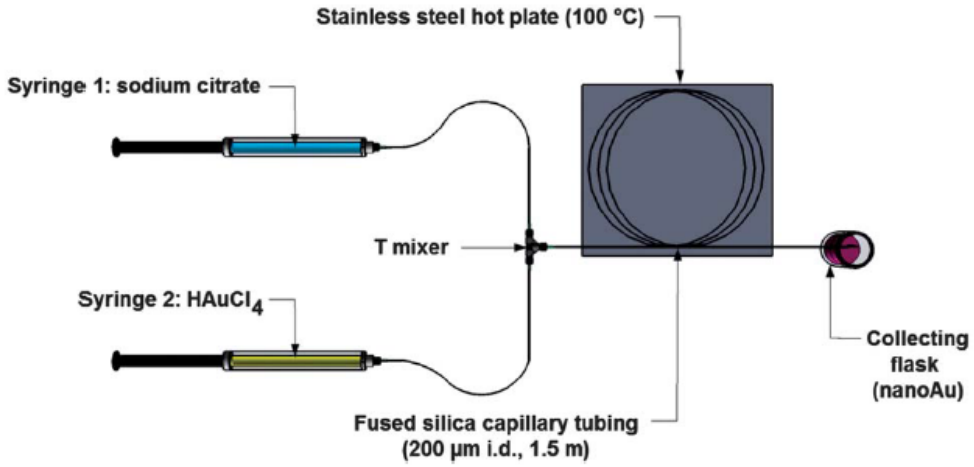

Figure 2-16: Synthesis of gold NPs using syringe pumps, t-mixer and fused silica capillary tubing set in a hot plate. Reproduced (Adapted) from Ref. 107 with permission of The Royal Society of Chemistry.

Sugano *et al*. synthesized gold NPs between 10-45 nm using a y-type micromixer with a pulsed flow of chloroauric acid and sodium citrate to mix the reagents within a small channel at room temperature.[108] They investigated how mixing affected the synthesis by altering the pulsing rate between 50,100 and 200 Hz. Analysis of the mixing showed that increasing the pulsing rate improved the mixing efficiency. They used two collection methods, in the first method the fluid was allowed to collect at the outlet of the micromixer for 5 min before collection and in the second method the fluid was collected for a total of 5 min through a 0.5 mm tube which was connected to the outlet of the micromixer. The polydispersity of the resultant NPs showed the following behavior, collection method 2 produced relatively lower polydispersity than collection method 1 for all pulsing frequencies. This is attributed to the reasoning that collection method 1 allows fluid that has travelled through the mixer initially to mix and react with fluid that is travelling and exiting the mixer after the initial period, resulting in interaction of the fluid with different concentrations over a 5 min period. Collection method 2 saw a reduction in polydispersity from 50 Hz to 100 Hz, but further increase in frequency showed no improvements suggesting that faster mixing reduces polydispersity only up until 100 Hz and further reduction in mixing time has no effect. The size of the NPs was found to increase with a higher pulsing frequency, suggesting faster mixing resulted in larger NPs. This is most likely due to the reaction rate of precursor decreasing with mixing as the $AuCl_4^-$ species becomes more hydroxylated on contact with citrate.

Köhler *et al*. used a split and recombine type reactor (Figure 2-17) to mix tetrachloroauric acid, ascorbic acid, PVA, sodium metasilicate and Fe(II) sulfate to synthesise gold NPs.[109] Because they used 4 pumps which were individually controlled to feed reactants to the reactor which had 4 inlets, they were able to precisely control the concentrations simply by altering the flow rates. They obtained a wide array of gold NPs using this method including small 5 nm gold NPs, NPs arranged in a circle like structure, aggregates and larger hexagonal aggregates.

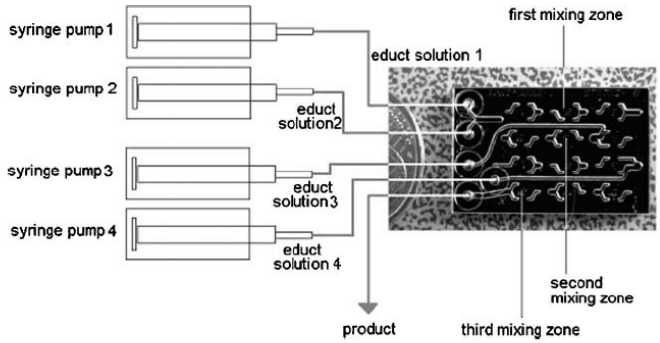

Figure 2-17: Split and recombine mixer employed for the synthesis of gold NPs. Reproduced from Ref. 109 with permission of The Royal Society of Chemistry.

Wagner and Köhler synthesized gold NPs in a split and recombine reactor (similar to that shown in Figure 2-17, but with 2 inlets instead of 4 using tetrachlorauric acid, ascorbic acid and polyvinylpyrrolidone. With increasing flow rate in the reactor, a decrease in NP size was observed from 35 nm at a flow rate of 1 ml/min to 24 nm at a flow rate of 8 ml/min. A larger size at lower flow rates was attributed to a preferential nucleation at the walls of the reactor, where a dark violet film which gradually deepened and became opaque was observed. Supposedly this effect is lessened with increasing flow rate because of an increased sheer at the walls of the reactor, though if an equal sample volume was taken for each experiment, this may have been because the reactor was operated over a shorter period of time at the higher flow rate and hence there was less time for the dark violet film to build up. Another reason for the smaller NP size at higher flow rates was suggested to be an increased nucleation rate because of more efficient mixing, which would lead to a quicker contact of excess reducing agent with the precursor ions. Mean diameter and dispersity also decreased with increasing ascorbic acid concentrations, due to the increased nucleation rate obtained at a higher reducing agent concentration. Smaller and less disperse NPs were obtained at higher pH (21 nm at pH 2.8, 8 nm at pH 9.5), attributed to the increasing redox potential of ascorbic acid at higher pH resulting in increased nucleation rate. Increasing PVP concentration also resulted in smaller NPs, attributed to the suppression of growth around newly formed nuclei which occurs because of the large PVP molecule slowing the approach of gold precursor to the surface of a nuclei stabilized by PVP. Reduction of fouling was also attained using two different approaches, elevated pH and silanization of the reactor walls to produce a hydrophobic surface. Both approaches achieved similar results in obtaining much higher peak absorbance than the standard approach at lower pH. Köhler *et al*. and Wagner *et al*. also used the split and recombine reactors to synthesize gold NPs using borohydride.[71, 72]

Shalom *et al*. synthesized small gold NPs using the Brust-Schiffrin method within a micromixer which splits two streams into 16 sub streams and subsequently interdigitates the streams for improved mixing (Figure 2-18).[110] Tetrachloroauric acid was reduced via sodium borohydride with 1-dodecanethiol being used as a stabilizing agent. NPs between 3-4 nm were synthesized within the reactor and a significant reduction in size and dispersity was achieved as compared to similar conditions using a batch reactor. This was proposed to be because of more efficient mixing, and supposedly the rate of sodium

borohydride addition affects the NP size. NPs will be more polydisperse when addition is slow because nuclei generated early in the reaction are exposed to an increased thiol concentration and those nuclei generated later as more sodium borohydride is added grow to a larger concentration because of decreased thiol concentration. However, it is not mentioned that borohydride has an abundance of electrons available to reduce the gold precursor, and hence if mixing is slow this may lead to a reduction of many gold ions to metal via a single borohydride molecule, which subsequently doesn't provide enough surface charge to stabilize the formed nuclei leading to aggregation because of poorly distributed sodium borohydride. Therefore one could argue that the polydispersity observed in the batch is due to poorly dispersed borohydride, leading to larger NPs produced initially rather than smaller NPs because of an increased thiol concentration. However, this would still explain why dispersity is reduced in the microfluidic system, since there is a better dispersion of sodium borohydride earlier in the mixing process.

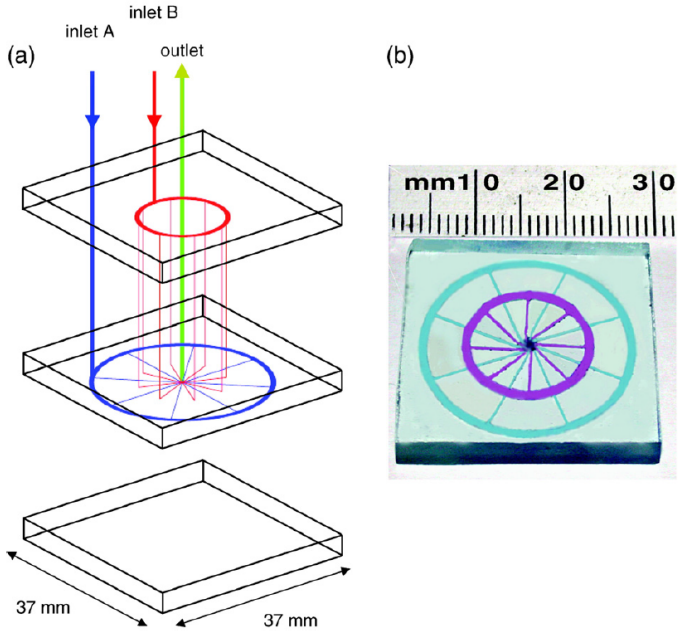

Figure 2-18: Interdigitating micromixer used by Shalom *et al*. for the synthesis of gold NPs via the Brust-Schiffrin method.[110] Reprinted from Ref. 110, Copyright (2007), with permission from Elsevier.

Cabeza *et al*. synthesized gold NPs within a microchannel in which segmented flow was generated with an aqueous phase that was segmented with either air, toluene or silicone oil (Figure 2-19).[111] Sodium borohydride was mixed with tetrachloroauric acid and tetradecyltrimethylammonium bromide in the aqueous phase and then segmented by the inert fluid at room temperature before being introduced into a heated channel with a temperature of 100°C. They found increasing residence time resulted in larger and more polydisperse NPs, with size increasing from 3.8 ± 0.3 to 4.9 ± 3.0 nm at a residence time from 10 to 40 s, for a water-toluene system where toluene was the dispersed phase and water the continuous phase. Smaller slugs of fluid were obtained at a lower residence time, indicating that these types are more beneficial for controlling the size and polydispersity of the resultant NPs in the continuous phase. This is probably because of the decreased size of the continuous phase slugs which would result in faster mixing and therefore decreased polydispersity. Considering this, they further

investigated the effect of changing the dispersed phase fluid on NPs synthesized in the continuous aqueous phase and found that air as the dispersed phase produced the smallest and most monodisperse NPs (2.8 ± 0.2 nm) followed by toluene (3.8 ± 0.3 nm) and silicone oil produced a bimodal distribution (7.8 ± 6.5 nm and 15.5 ± 3.1 nm). This was determined to be because of how well the continuous aqueous slug phase recirculated material, with air producing the highest circulation rate followed by toluene and silicone oil. This was down the hydrodynamics within the microchannel and the difference in material properties of the inert dispersed phase.

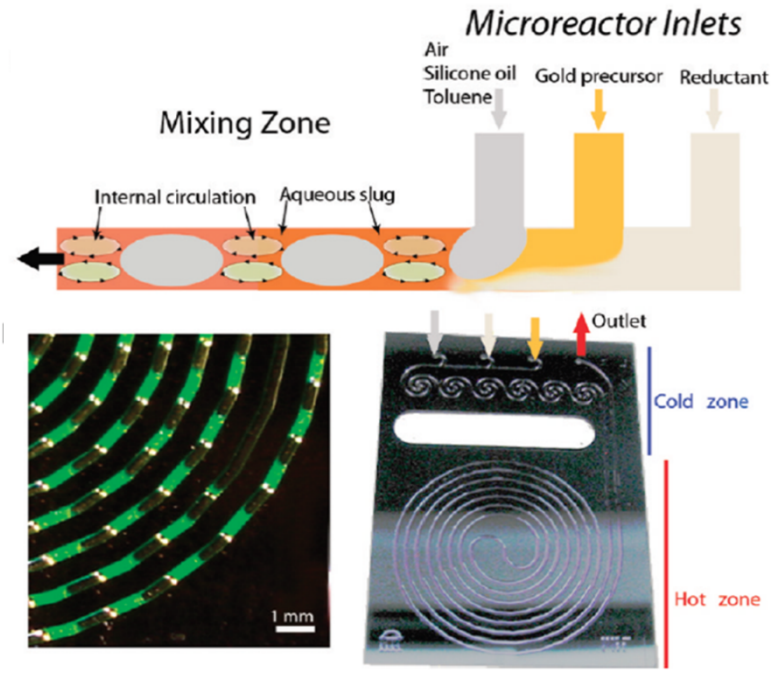

Figure 2-19: Segmented flow in microchannel employed for synthesis of gold NPs by Cabeza *et al*. Reprinted with permission from Ref. 111. Copyright (2012) American Chemical Society.

Tsunoyama *et al*. synthesized small gold NPs of around 1 nm by reducing tetrachlorauric acid with sodium borohydride in the presence of polyvinylpyrrolidone in an interdigitating micromixer (Figure 2-20).[112] Smaller clusters were obtained when the flow rate was increased and when the concentration of the precursor and reducing agent was increased.

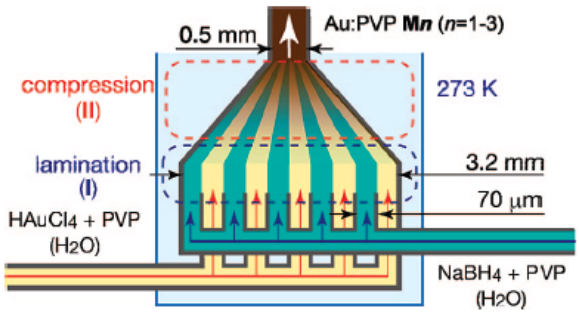

Figure 2-20: Interdigitating mixer used by Tsunoyama *et al*. for the synthesis of gold NPs. Reprinted (adapted) with permission from Ref. 112. Copyright (2008) American Chemical Society.

The gold NP synthesis in microfluidic devices studies presented show the wide range of possibilities and potential benefits that microfluidic devices offer for the synthesis of NPs, and also highlight the importance of mass transfer in controlling size and dispersity of the NPs.

2.3.3 Mechanistic studies of gold nanoparticle synthesis

One of the more commonly held views of the mechanism for gold NP formation is a burst nucleation process, as described by LaMer and Dinegar,[113] in which the nuclei are formed in a short period of high nucleation rate, causing the supersaturation to drop below the required level for nucleation and into a growth phase which results in monodispersed particles. Turkevich *et al*. conducted a study to investigate the mechanisms involved in the nucleation and growth of gold NPs in the chloroauric acid and citrate system.[114] The nucleation mechanism was suspected to have four distinct regions: induction period, an auto-accelerating period, a linear period and a decay period. Briefly, the induction period was believed to be caused by the oxidation of citrate ions into acetonedicarboxylate ions which when reaching a sufficient level, induces nucleation through the reduction of precursor. The auto-accelerating portion is suspected to be caused by the increase in production of acetonedicarboxylate ions past the speed at which they can be utilised for reduction. The linear proportion is when nucleation achieves a constant rate and the limiting factor is the speed at which the precursor is reduced to form nuclei. The decay period occurs when nucleation gives way to the growth of the NPs, i.e. the precursor begins to be utilised at the surface of existing nuclei surfaces rather than nucleating new particles. It is important to note that at the decay stage, it was observed that less than 5% of the gold precursor and citrate had been consumed, so the decay period doesn't seem to be due to the exhaustion of reagents.

Biggs *et al*. investigated the colloidal stability of the gold NPs and the role of the $AuCl_4^-$ ion and the citrate ion.[115] Using AFM measurements, it was shown that the citrate ion binds onto the surface of gold causing a repulsive force, but when the $AuCl_4^-$ ion was introduced; the repulsive force is greatly reduced suggesting that the citrate is displaced by $AuCl_4^-$. The preferential attachment of $AuCl_4^-$ onto the surfaces of the gold NPs causes a reduction in the repulsive force of the NPs leading to flocculation. This flocculation is the cause of the purplish-blue color usually observed in the Turkevich synthesis, and as the $AuCl_4^-$ is consumed through surface reduction, there is a subsequent increase in repulsion forces at the surface as more citrate attaches leading to the formation of a well-dispersed gold sol. Injection of a mixture of gold precursor and citrate onto a gold plate surface that had been previously equilibrated with citrate showed that the surface potential went from repulsive to attractive and remained attractive because of the slow reduction of the Au(III) onto the surface of the gold plate.[116] Further work was done on this by Wall *et al*. using the same techniques but with a thiol coated cantilevers to prevent NP formation, and the results revealed that the behavior was consistent with a multilayer adsorption of citrate onto the surface of the gold and because of the low charge density, there was most likely some counter-ion pairing with the citrate.[117] The possibility of the $AuCl_4^-$ ion adsorbing with a counter-ion or with a Cl^- displacement was likely according to the results of the study.

Chow and Zukoski suggest a growth mechanism were large fluffy NPs are formed in the initial stages of the reaction and then subsequently these larger agglomerated NPs break down to form smaller and more monodispersed NPs.[91] They suggest that the concentration of small NPs increases and larger NPs decreases through the course of the reaction. The proposed mechanism can be briefly described as follows. Aurate ions are reduced by citrate to form gold atoms which form clusters consisting of gold metal, with adsorbed citrate and aurate ions. Since aurate ions are preferentially binded over citrate to the surface of the gold, there is a lower surface potential which results in a loose aggregation. Over time the aurate ions are reduced onto the surface to grow the NP, resulting in an increase in surface potential eventually leading to an electrostatic repulsion which causes the loosely aggregated NPs to break off into smaller NPs. This describes how the large fluffy NPs eventually break down to form a monodispersed and stable sol.

Pei *et al*. monitored the evolution of gold at various reaction times by monitoring the concentration of the precursor species ($AuCl_4^-$) and the total gold concentration, which allowed the concentration of metallic gold to be inferred.[93] It was found that the reduction in $AuCl_4^-$ ion was faster with a higher citrate to precursor ratio which is natural since the citrate behaves as a reducing agent. Nanowires remained in solution if there was $AuCl_4^-$ ions still in solution and in the case of ratios 0.2 and 0.3, nanowires persisted until at least 180 min, supporting the idea that the $AuCl_4^-$ does lead to an aggregation of NPs as suggested by the studies above. As soon as $AuCl_4^-$ was consumed, the blue color of the nanowires disappeared and the red color of spherical NPs was obtained. Hence excessive $AuCl_4^-$ ion was important in nanowire formation, and it was observed that exposure to hydrogen gas caused the breakdown of nanowires into NPs presumably because of a reduction of excess $AuCl_4^-$. It is suggested that the mechanism is as follows: nucleation of small gold particles, subsequent attachment of further $AuCl_4^-$ onto the particle surface, this $AuCl_4^-$ ion results in an attractive force between NPs which causes them to stick together, followed by growth of nanowires and large 2-D structures of nanowires.

Kimling *et al*. found that the crystal sizes within citrate prepared gold NP were usually smaller than the particle diameter indicating a polycrystalline nature.[94] This supports the idea of nucleation followed by growth through coalescence. They propose a four step process described here briefly as: cluster formation, agglomeration of clusters into NPs with a defined surface plasmon resonance (SPR), fusion of these NPs into larger entities and finally there is a significant amount of atoms in solution which continue to aggregate leading to their incorporation into the larger entities resulting in a homogenous density and improved symmetry of NPs resulting in a blue shift of the SPR. This growth mechanism applied for UV-assisted NP formation and using ascorbic acid as a reducing agent, and was based on the movement of the SPR which starts from an initial phase which blue shifts, followed by a red shift and then finally a blue shift. This behavior could also be explained by a loose aggregation of NPs due to unreduced $AuCl_4^-$ on the surface , explaining the red shift, and eventual surface reduction leading to uniform stable NPs, explaining the subsequent blue shift.

Kumar *et al*. proposed a model for the formation of gold NPs based on reactions they deduced from evidence in the literature pertaining to stoichiometry of reactions and suggestions for the oxidation of citrate into the DCA molecule.[118] Briefly, the mechanism is described by a reduction of the Au_3^+ ion to Au^+ via the oxidation of the citrate molecule to DCA, which subsequently forms a complex with the Au^+. The DCA organizes the Au^+ and disproportionation of the gold ions into gold atoms occurs. These atoms pick up further Au^+ ions to form larger aggregates and further disproportionation occurs leading to larger gold clusters and subsequent formation of gold nuclei. Based on this, a model is presented with mass balances for the species involved, which accounts for the mass of auric chloride, aurous chloride, citrate, DCA and acetone (acetone is also proposed as a reagent which can reduce auric chloride to aurous chloride). A population balance model is also included so that the number concentration of particles, which plays a role in the consumption of precursor through surface growth, can be deduced. Kinetic rate constants for each step of the proposed mechanism are then obtained through fitting to the experimental data presented by Frens.[89] A reasonable fit to the experimental data in the literature is obtained, suggesting that the proposed mechanism is able to account for at least some of the physical mechanisms occurring in the synthesis of gold NPs in the Turkevich synthesis. Interestingly there is no suggestion of particle aggregation to form wire like structures and subsequent reduction into monodisperse NPs which is observed experimentally by many studies discussed in this section.

Ji *et al*. propose a mechanism for two different sets of ratios of citrate to gold precursor, one for low citrate to gold ratios (< 3.5) and the other for high citrate ratios (> 3.5), shown in Figure 2-21.[95] At high citrate ratios, where the pH is closer to neutral there is nucleation followed by a slow diffusion controlled growth, evidenced by small spherical NPs at the initial stage followed by growth into larger spherical NPs. At the lower citrate ratios, dense nanowires with fatter heads and thinner tails were observed which eventually lead to spherical NPs. It is suggested this is far more likely because of intra-particle ripening rather than through the cleaving of material from the nanowires which then grow to larger spherical NPs which is suggested by Pong *et al*.[119] This is because the evolution from nanowires to spherical NPs takes much longer than the reduction of gold precursor into gold metal, hence there would be a lack of monomers available for growth of any cleaved NPs and most of the precursor has already been utilized to form the nanowire structures. There is also an observed fattening of the head and thinning of the tail over time which supports the idea of intra-particle ripening. The mechanism was found to be controlled by the reactivity of the precursor which was determined by its speciation. By tuning the pH, it was found that the reactivity of precursor corresponded with the switching points of the gold ion complexes i.e. reactivity fell as the pH increased as a result of increasing the hydroxylation of the gold ion from $AuCl_4^-$ to $AuCl_3OH^-$ to $AuCl_2OH_2^-$. This reactivity is suggested to be the reason for nanowire like structures at lower pH and spherical NPs at higher pH. Sivaraman *et al*. also found the rate of reduction of gold species was highest when the tetrachloroauric acid was present in its most reactive form (i.e. $AuCl_4^-$).[102] The extent of protonation/deprotonation of citrate may be important also, since the point at which a minimum in size occurred was at pH around 6.5, corresponding to the third pK_a value of 6.4 for citric acid where it is completely deprotonated (Ct^{3-}).

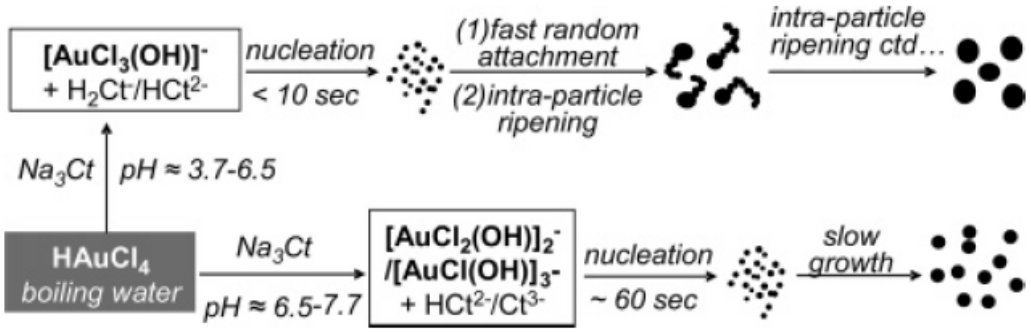

Figure 2-21: Mechanism suggested by Ji et al. for gold NP synthesis. Two pathways exist dependent on pH.[95] Reprinted with permission from Ref. 84. Copyright (2007) American Chemical Society.

Polte *et al*. observed the nucleation and growth of the gold NPs using the Turkevich synthesis at 75 and 85°C through the use of UV-Vis, SAXS and XANES analysis.[120] In contrast to mechanisms which suggest the formation of larger NPs which eventually form smaller and more spherical and monodisperse NPs, there were no larger NPs observed in this study. Instead the mechanism is proposed to be consisting of four main steps: the reduction followed by nucleation of gold, the coalescence of gold nuclei to form larger gold NPs, slow growth of the larger gold NPs through reduction of precursor onto existing NPs, and finally a more rapid growth onto existing NPs possibly because of an autocatalytic effect (Figure 2-22). Polte *et al*. also observed a coalescence of smaller NPs to form larger NPs when using sodium borohydride as a reducing agent.[121] Goia and Matijevic used iso-ascorbic acid to reduce tetrachloroauric acid and found a coalescence of gold NPs of a crystal size of 30 nm which formed much larger micrometer sized particles.[122] Park *et al*. modelled the process of burst nucleation followed by aggregation of primary particles to form larger secondary particles and the model was found to sensitive to the surface tension of the particles and singlet-singlet aggregation rate.[123]

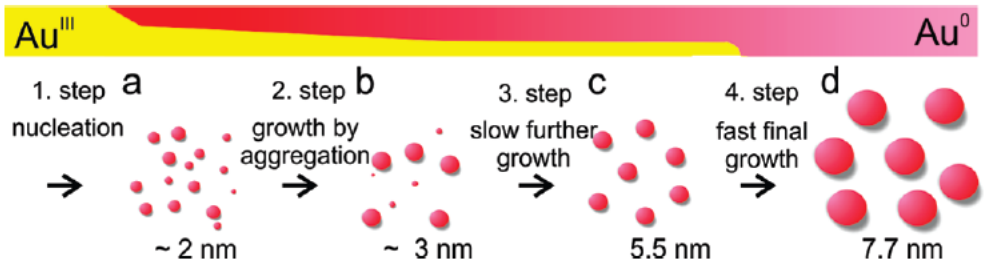

Figure 2-22: Mechanism of gold NP formation suggested by Polte *et al*. Reprinted (adapted) with permission from Ref. 120. Copyright (2010) American Chemical Society.

Wuithschick *et al*. investigated the mechanism from the speciation of reagents aspect and answered some questions pertaining to the control of the size of the NPs.[104] They present a suggested mechanism for gold NP formation for the Turkevich synthesis, based on that proposed by Polte (Figure 2-23).[124] The main suggestion is that the speciation of the $AuCl_4^-$ controls the nucleation of the gold NPs which

ultimately determines their final size. The degree of hydroxylation of the $AuCl_4^-$ affects the reactivity as highlighted by Ji *et al.*,[95] and that the Turkevich method produces monodisperse NPs because of the change in speciation of the precursor which creates a separation of nucleation and growth as $AuCl_4^-$ is both consumed and transitions into more hydroxylated forms as pH goes from acidic to neutral. They note that once the nucleation is over, the kinetics of growth has little effect on the final size which is determined in the nucleation phase, suggested to be of the order of 30 s long for the conditions tested. They emphasize that, contrary to the majority of studies elucidating the mechanism of gold NP synthesis using the Turkevich method, there is no aggregate or agglomerate formation leading to the formation of wire like structures according to the SAXS analysis by Polte *et al.*[120] The bluish-gray color which is observed in the Turkevich synthesis is suggested to be due to an optical alteration of gold NPs with precursor ions adsorbed onto the surface rather than because of an aggregation or agglomeration of NPs. Plech *et al*. synthesised NPs using a modified Turkevich method in which X-rays were used to induce nucleation.[125] They introduced a mixture of chloroauric acid and trisodium citrate into an X-ray capillary, where it was exposed to X-rays and formed NPs. In the early stages of the process, they suggest a bimodal distribution centred around 7.8 and 3.9 nm at 38s, and 9 and 4.6 nm at 83s. Following this period, the data suggests that the particles are close in distance and that there is clustering of particles to bigger aggregates (20-40 particles). Finally after 2h, the data can be fitted by isolated particles with a few clusters still present. The final size of the NPs was not different to the aggregates detected in the earlier stages, supporting the idea of coalescence of smaller NPs to form larger ones.

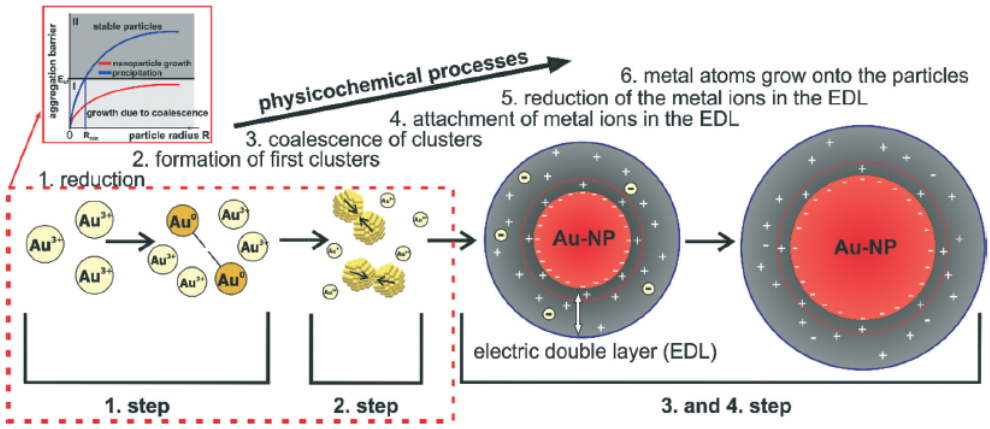

Figure 2-23: Mechanism of gold NP formation in the Turkevich synthesis suggested by Polte. Ref.124 – Published by The Royal Society of Chemistry.

Kettemann *et al*. investigated the importance of the speciation of the citrate species in the Turkevich synthesis.[106] Depending on the pH, the protonation/deprotonation of the citrate species changes, increasing pH from acidic to basic deprotonates the species. They deduced that the $HCit_2^-$ was the likely species which reduced the $AuCl_4^-$ and if the synthesis is manipulated to ensure a reproducible concentration of $HCit_2^-$, the synthesis becomes highly reproducible. $HAuCl_4^-$ was also prone to differences

from batch to batch, it was found that boiling and refluxing the precursor for 1 h enabled reproducibility.

Much work has been carried out to understand the mechanisms involved in gold NP formation, with particular focus on the reduction of gold precursor using citrate at elevated temperatures. The color changes observed in the synthesis can best summarize the mechanisms. Initially there is a color change from the yellow of $AuCl_4^-$ to clear, which is most likely the transition of the Au^{3+} ion to some intermediate such as Au^+ as suggested by Kumar *et al*.[118] Following this, a purple-blue color is usually observed. The consensus is that this color arises from flocculation or loose aggregation of newly formed gold nuclei, observed to be large fluffy NPs,[91] or wire like structures.[93, 95] The explanation of this seems to arise from the preferential binding of gold precursor to the surface of gold nuclei over the citrate molecule, as highlighted by the work of Biggs *et al*. and Wall *et al*.[115-117] This then leads to the color of the solution deepening and eventually turning ruby red, indicating the formation of monodispersed gold NPs of 10-20 nm. This is suggested to be caused by the slow surface reduction of the gold precursor, which eventually leads to increasing stability of NPs as citrate begins to attach onto the surface. This increased stability causes a repulsion, which enables the flocculated NPs to break apart. There seems to be an agreement that a coalescence of nuclei in the initial phase to form small gold NPs, indicated by their polycrystalline nature and the SAXS studies by Polte *et al*. and Plech *et al*.[120, 125] There is a suggestion that the formation of wire like structures or larger NPs doesn't exist in solution and that the purple blue color is caused by an optical effect of gold precursor binding onto the surface of gold NPs.[104] However, it is still seems like flocculation is a strong possibility because of the preferential binding of gold precursor on the surface of gold NPs, which would create attractive rather than repulsive forces. The speciation of the components in the Turkevich synthesis have also been identified to be important in determining the mechanisms, reactions rates and resultant NP size.

The disadvantage of using reactors with a high surface area to volume ratio is that there is a higher chance of fouling and accumulation of material on the walls of the channel. Hence, microreactors which are not easily susceptible to accumulation of material on their walls are desirable. There are various studies which implemented different strategies to avoid fouling, such as the segmented-flow approach and the reduction of wall interactions through pH alteration and surface silanization of the channel walls.[76, 126, 127] One type of design that alleviates the occurrence of fouling is the coaxial flow reactor (CFR) which allows an inner stream of reagent to be surrounded by an outer stream, creating a reaction interface between the streams.[35, 36, 128-130] The CFR is less susceptible to fouling because the reduction of precursor ions and nucleation of metal NPs occur at the interface between the inner and outer streams, rather than near the channel walls. This reduction in fouling relies on the flow profile of the channel remaining in a stable laminar regime. This has adverse effects with regards to mixing efficiency, unless a reduction of diffusion distances or sufficient contact time is applied.

Examples of CFRs are found in the studies by Takagi *et al*. who produced titania NPs using an axial dual-pipe microdevice.[128] Using various flow conditions and tuning of solvent properties such as viscosity and surface tension, the flow characteristics in their device were tuned and led to increased control over mass transfer. The mass transfer of the reagents in the microdevice determined the size and monodispersity of the NPs which was demonstrated by using different solvent types, tube diameters and precursor concentrations. Maki *et al*. employed a concentric-axle dual-pipe microreactor to synthesize zirconia NPs,[128, 129] and showed that increasing residence time resulted in larger NPs. Abou-Hassan *et al*. used a coaxial flow device operated under laminar flow conditions to synthesize iron oxide, goethite and Fe_2O_3@SiO_2 core/shell NPs.[35, 36, 130] 7 nm iron oxide NPs were synthesized in the coaxial flow device and polydispersity decreased from 35% in a typical batch synthesis to ca. 20% in the coaxial flow device.[130] Goethite NPs were synthesized using the coaxial flow device as a nucleation section before a long residence loop in a temperature controlled bath. The goethite NPs were produced with a residence time of around 15 min as opposed to several hours using traditional batch methods, and were also smaller than those made in batch vessels.[35] Similarly, a multistep approach using the coaxial flow devices was used to synthesize Fe_2O_3@SiO_2 core/shell NPs within a much shorter timescale as compared to batch.[36] Lim *et al*. operated a CFR in the turbulent regime to produce various NPs such as iron oxide with an ability to tune the size through changing the flow conditions.[131] Schülein *et al*. used a micro coaxial-injection flow mixer for the synthesis of nickel NPs. The process for synthesizing nickel NPs quickly blocked commercially available microstructured mixers and the coaxial-injection mixer was used in a pilot plant scale process mainly because it could avoid fouling and blockage issues.[132]

Synthesis of silver NPs using silver nitrate, sodium borohydride (with sodium hydroxide) and trisodium citrate in a coaxial flow reactor in this study has not been reported in the literature. Shirtcliffe *et al*. reported the synthesis of silver NPs using sodium borohydride and sodium hydroxide as a reducing agent for silver nitrate using a PTFE flow chamber and also using Eppendorf pipettes to mix reagents directly into plastic cuvettes.[65] Wagner *et al*. synthesized silver NPs in a split and recombine mixer using

borohydride as a reducing agent for silver nitrate and despite fouling were able to control the size of the NPs by tuning the borohydride ratio, obtaining NPs in the range of 10-20 nm for borohydride to silver nitrate ratios ranging from 3 to 40.[71] Further studies using borohydride as a reducing agent for the reduction of a silver precursor to form silver NPs in the aqueous phase were mainly in batch reactors with NP sizes ranging between 1-100 nm.[5, 64, 67, 69]

The main objective of this work is to study how the size and monodispersity of silver NPs can be controlled by changing the operating parameters of flow rate and concentration of ligand (trisodium citrate) and precursor (silver nitrate). The motivation for using a CFR was to avoid fouling issues and blockages, an issue which was encountered when synthesising NPs using the same chemical system in a split and recombine type micromixer (see Appendix B, Figure B1 for images of fouling in such a micromixer).

3.1 Experimental

3.1.1 Chemicals

Silver nitrate ($AgNO_3$, 0.01 M stock solution), trisodium citrate ($HOC(COONa)(CH_2COONa)_2 \cdot 2H_2O$, powder form) and sodium borohydride solution ($NaBH_4$, ~12 wt% in 14 M NaOH stock solution), were obtained from Sigma Aldrich Company Ltd., UK. All chemicals were used without further purification and solutions were prepared with ultrapure water (resistivity 15.0 MΩ·cm) and diluted to the desired concentrations before being introduced into the CFR.

3.1.2 Experimental Setup

Syringe pumps (Pump 11 Elite OEM Module, Harvard Apparatus) were used in the experiments to deliver the two streams of silver nitrate/trisodium citrate solution and sodium borohydride solution to the CFR. The CFR used in this study consisted of a small inner tube which was inserted into the center of a larger outer tube (Figure 3-1). Both the inner and outer tubes were made of glass and inner tubes of two different internal channel diameters of 0.556 mm (0.8 mm external diameter) and 0.798 mm (1.09 mm external diameter) were used in separate experiments. The outer tube had an internal channel diameter of 2 mm. The distance from the inner tube outlet to the outlet of the CFR was 130 mm. A 1.59 mm PTFE tube sleeve with a suitable inner diameter is placed around the inner tube to keep the tube stable within the larger outer tube. The capillaries were connected together using a T-piece connector (0.508 mm thru-hole, Upchurch Scientific) which was drilled to a size of 2 mm internal diameter (I.D.) to allow the inner tube to be inserted into the outer tube. The flow ratio between the inner and outer stream, Q_{out}:Q_{in}, was fixed at 1:1 and the CFR operated in the laminar flow regime for all experiments.

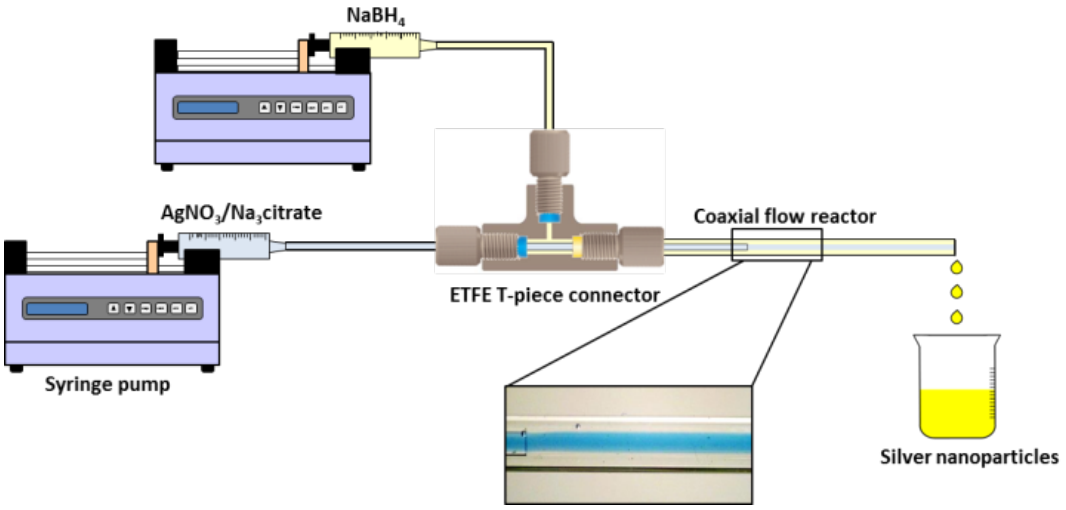

Figure 3-1: Schematic of the coaxial flow reactor setup. Insert shows flow visualization of laminar flow inside the coaxial flow reactor with blue dye flowing through the inner tube and water flowing through the outer tube.

3.1.3 Synthesis of silver nanoparticles

A typical synthesis was as follows: silver nitrate and trisodium citrate were mixed together in solution and introduced via the inner tube of the CFR, while the sodium borohydride solution was introduced via the outer tube of the reactor. Fresh trisodium citrate solution was made by dissolving the powder in ultrapure water before each synthesis. All reactions were carried out at room temperature (typically between 22-24 °C). All concentrations, unless otherwise stated, are concentrations of the individual streams being introduced into the CFR. Since the sodium borohydride was stored in 14 M sodium hydroxide, the concentration of sodium hydroxide was 3.21 times higher than the stated sodium borohydride concentration in all cases.

The literature shows that borohydride can supply up to eight molar equivalents of electrons to reduce the silver ions to silver metal.[133-135] The amount of electrons released from the borohydride molecule depends on whether the formed H^+ ions react with H^- ions from the molecule to form hydrogen gas, which would limit the electrons available for reducing metal ions. Highly basic conditions reduce the formation of hydrogen gas hence freeing up more electrons for reduction of the metal ion. In this study sodium borohydride was stored and used under basic conditions which should produce a higher amount of electrons for reducing the metal ions. Samples were stored for months without noticeable formation of hydrogen bubbles whereas when sodium hydroxide was not used to arrest the hydrolysis reaction, hydrogen bubbles formed within the samples after a short time. The actual amount of electrons utilized to reduce silver is unknown, though it is suggested by Shirtcliffe *et al*. that six of the available eight electrons are utilized to reduce silver ions under basic conditions.[65]

The primary purpose of sodium borohydride is to reduce the silver ions to silver metal; however, it also affects the growth of the NPs. The surface charge of the particles is affected by borohydride and hydroxide ion adsorption and it is well established that the conversion of borohydride to borate in aqueous solution results in changes in the particle charge.[68, 136] Under basic conditions the conversion of borohydride slows down.[137, 138] However, trisodium citrate is used as the primary stabilizing agent in this study. The concentrations of the reducing agent (sodium borohydride) and ligand (trisodium citrate) in

relation to the precursor concentration (silver nitrate) determine the nucleation, growth and stabilization of the NPs. Since the concentration is important in determining the size and dispersity of resultant NPs, the mass transfer during the reaction becomes important as this dictates the concentration at which the reaction takes place at any given time during the reaction. The reproducibility of the synthesis in the CFR over a range of flow rates was assessed by repeating the synthesis 4 times for each flow rate (Figure B2 in Appendix B shows UV-Vis analysis of the repeated syntheses).

3.1.4 Characterization of nanoparticles

The silver NPs were analyzed within an hour of the synthesis using a UV-Vis spectrometer (USB 2000+ Spectrometer and DT-Mini-2-GS light source, Ocean Optics). Transmission electron microscope (TEM) images were captured using a JEOL 1200 EX ii microscope with a 120 kV acceleration voltage. Carbon coated copper TEM grids were prepared within an hour of synthesis by pipetting approximately 15 µl sample onto the grid and allowing it to dry at room temperature. It was important to keep the droplet small enough to only partially cover the grid. This has two beneficial effects. Firstly, the drying time of grid is shorter because of a lower volume of solution. The second reason relates to the well-known 'coffee ring' effect, where particles are pushed towards the edges of a droplet that is evaporating, meaning that these areas will contain aggregated NPs which are not representative of the sample but rather an artefact of sample preparation. When the grid is prepared in such a way, the ring of aggregated NPs can be physically identified on the small copper grid and easily visible when analysing the sample using TEM. This allows the differentiation between aggregates that are in the sample and those that are artefacts of sample preparation. The TEM images have in the inset particle size distributions, average diameter, d, standard deviation, δd, indicating polydispersity and number of particles counted to obtain the particle size distribution, n. PEBBLES software was used for the counting and sizing of TEM images of the synthesised NPs.

3.2 Investigation on variance in nanoparticle morphology using parametric studies

3.2.1 Effect of total flow rate

Experiments were carried out in the CFR with an inner tube channel diameter of 0.798 mm at various flow rates. The CFR was used to synthesize silver NPs at concentrations of 0.2 mM silver nitrate, 0.2 mM trisodium citrate and 0.6 mM sodium borohydride at total flow rates ranging from 1 ml/min to 14 ml/min. The molar ratio of sodium borohydride to silver nitrate is 3:1, but the ratio of electrons to silver ions is many times greater than this. Figure 3-2 shows TEM images of silver NPs synthesized at 1 ml/min, 2.5 ml/min, 8 ml/min and 14 ml/min along with their respective particle size distributions. The particle size synthesized at the lower flow rates of 1 ml/min (3.1 ± 1.6 nm) and 2.5 ml/min (3.3 ± 2.2 nm) are statistically smaller than those at the higher flow rates of 8 ml/min (5.6 ± 2.7 nm) and 14 ml/min (5.4 ± 3.4 nm) while the polydispersity steadily increases from ± 1.6 nm to ± 3.4 nm. However, the particle sizes at 8 ml/min and 14 ml/min were not found to be statistically different using a t-test ($p = 0.209$).

According to Mie theory, for NPs in the range between 6-10 nm the peak absorbance increases with size (for a given concentration) but the peak wavelength does not shift significantly.[139] From the

UV-Vis analysis (see Appendix B, Figure B3), the peak wavelength does not change significantly (between 392-393 nm for all flow rates) in agreement with theory. However, the peak absorbance of the spectra decreases minimally from 1.35 to 1.27 (statistically different, $p < 0.01$) with increasing flowrate even though TEM shows an increasing average size of NPs from 3.1 nm to 5.4 nm. This can be explained by the increased polydispersity observed at higher flow rates where NPs larger than 10 nm are formed. This results in increased full width at half maximum of the resonance peaks at higher flow rates, and since the mass of silver used in each experiment is constant, the peak absorbance decreases.

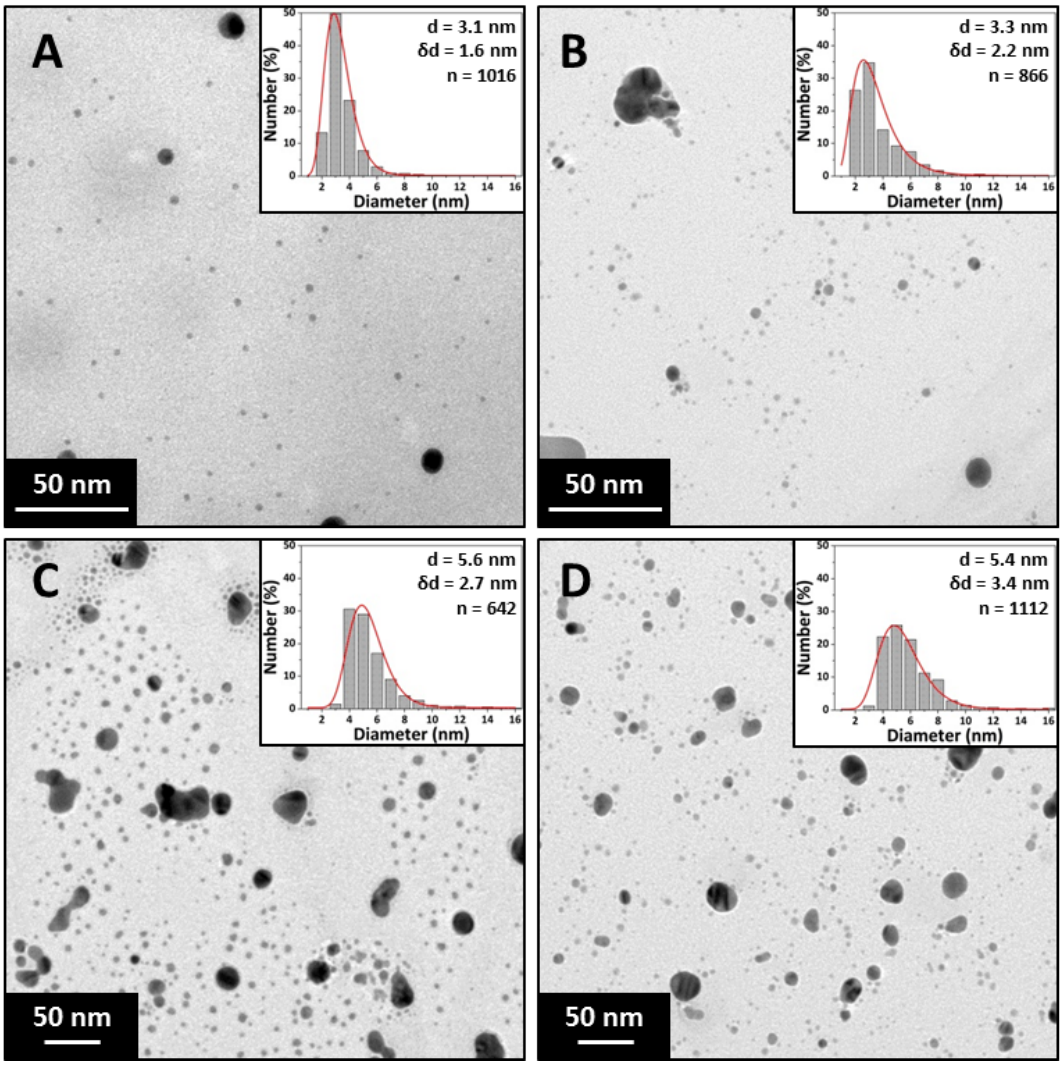

Figure 3-2: TEM images and particle size distributions of silver NPs synthesized at different total flowrates. A: 1 ml/min, B: 2.5 ml/min, C: 8 ml/min and D: 14 ml/min. Concentration of silver nitrate 0.2 mM, trisodium citrate 0.2 mM, sodium borohydride 0.6 mM. 0.798 mm inner tube I.D.

The concentrations of precursor, reducing agent and ligand are important factors in controlling nucleation and growth and hence size of the synthesized NPs. The evolution of the concentration profiles along the length of the reactor is controlled by mass transfer, i.e. the mixing characteristics. Mixing in the CFR occurs by diffusion, since it operates in the laminar flow regime for the flow rates employed. We can use a simple relationship:[140]

$$t \approx \frac{(x/2)^2}{2D}$$

where t is time, x is the thickness of the stream and D is the diffusion coefficient, to estimate the time required for the reagent to diffuse significantly along the radial direction in the CFR (i.e. the mole fraction becomes approximately uniform across the channel diameter in the absence of reaction). Using a diffusion coefficient of 1.7×10^{-9} m^2/s for $AgNO_3$,[141] and a stream thickness of 1 mm (half the diameter of the outer tube), a time of 73 s is calculated. Using a diffusion coefficient of 3.5×10^{-9} m^2/s for $NaBH_4$ in NaOH solution,[142] a time of 36 s is calculated. The volume of the reactor is 0.4 ml, yielding an average residence time of 1.75 - 24.5 s for flowrates between 1 - 14 ml/min. Hence, complete mixing does not occur because the residence times are shorter than the characteristic diffusion times. At higher flow rates, minimal mixing occurs in the channel as the molecules have very little time for diffusion. The majority of the reagent mixing in this case is at the outlet of the CFR where droplets form and are collected. A high reactant concentration in the streams is maintained in the CFR because of the slow mixing. This is confirmed when considering the Peclet number of the conditions tested. For a characteristic length of 2 mm (inner diameter of the outer tube) the Peclet number varies between *ca*. 3000-42000 for sodium borohydride and *ca*. 6000-87000 for silver nitrate. This indicates that for the flow conditions tested, the mass transport is dominated by advection. This is because the residence time within the channel is quite short compared to the time needed for diffusion along the cross-section of the channel. Even given the advection dominated mass transport (because the residence time is quicker than diffusion time), the size and dispersity of the NPs is still significantly affected with varying flow rate which highlights the speed at which the reactions take place with the limited diffusion time available.

Literature suggests that reaction and nucleation in silver NP synthesis have very fast kinetics evidenced by the timescales of NP appearance in studies by Polte *et al*. which suggests reduction occurs in less than 200 ms,[68] and Takesue *et al*. in which nucleation is observed in less than 1 ms.[82] Thus, the reaction is likely to occur at or very close to the interface between the two streams, at least in the initial part of the reactor and at high flowrates. The inner and outer streams behave as reservoirs of precursor and reducing agent respectively which supply the necessary reagents at the interface region for reduction of silver ions to silver metal and subsequent clustering and stabilization. Comparing the average residence times with characteristic times for diffusion, we can conclude that at high residence time (24.5 s) most silver nitrate in the inner stream would be consumed, because of the fast kinetics and sufficient diffusion time of the borohydride (36 s). This is likely not to be the case at low residence time (1.75 s).

Higher flow rates resulted in the appearance of larger silver NPs. This may be rationalized as follows. The reaction occurring at the interface within the CFR results in silver atoms being formed in that region. The concentration of silver atoms increases until they form clusters (synthesis mechanisms in the literature strongly suggest that the metal atoms form clusters which coalesce to form small NPs).[68, 82, 143] A smaller amount of silver precursor is consumed and smaller amounts of clusters are formed within the CFR at low residence time. A higher amount of silver nitrate is left unreacted at the outlet of the CFR, where droplets form and mixing and consumption of reagents continue within them.

Mixing there is through recirculation patterns as the droplets form. Even though these convective patterns promote faster mass transfer than diffusion, they result in non-homogenous concentration areas. Thus, the larger amount of remaining silver ions reacts and moves to areas where the concentration of silver nitrate may be high relative to borohydride. The resultant NPs would have a lower surface charge because of the low amount of borohydride ions which adsorb onto their surface. This in turn allows the NPs to aggregate and grow to a larger size, since it is established that a decrease of surface charge of the NPs (most likely because of borohydride ion depletion) causes NPs to grow to a larger size.[136] The appearance of higher amount of larger NPs, further gives rise to the increased polydispersity observed. The increasing Peclet number (with increasing flow rate) also quantifies the diminishing significance of the diffusion mechanism on the mass transport with increasing flow rate, further supporting the idea that there is less reaction occurring within the channel at higher flow rates.

An interesting observation was that a layer of silver formed on the inner wall near the outlet of the inner tube through which the silver nitrate was flowing. This fouling occurred on the outer wall of the inner tube when silver nitrate was flowing through the outer tube. Fouling only occurred on the side of the inner tube where silver nitrate was flowing i.e. a silver nitrate rich zone (see Figure B4 and Figure B5 in Appendix B for images of fouling on the channel walls). The reason fouling did not occur on the sodium borohydride side during experiments may be because silver metal atoms produced in sodium borohydride rich zones would have a high negative surface charge and hence cannot grow and deposit on the negatively charged glass channel wall in the sodium borohydride stream.[144] This is consistent with the larger NPs obtained at higher flow rates, which increases the polydispersity. Another point to note is that citrate molecules were also available in the silver nitrate stream, but they did not prevent the deposition of silver metal on the inner tube.

3.2.2 Effect of trisodium citrate concentration

The effect of surfactant concentration on the NP morphology was investigated by varying the trisodium citrate concentration. The silver nitrate and sodium borohydride concentrations were kept constant at 0.1 mM and 0.3 mM respectively. The role of sodium borohydride and why it was in such high excess was discussed previously. Trisodium citrate concentration was varied between 0.025 mM and 1.5 mM. Due to these high citrate concentrations, the silver nitrate and sodium borohydride concentration was reduced (though still using a 3 to 1 ratio of sodium borohydride to silver nitrate) to keep the ionic strength as low as possible. The flow rate of each stream was 1.25 ml/min making a total flowrate of 2.5 ml/min. Figure 3-3 shows TEM images and particle size distribution of the silver NPs synthesized at various citrate concentrations (0.025 mM to 0.75 mM) with average diameter and standard deviation for each concentration. It can be seen that the polydispersity and average size of the NPs decreases with increasing citrate concentration because of the reduction in the amount of large fused NPs present.

Figure 3-4 shows the UV-Vis spectra of the silver NP samples for each citrate concentration tested. The resonance peaks at lower citrate concentration are characterized by a lower plasmon peak absorbance and a higher absorbance at longer wavelengths; and as the citrate concentration is increased up to 0.25 mM the plasmon peak increases and the peak at higher wavelengths is reduced. The tail in the resonance peak is indicative of the presence of larger fused NPs, as confirmed by TEM

imaging at lower citrate concentrations, suggesting citrate plays a key role in reducing formation of larger fused NPs. Increasing the concentration of citrate above 0.5 mM up to 1.5 mM does not alter the synthesized silver NP characteristics. This shows that a minimum citrate concentration is needed to obtain relatively monodispersed NPs and to prevent the formation of larger fused NPs with irregular shapes. Henglein and Geirsig also showed in a study using radiolysis for the reduction of $AgClO_4$ that larger fused NPs were formed when insufficient amounts of citrate were used (they also showed large fused NPs when the citrate concentration was too high).[83] Further qualitative analysis of the TEM images shows that at lower concentration, there are smaller NPs which surround the larger NPs. Because of the high contrast of the larger fused NPs, these smaller NPS may be harder to identify since they do not yield as high of a contrast. Table 3-1 shows the full width at half maximum (FWHM) and peak wavelength of the silver NPs synthesised at the various citrate concentrations, obtained from the UV-VIS spectra. As expected the FWHM decreases with increasing concentration (lower FWHM indicates lower dispersity), in line with the TEM images showing decreased polydispersity with increasing citrate concentration. Interestingly, the peak wavelength shows increase with increasing citrate concentration (higher peak wavelengths indicate increasing NP size). This is obviously not the case according to the TEM images as well as the large shoulder peaks in the UV-Vis, but it does support the idea that at lower citrate concentrations, there is a possibility of smaller NPs existing (in particular, smaller than the smallest NPs present in the synthesis at higher citrate concentration).

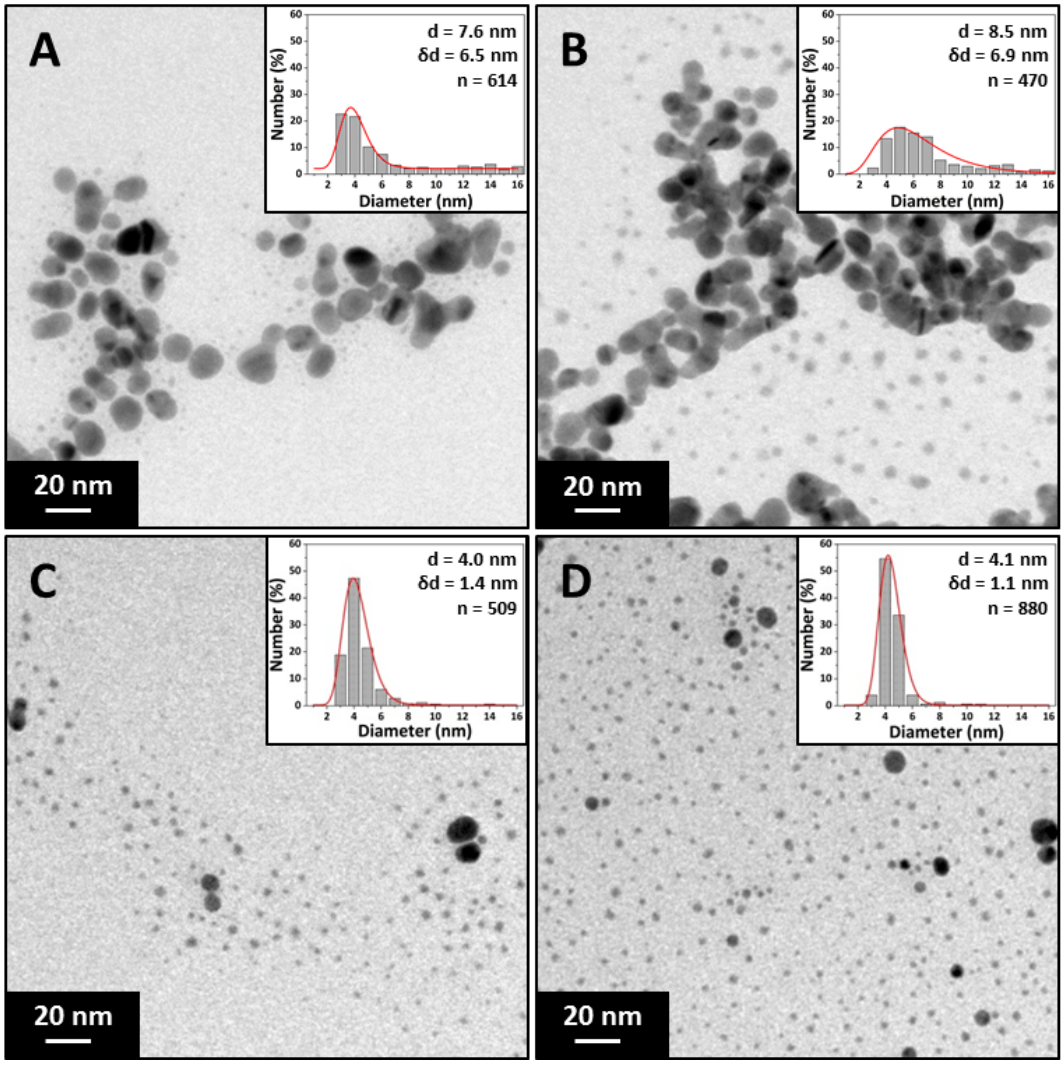

Figure 3-3: TEM images and particle size distributions of silver NPs synthesized at different trisodium citrate concentrations. A: 0.05 mM , B: 0.1 mM , C: 0.25 mM and D: 1.5 mM. Concentration of silver nitrate 0.1 mM, sodium borohydride 0.3 mM. Total flow rate 2.5 ml/min, 0.556 mm inner tube I.D.

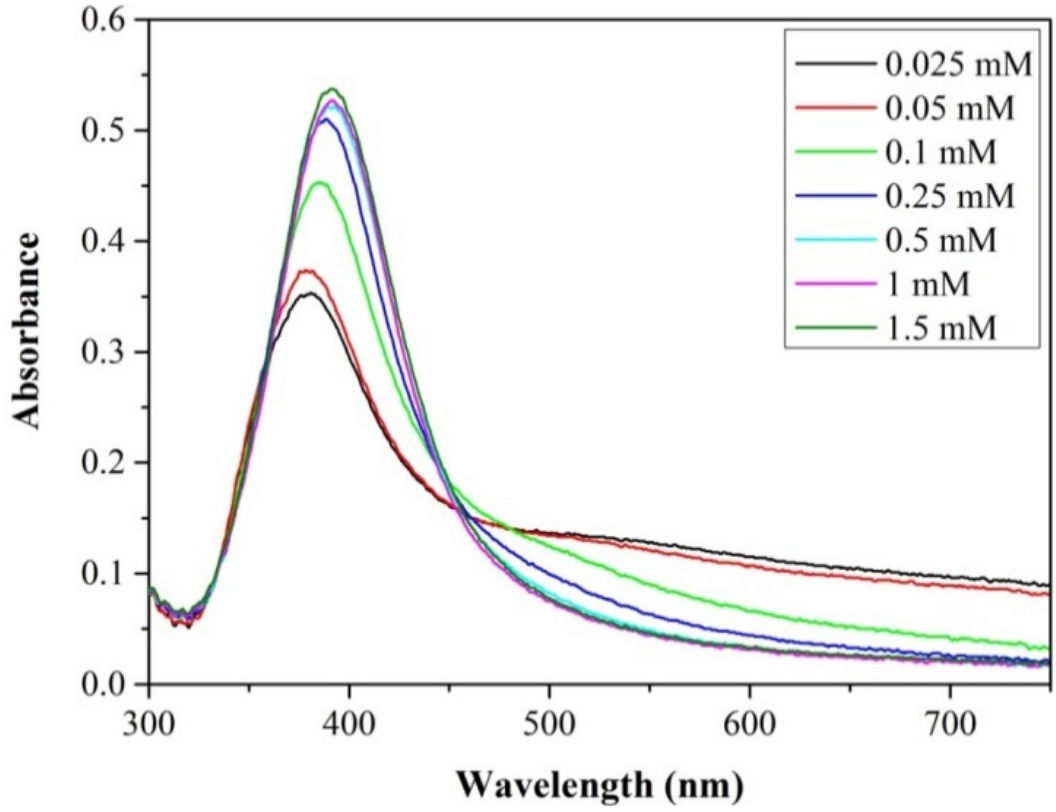

Figure 3-4: Absorbance peaks of silver NPs synthesized at various trisodium citrate concentrations in the range 0.025- 1.5 mM. Total flow rate 2.5 ml/min, concentration of silver nitrate 0.1 mM, sodium borohydride 0.3 mM. 0.556 mm inner tube I.D.

Table 3-1: FWHM and peak wavelength of silver NPs at various trisodium citrate concentrations in the range 0.025-1.5 mM. Total flow rate 2.5 ml/min, concentration of silver nitrate 0.1 mM, sodium borohydride 0.3 mM. 0.556 mm inner tube I.D.

Citrate concentration (mM)	FWHM (nm)	Peak wavelength (nm)
0.025	96	381
0.05	91	379
0.1	84	385
0.25	77	389
0.5	77	393
1	75	392
1.5	77	392

3.2.3 Effect of silver nitrate concentration

The effect of precursor concentration on the NP size and polydispersity was investigated by varying the concentration of silver nitrate. The trisodium citrate and sodium borohydride concentrations were kept constant at 0.5 mM and 0.3 mM respectively. The silver nitrate concentration was varied between 0.05 mM and 0.4 mM. Sodium borohydride is expected to reduce all silver ions even at the highest precursor concentration used since it is expected to supply an excess of electrons for reduction. The flow rate of each stream was 1.25 ml/min making a total flowrate of 2.5 ml/min. The Beer-Lambert law applied for

synthesized Ag NPs having peak absorbance values below 1.5. Therefore, samples were diluted if the absorbance was above this value for normalization.

Figure 3-5 shows TEM images of the silver NPs along with their respective particle size distributions. The size increased from 3.7 ± 0.8 nm to 9.3 ± 3 nm with increasing silver concentration. It can be seen that small and relatively monodisperse NPs form at the lowest concentration with a transition into a more polydisperse bimodal distribution occurring at 0.15 mM silver nitrate. The higher polydispersity may be related to a larger extent of reduction taking place in the droplets at the exit of the CFR, as discussed earlier. Figure 3-6 shows the UV-Vis spectra for each synthesis carried out at various silver nitrate concentrations. The peak absorbance increases with increasing concentration showing a linear dependence. The increase is most likely because of a higher concentration of NPs and increased average size of the NPs (absorbance increases with size for NPs below 10 nm).[139] Table 3-2 shows the FWHM and peak absorbance of the silver NPs synthesised at various silver nitrate concentrations, obtained from the UV-Vis spectra. At the lowest concentration the spectra is diffuse and has a larger peak wavelength (which indicates large and polydisperse NPs). However, the NPS are 3.7 nm according to TEM. At this size, the NPs would show very little absorbance, so the absorbance shown in the spectra could be from small amounts of larger NPs which would have a much higher absorbance. The large FWHM could be because the larger NPs that exist in the solution are polydisperse. This can explain to an extent the FWHM and peak wavelength at a concentration of 0.15 mM also. With increasing concentration after 0.15 mM, the FWHM and peak wavelength shows little variation indicating that there is minimal change in NP size and polydispersity.

As discussed previously, high amounts of silver nitrate in the droplets forming at the outlet of the CFR can lead to silver nitrate rich zones (due to imperfect mixing) which lead to larger NPs forming (as well as increased polydispersity). In the case of the lowest silver nitrate concentration (0.05 mM) there is a low amount of silver nitrate in the droplets at the outlet of the CFR, leading to a lower possibility of silver nitrate rich zones. At higher silver nitrate concentrations there is a larger amount within the droplets at the outlet of the CFR, increasing the likelihood of reactions occurring in silver nitrate rich zones leading to an increased formation of larger NPs and polydispersity.

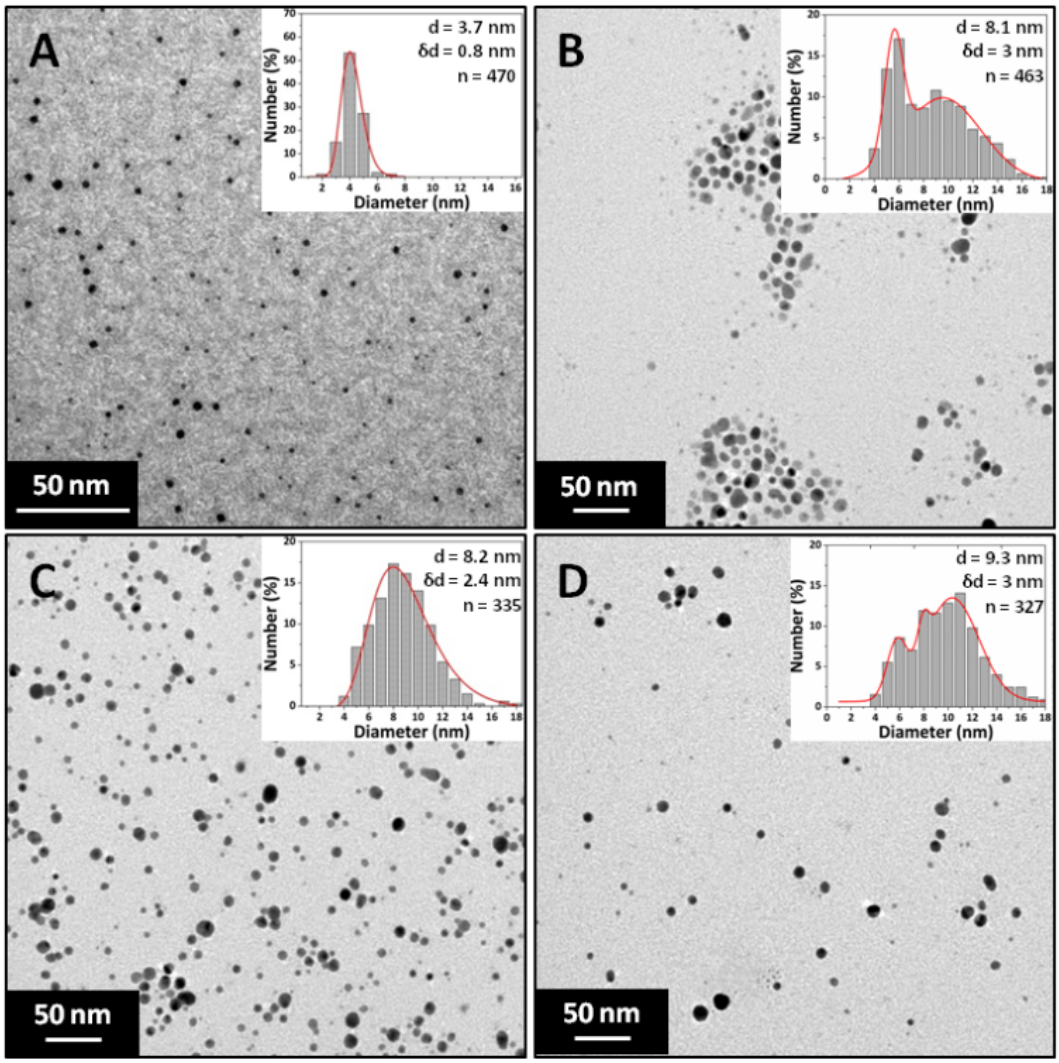

Figure 3-5: TEM images and particle size distributions of silver NPs synthesized at different silver nitrate concentrations. A: 0.05 mM, B: 0.15 mM, C: 0.25 mM and D: 0.4 mM. Concentration of trisodium citrate 0.5 mM, sodium borohydride 0.3 mM. Total flow rate 2.5 ml/min, 0.556 mm inner tube I.D.

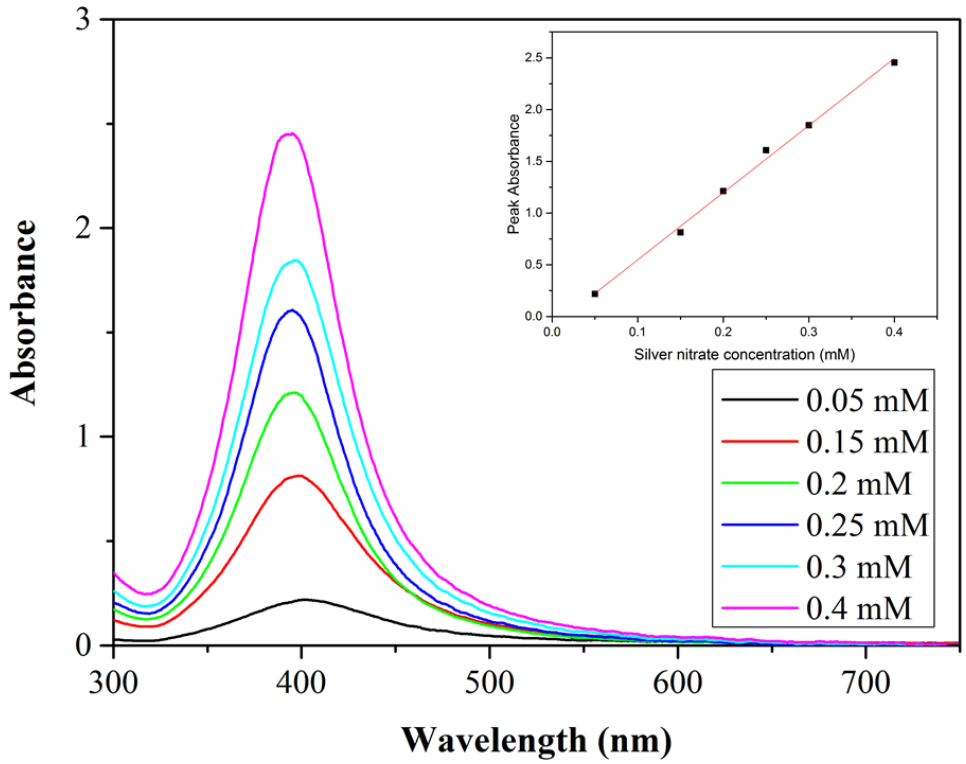

Figure 3-6: Absorbance peaks of silver NP synthesized at various silver nitrate concentrations in the range 0.05-0.4 mM. Total flow rate 2.5 ml/min, concentrations of trisodium citrate 0.5 mM, sodium borohydride 0.3 mM. 0.556 mm inner tube I.D. Inset: Silver nitrate concentration vs. peak absorbance for resonance peaks.

Table 3-2: FWHM and peak wavelength of silver NPs at various silver nitrate concentrations in the range 0.05 – 0.4 mM. Total flow rate 2.5 ml/min, concentrations of trisodium citrate 0.5 mM, sodium borohydride 0.3 mM. 0.556 mm inner tube I.D.

Silver concentration (mM)	FWHM (nm)	Peak Wavelength (nm)
0.05	88	402
0.15	76	399
0.2	67	397
0.25	64	395
0.3	68	396
0.4	66	395

3.3 Conclusions

The performance of a Coaxial Flow Reactor (CFR) was investigated for silver NP synthesis. The reaction was confined to the interface between the inner and outer streams resulting in the generation of silver clusters which increase in concentration along the length of the CFR. Hence the residence time is an important parameter which determines the amount of the precursor consumed before the advective mixing within the droplets at the end of the CFR. Residence time determines the amount of silver nitrate consumed in the CFR, and it is shown that shorter residence times where less silver nitrate is consumed, results in larger NPs being formed. This is possibly because reactions in silver nitrate rich zones (i.e. reactor outlet at high flow rates) lead to the formation of NPs with low surface charge which have reduced stability and hence have a tendency to grow by coalescence. For the same reason, increasing

silver nitrate concentration, while maintaining a constant residence time resulted in an increase of NP size and polydispersity. Increasing citrate concentration reduced the amount of larger fused NPs resulting in a smaller average size and reduced polydispersity. Such fused NPs disappeared above a citrate concentration of 0.25 mM. Increasing the concentration of citrate past this amount did not decrease the size of the NPs further, indicating that a threshold is reached. The CFR offers a simple method to control the size of the NPs because of its unique design. By keeping advective mixing to a minimum, the reaction is maintained at the interface region between the two streams. This avoids the problem of blockage of the channels by containing the reaction away from the channel walls, unlike other types of microfluidic devices where the reaction can take place close to the channel walls.

4 Synthesis of silver nanoparticles using a microfluidic impinging jet reactor

The synthesis of silver NPs using sodium borohydride as a reducing agent typically leads to small NPs because borohydride is a strong reducing agent, however it tends to give polydisperse NPs. Our previous study using a coaxial flow reactor produced silver NPs in the 4-10 nm range and showed that mixing is an important parameter when using borohydride as a reducing agent.[145] Split and recombine type flow reactors[71] and PTFE flow chambers[65] have been utilized to synthesize silver NPs using borohydride obtaining NPs in the range of 10-20 nm for borohydride to silver nitrate ratios ranging from 3 to 40. Batch reactor syntheses of silver NPs using borohydride as a reducing agent produced NPs in the 1-100 nm range.[5, 64, 67, 69]

A non-confined impinging jet reactor (IJR) with characteristic dimensions in the micrometer range is employed in this study to investigate how manipulating mass transfer affects the NP characteristics, in particular the size and dispersity. IJR is a particularly useful device to use in the synthesis of NPs since it doesn't clog because of absence of channel walls. Fouling is particularly problematic in microfluidic devices since their small dimensions make them potentially vulnerable to blockage, and various strategies in the literature have been used to avoid fouling such as segmented flow,[126] coaxial flow[128, 145] and surface silanization.[127]

The IJR has found most common application in bipropellant liquid rocket engines[146] but it also presents some very distinct advantages for reactions which produce solids. Mahajan and Kirwan characterized the mixing times in an IJR using the Bourne reaction scheme.[147] They subsequently carried out a precipitation reaction for the synthesis of lovastatin crystals and compared the size of crystals obtained when the mixing time was i) slower and ii) faster than the induction time for crystallization. They concluded that a more monodisperse particle size distribution (PSD) was obtained when mixing time was faster. They also concluded that if the mixing time is faster than the induction time (elapsed time period between achievement of supersaturation and the appearance of crystals),[148] further improvements to the mixing time do not significantly affect the resultant crystals. Erni and Elabbadi studied the hydrodynamic properties of the IJR and characterized various flow regimes before using the IJR for an acid induced crystallization of sodium benzoate. They found a decrease in both size and dispersity with an increasing jet velocity.[149] Kumar *et al.* employed an IJR for the synthesis of nanocrystalline MgO, a process which yields a rigid gel which can quickly clog microchannels. A change in impingement angle and velocity of the jets was found to affect the surface area of the nanocrystalline MgO formed and for each parameter there was an optimum that existed to obtain maximum surface area. It is suggested that this optimum exists because of a change in hydrodynamics in the impingement zone, where too high a flow rate or impingement angle led to non-optimal mixing conditions resulting in a reduced contact time for reaction.[150] Hosni *et al.* used impinging jet reactors for the synthesis of ZnO NPs, comparing results against those formed in a batch stirred vessel and a T-mixer type reactor. The size of the NPs synthesized in each reactor depended on the energy dissipation used for mixing, with the

IJR having intermediate energy dissipation versus the other two types of reactors and hence producing an intermediate size of ZnO NPs.[151]

Confined impinging jet reactors (CIJR) are a similar type of reactor for the use in reactions involving precipitation of solids. Johnson and Prud'homme employed a CIJR for the precipitation of hydrophobic organic actives NPs; importantly the CIJR allows for homogeneous conditions prior to precipitation of NPs (i.e. formation of block copolymer NPs and nucleation and growth of organic actives) which ultimately separates the effect of mixing on the final size of the NPs.[152] The NP size decreased with increasing mixing efficiency up until a 'breakpoint' was reached, at which point the size of the block copolymer NPs remained constant. They also observed the same effect when using a different block copolymer, and the 'breakpoint' corresponded to a Dahmköhler number of 1.[153] Marchisio *et al*. studied the precipitation of barium sulfate NPs in a CIJR and similarly observed a reduction in particle size with increasing mixing intensity, but no further improvements were observed when the characteristic mixing time scale reached the reaction time scale.[154] Reduction in size of precipitated barium sulfate NPs with increasing mixing intensity was also observed by Schwarzer and Peukert using a T-mixer.[155] Siddiqui *et al*. used a CIJR for the synthesis of iron oxide NPs where they found a reduction from 800 nm to 200 nm in agglomerate size by increasing the flow rate under high concentration conditions.[156] These studies show the importance of mixing for reactions which lead to formation of NPs, since they typically have reaction times that are small and hence need very good mixing efficiency to approach monodispersity. According to the literature above, a reduction in NP size is reported with increasing mixing efficiency attributed to increasing supersaturation levels which would favor a higher nucleation rate and hence smaller particles.

The IJR used in this study presents a convenient platform for the synthesis of silver NPs because the reactor has no channel walls in the reaction zone, eliminating the need for lengthy cleaning procedures which are needed in traditional microchannels because of fouling. The IJR can synthesize silver NPs in a highly repeatable manner, associated with the lack of fouling which can occur in other types of reactors where surfaces are present near the reaction zone. The main objective of this work is to investigate the effect of mixing on the size and dispersity of silver NPs synthesized using two different ligands: i) trisodium citrate and ii) polyvinyl alcohol (PVA). The hydrodynamics and mixing efficiency of the IJR have also been studied.

4.1 Experimental

4.1.1 Chemicals

Silver nitrate ($AgNO_3$, 0.01 M stock solution), trisodium citrate ($HOC(COONa)(CH2COONa)_2 \cdot 2H_2O$, powder form, PVA (molecular weight 89000-98000 Da), sodium borohydride solution ($NaBH_4$, ~12 wt% in 14 M NaOH stock solution), potassium iodide (KI, 99%) potassium iodate (KIO_3, 98%), boric acid (H_3BO_3, 99.5%) and sulfuric acid (H_2SO_4, 3 M stock solution) were obtained from Sigma. All chemicals were used without further purification and solutions were prepared with ultrapure water (resistivity 15.0 MΩ·cm).

4.1.2 Experimental Setup

Syringe pumps (Pump 11 Elite OEM module, Harvard) were used in the flow experiments to deliver the reagents to the IJR. Figure 4-1 shows a schematic representation of the IJR, which consisted of two stainless steel tubes with equal internal diameters of 0.25 mm or 0.5 mm aligned at an angle, θ = 48°. This was achieved by inserting the tubes into a perspex plate which had 1.5 mm (depth and width) channels milled at a 48° angle using a Roland EGX-400 engraving machine. The outer diameters of the tubing was 1.59 mm. Spacing between the centers of the fluid jets at the point of tube outlets, d, was 3 mm.

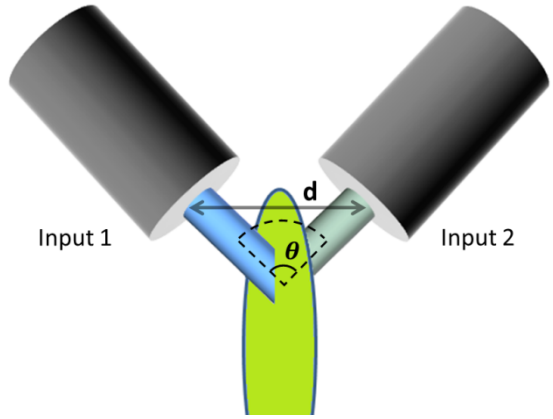

Figure 4-1: Representation of the impinging jet reactor.

4.1.3 Nanoparticle Synthesis

A mixture was made by combining silver nitrate and ligand (trisodium citrate or PVA) into a solution and diluting to the appropriate concentration for input 1 (Figure 4-1) and diluting sodium borohydride/sodium hydroxide solution to the appropriate concentration for input 2. Since the sodium borohydride was stored in 14 M sodium hydroxide, the concentration of sodium hydroxide was 3.21 times higher than the stated sodium borohydride concentration in all cases. The syringe pumps delivered reagents to input 1 and input 2 at the appropriate flow rates to produce the desired jets. As the two jets collide, the reagents mix followed by subsequent reaction and formation of silver NPs. Reactions were carried out at room temperature (22-24°C). All concentrations stated are those at the inlets before any mixing of reagents occurs.

4.1.4 Characterisation of Nanoparticles

The silver NPs were analyzed using a UV-Vis spectrometer (USB 2000+ Spectrometer and DT-Mini-2-GS light source, Ocean Optics) between 45 to 60 min after synthesis (the signal of the samples were stable in this window of time). Silver NP samples were diluted with additional ultrapure water to bring the absorbance into a suitable range (i.e. obeying the Beer-Lambert law and avoiding saturation of the light detector) and the data were normalized so that the maximum absorbance in the flow rate range tested represented an absorbance of 1. Transmission electron microscope images were captured using a JEOL 1200 EX ii microscope with a 120 kV acceleration voltage. Carbon coated copper TEM grids were prepared between 45 to 60 min after synthesis by pipetting a 5 µl sample onto the grid and allowing it to dry at room temperature. Care was taken to not cover the entire TEM grid with sample but rather only a portion of it (as discussed in Chapter 3). Particle size distributions (insets for each TEM image

presented) have the following nomenclature: *d* is average diameter, *δd* is the standard deviation of the NP distribution and *n* is the number of particles counted to obtain the particle size distribution. PEBBLES software was used for the counting and sizing of TEM images of the synthesised NPs.

4.2 Mixing characterization methods

For single phase mixing, two types of experimental technique can be considered for mixing characterisation: dilution-based methods and reaction-based methods.[157]

4.2.1 Dilution-based methods

These methods involve the contacting of a clear liquid with a coloured dye and observing the change in concentration of the coloured dye along the channel. Mixing is considered complete when the concentration of the coloured dye is uniform across the diameter of the channel. There are two limitations to this kind of characterisation. The channel must be optically transparent for visual observations using a microscope to be made. Because the observation is made perpendicular to the channel, the concentration that is visually observed is actually an average of the concentration of the dye over the depth of the channel. Examples of this type of characterisation are: Mixing concentrated dye with colourless water solution,[158] and dilution of fluorescent species such as fluorescein and rhodamine B.[50]

4.2.2 Reaction-based methods

Three types of reaction exist in this branch of characterisation:

1. Acid-base reactions:
2. Reactions producing a coloured species product
3. Competing parallel reactions

The first two methods also rely on optical observation of the product. Acid-base reactions rely on the presence of a pH indicator such as methyl orange, bromothymol blue and phenolphthalein. Reactions producing coloured species include the reduction of potassium permanganate in alkaline ethanol and the iron rhodanide reaction. Both these methods give similar disadvantages to dilution-based methods (not being able to obtain concentrations across the depth of the channel, but obtain an average of the concentration over the depth of the channel).

Competing parallel reactions rely on parallel reactions which compete for a single reactant. One of these reactions will be faster than the other. The degree to which the slower reaction occurs depends on the measure of mixing. There are two types of these reactions used for measuring the mixing performance in microreactors: the Villermaux-Dushman reaction and the second Bourne reaction scheme (the simultaneous diazo coupling of 1- and 2-napthol with diazotized sulfanilic acid). Both methods involve measuring the concentration of specific products using UV-Vis spectroscopy, which allows certain parameters to quantify mixing to be calculated such as segregation index. For this study, the Villermaux-Dushman reactions were chosen to characterize mixing.

4.3 Villermaux-Dushman reaction scheme

The Villermaux-Dushman test reaction system is a well-known method to characterize mixing efficiency in a reactor.[159] Mixing time within a micromixing device can be obtained using this reaction system by tuning the concentrations appropriately. The Villermaux-Dushmann reaction system can be described as follows: A stoichiometric defect of sulphuric acid is introduced to a mixture of borate, iodide and iodate ions. The following reactions occur:

$H_2BO_3^- + H^+ \leftrightarrow H_3BO_3$ **(4.1)** *instantaneous*

$5I^- + IO_3^- + 6H^+ \leftrightarrow 3I_2 + 3H_2O$ **(4.2)** *very fast*

$I_2 + I^- \leftrightarrow I_3^-$ **(4.3)**

Reaction 1 is much faster than reaction 2, and since there is a stoichiometric defect of acid, only reaction 1 occurs if there is perfectly efficient mixing. In practice, reaction 2 increases as the mixing efficiency decreases because iodide and iodate will react with acid if the local concentration of orthoborate ions has been depleted (this only occurs if the mixing is not perfectly efficient). Reaction 2 produces iodine, which further reacts with iodide ions to form triiodide (reaction 3). A defect of acid amount is needed because the mean pH must be within a narrow range close to the value for the iodine dismutation pH (pH*). If the pH is lower than pH*, iodine can form in acid solution irrespective of micromixing effects, while on the other hand the pH cannot be too basic since formation of iodine becomes thermodynamically unstable.[159] By measuring the triiodide concentration, the extent to which reaction 2 occurs can be measured, hence allowing the mixing efficiency to be estimated. Triiodide exhibits a strong peak at 353 nm enabling its concentration to be calculated. The extinction coefficient of triiodide was found to be 23209 $M^{-1}\cdot cm^{-1}$ at 353 nm, which is similar to the values reported in the literature (details on this procedure can be found in Appendix A and calibration curve is shown in Figure A2).[159] The micromixing quality is quantified by the segregation index which is discussed in detail in other studies.[159, 160] The segregation index can be linked to the mixing efficiency through the use of a phenomenological mixing model.

4.4 The interaction by exchange with the mean mixing model

The interaction by exchange with the mean (IEM) model was used to estimate the mixing time from the experimental results, and can be expressed as follows:[161, 162]

$$\frac{dC_{k,1}}{dt} = \frac{<C_k> - C_{k,1}}{t_\mu} + R_{k,1} \quad \textbf{(4.4)}$$

$$\frac{dC_{k,2}}{dt} = \frac{<C_k> - C_{k,2}}{t_\mu} + R_{k,2} \quad \textbf{(4.5)}$$

$$<C_k> = \alpha C_{k,1} + (1-\alpha) C_{k,2} \quad \textbf{(4.6)}$$

where C is concentration of species k, $<C_k>$ is the average concentration of the species k across acid and buffer streams, R is the reaction rate of species k, t_μ is the mixing time and α is the volume fraction of the acid stream. Equations 3.4 and 3.5 represent the acid stream (or injection) and the buffer stream (or volume in the tank) respectively, and hence the subscript following k in these equations represent either the acid (1) or buffer (2) stream. These equations form the differential mass balance equations that need to be solved to obtain a theoretical concentration of triiodide (or segregation index) for a given mixing time according to the model. The segregation index, X_s, is defined as:

$$X_s = \frac{Y}{Y_{ST}} \qquad \textbf{(4.7)}$$

where Y is the ratio of acid mole number consumed by reaction 2 divided by the total acid mole number injected:

$$Y = \frac{2\left((I_2)+\left(I_3^-\right)\right)}{\alpha(H_0^+)} \qquad \textbf{(4.8)}$$

and Y_{ST} is the value of Y when the mixing process is infinitely slow (perfect segregation):

$$Y_{ST} = \frac{\frac{6(IO_3^-)_0}{(H_2BO_3^-)_0}}{6\left(\frac{(IO_3^-)_0}{(H_2BO_3^-)_0}\right)+1} \qquad \textbf{(4.9)}$$

A curve of mixing time vs. segregation index can be obtained by setting a mixing time and the concentration of reagents, followed by solving for a range of mixing times. The differential mass balance equations were solved using gProms Model Builder 3.7.1. An example code for a flow reactor can be seen in Appendix A. By solving the IEM model for a range of mixing times, segregation index can be plotted against mixing time. By performing the experiments using the appropriate reactor, the triiodide concentration for the given set of conditions can be obtained and the segregation index can be determined. The corresponding mixing time is then determined by using the plot generated by the model i.e. see which mixing time corresponds with the segregation index determined experimentally from the plot. The relationship between mixing time and segregation index for the concentration sets used to characterise mixing time in the IJRs can be seen in Figure 4-2.

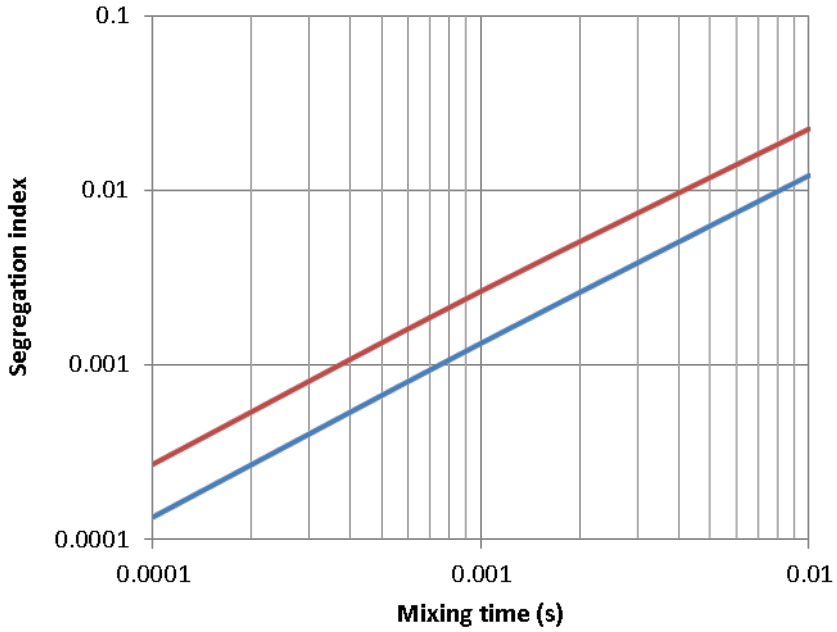

Figure 4-2: Segregation index vs. mixing time estimated using the IEM model for the Villermaux-Dushmann reaction scheme for 0.5 mm (blue line) and 0.25 mm (red line) IJRs. Concentrations of buffer solution were KI: 0.032 M, KIO_3: 0.006 M, NaOH: 0.045 M, H_3BO_3: 0.09 M in both IJRs. Concentration of H_2SO_4 was: 0.017 M and 0.02 M for 0.5 mm and 0.25 mm IJR respectively.

4.5 Experimental determination of mixing time in the impinging jet reactors

The Villermaux-Dushmann reaction system was carried out in the 0.5 mm and 0.25 mm IJRs. For input 1, 0.017 M and 0.02 M of sulphuric acid were used (corresponding to 0.034 M and 0.04 M H^+) for the 0.5 mm and 0.25 mm IJR respectively. The dissociation of sulphuric acid is considered to be almost complete for pH above 4, whereas if the reactions take place at a lower pH then the assumption of complete acid dissociation would result in overestimating the mixing efficiency. Commenge and Falk noted that the pH of the solution (acid and buffer combined) will increase as mixing takes place resulting in more dissociation, while suggesting that if the reaction takes place at pH 2.5, the mixing time will be underestimated by 25%.[160] Input 2, which is considered the buffer solution, had a concentration of 0.032 M potassium iodide, 0.006 M potassium iodate, 0.045 M sodium hydroxide and 0.09 M orthoboric acid. Figure 4-3 shows mixing time vs. Weber number obtained for the 0.5 mm and 0.25 mm IJRs.

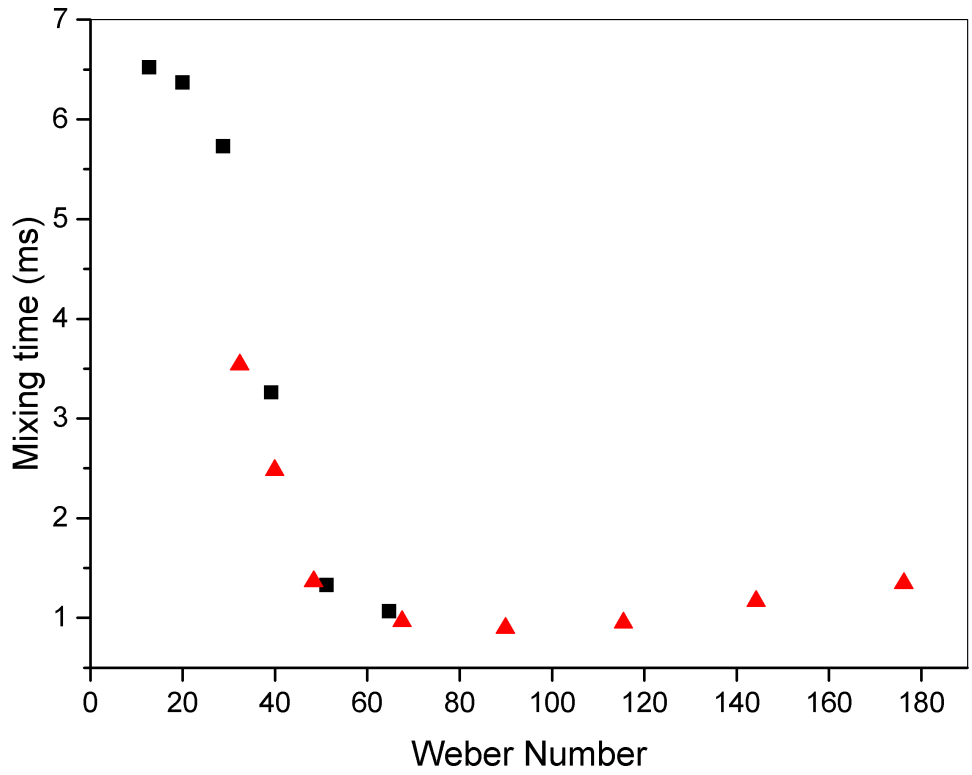

Figure 4-3: Mixing time calculated by the Villermaux-Dushmann reaction scheme vs. Weber number for 0.5 mm (black squares) and 0.25 mm (red triangles) IJRs. Concentration of acid solution (input 1) was 0.017 M and 0.02 M H_2SO_4 for 0.5 mm and 0.25 mm I.D. tubing IJR respectively. Concentrations of buffer solution (input 2) were KI: 0.032 M, KIO_3: 0.006 M, NaOH: 0.045 M, H_3BO_3: 0.09 M in both IJRs.

The Weber number is defined as:[163]

$$We = \frac{\rho u^2 d}{\sigma}$$

where ρ is the density of fluid, u is average velocity of fluid before impact, d is the diameter of the jet (taken as the tube internal diameter) and σ is the surface tension of the fluid. Values of fluid properties used are those for water at room temperature. The Weber number represents the ratio of inertial to surface tension forces, and is useful in describing what regime the IJR is operating in. The Weber number range for the 0.5 mm and 0.25 mm IJRs was 13-65 and 32-176 respectively. The Reynolds number is defined as:

$$Re = \frac{\rho u d}{\mu}$$

where μ is the dynamic viscosity. The Reynolds number represents the ratio of inertial to viscous forces, and describes whether the flow is a laminar, intermediate or turbulent regime. The Reynolds number range for the 0.5 mm and 0.25 mm IJRs was 680-1520 and 760-1770 respectively. From Figure 4-3 it can be seen that the mixing time for both reactors is similar when operating under similar Weber numbers. This indicates that the Weber number is a key parameter in determining the mixing efficiency of an IJR. Erni and Elabaddi propose that the mixing time for an impinging jet is proportional to the Weber

number according to a power law relationship ($t_m \propto We^{-0.75}$).[149] Fitting the data in our study for We < 80, the following relationship was found, $t_m \propto We^{-0.89}$. Mixing time decreases with increasing Weber number up to a value of *ca*. 90 where it reaches a minimum value of around 1 ms. Increasing the Weber number past *ca*. 90 using the 0.25 mm IJR results in a gradual increase in mixing time. In general, the specific power dissipation within a reactor can be used to estimate the mixing time and several studies have shown a correlation between the two.[52, 160, 161] The specific power dissipation for the IJR can be estimated using the following relationships:[147]

$$\epsilon = \frac{P}{\rho V} \quad \textbf{(4.10)}$$

$$P = \frac{1}{2}(m_1 u_1^2 + m_2 u_2^2) \quad \textbf{(4.11)}$$

$$V = \frac{\pi d^2}{4} h \quad \textbf{(4.12)}$$

where ϵ is overall energy dissipation per unit mass [W/kg], P is rate of overall mechanical energy dissipation [W] assumed to be equal to the kinetic energies of the two impinging jets, ρ is the fluid density [kg/m^3], V is the volume of the impingement zone [m^3], m is the mass flow rate of a jet [kg/s], u is the velocity of a jet [m/s] (with subscripts 1 and 2 denoting input 1 or 2), *d* is the diameter [m] and *h* is the effective thickness of the cylindrical micromixing region. It is difficult to estimate what the cylindrical micromixing region would be given the non-uniform shape of the liquid sheet after impingement and its changing dimensions depending on the flow rate. If *d* is assumed to be the jet diameter of the IJR while the value of *h* to be 10% of the internozzle distance,[147] mixing time can be estimated using the correlation suggested by Commenge and Falk:[160]

$$t_m = 0.15\epsilon^{-0.45} \quad \textbf{(4.13)}$$

where t_m is the mixing time [s]. Using the correlation, the mixing time estimate was found to be between 0.9-2.6 ms for the 0.5 mm IJR and 0.25-0.9 ms for the 0.25 mm IJR for the conditions used in this study. The mixing times found using the IEM model were between 1-6.5 ms for the 0.5 mm IJR and 0.9-3.5 ms for the 0.25 mm IJR. Considering that both the correlation and the IEM model only give an estimate of the mixing time, the order of magnitude agreement is satisfactory. Increasing specific power dissipation by increasing flow rate within the flow reactor should decrease mixing time. However this is not the case for the IJR where the mixing time levels off and begins to increase past a Weber number *ca*. 90, most likely because of droplet formation and breakup at the liquid rim of the sheet formed on impingement of the jets. Erni and Elabaddi observed that there is a transition from the liquid sheet to a fragmented sheet (unstable rim) at a We~30 at a surfactant concentration of 8.2 µM sodium dodecyl sulfate (SDS), We~80 at a concentration of 0.82 mM and We~200 at 82 mM.[149] They observed that the mixing quality deteriorates when there is excessive droplet fragmentation; droplets ejected from the sheet have little time for efficient mass transfer which is highest in the liquid sheet (they estimate that droplets took 0.6 ms to be ejected from the liquid sheet). Using the fourth Bourne reaction scheme,

they estimated mixing time in their system to be 4.9 ms, which is of the same order of magnitude as our work. The flow regime in our system was subsequently investigated to ascertain where this transition occurs.

4.6 Flow regime characterization of impinging jet reactor using high speed camera

The flow regime of the 0.5 mm and 0.25 mm IJR was investigated by capturing images of the IJR during operation using a high speed camera (Photron Fastcam SA1.1 high speed camera). Figure 4-4 shows the flow regime for the 0.5 mm IJR system, for flow rates between 32-72 ml/min (Weber number 13-65). From the images, it can be seen that the flow pattern changes across the flow rate range investigated. At the lowest flow rate the jets collide and coalesce, forming a small sheet. As the flow rate increases, the sheet increases in length and diameter. Further increase in the flow rate results in a wavy liquid film surrounding the liquid sheet. This behavior has been observed in other studies where a wavy film occurs, although it is usually accompanied by droplets leaving the stable sheet bounded by a liquid rim. This effect arises from Rayleigh-Plateau instability.[164, 165] It is possible that these waves, observed on the liquid rim and sheet, arise from small oscillations in the flow delivered from the syringe pumps. This wavy nature of the liquid sheet is also transferred into the chain of fluid following the initial sheet formed by the collision of the jets. The liquid following the collision of the jets remains continuous in all cases for the 0.5 mm IJR, with no droplet breakup in the region visualized. Figure 4-5 shows the flow regime for the 0.25 mm IJR system, for flow rates between 18-42 ml/min (Weber number 32-176). At lower flow rates, a stable sheet and liquid rim are formed at the point of impact. At flow rate above 26 ml/min, an unstable rim with droplets breaking off the main structure begins to form. From the front view it can be seen that the flow is also developing a spray in that plane. At this point the inertial forces overcome the surface tension forces of the fluid resulting in droplet breakaway from the main liquid sheet/rim. Also for the 0.25 mm IJR system, the chain of fluid following the liquid sheets after impact is non-continuous after the first few secondary liquid sheets are formed.

Taking the mixing time estimations and flow regime observations into account, the mixing behavior of the IJR system can be rationalized. There are two modes of atomization: reflective and transmitive. Between these two regions there exists a well-mixed atomization condition.[166] In the reflective atomization regime, which occurs at relatively low jet velocities, the jets essentially collide and coalesce forming a thin liquid sheet immediately after collision. Deflection of each jet will be equal as they bounce on each other because of equal momentum. In this region, the turbulence in the mixing layer following impingement increases as flow rate increases leading to an increasing mixing efficiency. However, because of the turbulent nature of the jets there will be a fluctuation in the trajectory of droplets/sheet as velocity increases; there is an eventual breakup of the liquid sheet where smaller droplets break away. At this point the atomization transitions into a transmitive mode, whereby droplets are ejected from the liquid rim of the sheet because of increased momentum. This is observed in Figure 4-5 at We > 90. The droplets that are ejected from the liquid rim have little contact time in the relatively efficiently mixed sheet and the mixing efficiency suffers because higher amounts of droplets are ejected. The results show that below a We ~ 90, we are in the reflective atomization regime. Above this Weber number the regime transitions into a transmitive regime. A We ~ 90 seems to yield optimal

mixing as confirmed by the mixing time estimation. The observed transition is somewhat higher than those observed by Erni and Elabaddi who at minimal surfactant concentration observed transition at We ~ 30.[149] However they use jets at an angle of 110° with a jet spacing of 10 mm which could affect the transition point.

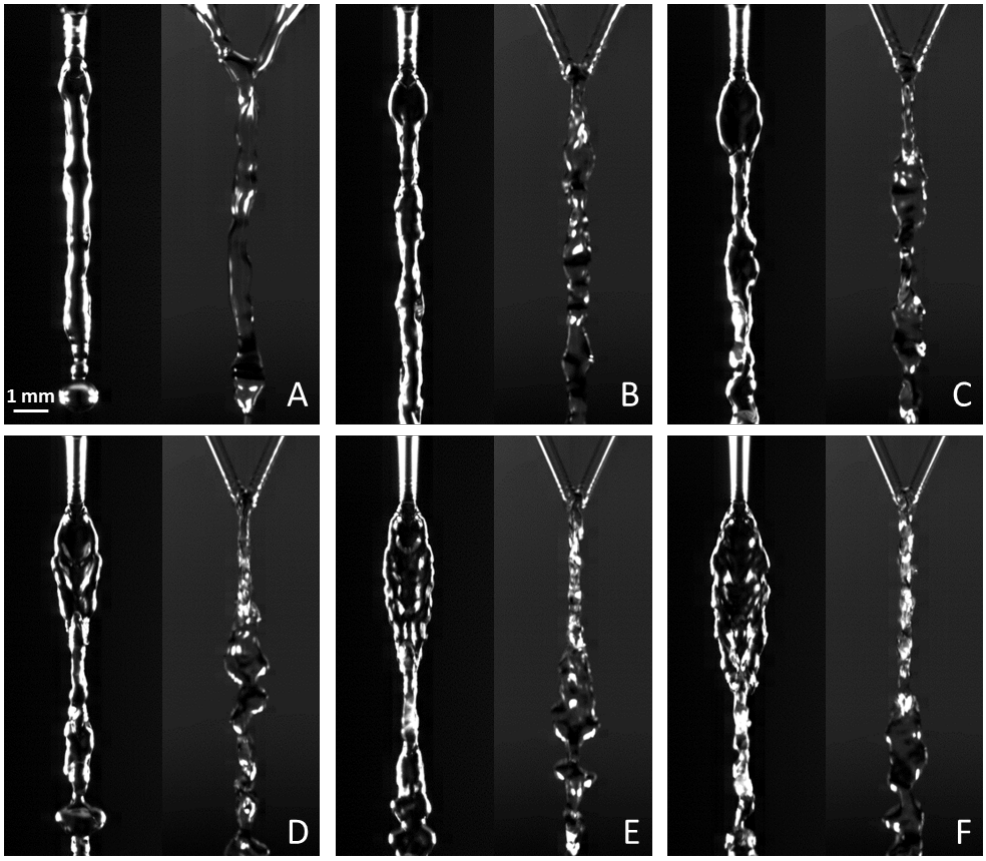

Figure 4-4: Flow visualization of jets emitted from 0.5 mm tubes at total flow rate: A: 32 ml/min (We: 13), B: 40 ml/min (We: 20), C: 48 ml/min (We: 29), D: 56 ml/min (We: 39), E: 64 ml/min (We: 51) and F: 72 ml/min (We: 65). Pictures show side view and front view.

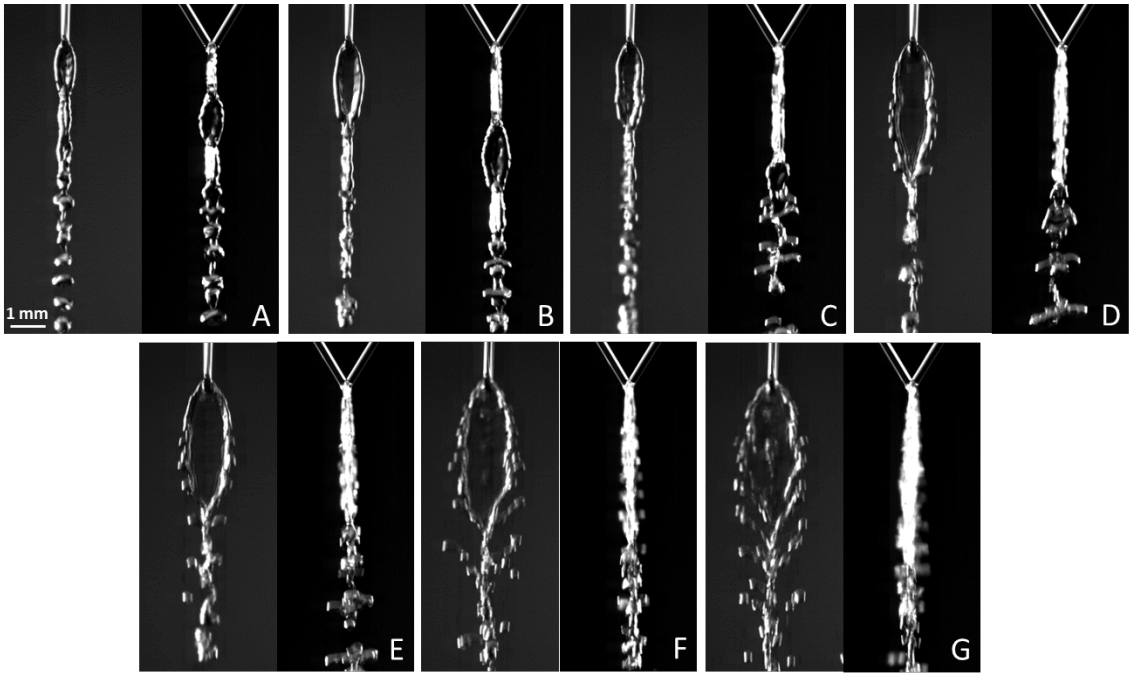

Figure 4-5: Flow visualization of jets emitted from 0.25 mm tubes at total flow rate: A: 18 ml/min (We: 32), B: 22 ml/min (We: 48), C: 26 ml/min (We: 68), D: 30 ml/min (We: 90), E: 34 ml/min (We: 115), F: 38 ml/min (We: 144) and G: 42 ml/min (We: 176). Pictures show side view and front view.

4.7 Investigating the effect of weber number on NP morphology

4.7.1 Effect of weber number on silver NP synthesis 1 (citrate system)

The effect that the Weber number has on the silver NPs was investigated in the 0.5 mm and 0.25 mm IJRs using trisodium citrate as a stabilizing agent. Concentrations of input 1 were 0.9 mM silver nitrate, 6 mM trisodium citrate and for input 2 were 1.8 mM sodium borohydride. Total flow rates for the 0.5 mm IJR ranged from 32 ml/min to 72 ml/min and for the 0.25 mm IJR ranged from 18 ml/min to 34 ml/min (repeatability of the synthesis is shown in Appendix C, Figure C1).

Figure 4-6 shows TEM images for NPs synthesized in the 0.5 mm IJR at 32, 48, 64 and 72 ml/min where the average diameter and dispersity of the NPs are 7.9 ± 5.8 nm, 7.7 ± 5.0 nm, 5.0 ± 2.8 nm and 3.4 ± 1.4 nm. Average diameter and polydispersity decrease with increasing Weber number (flow rate). T-tests showed p-values < 0.001 when comparing all the PSDs against each other. This suggests that the PSDs are all statistically different.

Figure 4-7 shows TEM images for NPs synthesized in the 0.25 mm IJR at 20, 24, 28 and 32 ml/min where the average diameter and dispersity of the NPs are 6.4 ± 3.4 nm, 5.9 ± 2.1 nm, 5.0 ± 2.5 nm and 5.1 ± 4.6 nm. It appears with increasing Weber number (flow rate) the NPs reduce in average size up to *ca*. 5 nm. T-tests showed p-values > 0.05 when comparing the PSDs of 20 and 24 ml/min, 24 and 32 ml/min and 28 and 32 ml/min (all other p-values where < 0.001). These suggest that the PSDs are not statistically different; however, this is most likely down to the large polydispersity. Visual analysis of the TEM images reveals two different populations of NPs, those that are smaller than 20 nm and those that are larger. Although the larger NPs were present in small frequencies (not larger than 15 counts for any flow rate), there were enough present to affect the average size and dispersity calculations of NPs

synthesized at 20 ml/min and 32 ml/min, but at 24 ml/min and 28 ml/min virtually no larger NPs are present. If NPs larger than 20 nm are removed from the t-test analysis, only NPs synthesized at 20 ml/min and 24 ml/min have a p-value > 0.05 with all other p-values being <0.001. From the PSDs in Figure 4-7 it can be seen that, as the Weber number is increased, the average size gets smaller and the dispersion is reduced in the < 20 nm range. However, the polydispersity is higher at the largest Weber number even though it has the least disperse curve for NPs < 20 nm. This is because synthesis at the highest Weber number produced the highest frequency of larger NPs (> 20 nm), and the disparity in size between the larger and smaller NPs is higher as compared to NPs produced at lower Weber numbers.

Figure 4-8 shows the peak absorbance vs. Weber number obtained from UV-Vis spectroscopy for the silver NPs obtained using the 0.5 mm IJR (We = 13-65) and the 0.25 mm IJR (We = 32-115). It is worth noting that the UV signal did not change significantly 24 hours after synthesis (~1% change in peak absorbance). For each jet diameter, the peak absorbance in general decreases with increasing Weber number. Since the NP size identified from TEM images was primarily below 10 nm, the decreasing peak absorbance is possibly because of a decrease in size of the NPs. For silver NPs the molar extinction coefficient increases with size,[167] and absorbance increases with increasing size below the 10 nm range, as predicted by Mie theory.[139] Table 4-1 and Table 4-2 show the FWHM and peak wavelength for silver NPs synthesised using trisodium citrate as a stabilising agent at various flow rates in the 0.5 mm and 0.25 mm IJR respectively. The FWHM for the 0.5 mm IJR increases significantly after a flow rate 48 ml/min while the peak wavelength remains fairly constant. There is a gradual increase in the FWHM with increasing flow rate for the 0.25 mm IJR, while the peak wavelengths again stay approximately constant.

The TEM images and peak absorbance of the NPs would suggest that the NPs decrease in size with increasing Weber number while the dispersity shows a more complex relationship. Firstly the results obtained from the 0.25 mm IJR will be discussed. In terms of the NP synthesis, the size and dispersity changes can be explained by taking into account mixing characteristics of the impinging jet at the particular Weber number. The NPs below 20 nm are referred to as *smaller* NPs and those above 20 nm are referred to as *larger* NPs. At low Weber numbers, the *smaller* NPs tend to be of a larger and more polydisperse nature. As the Weber number increases, the average size of these NPs decreases while the PSDs become tighter. This can be explained through the mixing characteristics within the liquid sheet, where increasing turbulence results in a shorter mixing time. Borohydride has a stabilizing effect on the NPs,[136, 139, 145] and can also supply a high amount of electrons per mole (up to a maximum of eight electrons in theory).[133-135] Therefore, if there is efficient mixing within the liquid sheet, there will be a sufficient supply of sodium borohydride in the local regions where reaction is taking place, resulting in increased stabilization and smaller NPs. If there are insufficient amounts of borohydride molecules, less stable NPs, which can grow relatively easily, are formed. Poor local mixing efficiency, which results in low local concentrations of borohydride, will lead to larger NPs, since borohydride can reduce many times its own molar equivalent of silver ions. The formation of *larger* NPs can be compared to the formation of iodine in the Villermaux-Dushmann reactions, which is caused by a local lack of

orthoborate ions. Hence, increasing the mixing efficiency (Weber number) decreases the size of the *smaller* NPs.

It is suggested that the *larger* NPs are formed in silver nitrate rich regions. The presence of large NPs was most frequent at a Weber number of 40 and 102. Intermediate Weber numbers of 58 and 78 had virtually no NPs over 20 nm. The appearance of *larger* NPs and their change in size and frequency can be explained by mixing efficiency and the transition from a reflective to a transmitive type of atomization. At the lowest Weber numbers, in the reflective atomization regime, there is lower turbulence within the mixing zone. This leads to the possibility of reactions occurring in poorly mixed regions, resulting in the formation of *larger* NPs. At the intermediate Weber numbers, very few *larger* NPs are formed because of the increasing mixing efficiency. At large Weber numbers, there is a transition into transmitive atomization. At this point an unstable rim is seen with droplets leaving the main body of fluid, resulting in a net decrease in mixing efficiency. Within these droplets, it is possible that *larger* NPs are formed especially if they are silver nitrate rich.

The reduction in size and dispersity is more obvious for the 0.5 mm IJR. This reduction is obtained as the mixing efficiency is increased within the liquid sheet, causing the average size of the NPs to decrease and minimizing the formation of *larger* NPs. Again this is because the reactions are taking place with a more efficient spread of sodium borohydride, which increases stability of formed NPs and decreases the formation of NPs in silver nitrate rich regions. There is reduction in size and polydispersity when the hydrodynamics of the IJR transition from a uniform liquid sheet ($We < 29$) to a liquid sheet with waves ($We > 39$) with the size and polydispersity ultimately reducing from 7.9 ± 5.8 nm to 3.4 ± 1.4 nm.

For NPs less than 10 nm, the peak wavelength doesn't change significantly with size.[139] This is in line with the approximately constant peak wavelengths shown in Table 4-1 and Table 4-2, and the TEM images show NPs with an average diameters of less than 10 nm. The increasing FWHM can possibly be explained by the change in the *larger* NPs, where the size increases (particularly in the 0.25 mm IJR case). These NPs which are larger than 10 nm, cause a shift in peak wavelength for this population of the NPs, causing a widening of the FWHM. This is one possible explanation and there could be some other phenomenon which explains the widening of the FWHM.

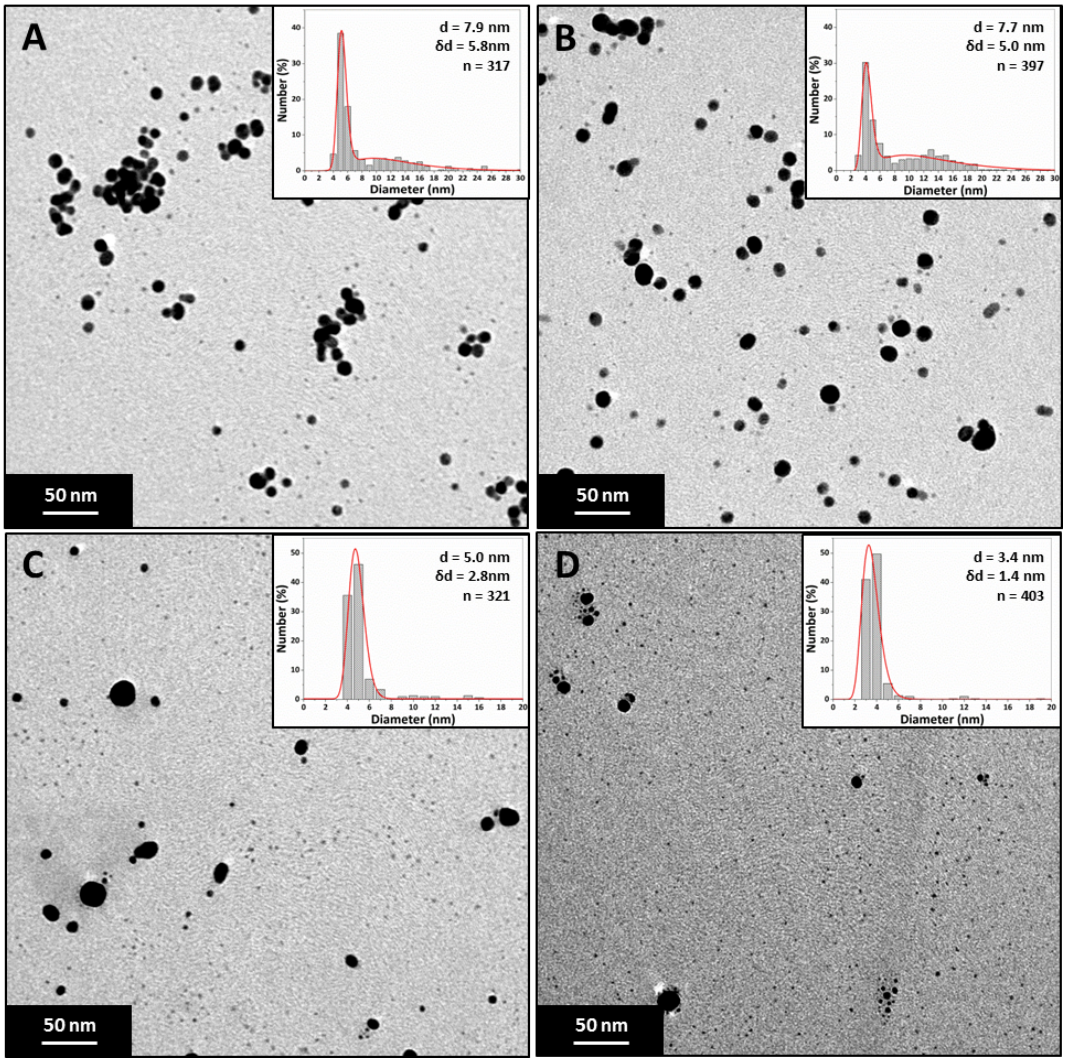

Figure 4-6: TEM images and particle size distributions of silver NPs synthesised at different total flow rates using a 0.5 mm I.D. tubing IJR. (A) 32 ml/min (We: 13), (B) 48 ml/min (We: 29), (C) 64 ml/min (We: 51) and (D) 72 ml/min (We: 65). Concentration of silver nitrate 0.9 mM, trisodium citrate 6 mM in input 1 and sodium borohydride 1.8 mM in input 2.

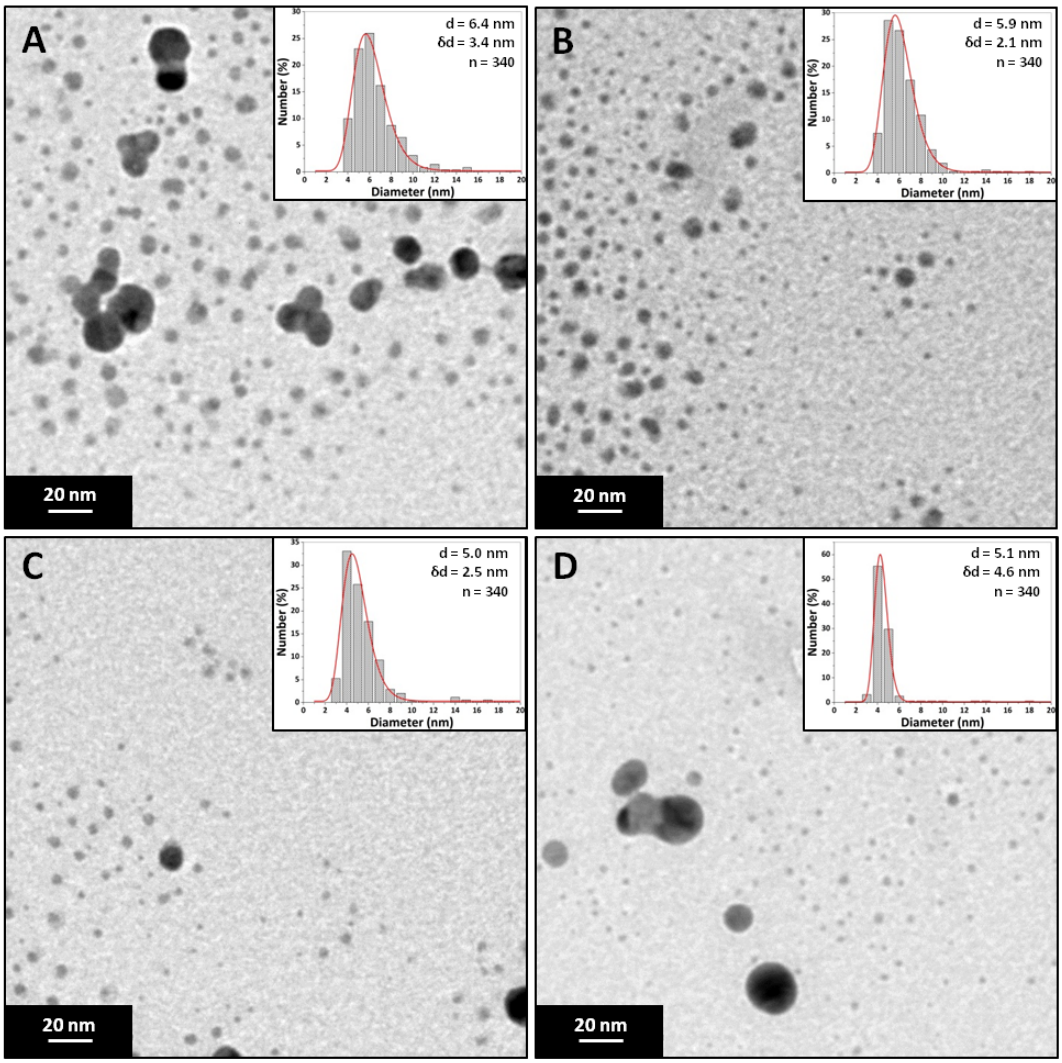

Figure 4-7: TEM images and particle size distributions of silver NPs synthesised at different total flow rates using a 0.25 mm I.D. tubing IJR. (A) 20 ml/min (We: 40), (B) 24 ml/min (We: 58), (C) 28 ml/min (We: 78) and (D) 32 ml/min (We: 102). Concentration of silver nitrate 0.9 mM, trisodium citrate 6 mM in input 1 and sodium borohydride 1.8 mM in input 2.

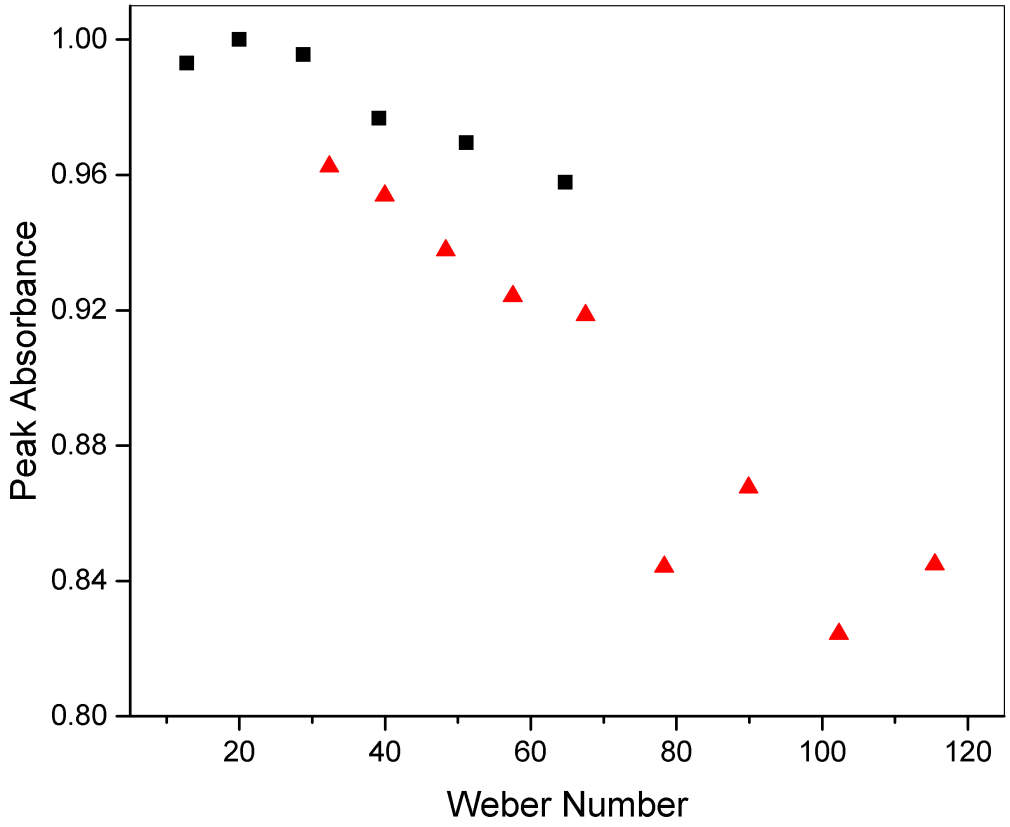

Figure 4-8: Dependence of peak absorbance (peak wavelength 386-389 nm) on Weber number obtained from UV-Vis spectroscopy of silver NPs synthesised at different total flow rates using: i) 0.5 mm (black squares) and ii) 0.25 mm I.D. tubing IJR (red triangles). Concentration of silver nitrate 0.9 mM, trisodium citrate 6 mM in input 1 and sodium borohydride 1.8 mM in input 2.

Table 4-1: FWHM and peak wavelength of silver NPs synthesised in the 0.5 mm IJR using trisodium citrate as a stabilising agent at flow rates between 32 and 72 ml/min. Concentration of silver nitrate 0.9 mM, trisodium citrate 6 mM in input 1 and sodium borohydride 1.8 mM in input 2.

Flow rate (ml/min)	Weber Number	FWHM (nm)	Peak wavelength (nm)
32	13	66	387
40	20	66	386
48	29	67	386
56	39	73	387
64	51	75	387
72	65	77	387

Table 4-2: FWHM and peak wavelength of silver NPs synthesised in the 0.25 mm IJR using trisodium citrate as a stabilising agent at flow rates between 18 and 34 ml/min. Concentration of silver nitrate 0.9 mM, trisodium citrate 6 mM in input 1 and sodium borohydride 1.8 mM in input 2.

Flow rate (ml/min)	Weber Number	FWHM (nm)	Peak wavelength (nm)
18	129	72	389
20	160	72	389
22	193	74	387
24	230	77	387
26	270	78	389
28	313	79	389
30	360	87	386
32	409	91	388
34	462	89	388

4.7.2 Effect of weber number on silver NP synthesis 2 (PVA system)

The Weber number effect on silver NPs was also investigated in the 0.5 mm and 0.25 mm IJRs using PVA as a stabilizing agent. Concentrations of input 1 were 0.9 mM silver nitrate, 0.02 wt% PVA and for input 2 were 1.8 mM sodium borohydride. Total flow rates for the 0.5 mm IJR ranged from 32 ml/min to 72 ml/min and for the 0.25 mm IJR ranged from 18 ml/min to 42 ml/min (repeatability of the synthesis is shown in Appendix C, Figure C2). PVA as a surfactant affects the surface tension of the aqueous solution. The surface tension for water is 72 mN/m and it is estimated that PVA reduces it to a value between 60-65 mN/m.[168] Although there is a small increase in Weber number because of reduced surface tension using PVA, the hydrodynamics observed showed minimal change when compared to using water only (see Appendix C, Figure C3).

Figure 4-9 shows TEM images for NPs synthesized in the 0.5 mm IJR at 32, 48, 64 and 72 ml/min, where the average diameter and dispersity of the NPs are 5.4 ± 1.6 nm, 4.9 ± 1.1 nm, 4.6 ± 1.1 nm and 4.2 ± 1.1 nm. Using this jet diameter, the NP size decreases with increasing Weber number (up to a maximum of We: 65). T-tests yielded p-values < 0.001 when comparing the PSDs. The dispersity of the NPs does not change significantly with increasing Weber number. One of the differences from the trisodium citrate stabilized system is a notable lack of larger NPs, resulting in lower polydispersity. This difference can be attributed to the PVA molecules used as ligands which provide a bulkier steric stabilization as opposed to the electrostatic stabilization of the smaller citrate molecule, leading to a stronger barrier to prevent growth through coalescence of NPs.

Figure 4-10 shows TEM images for NPs synthesized in the 0.25 mm IJR at 18, 26, 34 and 42 ml/min, where the average diameter and dispersity of the NPs are 4.3 ± 1.0 nm, 4.7 ± 1.3 nm, 4.3 ± 0.7 nm and 4.6 ± 1.1 nm. The size and dispersity do not seem to be correlated with the Weber number in this case. T-test yielded p-values of 0.68 when comparing 18 and 34 ml/min, 0.22 when comparing 26 and 42 ml/min and < 0.001 in all other cases. It appears that in the 0.25 mm IJR there is not a discernible change of NP size when compared to the 0.5 mm jets, especially with p-values suggesting there is no difference between 18 and 34 ml/min and 26 and 42 ml/min.

Figure 4-11 shows the peak absorbance vs. Weber number obtained from UV-Vis spectroscopy for the silver NPs obtained using the 0.5 mm IJR (We=13- 65) and the 0.25 mm IJR (We=32-176). In terms of stability, the UV signal changed in the first 15 min after synthesis, but remained stable after 30 min and up to 2 hr. After 24 hr there was a 16% increase in peak absorbance. For the 0.5 mm IJR, the peak absorbance decreases with increasing Weber number. For the 0.25 mm IJR, the peak absorbance decreases minimally as the Weber number increases. This indicates that in the 0.5 mm IJR case the NP size decreases with increasing Weber number, which is in agreement with the TEM observations. In the 0.25 mm IJR case, the peak absorbance trend indicates that the NP size changes minimally with increasing Weber number, again in agreement with TEM observations. Table 4-3 and Table 4-4 show the FWHM and peak wavelength for silver NPs synthesised using PVA as a stabilising agent at various flow rates in the 0.5 mm and 0.25 mm IJR respectively. Similar to the trisodium citrate system, the FWHM for the 0.5 mm IJR increases significantly after a flow rate 48 ml/min and the peak wavelength remains fairly constant. Again, similar to the trisodium citrate system, there is a gradual increase in the FWHM with increasing flow rate for the 0.25 mm IJR, while the peak wavelength stay approximately constant except for the highest flow rate where it decreases by 4 nm.

PVA has a much higher molecular weight than trisodium citrate and is expected to be more effective at stabilising the NPs through adsorption onto the silver NP surface through its hydroxyl groups, which are numerous along the chain.[169, 170] Citrate molecules, which are much smaller, adsorb on the surface of the NPs through their carboxyl groups (citrate has three carboxyl groups as opposed to the many hydroxyl groups on a PVA chain).[171] Another aspect of the two ligands is the effect they have on the kinetics of the reduction reaction and subsequent nucleation of NPs. It is possible that the ligands interact with the precursor in different ways; trisodium citrate behaves as a buffer and affects the solution pH, whereas PVA does not behave in this manner. Literature indicates that the PVA molecule slows down growth of silver NPs compared to reduction with no ligand present, by investigating the evolution of absorbance over time.[172] This reduction in growth rate is most likely because of the bulky nature of the PVA, which would make it more difficult for clusters of silver to approach a growing nucleus. It is suggested that, since trisodium citrate molecules are smaller than PVA, they would allow a closer approach for silver clusters in solution to the NP surface (literature suggests various cluster sizes such as formation of Ag_{13} and Ag_2^+).[82, 84] The presence of highly concentrated silver nitrate zones in the liquid using an IJR in the case of citrate capped NPs will likely result in growth at the surface of the NP through coalescence of silver clusters. The possible reason that no *larger* NPs are seen using the PVA are that it provides a much larger barrier on the NP surface, inhibiting the approach of silver clusters and rapid growth in areas that are rich in silver nitrate. At the same time, the stabilising effect of borohydride can be taken into account. There is a balance between how quickly reduced silver clusters can approach and incorporate onto the NP surface vs. the abundance of borohydride in the vicinity of the NP. As mixing efficiency increases, there is a better distribution of borohydride, resulting in a suppressed growth rate and smaller NPs, which is the observed effect using PVA as a ligand in the 0.5 mm IJR. Using the 0.25 mm IJR, which yields a more constant size with increasing flow rate, the size of the NPs does not fall below *ca*. 4 nm with increasing mixing efficiency. The size of the NPs using the 0.25

mm IJR fluctuates between 4.3 and 4.7 nm. The reason for this fluctuation seems to be due to the flow regime in the 0.25 mm IJR, with the unstable rim region contributing to a fluctuating size which is not as repeatable as a stable rim. The repeatability data for the PVA system (Appendix C, Figure C2) also indicates that silver NPs synthesized in the 0.25 mm IJR show more fluctuation in absorbance as compared to the 0.5 mm IJR, further suggesting that the unstable rim contributes to the fluctuating NP size in the 0.25 mm IJR system. It is expected that improved mixing efficiency should result in a reduction in size as explained above and observed in the 0.5 mm IJR. However this reduction in size is not seen with improving mixing efficiency in the 0.25 mm IJR because the PVA may be imposing a limit on the size of NPs. The synthesis was repeated in the 0.5 mm IJR at a We=65 using double the concentration of PVA (0.04 wt%). The size was reduced from 4.2 ± 1.1 nm to 3.7 ± 1.0 nm, suggesting that the PVA concentration is one of the factors that determine the NP size (TEM image and PSD for this experiment are shown in Appendix C, Figure C4). This suggests that to achieve NPs smaller than 4 nm, an increase in PVA would be required, otherwise once a certain mixing efficiency is achieved; the size of the NP doesn't decrease at a fixed PVA concentration. The increase in FWHM in the case of both the 0.5 mm IJR and 0.25 mm IJR is interesting, given the peak wavelength doesn't change. The decrease in peak absorbance and constant peak wavelength in consistent with a reduction in size of NPs below the 10 nm size and the dispersity doesn't seem to significantly increase according to the TEM analysis. Interestingly, the same effect was seen in terms of the FWHM trend when using trisodium citrate as a stabilising agent and this warrants further investigation.

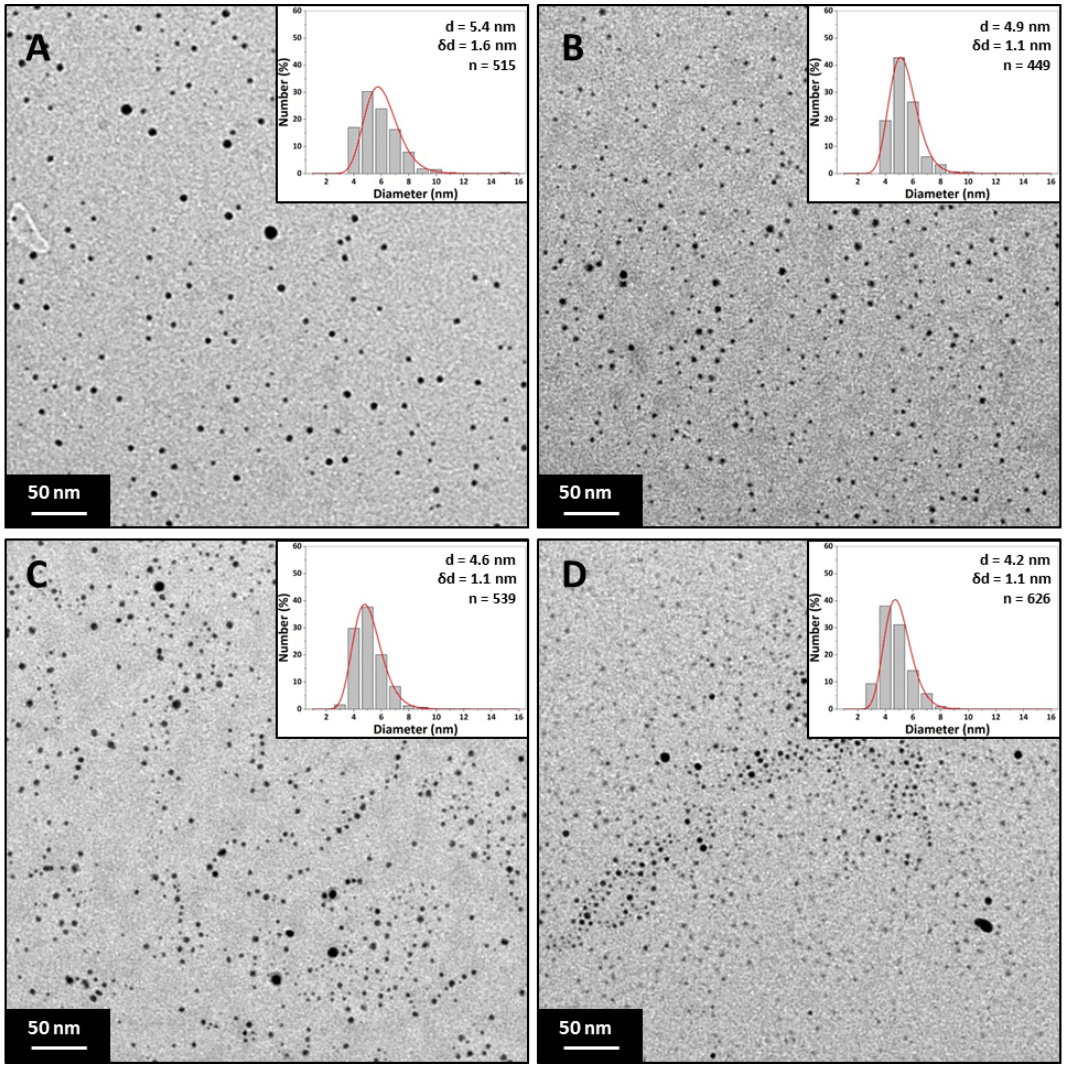

Figure 4-9: TEM images and particle size distributions of silver NPs synthesized at different total flow rates using a 0.5 mm I.D. tubing IJR. (A) 32 ml/min (We: 13), (B) 48 ml/min (We: 29), (C) 64 ml/min (We: 51) and (D) 72 ml/min (We: 65). Concentration of silver nitrate 0.9 mM, PVA 0.02 wt% in input 1 and sodium borohydride 1.8 mM in input 2.

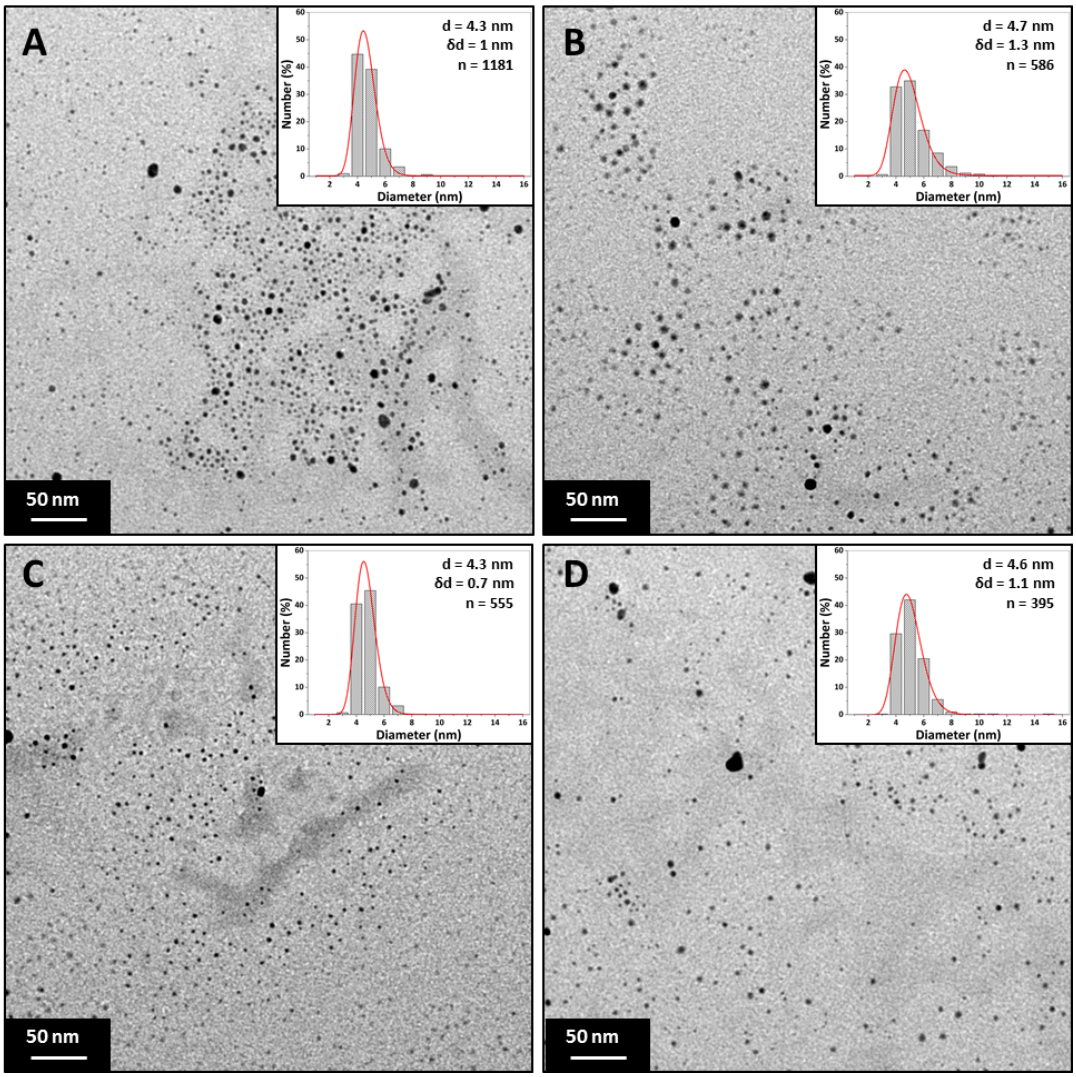

Figure 4-10: TEM images and particle size distributions of silver NPs synthesized at different total flow rates using a 0.25 mm I.D. tubing IJR. (A) 18 ml/min (We: 32), (B) 26 ml/min (We: 68), (C) 34 ml/min (We: 115) and (D) 42 ml/min (We: 176). Concentration of silver nitrate 0.9 mM, PVA 0.02 wt% in input 1 and sodium borohydride 1.8 mM in input 2.

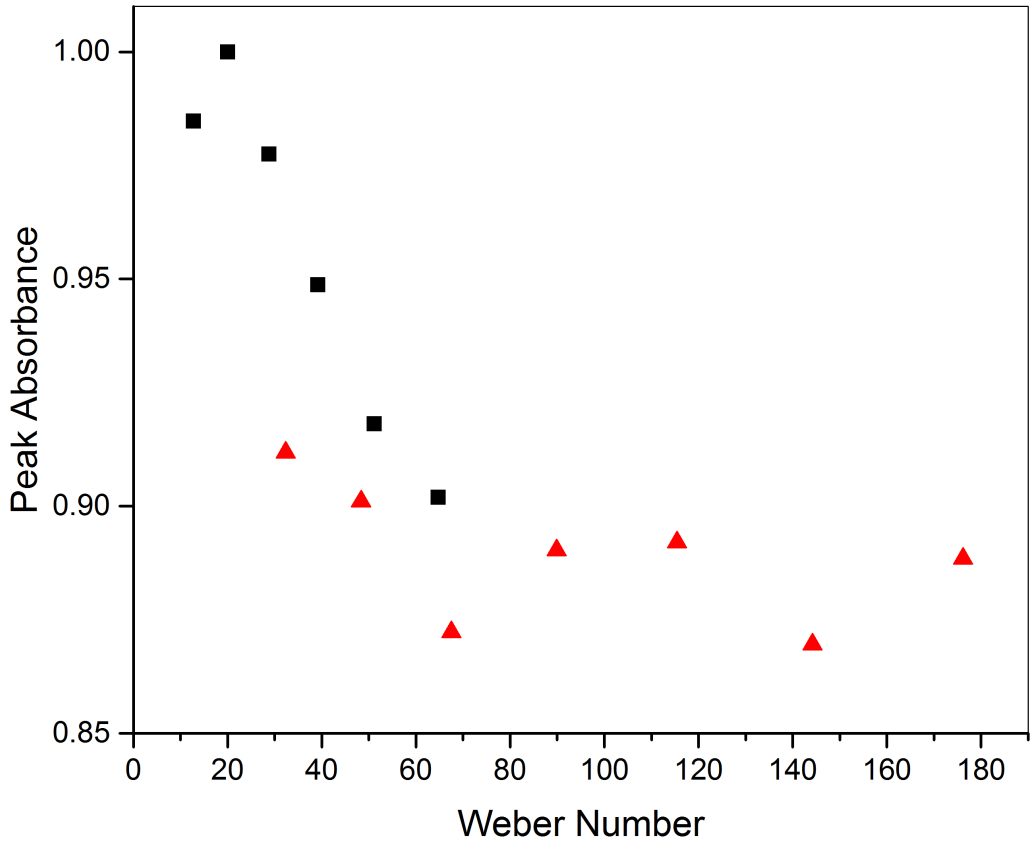

Figure 4-11: Dependence of peak absorbance (peak wavelength 398-401 nm) on Weber number obtained from UV-Vis spectroscopy of silver NPs synthesised at different total flow rates using: i) 0.5 mm (black squares) and ii) 0.25 mm (red triangles) I.D. tubing IJR. Concentration of silver nitrate 0.9 mM, PVA 0.02 wt% in input 1 and sodium borohydride 1.8 mM in input 2.

Table 4-3: FWHM and peak wavelength of silver NPs synthesised in the 0.5 mm IJR using PVA as a stabilising agent at flow rates between 32 and 72 ml/min. Concentration of silver nitrate 0.9 mM, PVA 0.02 wt% in input 1 and sodium borohydride 1.8 mM in input 2.

Flow rate (ml/min)	Weber Number	FWHM (nm)	Peak wavelength (nm)
32	13	80	400
40	20	81	401
48	29	82	398
56	39	86	400
64	51	91	400
72	65	93	400

Table 4-4: FWHM and peak wavelength of silver NPs synthesised in the 0.25 mm IJR using PVA as a stabilising agent at flow rates between 18 and 34 ml/min. Concentration of silver nitrate 0.9 mM, PVA 0.02 wt% in input 1 and sodium borohydride 1.8 mM in input 2.

Flow rate (ml/min)	Weber Number	FWHM (nm)	Peak wavelength (nm)
18	32	93	401
22	48	95	400
26	68	93	399
30	90	97	400
34	115	99	400
38	144	101	399
42	176	100	395

4.8 Conclusions

The impinging jet reactor (IJR) was characterized visually and using the Villermaux-Dushmann test reaction system to investigate the flow regime and mixing efficiency under a range of flow rates and jet diameters of 0.25 mm and 0.5 mm. A maximum mixing efficiency was identified at a Weber number of ca. 90, and it was found to correspond to the point at which the flow regime transitions from a stable rim sheet/chain like pattern to an unstable rim according to visual observation of the impinging jets. This point is identified as the transition from a reflective to a transmitive type atomization.

Two different ligands for silver NP synthesis were investigated using the IJR: trisodium citrate, which electrostatically stabilizes NPs, and PVA, which is a large chain molecule that sterically stabilizes NPs. Trisodium citrate produced more polydisperse silver NPs. Average size was reduced with increasing flow rate because of increased mixing efficiency, reducing the silver nitrate rich zones occurring in the mixing zone after impingement. Increasing mixing efficiency in the PVA system past a Weber number *ca*. 60 did not yield smaller size NPs suggesting a limit of size achievable using PVA as a ligand, possibly due to the small amount of PVA present. More monodispersed NPs are obtained using PVA, indicating that it is more efficient at stabilizing the NPs since it has more potential sites available for adsorption onto the surface of the NP than the citrate molecule, and it kinetically hinders growth during NP formation. Figure 4-12 shows the diameter of the synthesised silver NPs against the Weber number for all the synthesis conditions tested. The overall trend shows that the NP diameter decreases with increasing Weber number when the Weber number is relatively low, and then the decrease is less pronounced and levels off as Weber number increases to relatively high numbers. The trend matches well with that of the dependence of mixing time on the Weber number, however it must be noted that the trend is also influenced by the surfactant that is used (PVA concentration appears to limit the size that can be achieved in that synthesis). The decreasing size of NP with increasing number was more apparent when citrate was used as a surfactant. The lack of fouling and the efficient mixing in the IJR are the main benefits for the synthesis of NPs. The size of the NPs can be reduced with increasing mixing efficiency while also reducing polydispersity. The IJR is scalable through a 'scale-out' procedure of essentially increasing the number of IJRs operating in tandem, making it suitable for large scale synthesis of NPs.

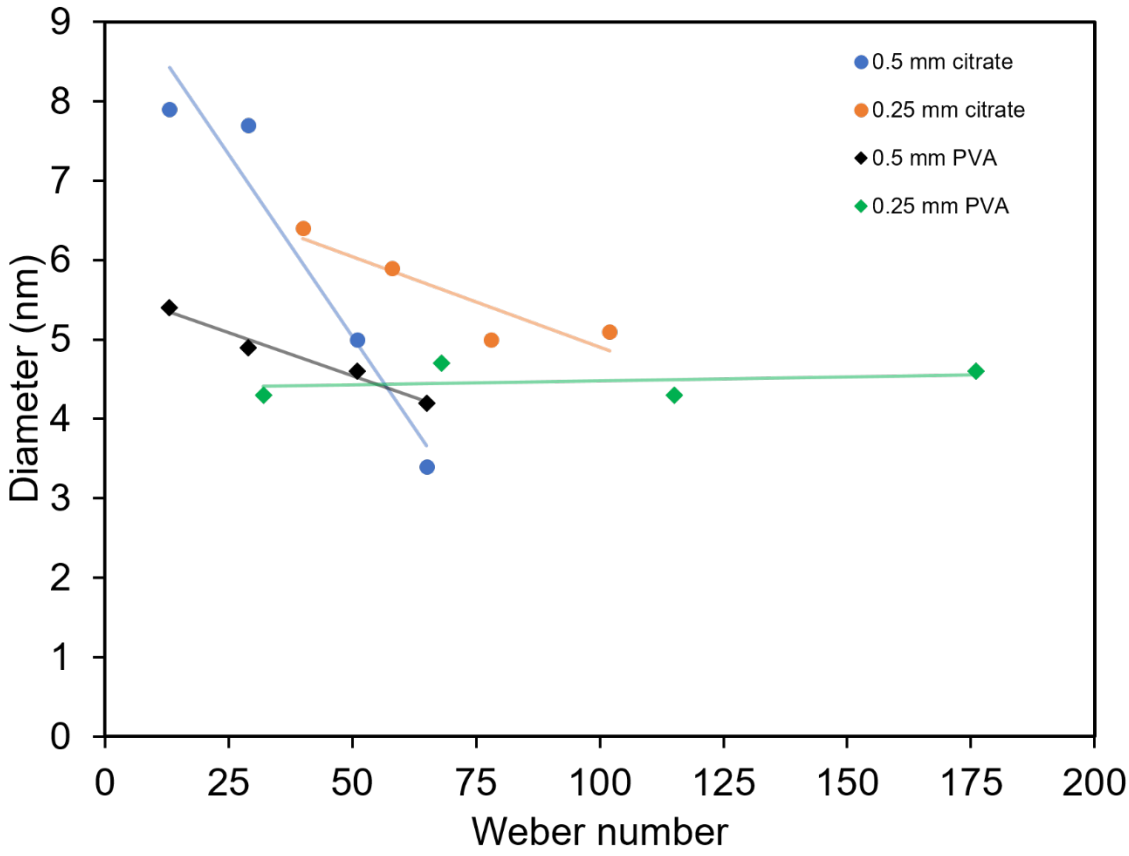

Figure 4-12: Dependence of silver nanoparticle diameter on the Weber number. Data shown is for 0.5 mm and 0.25 mm IJRs and for both citrate and PVA surfactants.

5 Effect of hydrodynamics and mixing conditions on the continuous synthesis of gold and silver nanoparticles in a coaxial flow device

There are many studies in the literature on the synthesis of gold and silver NPs. Two more common synthesis methods were used in this study: the well-known Turkevich synthesis for gold NPs[88] and the reduction of silver nitrate via sodium borohydride in the presence of trisodium citrate for silver NPs.

The Turkevich method for synthesising gold NPs is perhaps the most common, and there are many studies in which batch reactors were used.[89-106, 173] Flow syntheses of gold NPs using the Turkevich method are less common. Ftouni *et al*. synthesized gold NPs with the Turkevich method using a fused silica capillary and a t-mixer to mix chloroauric acid to sodium citrate prior to introducing them into the heated capillary.[107] Residence times within the capillary were varied between 35 to 94 s and they obtained NPs in the size range between 1.5 and 3 nm, with larger NPs being obtained at longer residence times. A minimum size of NPs was found at around 3.15 ratio of citrate to gold. The temperature effect was investigated, and NP size decreased with increasing temperature in the range between 60 and 100°C. Sugano *et al*. synthesized gold NPs in the size range 10-45 nm using a y-type micromixer with a pulsed flow of chloroauric acid and sodium citrate to mix the reagents within a small channel at room temperature.[108] Mixing efficiency was altered by adjusting the pulsing rate between 50,100 and 200 Hz. The NP size increased with a higher pulsing frequency, suggesting faster mixing resulted in larger NPs. Weng *et al*. synthesized gold NPs using the Turkevich method recipe using a novel microfluidic device.[40] Hexagonal NPs of around 35 nm were obtained at a temperature of 115°C with reaction time in the order of 2 to 5 min. There are also various studies in which gold NPs were synthesized with methods other than that of Turkevich in flow reactors.[109-112, 127]

Silver NPs are commonly synthesized in batch with sodium borohydride used to reduce the silver precursor.[5, 64, 66, 67, 69, 70] SAR mixer type reactors[71] and PTFE chambers[65] have been utilized to synthesize silver NPs in flow using borohydride, obtaining NPs in the range of 10-20 nm for borohydride to silver nitrate ratios ranging from 3 to 40. We have also previously used the CFR and an impinging jet reactor for synthesis of silver NPs using borohydride as a reducing agent.[145, 174]

The CFR has been used to synthesize a variety of different NPs such as titania,[128] zirconia,[129] iron oxide,[35, 36, 130] polymer,[131, 175, 176] nickel,[132] palladium[177] and gallium nitride.[178] The SAR mixer uses the principle of reducing the diffusion distance between multiple streams that are required to mix and can be categorized as a serial lamination device. SAR mixers have been employed for the synthesis of gold and silver NPs.[71, 109, 127] Parallel lamination devices are similar to serial lamination but the reduction in diffusion distance is done in one step rather than multiple ones, and these have also been used for the synthesis of NPs.[110, 112] The CFI is primarily used as a heat transfer device in the literature,[179, 180] and can be used as an inline mixer[181] but has not been used specifically for the synthesis of NPs.

A variety of different configurations were used in this study, with the focal point being the CFR, for the synthesis of gold and silver NPs were employed in this study. The CFR works on the basis of a cylindrical inner stream of reagent which is sheathed by a cylindrical outer stream of reagent, creating a

reaction interface between the streams. The configurations used either: added an extra flow component following the CFR for a specific purpose or, by altering the hydrodynamics within the CFR. Flow components that were used in conjunction with the CFR were: coiled flow inverter (CFI) for the synthesis of gold NPs using a Turkevich recipe where tetrachlorauric acid and trisodium citrate are mixed and heated, and a split and recombine (SAR) mixer for the synthesis of silver NPs through reduction of silver nitrate by sodium borohydride in the presence of trisodium citrate. Schematic representations of these flow components can be seen in Figure 5-1.

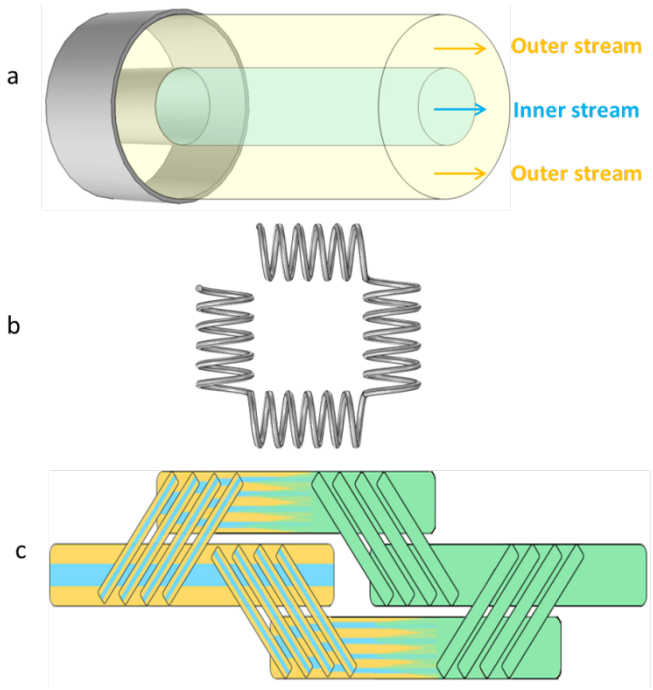

Figure 5-1: Schematic representations of components used in the microfluidic flow setup: a: coaxial flow reactor, b: coiled flow inverter and c: split and recombine mixer.

The CFI was used as a residence loop following the CFR because of its mixing characteristics. It has ideal properties in synthesizing NPs because of an improved residence time distribution.[182] This improvement arises from enhanced mass transfer because of a secondary flow developing within a helically coiled channel, known as 'Dean flow'. This is characterized by the Dean number, which is the ratio between the square root of the product of inertial and centripetal forces over viscous forces:

$$De = \sqrt{\frac{d}{2r}}\,\frac{\rho u d}{\mu} = \sqrt{\frac{d}{2r}}\,Re$$

where d is the diameter of the channel, r is the radius of curvature of the coil, ρ is the fluid density, u is the mean velocity of the fluid, μ is the viscosity of the fluid and Re is the Reynolds number, the ratio of inertial to viscous forces. The mixing is further improved when this secondary flow is inverted, as in the CFI, by introducing 90° bends in the helically coiled channel. The SAR is a device which improves mixing by reducing the diffusion distance between streams by continuously splitting and recombining the flow

into thinner and thinner interdigitated lamellae. Hydrodynamic changes in the CFR when one operates at a higher Re number as opposed to laminar flow by increasing the velocity of the inner stream or when one changes the thickness of the inner stream to reduce the diffusion distance. The various components and hydrodynamic conditions were chosen in an effort to demonstrate what the effect of mass transfer is on the synthesis of gold and silver NPs in the CFR.

NPs were synthesized under a variety of different hydrodynamics and mixing conditions to understand how these could affect size and dispersity. As mentioned previously, understanding how to control size and dispersity is important because it allows NPs to be tailored for specific applications. Two systems were studied in this work: the synthesis of gold NPs in the CFR in conjunction with the CFI using the Turkevich method recipe and the synthesis of silver NPs in the CFR in conjunction with the SAR mixer, as well as the CFR in isolation, using sodium borohydride to reduce silver nitrate in the presence of trisodium citrate. The effect of flow rate (or residence time) and temperature on NP size and dispersity were investigated for the gold NP system. The effect of silver concentration on the NP size and dispersity was investigated using the CFR with SAR mixer system. Using the CFR in isolation, the silver NP synthesis was performed at high Re, to investigate the effect of hydrodynamics silver NP size and dispersity, and the effect of changing the internal diameter of the inner tube in a laminar flow regime (to reduce the diffusion distance of the inner stream) on NP size and dispersity was investigated.

5.1 Experimental

5.1.1 Chemicals

Silver nitrate ($AgNO_3$, 0.01 M stock solution), trisodium citrate ($HOC(COONa)(CH_2COONa)_2 \cdot 2H_2O$, powder form, sodium borohydride solution ($NaBH_4$, ~12 wt% in 14 M NaOH stock solution) and gold (III) chloride hydrate ($HAuCl_4.xH_2O$, powder form) were obtained from Sigma. All chemicals were used without further purification and solutions were prepared with ultrapure water (resistivity 15.0 MΩ·cm).

5.1.2 Experimental Setup

Syringe pumps (Pump 11 Elite OEM module, Harvard) were used to deliver the reagents. The setup for gold NP synthesis using the CFR followed by a CFI acting as a residence time loop, as can be seen in Figure 5-2. The CFR consisted of a 0.798 mm internal diameter (I.D.) inner glass tube (1.09 mm external diameter) and a 2 mm I.D. outer glass tube with the length from the outlet of the inner tube to the outlet of the CFR of 21 mm. Upstream, the capillaries were connected using an ETFE T-piece connector (0.5 mm thru-hole, Upchurch Scientific) which was drilled to a diameter of 2 mm to allow the inner tube to be inserted into the outer tube. The inner tube was inserted into a 1 mm I.D. PTFE tube sleeve (1.59 mm external diameter) to keep the tube stables within the larger outer tube. Downstream, the CFR was connected to the CFI by using an ETFE union (0.75 mm thru-hole, Upchurch Scientific). The CFI was a 3.5 m 1 mm I.D. PTFE tube that had nineteen 90° bends with 20 arms, each arm consisting of 5.5 coils (length also includes entrance and exit length of tubing). The coils had an axial pitch of 3 mm, while the coil diameter was 8 mm. The coils were fabricated by drilling 1.6 mm holes (using a Roland EGX-400 engraving machine) into a PTFE plate (2 mm thickness, Direct Plastics) and the PTFE tubing was threaded through these holes which were arranged to result in coiling with the dimensions stated above. The CFR

and CFI were immersed in a glycerol bath (GR150, Grant Instruments) with temperature being varied between 60-100°C. The tetrachloroauric acid was fed through a preheating CFI consisting of four 90° bends and similar axial pitch and coil diameter as the CFI described above to ensure it came into contact with the trisodium citrate at the desired temperature. The outlet of the CFI was split to a waste container and a sample container. These containers were pressurized using nitrogen gas and a backpressure regulator, which was set to 2 bars to prevent vaporization of water within the reactor.

The setups used for the synthesis of silver NPs can be seen in Figure 5-3. The CFR used was similar to that in the gold NP synthesis, but the length from the inner tube outlet to the outlet of the CFR was 130 mm (a longer length was used for additional residence time) while the inner tube I.D. used was between 0.142mm and 0.798 mm (between 0.559 mm and 1.09 mm external diameter). A glass SAR mixer (Micromixer chip, Dolomite microfluidics) was placed downstream of the CFR in order to enhance the mixing by laminating the stream into thinner striations. The SAR mixer had an internal channel diameter of 0.125 mm x 0.35 mm (depth x width) of the main channel and 0.05 mm x 0.125 mm of the secondary channels responsible for splitting the flow. The internal volume was 8 µl. The CFR was connected to the SAR using an ETFE union (0.75 mm thru-hole, Upchurch Scientific). Following the SAR, a 10 cm long 1 mm I.D. PTFE tube delivered the silver NPs to the sample container.

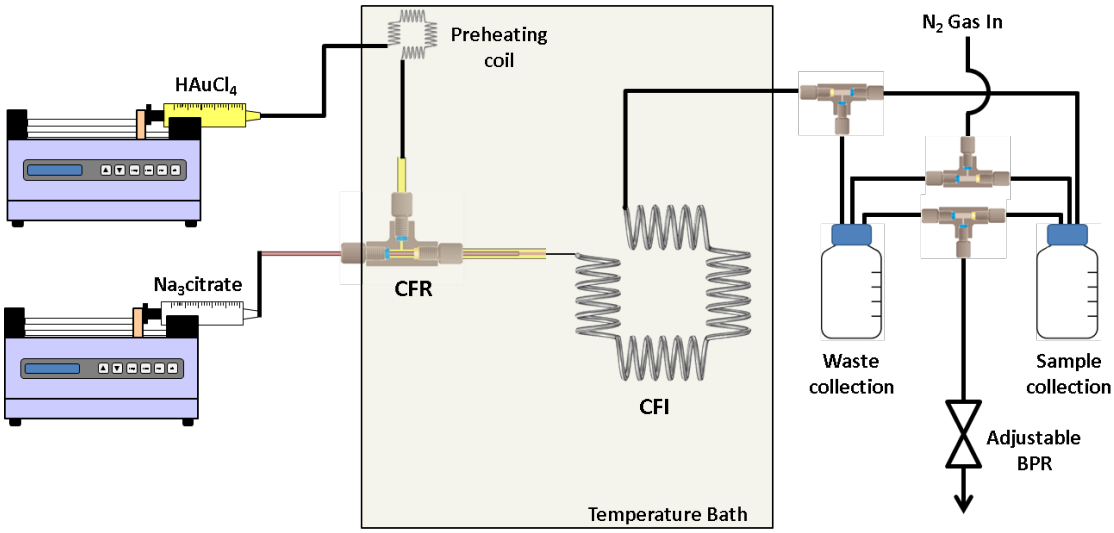

Figure 5-2: Schematic representation of experimental setup for gold NP synthesis.

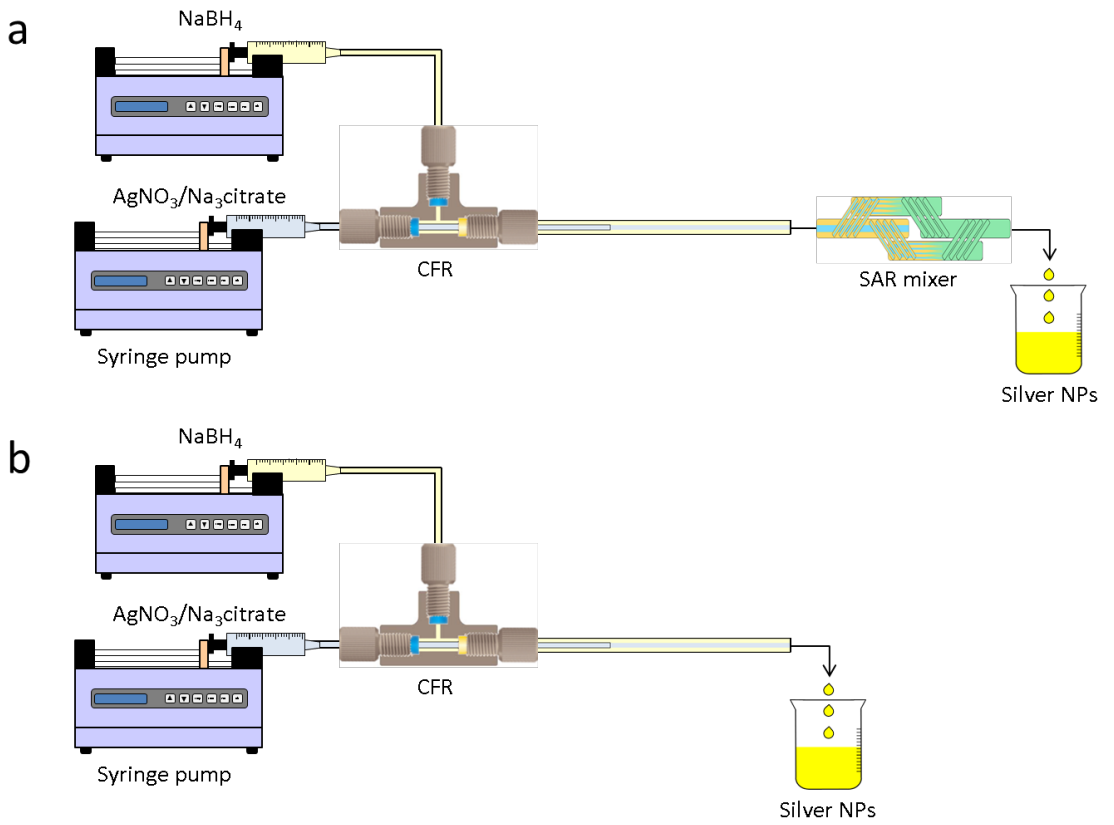

Figure 5-3: Schematic representation experimental setup for silver NP synthesis: a) CFR used in conjunction with SAR and b) CFR used in isolation.

5.1.3 Nanoparticle synthesis

For the gold NP synthesis, initially the reactor setup was filled with tetrachloroauric acid before the system was pressurized using nitrogen gas and a backpressure regulator set to 2 bar. The reactor setup was then immersed in the temperature bath (60-100°C). A trisodium citrate solution and tetrachloroauric acid were diluted to the appropriate concentrations and pumped through the inner and outer streams of the CFR respectively. It was found that filling the reactor with tetrachloroauric acid prior to synthesis reduced the amount of fouling drastically. The reactor was then operated at the appropriate flow rate, and one reactor volume was allowed to pass through at high temperature and collected in the waste container before the outlet of the CFI was switched to sample collection to collect 10 ml of sample. Small amounts of fouling were observed when the reactor was operated at a flow rate of 0.25 ml/min towards the end of the CFI. It was suspected this is because the long residence time enabled citrate to diffuse towards the channel walls which would increase pH. The surface charge of PTFE is close to zero at pH 3.5, which is coincidentally around the pH of the tetrachloroauric acid.[183] This was the reason for the reduction in fouling, since a reactor filled with a mixture of citrate and precursor prior to immersion in the temperature bath resulted in increased fouling at the channel walls. The surface charge would be negative in the pH range near neutral (which is the pH when mixing citrate and tetrachlorauric acid at these concentrations), which probably attracts NPs in the growth phase because of the positive Au ion adsorbed onto the surface of the NP. Thus it is beneficial to allow a small layer of tetrachloroauric acid to remain at the wall to keep the surface charge neutral. In laminar flow the layer

will remain for some time before citrate diffuses near the wall because of the flow profile and non-slip condition at the walls of the reactor. This is evidenced by small amounts of fouling only occurring at 0.25 ml/min where the relative residence time is longer.

For the silver NP synthesis, silver nitrate and trisodium citrate solutions were premixed to the appropriate concentration and pumped through the inner stream. Sodium borohydride/sodium hydroxide solution was diluted to the appropriate concentration and pumped through the outer stream of the CFR. Sodium borohydride was stored in 14 M sodium hydroxide; hence the concentration of sodium hydroxide was 3.21 times higher than the stated sodium borohydride concentration in all cases. Silver NP syntheses were carried out at room temperature (22-24°C). All concentrations are those at the inlets before any mixing of reagents occurs, unless stated otherwise.

5.1.4 Characterization of nanoparticles

NPs were analysed using a UV-Vis spectrometer (USB 2000+ Spectrometer and DT-Mini-2-GS light source, Ocean Optics). Silver NPs were analysed within an hour of synthesis (the signal of the samples were stable in this window of time). Gold NPs were analysed over time and were analysed once the signal was stable (the signal became stable usually after 1-2 days). NP samples were diluted with additional ultrapure water to bring the absorbance into a suitable range (i.e. obeying the Beer-Lambert law and avoiding saturation of the light detector) if necessary and the data were normalized so that the maximum absorbance in the particular set of experiments tested represented an absorbance of 1. Transmission electron microscope images were captured using a JEOL 1200 EX ii microscope with a 120 kV acceleration voltage. Carbon coated copper TEM grids were prepared within an hour of synthesis for silver NPs and when the sample was stable for gold NPs by pipetting a 5 µl sample onto the grid and allowing it to dry at room temperature. When preparing the sample, the droplet placed on the grid is small to allow for quicker drying and for the ring of aggregated NPs to be identified easily (as discussed in Chapter 3). Particle size distributions (insets for each TEM image presented) have the following nomenclature: d is average diameter, δd is the standard deviation of the NP distribution and n is the number of particles counted to obtain the particle size distribution. Differential centrifugal sedimentation analysis (CPS disc centrifuge UHR, Analytik) was carried out on gold NPs when the samples were stable. PEBBLES software was used for the counting and sizing of TEM images of the synthesised silver NPs. ImageJ software was used for the counting and sizing of TEM images of the synthesised gold NPs. PEBBLES software tends to be better for lower contrast images where the outlines of the NPs are harder to distinguish, in this case it was more suitable to use this program for silver NPs. The ImageJ software can count and size NPs faster than PEBBLES, but works better with higher contrast images. Gold NP images were suitably high contrast to obtain accurate size distributions using ImageJ.

5.2 Results and discussion

5.2.1 Effect of increasing flow rate on gold nanoparticle size and dispersity

The effect that the flow rate has on the gold NPs was investigated in the CFR with an inner tube internal I.D. of 0.798 mm and an outer tube I.D. of 2 mm. The concentration of trisodium citrate was 0.09 M

through the inner tube; the concentration of tetrachlorauric acid was 0.557 mM through the outer tube. The volumetric flow rate ratio was fixed at 32.3:1 (Q_{out}:Q_{in}) and the total flow rate was varied between 0.25 and 3 ml/min. The molar flow rate ratio was 1:5 ($HAuCl_4$:Na_3citrate). The Reynolds numbers varied between 3 and 32 in the CFR and between 5 and 63 in the CFI. The Dean numbers were ranged from 1.9 to 22.4 in the CFI which is above the threshold of 1.5 required for fully developed Dean flow.[182]

Figure 5-4 shows TEM images of gold NPs synthesized at a flow rate of 0.25, 0.5, 0.75, 1, 1.5, 2 and 3 ml/min where the average diameter and dispersity of the NPs are 18.9 ± 2.3 nm, 18.4 ± 2.8 nm, 19.7 ± 2.4 nm, 17.9 ± 2.1 nm, 20.6 ± 7.2 nm, 21.7 ± 3.3 nm and 23.9 ± 4.7 nm respectively. Figure 5-5 shows corresponding DCS measurements, where the average diameter is 16.7 ± 2.8 nm, 15.1 ± 3.6 nm, 16.4 ± 3.0 nm, 14.9 ± 2.3 nm, 18.5 ± 3.1 nm, 22.5 ± 3.8 nm and 26.4 ± 4.0 nm nm respectively. The trend of the average diameter of the NPs matches with that observed from TEM images. Figure 5-6 shows UV-Vis spectra of gold NPs synthesized at a flow rate of 0.25, 0.5, 0.75, 1, 1.5, 2 and 3 ml/min. Experiments at selected flow rates were repeated three times and analyzed using DCS (shown in Appendix D, Figure D1).The average size of the NPs from 0.25 ml/min to 1 ml/min changes minimally according to the TEM and DCS analysis (although t-tests show that all PSDs are statistically different to a significance value of at least 0.05). The molar extinction coefficient increases with size for gold NPs,[184, 185] therefore for a constant number concentration of NPs, an increase in peak absorbance would indicate increasing size. However, the number concentration of NPs of changing size would change for a constant gold concentration i.e. larger NPs synthesized at the same gold concentration would have a lower number concentration. Hendel *et al*. showed that the absorbance at 400 nm of citrate capped gold NPs in the 15-30 nm range increases linearly with increasing size for a constant gold concentration.[186] This suggests a larger size has a more significant effect on the absorbance then number concentration of NPs. Figure 5-6 shows that there is an increase in the absorbance at 400 nm with increasing flow rate but it is unlikely that this is because of increasing size since TEM and DCS show a more constant size in the 0.25-1 ml/min range. The peak wavelength should redshift with increasing size,[184] but the wavelength changes minimally between 523 - 525 nm further suggesting there is a minimal change in size. One possible explanation for the increase in absorbance up to 1 ml/min may be related to fouling. Fouling was observed at the lowest flow rate suggesting an increase of fouling with decreasing flow rate. This explains the decrease in absorbance at lower flow rates (despite a constant NP size) since some of the gold remains within the reactor. Increasing the flow rate from 1.5 ml/min to 3 ml/min shows an increase in the size of the NPs from 20.6 to 23.9 nm according to TEM analysis, and from 18.5 to 26.4 nm according to DCS analysis. The peak absorbance increases with increasing flow rate in this range and the peak wavelength increases from 525 to 529 nm, which indicates an increase in the size of the NPs consistent with DCS and TEM data.

The data shows that the size stays fairly constant between 0.25 and 1 ml/min and thereafter increases up to a flow rate of 3 ml/min. This can be rationalized as follows. In the CFR section, there is a laminar flow where the outer flow of tetrachloroauric acid focuses the inner flow of trisodium citrate. There is little mixing in this region. Mass transfer occurs through diffusion at the interface between the two streams. In the more acidic conditions of the tetrachloroauric acid stream, the reaction rate is faster

and nucleation is favored. In the more basic conditions in the trisodium citrate stream, the reaction rate is slower. This is because of the speciation of the precursor, in acidic conditions the speciation is favoured towards $AuCl_4^-$,[95, 102, 104] whereas in more basic conditions the speciation passes through various forms from $AuCl_3OH^-$ to $AuOH_4$. As the gold species acquire more hydroxyl ions, the reactivity decreases and there is a transition from nucleation of gold atoms into clusters to growth of gold onto existing clusters. In the CFR region of the reactor, the tetrachloroauric acid and the trisodium citrate remain well separated and only exchange material through diffusion at the interface. In this region, a higher reaction rate and hence nucleation will occur in the tetrachloroauric acid stream. Therefore, the CFR behaves as a nucleation section. Further along in the CFI residence loop, the streams are subjected to Dean flow and flow inversion. These enhance the mixing and lower the reduction rate of gold ions, hence transitioning from the nucleation section in the CFR to a growth section in the CFI. Given this, the longer nucleation can be maintained, the smaller the resultant NPs should be obtained. In this study, there is a marked increase in the size of the NPs as the flow rate increases past 1 ml/min, supporting the hypothesis of nucleation dominating in the CFR, since at higher flow rates, reactions at the interface of streams do not persist as long. There is a limitation on size reduction when operating below 1 ml/min, which may be related to a decrease in citrate concentration. The decrease in citrate concentration would result in a decrease in reduction of gold precursor, leading to a suppression of nucleation within the CFR section. Finally, the Peclet number for the syntheses was >> 1 at all flow rates, indicating that mass transport was advection dominated (Table 5-1 shows Peclet number for the CFR section where the I.D. was 2 mm and the diffusion coefficient used was 1.4×10^{-9} m^2/s,[187] which is for tetrachlorauric acid, the Peclet number is doubled for those shown in the table for the CFI where the I.D. was 1 mm). Increasing Peclet number indicated decreasing significance of diffusion on the process, so agrees with the ideas discussed above to explain why the gold NP size increases with increasing flow rate.

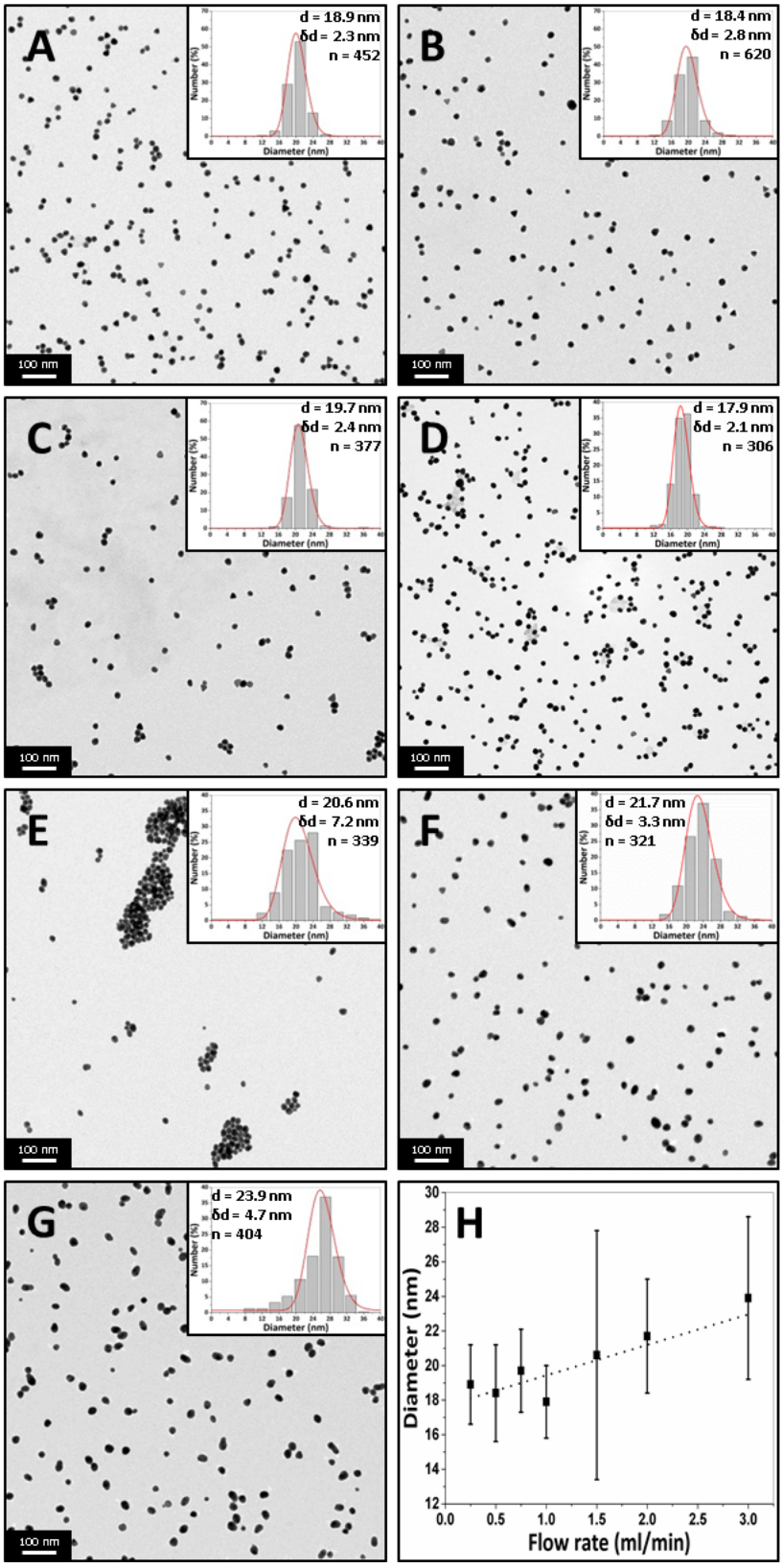

Figure 5-4: TEM images of gold NPs synthesized using the CFR with a CFI residence loop at a flow rate of A: 0.25 ml/min ,B: 0.5 ml/min, C: 0.75 ml/min, D: 1 ml/min, E: 1.5 ml/min, F:2 ml/min and G: 3 ml/min. H: Average diameter of gold NPs vs flow rate of synthesis (bars represent standard deviation of the size). Concentration of tetrachloroauric acid, 0.557 mM; concentration of trisodium citrate, 0.09 M; volumetric flow rate ratio, 32.3: 1 (Q_{out}:Q_{in}, $HAuCl_4$: Na_3citrate); molar flow rate ratio, 1:5 ($HAuCl_4$: Na_3citrate); temperature, 80°C.

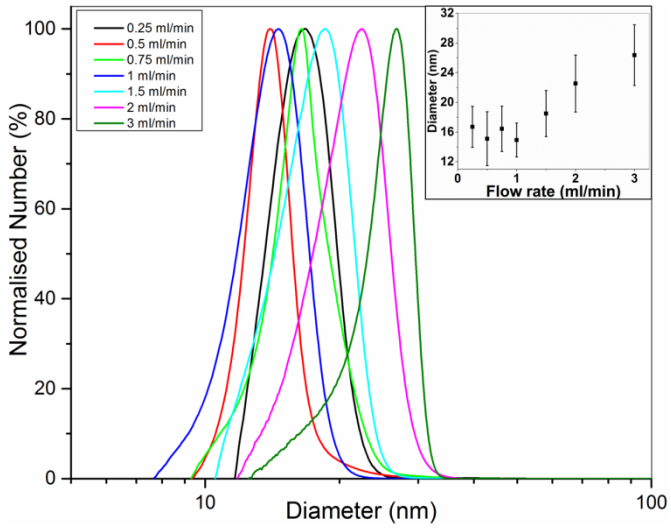

Figure 5-5: Normalized DCS curves of gold NPs synthesized using the CFR with a CFI residence loop at flow rates between 0.25 and 3 ml/min. Inset: Diameter of gold NPs vs. flow rate of synthesis (bars represent standard deviation of size). Concentration of tetrachloroauric acid was 0.557 mM and concentration of trisodium citrate was 0.09 M. Concentration of tetrachloroauric acid, 0.557 mM; concentration of trisodium citrate, 0.09 M; volumetric flow rate ratio, 32.3: 1 (Q_{out}:Q_{in}, $HAuCl_4$: Na_3citrate); molar flow rate ratio, 1:5 ($HAuCl_4$: Na_3citrate); temperature, 80°C.

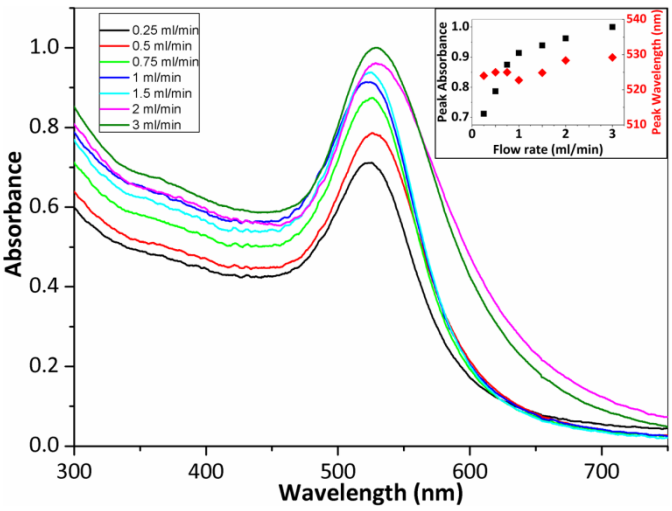

Figure 5-6: UV-Vis spectra of gold NPs synthesized using the CFR with a CFI residence loop at flow rates between 0.25 and 3 ml/min. Inset: Peak absorbance (black squares) and peak wavelength (red diamonds) of gold NPs vs. flow rate of synthesis analyzed using UV-Vis spectroscopy. Concentration of tetrachloroauric acid, 0.557 mM; concentration of trisodium citrate, 0.09 M; volumetric flow rate ratio, 32.3: 1 (Q_{out}:Q_{in}, $HAuCl_4$: Na_3citrate); molar flow rate ratio, 1:5 ($HAuCl_4$: Na_3citrate); temperature, 80°C.

Table 5-1: Diameter and dispersity of gold NPs synthesised at various flow rates with corresponding Peclet number

Flowrate (ml/min)	Peclet Number	Diameter (nm)	Dispersity (nm)
0.25	1.9×10^3	18.9	± 2.3
0.5	7.6×10^3	18.4	± 2.8
0.75	11.4×10^3	19.7	± 2.4
1	15.2×10^3	17.9	± 2.1
1.5	22.7×10^3	20.6	± 7.2
2	30.3×10^3	21.7	± 3.3
3	45.5×10^3	23.9	± 4.7

5.2.2 Effect of temperature on gold nanoparticle size and dispersity

The effect that the temperature has on gold NPs synthesis was investigated in the CFR with an inner tube internal I.D. of 0.798 mm and an outer tube internal I.D. of 2 mm. The concentration of trisodium citrate was 0.09 M through the inner tube, while the concentration of tetrachlorauric acid was 0.557 mM through the outer tube. The volumetric flow rate ratio was fixed 32.3:1 (Q_{out}:Q_{in}) and the total flow rate was fixed at 1 ml/min. The molar flow rate ratio was 1:5 ($HAuCl_4$:Na_3citrate). The Reynolds number in the CFR was 11 and in the CFI was 21. In the CFI, the Dean number was 7.5.

Figure 5-7 shows TEM images of gold NPs synthesized at a temperature of 60, 70, 80, 90 and 100°C where the average diameter and dispersity of the NPs are 25.5 ± 5.7 nm, 22.7 ± 3.9 nm, 17.9 ± 2.1 nm, 18.6 ± 2.1 nm and 19.4 ± 2.4 nm respectively. T-tests for the PSDs showed p-values of < 0.001 when comparing all PSDs, indicating statistical difference to a significance level of 0.001. Figure 5-8 shows corresponding DCS measurements, where the average diameter is 31.1 ± 5.5 nm, 18.4 ± 3.8 nm, 14.9 ± 2.3 nm, 16.2 ± 3.4 nm and 17.6 ± 2.7 nm respectively. The trend of the average diameter of the NPs matches that observed in the TEM images. Figure 5-9 shows corresponding UV-Vis spectra.

The average size of the NPs decreased from 25.5 nm to 17.9 nm when increasing the temperature from 60 to 80°C and then increased slightly to 19.4 nm when increasing the temperature from 80 to 100°C. DCS characterization also shows similar trends. The peak absorbance is highest at 70°C after which it decreases with increasing temperature while the peak wavelength changes from 528 to 523 nm from 60 to 80°C and from 523 to 525 nm from 80 to 100°C. The characterization confirms that there is a minimum at 80°C. Turkevich *et al*. also observed a minimum size of 16.5 nm at 80°C.[88] Chow and Zukoski found that NPs had approximately the same size at synthesis temperatures of 60, 70 and 80°C but it took longer for NPs at lower temperatures to arrive at the final size.[91] Wuithschick *et al*. found a minimum of NP size at 60°C using the Turkevich method,[104] while Piella *et al*. found a minimum at 70°C.[105] Increasing temperature affects a number of factors in the synthesis. The conversion of $AuCl_4^-$ species to hydroxylated species speeds up at higher temperatures meaning that nucleation period also terminates faster as the more reactive species is converted to less reactive species. Note also that the equilibrium shifts to more hydroxylated forms at higher temperatures.[104] However, the rate of reduction of $AuCl_4^-$ at higher temperatures would also speed up, resulting in a higher nucleation rate in a shorter

time period. Finally, the size of the stable nuclei would also be slightly larger at higher temperatures because of the larger thermal energy available.[104] Thus, there is a balance of competing effects, resulting in a minimum size at an intermediate temperature. A further point to note is that the heat transfer and mixing would also play a role in how the temperature affects the resultant NPs. For instance in batch synthesis, the citrate is injected at room temperature to boiling citrate, and so, depending on the amount and nature of the injection, the reaction could take place at different temperatures in localized regions around the injection point, which may explain the variety of results reported in the literature.

The repeatability of the synthesis was investigated by repeating the experiment at each temperature three times and characterizing the size using DCS (Appendix D, Figure D2). The repeatability in size was found to be worst at 60°C and improved with increasing temperature up to 80°C, after which it remained fairly constant.

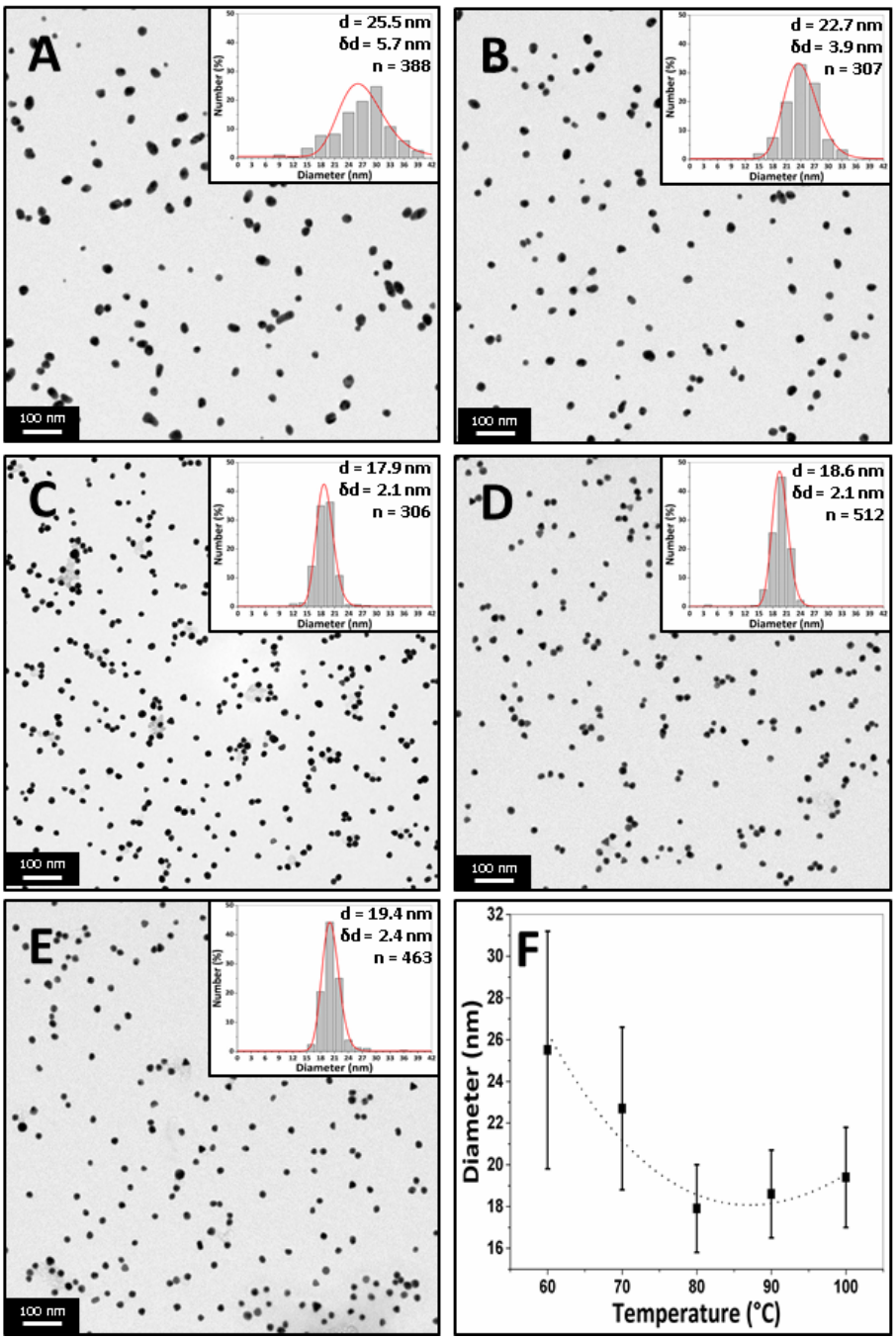

Figure 5-7: TEM images of gold NPs synthesized using the CFR with a CFI residence loop at a temperature of A: 60°C, B: 70°C, C: 80°C, D: 90°C, E: 100°C. F: Average diameter of gold NPs vs temperature of synthesis (bars represent standard deviation of the size). Concentration of tetrachloroauric acid, 0.557 mM; concentration of trisodium citrate, 0.09 M; volumetric flow rate ratio, 32.3: 1 (Q_{out}:Q_{in}, $HAuCl_4$: Na_3citrate); molar flow rate ratio, 1:5 ($HAuCl_4$: Na_3citrate); flow rate, 1 ml/min.

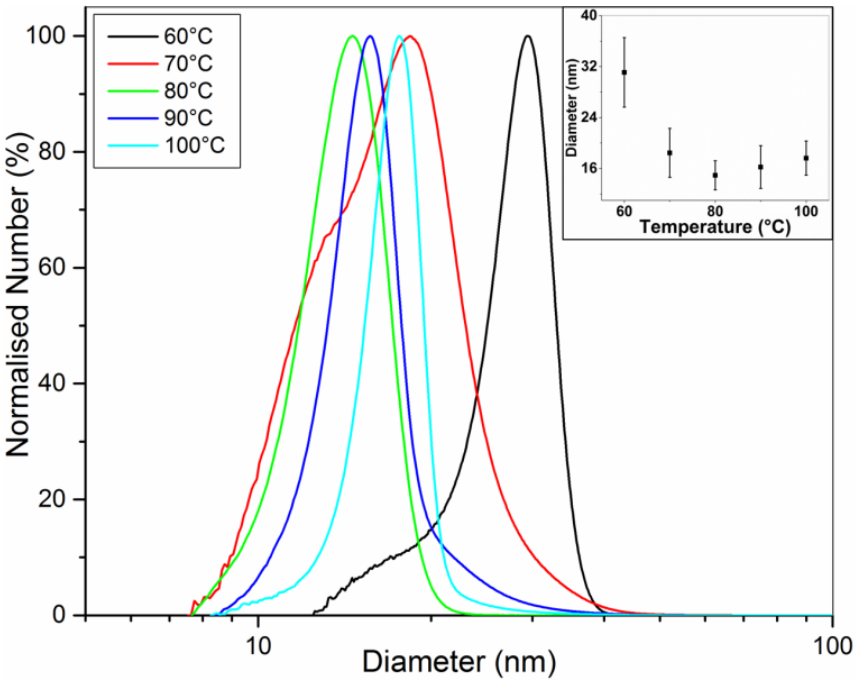

Figure 5-8: Normalized DCS curves of gold NPs synthesized using the CFR with a CFI residence loop at temperatures between 60 and100°C. Inset: Diameter of gold NPs vs. temperature of synthesis (bars represent standard deviation of size). Concentration of tetrachloroauric acid, 0.557 mM; concentration of trisodium citrate, 0.09 M; volumetric flow rate ratio, 32.3: 1 (Q_{out}:Q_{in}, $HAuCl_4$: Na_3citrate); molar flow rate ratio, 1:5 ($HAuCl_4$: Na_3citrate); flow rate, 1 ml/min.

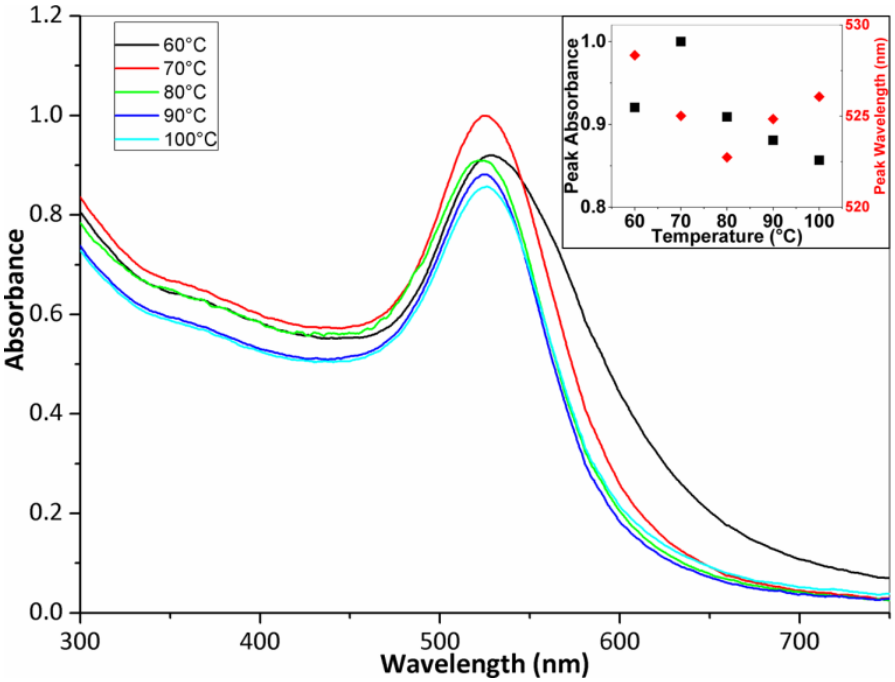

Figure 5-9: UV-Vis spectra of gold NPs synthesized using the CFR with a CFI residence loop at temperatures between 60 and 100°C. Inset: Peak absorbance (black squares) and peak wavelength (red diamonds) of gold NPs vs. temperature of synthesis. Concentration of tetrachloroauric acid, 0.557 mM; concentration of trisodium citrate, 0.09 M; volumetric flow rate ratio, 32.3: 1 (Q_{out}:Q_{in}, $HAuCl_4$: Na_3citrate); molar flow rate ratio, 1:5 ($HAuCl_4$: Na_3citrate); flow rate, 1 ml/min.

5.2.3 Silver nanoparticle synthesis using a coaxial flow device followed by a split and recombine mixer

A SAR mixer was attached onto the CFR to see the effect that multi-lamination would have on the silver NP synthesis. The CFR had an inner tube I.D. of 0.556 mm and an outer tube I.D. of 2 mm. The distance from the inner tube outlet to the outlet of the CFR was 130 mm. The effect that the silver nitrate concentration had on the silver NPs was investigated using this configuration, previously we have studied the effect of silver nitrate concentration using the CFR in isolation.[145] Silver nitrate and trisodium citrate solutions were premixed before pumping through the inner tube with concentration of silver nitrate varied between 0.05 and 0.4 mM, the trisodium citrate concentration was fixed at 0.5 mM. Concentration of sodium borohydride was fixed at 0.3 mM and pumped through the outer tube. The volumetric flow rate ratio was fixed at 1:1 (Q_{out}:Q_{in}) and the total flow rate was fixed at 2.5 ml/min. Experiments were carried out at room temperature between 22-24°C.

Figure 5-10 shows TEM images of silver NPs synthesized at a silver nitrate concentration of 0.05, 0.15, 0.25 and 0.4 mM. The average diameter and dispersity of the NPs were 5.5 ± 2.4 nm, 4.7 ± 2.8 nm, 4.4 ± 1.8 nm and 3.4 ± 1.4 nm. T-tests for the PSDs showed p-values of < 0.001 when comparing all PSDs except when comparing 0.15 and 0.25 mM where the p-value was 0.15. In this case there is no statistical difference between 0.15 mM and 0.25 mM according to the p-value. Figure 5-11 shows corresponding UV-Vis spectra. Peak absorbance increases with increasing concentration, the peak wavelength stays relatively constant between 398-400 nm between 0.05-0.25 mM, however at 0.3 mM the wavelength decreases to 395 nm and at 0.4 mM the wavelength is 392 nm. Although peak wavelength shouldn't change according to Mie theory for silver NPs less than 10 nm,[139] a blue shift in peak wavelength generally indicates smaller NPs.

The laminar flow profile inside the CFR creates an interface between the silver nitrate and sodium borohydride, resulting in mixing through diffusion rather than enhanced by a stretching and thinning of the lamellae though turbulent flow for example. The laminar flow profile prevents reaction in silver nitrate rich zones resulting in smaller NPs. Larger NPs occur in silver nitrate rich zones because the sodium borohydride can reduce multiples of its own stoichiometric equivalent in silver ions,[133-135] resulting in larger and less stable NPs which are able to grow. Through the SAR mixer the laminar flow condition is maintained but the mixing efficiency is increased since the diffusion distance is reduced as the stream is continuously split and recombined in a way to serially laminate the flow into thinner and thinner multiples of the original stream, as well as the creation of an increased number of interfaces between reagents. In the experiments above, increasing silver nitrate concentration, led to higher supersaturation levels and thus a higher nucleation rate resulting in smaller NPs. In previous experiments we have conducted using only the coaxial flow reactor, the opposite trend was observed; NP size increased from 3.7 ± 0.8 nm to 9.3 ± 3 nm with increasing silver concentration from 0.05-0.4 mM with the same sodium borohydride and trisodium citrate concentrations (a comparison is shown in Figure 5-12).[145] This occurred because reaction was not complete in the CFR and the advective mixing in the droplets at the end of the CFR allowed the possibility of sodium borohydride to travel into silver nitrate rich zones, which as discussed previously, would lead to larger NPs. Since downstream mixing is

more controlled with the SAR mixer, silver nitrate rich zones which give rise to larger NPs are less likely to occur. The above indicates that the mixing condition of the fluid at the exit of the CFR has a pronounced effect on NP synthesis.

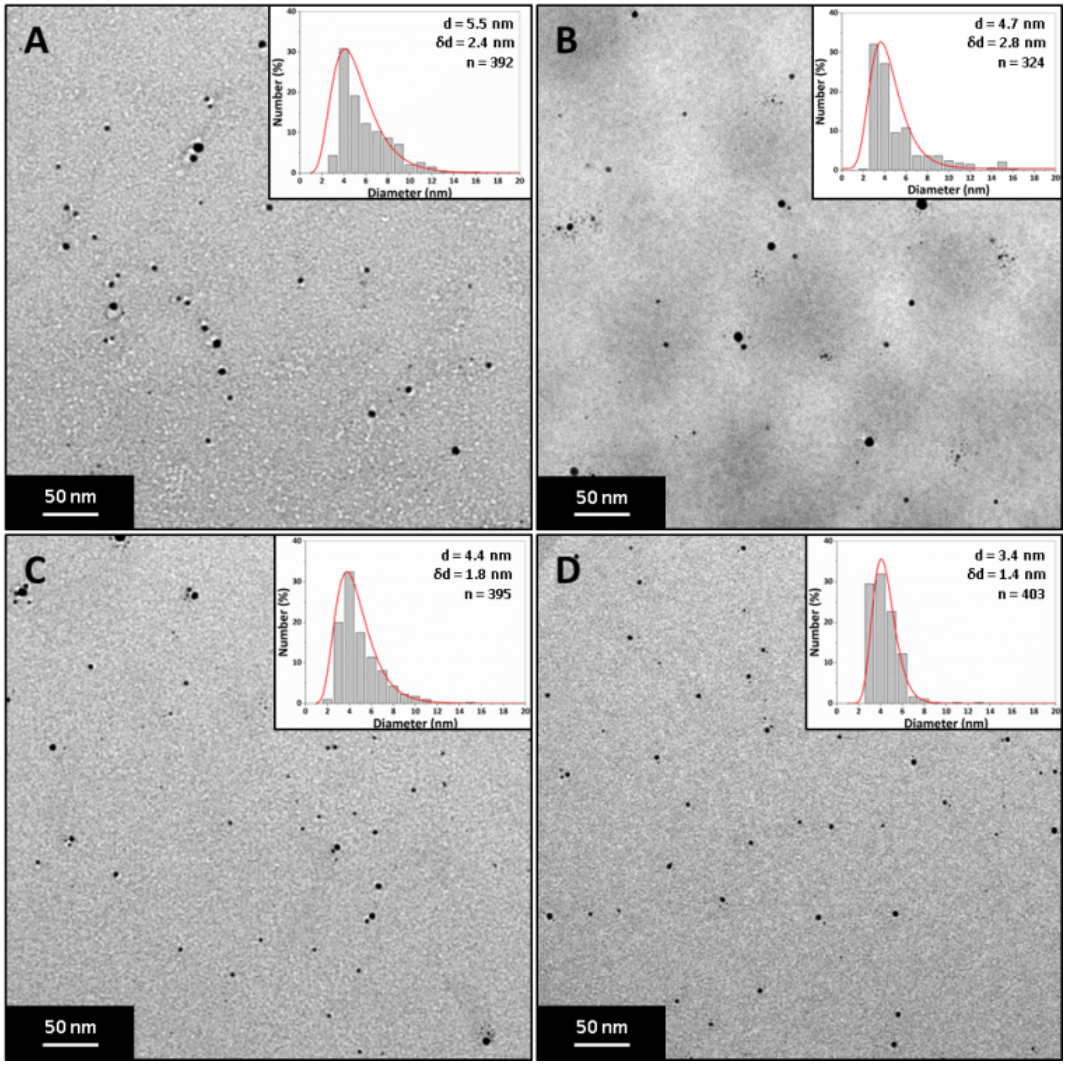

Figure 5-10: TEM images of silver NPs synthesized using the CFR followed by a SAR mixer at a silver nitrate concentration of A: 0.05 mM, B: 0.15 mM, C: 0.25 mM, D: 0.4 mM. Concentration of sodium borohydride, 0.3 mM; concentration of trisodium citrate, 0.5 M; volumetric flow rate ratio, 1: 1 (Q_{out}:Q_{in}, $NaBH_4$: $AgNO_3$); molar flow rate ratio, 0.5-4:3:5 ($AgNO_3$:$NaBH_4$:Na_3citrate); flow rate, 2.5 ml/min; temperature, 22-24°C.

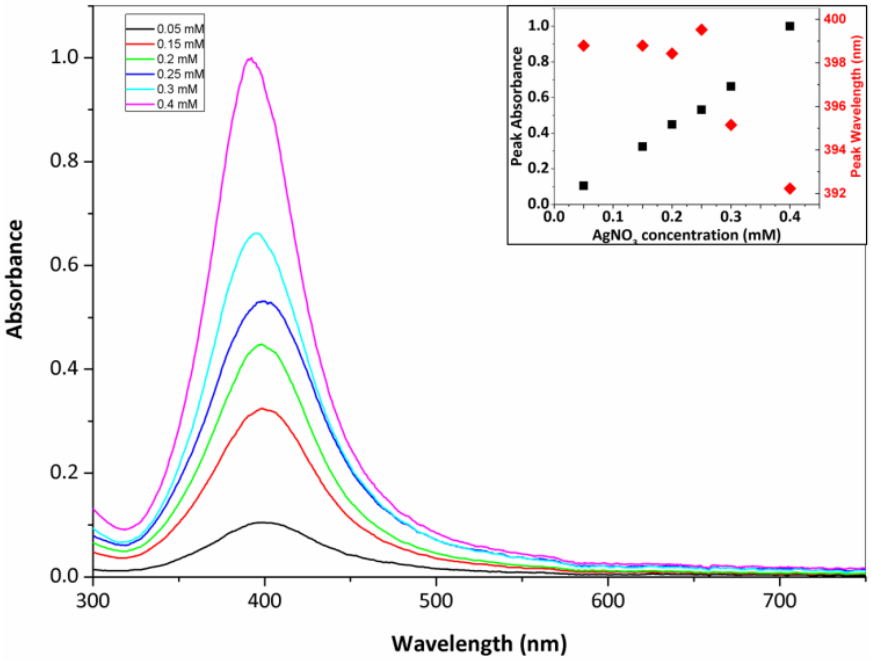

Figure 5-11: UV-Vis spectra of silver NPs synthesized using the CFR followed by a SAR mixer at a silver nitrate concentrations ranging between 0.05 and 0.4 mM. Inset: Peak absorbance (black squares) and peak wavelength (red diamonds) of silver NPs vs. silver nitrate concentration of synthesis. Concentration of sodium borohydride, 0.3 mM; concentration of trisodium citrate, 0.5 M; volumetric flow rate ratio, 1: 1 (Q_{out}:Q_{in}, $NaBH_4$: $AgNO_3$); molar flow rate ratio, 0.5-4:3:5 ($AgNO_3$:$NaBH_4$:Na_3citrate); flow rate, 2.5 ml/min; temperature, 22-24°C.

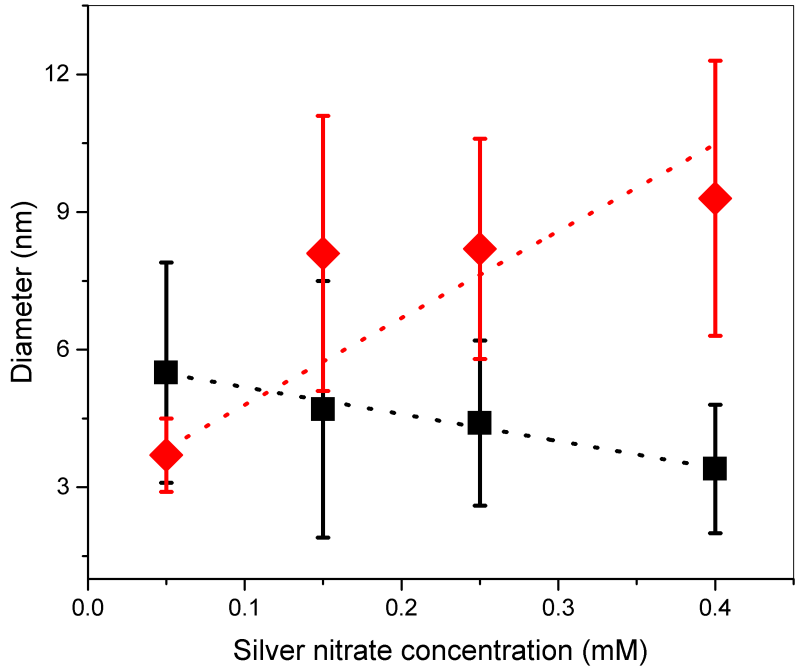

Figure 5-12: Diameter vs. silver nitrate concentration for the CFR operated followed with a SAR (black squares) and without a SAR (red diamonds). Concentration of sodium borohydride, 0.3 mM; concentration of trisodium citrate, 0.5 M; volumetric flow rate ratio, 1: 1 (Q_{out}:Q_{in}, $NaBH_4$: $AgNO_3$); molar flow rate ratio, 0.5-4:3:5 ($AgNO_3$:$NaBH_4$:Na_3citrate); flow rate, 2.5 ml/min; temperature, 22-24°C.

5.2.4 Silver nanoparticle synthesis using a coaxial flow device operated at high Re

In the previous section (5.2.3), we have observed differences in NP synthesis when mixing conditions are altered downstream of the CFR. In this section we investigate the effect of mixing conditions in the CFR itself. This is achieved by using a CFR with low I.D and high flowrate of the inner tube, to increase the Re. Even though turbulent conditions are not achieved, mixing is enhanced by recirculation vortices that appear under these conditions.[188] The CFR had an inner tube I.D. of 0.798 mm and an outer tube I.D. of 2 mm. The distance from the inner tube outlet to the outlet of the CFR was 130 mm. The concentrations of silver nitrate, trisodium citrate and sodium borohydride were varied so that the concentration (assuming full mixing of the streams) for each flow rate tested was fixed at 0.1 mM, 0.5 mM and 0.3 mM respectively. Silver nitrate and trisodium citrate were pumped through the inner tube and sodium borohydride was pumped through the outer tube. The volumetric flow rate ratio was varied between 1:50 and 1:200 (Q_{out}:Q_{in}) and the total flow rate was varied between 5.1 and 20.1 ml/min. The molar flow rate ratio was fixed at 1:3:5 ($AgNO_3$:$NaBH_4$:Na_3citrate). Experiments were carried out at room temperature between 22 and 24°C.

Figure 5-13 shows TEM images of silver NPs synthesized in the CFR with vortex flow. The Reynolds number in the inner tube was in the range 132-530 and in the main channel was in the range 54-212. The average diameter and dispersity was 5.9 ± 1.5 nm, 6.2 ± 2.7 nm, 7.7 ± 3.4 nm and 6.2 ± 2.2 nm for 5.1, 10.1, 15.1 and 20.1 ml/min respectively. Figure 5-14 shows flow visualization of the CFR at a flow rate of 20.1 ml/min to demonstrate the turbulent nature of the flow. Flow visualization using dye and water at other flow rates can be seen in Appendix D (Figure D3).

Flow rates of 5.1, 10.1 and 20.1 ml/min showed similar sizes, although 5.1 ml/min had a lower polydispersity. T-tests showed that p-values were < 0.001 when comparing 15.1 ml/min to any other flow rate, and < 0.05 when comparing 5.1 and 20.1 ml/min. All other flow rate comparisons showed the NP population was not statistically different to any degree of confidence.

The NPs obtained using the CFR operated in vortex flow showed that there were minimal changes and no observable trends as flow rate was increased. Other systems such as iron oxide NPs and polystyrene NPs were synthesized successfully with low dispersity using a CFR operated in turbulent flow,[131] in this case increasing mixing efficiency seemed to have no significant effect on the synthesized NPs in terms of size and polydispersity. This suggests that increasing mixing efficiency doesn't necessarily lead to increased monodispersity because of a perceived improvement in mixing efficiency, although the smallest and least disperse NPs were obtained at the lowest flow rate 5.1 ml/min. Observing the hydrodynamics near the outlet of the inner tube, the concentration of the dye (this would represent silver nitrate in the NP synthesis) spreads across the entire cross section of the channel. The steady state concentration of dye near the channel walls in the section immediately after jet emission from the outlet the inner tube is most dilute at the lowest flow rate and then subsequently becomes more concentrate at higher flow rates. This area then becomes more concentrated in silver nitrate as the flow rate increases. This would explain why there is a lower size and dispersity at the lowest flow rate, where the ratio of silver nitrate to sodium borohydride is lower and hence more stable NPs which are less prone to growth through coalescence are synthesized.

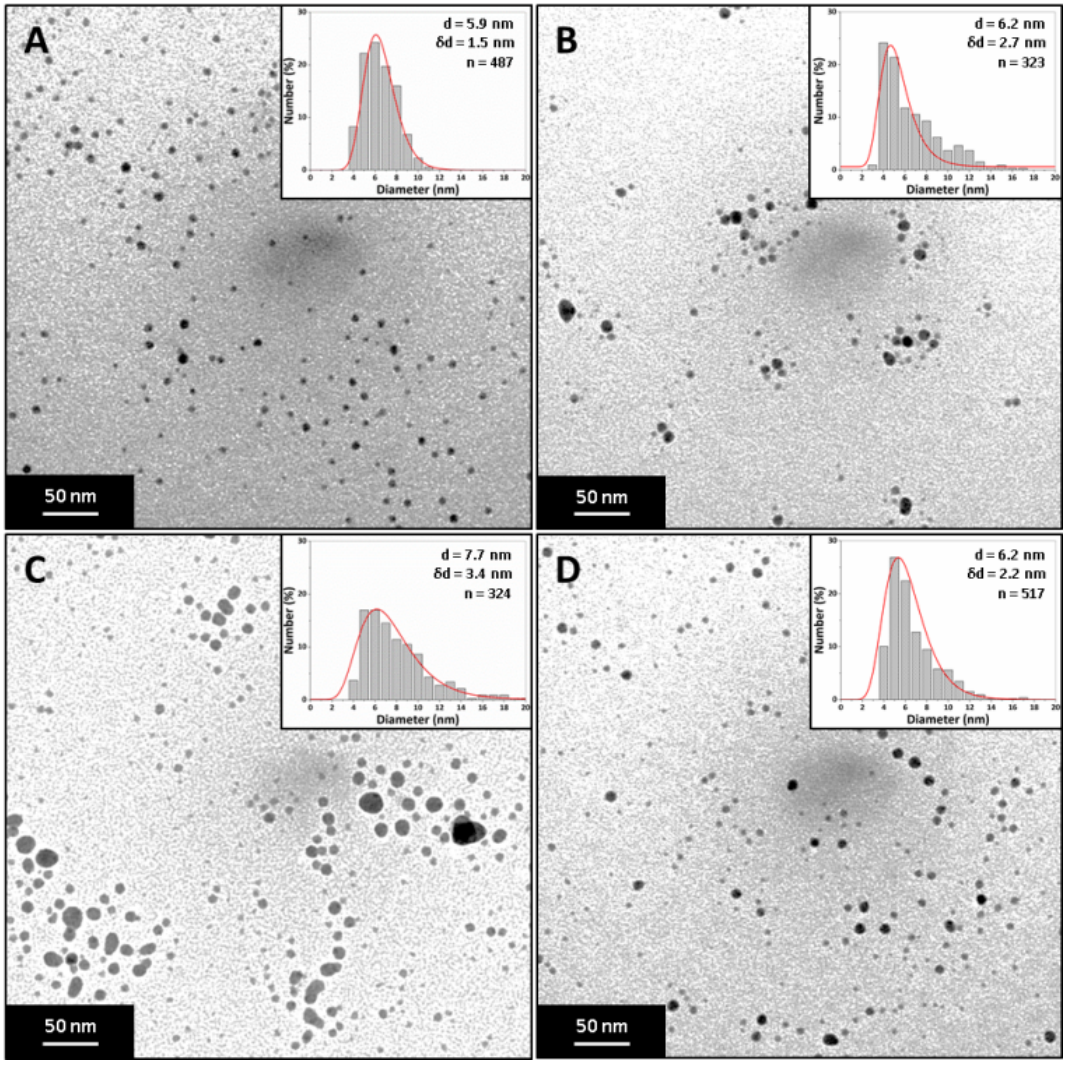

Figure 5-13: TEM image of silver NPs synthesized using the CFR with inner tube I.D. of 0.798 mm operated under high Re with a total flow rate of A: 5.1 ml/min, B: 10.1 ml/min, C: 15.1 ml/min, D: 20.1 ml/min . The outer tube flow rate was fixed at 0.1 ml/min. Concentration of silver nitrate, 0.1 mM; of sodium borohydride, 0.3 mM; concentration of trisodium citrate, 0.5 M (all concentrations stated are those after complete mixing); molar flow rate ratio, 1:3:5 ($AgNO_3$:$NaBH_4$:Na_3citrate); temperature, 22-24°C

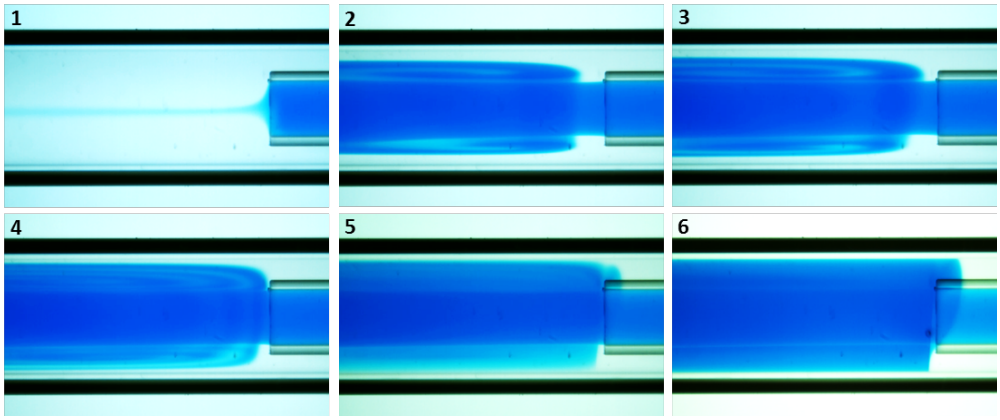

Figure 5-14: Flow visualization of CFR with inner tube I.D. of 0.798 mm operated under turbulent flow conditions. Basic Blue dye was pumped through the inner tube at 20 ml/min and water was pumped through the outer tube at 0.1 ml/min. Re is 520 in the inner tube and 212 in the main channel. Picture 1 is taken before dye is pumped through the inner tube up, Pictures 2-5 as operational time increased, Picture 6 after steady state is reached.

5.2.5 Effect of inner tube internal diameter on silver NP synthesis using the CFR

The effect of the inner tube I.D. on the synthesis of silver NPs in the CFR was investigated by varying the inner tube I.D. between 0.147 and 0.798 mm. The outer tube I.D. was 2 mm and the distance from the inner tube outlet to the outlet of the CFR was 130 mm. The concentration of silver nitrate was 0.1 mM, while the trisodium citrate concentration was fixed at 0.5 mM. These two components were premixed and pumped through the inner tube. Concentration of sodium borohydride was fixed at 0.3 mM; this component was pumped through the outer tube. The volumetric flow rate ratio was fixed at 1:1 (Q_{out}:Q_{in}) and the total flow rate was fixed at 1 ml/min.

Figure 5-15 shows TEM images of silver NPs synthesized at an inner tube diameter of 0.147, 0.345, 0.447, 0.556, 0.701 and 0.798 mm where the average diameter and dispersity of the NPs are 4.7 ± 1.4 nm, 5.9 ± 2.4 nm, 5.9 ± 2.2 nm, 6.6 ± 3.7 nm, 8.8 ± 2.6 nm and 10.5 ± 4.0 nm. T-tests for the PSDs showed p-values of < 0.001 when comparing all PSDs except when comparing 0.345 and 0.447 mm (p-value = 0.91), 0.345 and 0.556 mm (p-value = 0.0012) and 0.447 and 0.556 mm (p-value = 0.0012). In this case there is no statistical difference between 0.345 and 0.447 mm inner tube I.D. according to the p-value. 0.345 and 0.447 mm are statistically different to 0.556 mm to a significance level of 0.01. Figure 5-16 shows corresponding UV-Vis spectra. The peak absorbance showed a maximum at 0.447 mm (UV-vis data of repeats can be seen in Appendix D, Figure D4) and the peak wavelength remained relatively constant between 392 and 394 nm for all diameters.

The size of the NPs increased with an increase in the inner tube I.D. The internal tube I.D. controls the thickness of the inner stream, and hence the diffusion distance across the stream. By using smaller inner tubing I.D., the diffusion distance is reduced. By reducing the diffusion distance, more of the silver nitrate in the inner stream can react with sodium borohydride. As the diffusion distance increases with increasing diameter, there is a larger amount of unreacted silver nitrate at the end of the channel. When droplets form at the outlet, this increases the likelihood of reactions and uncontrolled growth of NPs occurring in silver nitrate rich regions within the droplets. Hence smaller NPs are obtained by reducing the diffusion distance of the silver nitrate stream within the CFR.

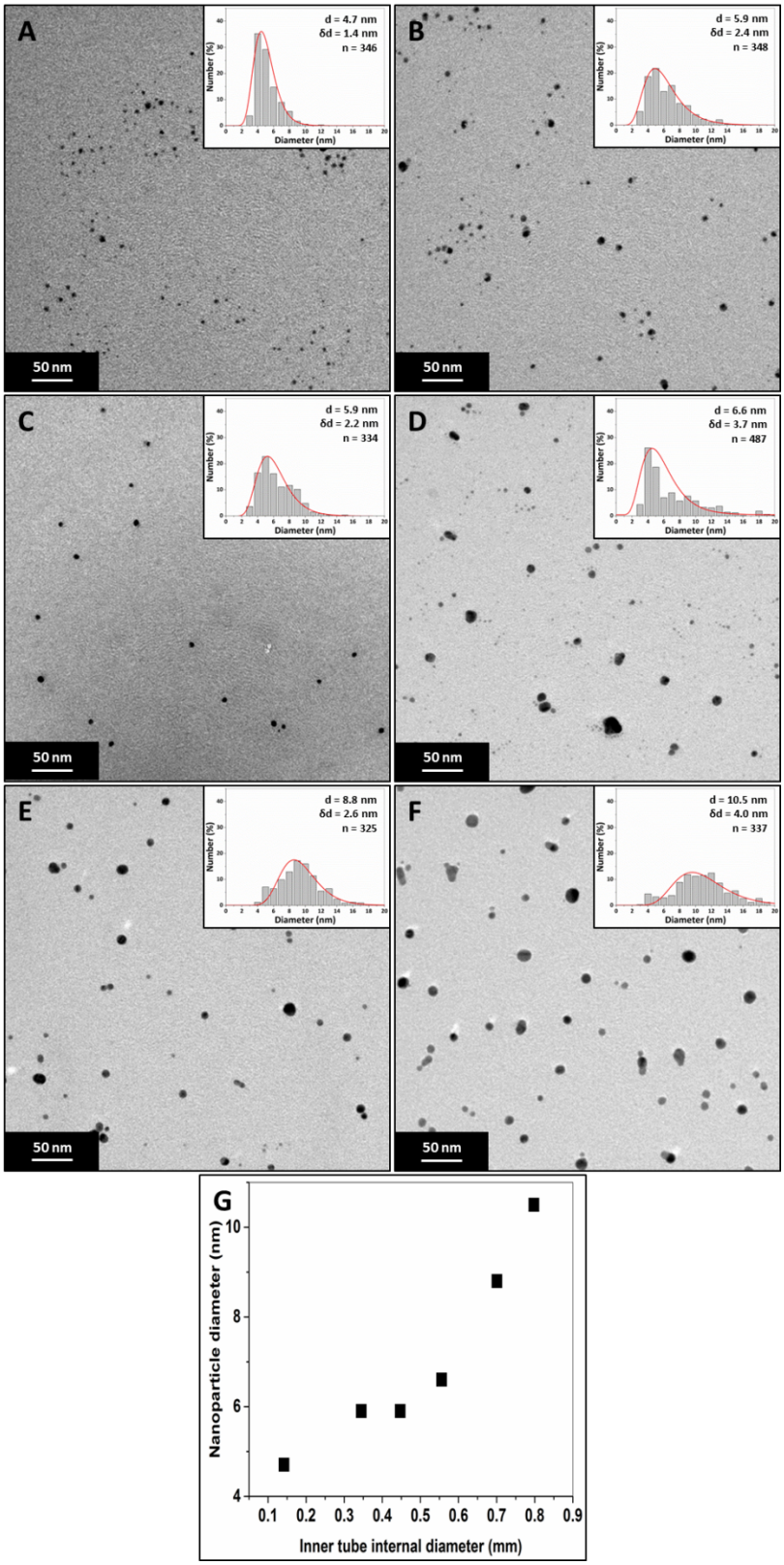

Figure 5-15: TEM images of silver NPs synthesized using the CFR with inner tube diameters of A: 0.142 mm, B: 0.345 mm, C: 0.447 mm, D: 0.556 mm, E: 0.701 mm, F: 0.798 mm, G: Nanoparticle diameter vs. inner tube internal diameter. Concentration of silver nitrate, 0.1 mM; concentration of sodium borohydride, 0.3 mM; concentration of trisodium citrate, 0.5 M; volumetric flow rate ratio, 1: 1 (Q_{out}:Q_{in}, $NaBH_4$: $AgNO_3$); molar flow rate ratio, 1:3:5 ($AgNO_3$:$NaBH_4$:Na_3citrate); flow rate, 1 ml/min, temperature 22-24°C.

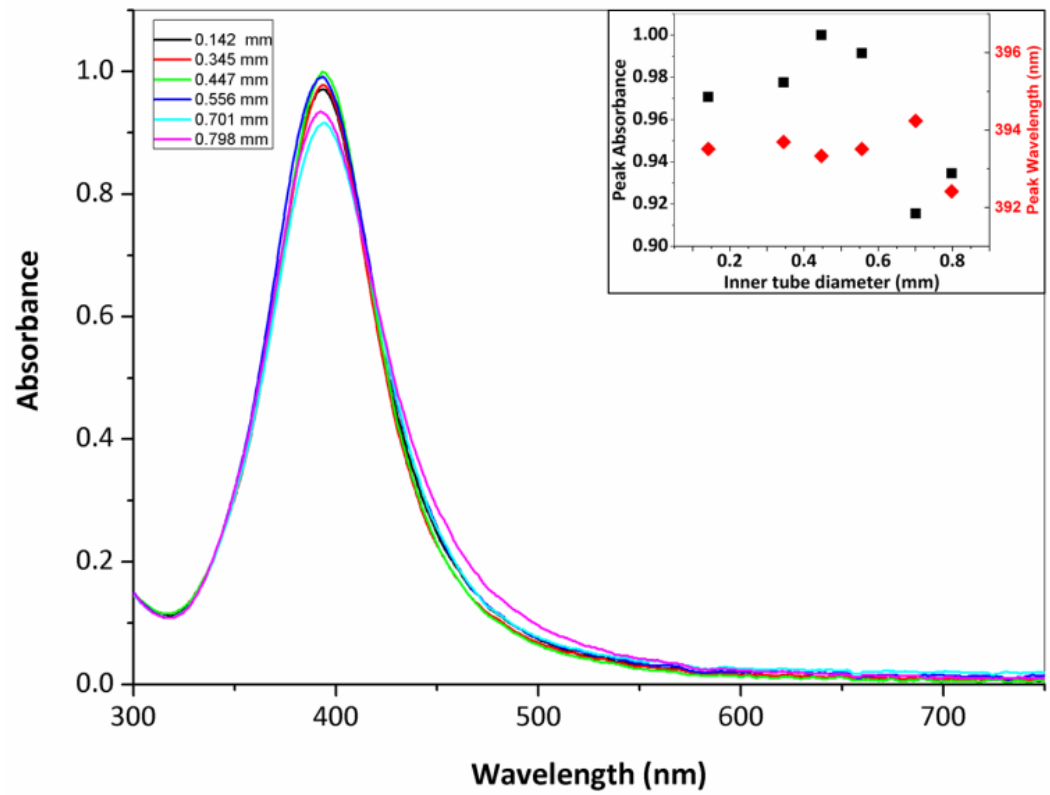

Figure 5-16: UV-Vis spectra of silver NPs synthesized using the CFR with inner tube diameters ranging between 0.142 and 0.798 mm. Inset: Peak absorbance (black squares) and peak wavelength (red diamonds) of silver NPs vs. inner tube internal diameter used in the CFR. Concentration of silver nitrate, 0.1 mM; concentration of sodium borohydride, 0.3 mM; concentration of trisodium citrate, 0.5 M; volumetric flow rate ratio, 1: 1 (Q_{out}:Q_{in}, $NaBH_4$:$AgNO_3$); molar flow rate ratio, 1:3:5 ($AgNO_3$:$NaBH_4$:Na_3citrate); flow rate, 1 ml/min, temperature 22-24°C.

5.3 Conclusions

Silver and gold NPs were synthesized in continuous flow mode in a Coaxial Flow Reactor (CFR) in conjunction with other microfluidic components such as a Continuous Flow Inverter (CFI) as a residence tile loop for gold NP synthesis or a SAR mixer for silver NP synthesis. Size control was achieved in the synthesis of gold NPs by varying the flow rate. The CFI provided a laminar region in which nucleation occurred at the interface of the two streams and the CFI provided a mixing region (due to secondary flow circulation) with an improved residence time (because of flow inversion) for growth to occur. In this way nucleation and growth periods could be controlled, resulting in an NP size range of 17.9-23.9 nm for a flow rate range of 0.25-3 ml/min. A minimum size of 17.9 nm existed at 80°C when the synthesis was tested in temperature range of 60-100°C. In batch syntheses, a change in size is achieved by altering the concentrations or order of reagent addition rather than the mixing conditions. Using this approach, the system offers a higher precision of control over the mass transfer, as opposed to a batch reactor, in a relatively simple manner (changing the flow rate of reagents) to achieve a variation in size of gold NPs. The CFR used in conjunction with the SAR mixer produced a decreasing silver NP size from 5.5 to 3.4 nm with increasing silver concentration, which is the opposite trend to using the CFR in isolation. This is because the SAR mixer provided very efficient mixing in a well-controlled manner to prevent reaction in silver nitrate rich regions. The CFR also allows some of the reaction to occur before entering the SAR

mixer. This reduced the fouling occurring in the very small and complex geometry of the SAR (using the SAR in isolation resulted in a higher amount of fouling). A vortex flow regime at higher Re number was tested in the CFR with size range of 5.9-7.7 nm for a flow rate range of 5.1-20.1 ml/min. No trend in size or dispersity was observed using this type of flow regime, even though the mixing efficiency was increased with increasing flow rate. Interestingly, the smallest and least disperse NPs were observed at the lowest flow rate, which was most likely because of the region close to the outlet of the inner tube. The spread of silver nitrate across the channel under these conditions was relatively small compared to higher flow rates and NPs prone to less growth would be formed in regions dilute in silver nitrate and concentrated in sodium borohydride. Decreasing the inner tube I.D. in the CFR resulted in a decrease in NP size from 10.5 to 4.7 nm, due to the reduced diffusion distance of the inner stream resulting in a faster consumption of silver nitrate in a well-controlled mass transfer region (i.e. within the CFR rather than at the outlet), which was supported by CFD modelling of the reaction within the CFR. The study demonstrates the versatility of using microfluidic devices and the potential benefits arising from manipulating the mass transfer and hydrodynamics on NP size and dispersity by using the CFR and/or other components in conjunction with the CFR for synthesis. This level of control over mass transfer is not easily achieved using batch reactors.

6 Mass transfer effects in the batch synthesis of silver and gold nanoparticles

There are many syntheses which investigate how concentrations affect the size of the NPs and naturally different conditions yield different sizes. One factor that is rarely investigated in depth in batch synthesis studies is the mass transfer, which is an important factor since it also has a major role to play in determining at what concentrations reactions occur in localized regions within the reactor.

The batch reactors used in the following chapter employ active mixing where external energy is applied to mix the fluids within (in this case a magnetic stir bar and stirrer motor). This type of mixing enhances advection in the fluid, leading to more efficient mixing. The microfluidic devices do not rely on external energy being applied, but rather their small dimensions and manipulations of the channel geometry to enhance mixing. As discussed in the introduction (Chapter 1), mass transport has two main mechanisms which are diffusion and advection. Microfluidic devices rely mainly on diffusion for mass transport, in contrast the batch reactors used in the following chapter also employ advection as a major component to the overall mass transport.

Silver NPs are commonly synthesized using sodium borohydride as a reducing agent within a batch reactor vessel (chapter 2). [5, 64-70] In general, altering the molar ratios of reducing agent to precursor was the main method to achieve control over the size of the silver NPs. This highlights the importance of concentration in the resultant NP size. Similarly for gold NPs, the Turkevich method is a very common method employed. This involves the reduction of tetrachloroauric acid via the citrate molecule at an elevated temperature. Many studies investigate this method for synthesis of gold NPs using batch reactors (chapter 2).[88-98, 100-106] The batch syntheses studies on the Turkevich method investigate changing the order of reagent addition, but there is a lack of studies which focus specifically on mass transfer and how it affects the resultant NP size and dispersity.

This study takes these two popular methods for the synthesis of silver NPs and gold NPs in batch vessels, and investigates the role mass transfer plays in the resultant size and dispersity of the respective NP system. The mixing time is characterized using the Villermaux-Dushman reaction scheme and various mixing configurations and order of addition of the reagents is investigated to draw conclusions on the effect of mass transfer. For all of the mixing configurations, the final concentration after mixing resulted in the same concentration of reducing agent and precursor.

6.1 Methodology

6.1.1 Chemicals

Silver nitrate ($AgNO_3$, 0.01 M stock solution), trisodium citrate ($HOC(COONa)(CH2COONa)_2 \cdot 2H_2O$, powder form, sodium borohydride solution ($NaBH_4$, ~12 wt% in 14 M NaOH stock solution) and gold (III) chloride hydrate ($HAuCl_4.xH_2O$, powder form), potassium iodide (KI, 99%) potassium iodate (KIO_3, 98%) and boric acid (H_3BO_3, 99.5%) were obtained from Sigma. Sulfuric acid (H_2SO_4, 3 M stock solution) was

obtained from Alfa Aesar. All chemicals were used without further purification and solutions were prepared with ultrapure water (resistivity 15.0 MΩ·cm).

6.1.2 Experimental Setup

Syringe pumps (Pump 11 Elite OEM module, Harvard) connected to a 0.5 mm internal diameter (I.D.) 316L stainless steel tube for silver NPs and a 0.5 mm I.D. PTFE tube for gold NPs were used to deliver one of the reagents to the batch vessel. The batch vessel was a 50 ml small neck glass Erlenmeyer flask (Fisher Scientific). A digital hotplate stirrer with temperature control (Stuart) was used together with PTFE stir bars (15 mm x 1.5 mm, VWR international) to mix the reagents within the vessel. A glycerine bath was used together with the temperature controller to heat the reagents within the batch vessel in the case of the gold NP synthesis. A cap was used to cover the batch vessel and the tube was inserted through the cap for addition of reagents. The length of the tube could be adjusted to allow addition of reagents from above the solution or near the tip of the magnetic stir bar. This was done to allow for variation in mixing conditions. Figure 6-1 shows a schematic of the experimental setups for silver and gold NP synthesis.

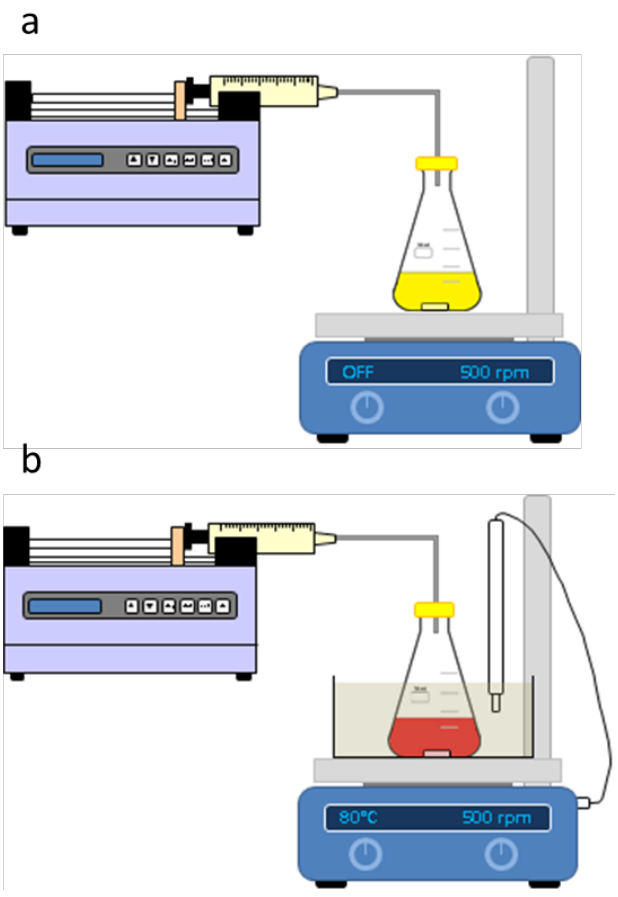

Figure 6-1: Schematic of experimental setup for silver and gold NP synthesis consisting of an Erlenmeyer flask with precursor or reducing agent stirred via a magnetic stirrer with a syringe pump reagent via tubing a) silver NP system using a stainless steel 0.5 mm I.D. tubing and b) gold NP system using a PTFE 0.5 mm I.D. tubing with a glycerine bath and temperature probe for temperature control at 80°C. Stirrer speed was set at 500 rpm in both cases.

6.1.3 Nanoparticle synthesis

In a typical silver NP synthesis, 20 ml of reagent were placed within the batch vessel and stirred at 500 rpm. To this, 0.6 ml of the other reagent was added via the syringe pump and tube at either: 0.5 ml/min from above the solution in droplets or, 50 ml/min with the tube inserted into the solution within the batch vessel near the stir bar tip. The reagents were a mixture of silver nitrate and trisodium citrate, and the sodium borohydride solution. The order of mixing was tested by switching which reagent was placed in the batch vessel, either 20 ml of silver nitrate and trisodium citrate or 20 ml of sodium borohydride (sodium borohydride was stored in 14 M sodium hydroxide leading to NaOH concentration being 3.21 times higher than the sodium borohydride concentration in all cases). Similarly, in the gold NP synthesis 20 ml of reagent was placed in the batch vessel and 0.6 ml of reagent was added to this in a similar manner to the silver NP synthesis. 20 ml of tetrachlorauric acid or 20 ml of trisodium citrate were placed in the batch vessel. This solution was placed in the glycerine bath which was heated to 80°C. To test the length of time required to bring 20 ml of solution to 80°C, temperature was measured over time after inserting solution at room temperature into the glycerine bath and it was found that after 7 min the temperature reached a steady state of 80°C. Hence the solution in the experiments was heated and stirred for 15 min before addition of 0.6 ml of reagent from the syringe pump.

6.1.4 Characterization of nanoparticles

For UV-Vis analysis, NPs were analyzed using a UV-Vis spectrometer (USB 2000+ Spectrometer and DT-Mini-2-GS light source, Ocean Optics). Silver NPs were analyzed within an hour of synthesis (the signal of the samples were stable in this window of time). Gold NPs were analyzed over time and were analyzed once the signal was stable (usually 1-2 days). NP samples were diluted with additional ultrapure water to bring the absorbance into a suitable range (i.e. obeying the Beer-Lambert law and avoiding saturation of the light detector) if necessary. Transmission electron microscope images were captured using a JEOL 1200 EX ii microscope with a 120 kV acceleration voltage. Carbon coated copper TEM grids were prepared within an hour of synthesis for silver NPs and when the sample was stable for gold NPs by pipetting a 5 µl sample onto the grid and allowing it to dry at room temperature. Care was taken to not cover the entire TEM grid with the droplet, so that the aggregated ring around the edge of the droplet could easily be identified as an artefact of sample preparation. Particle size distributions (insets for each TEM image presented) have the following nomenclature: d is average diameter, δd is the standard deviation of the NP distribution and n is the number of particles counted to obtain the particle size distribution. Differential centrifugal sedimentation analysis (CPS disc centrifuge UHR, Analytik) was carried out on gold NPs when the samples were stable. PEBBLES software was used for the counting and sizing of TEM images of the synthesised silver NPs and ImageJ software was used for the counting and sizing of TEM images of the synthesised gold NPs.

6.2 Results and discussion

6.2.1 Mixing Characterization

1 ml of 0.07 M sulfuric acid was added to 20 ml of a buffer solution consisting of 0.1818 M orthoboric acid, 0.0909 M sodium hydroxide, 11.67 mM potassium iodide and 2.33 mM potassium iodate. Stirrer speed was set to 500 rpm and the two mixing configurations used in the NP synthesis were tested. These were: acid was injected from the centre above the buffer solution or near the stir bar tip. Figure 6-2 shows a schematic illustrating the two configurations. Figure 6-3 shows the computed segregation index vs. mixing time for the concentration set of the experiments using the IEM mixing model (details can be found in Appendix A). Each mixing configuration was repeated three times and the triiodide concentration was measured (extinction coefficient was found to be 23209 l/mol.cm, details on the procedure used to find this can be found in the Appendix A). The mixing time averaged over three repeat experiments for the injection from above the solution was 209 ms while the injection near the stir bar tip was 46 ms. A reduction in mixing time was expected since there is a much higher shear rate near the stir bar tip, resulting in improved mixing efficiency. Since both experiments used the same concentration set, injection near the stir bar tip was approximately 4 times more efficient then injection from above the buffer solution.

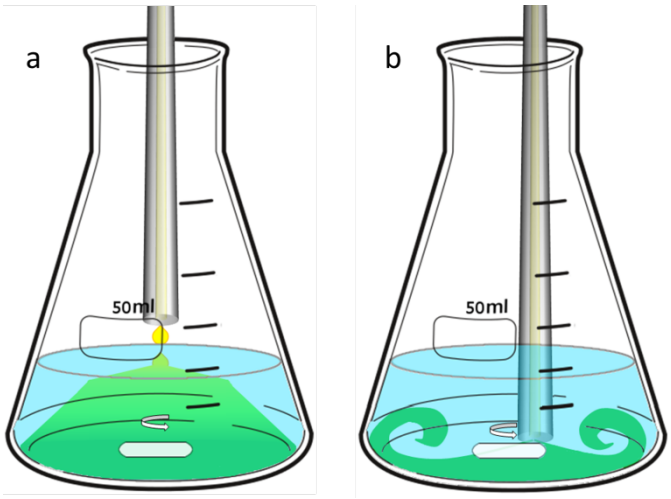

Figure 6-2: Schematic representation of injection points within the batch vessel to vary mixing efficiency a) injection is added from above the solution in the batch vessel and b) injection is added close to the stir bar tip.

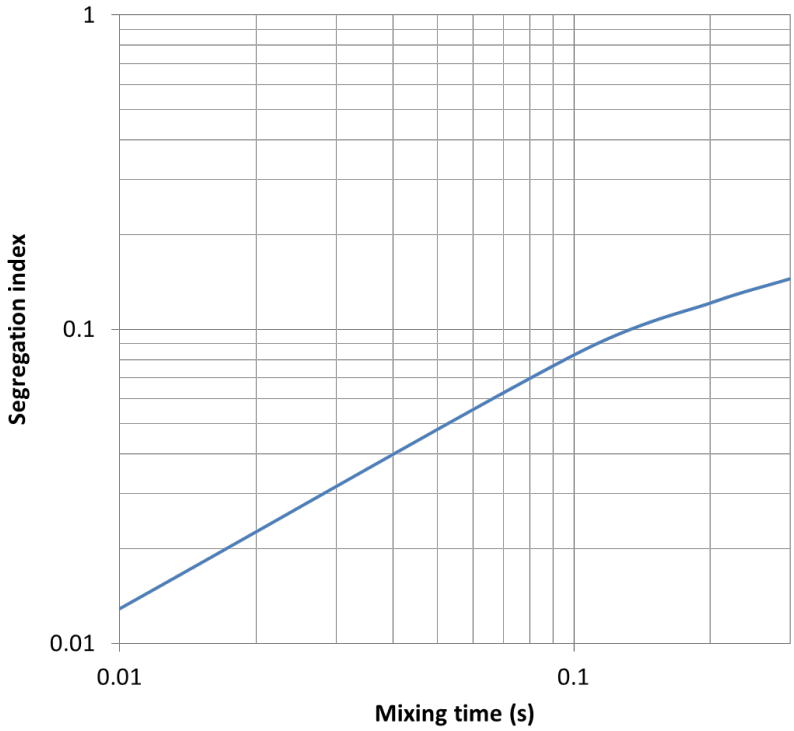

Figure 6-3: Segregation index vs. mixing time estimated using the IEM model for the Villermaux-Dushmann reaction scheme. Concentrations of buffer solution were KI: 0.0117 M, KIO_3: 0.0023 M, NaOH: 0.0909 M, H_3BO_3: 0.1818 M. Concentration of H_2SO_4 was: 0.07M.

6.2.2 Silver nanoparticle synthesis

Silver NPs were synthesized in the batch vessel by reduction of silver nitrate via sodium borohydride in the presence of trisodium citrate. The effect of changing the mixing configuration and the effect of changing the order of reagent addition on the size and dispersity of the NPs was investigated. Mixing configurations were those described in the previous section i.e. injection of reagent from above the solution or injection near the stir bar tip, and the order of reagent addition was achieved by swapping the reagent that started in the batch vessel i.e. a silver nitrate and trisodium citrate mixture or sodium borohydride. The general procedure was to inject 0.6 ml of reagent via tubing into 20 ml of reagent which was being stirred in the batch vessel. Four conditions were tested and will be described as A-Ag-R-S, B-Ag-R-F, C-Ag-P-S and D-Ag-P-F. The order of reagent addition is denoted by the letters R and P, R represents the addition of 0.6 ml of reducing agent to the batch vessel and P represents the addition of 0.6 ml of precursor to the batch vessel. The mixing configurations are denoted by the letters S and F, S denotes the addition of 0.6 ml of reagent via droplets at a rate of 0.5 ml/min from above the 20 ml mixture while F denotes the addition of 0.6 ml of reagent near the stir bar tip at a rate of 50 ml/min (for example, the condition A-Ag-R-S describes the addition of 0.6 ml of reducing agent at a rate of 0.5 ml/min to 20 ml of precursor). Table 6-1 summarizes the concentrations for each mixing condition (3 to 1 molar ratio of borohydride to silver nitrate was used in all cases).

Table 6-1: Summary of concentrations for each mixing condition used in the silver NP synthesis

Condition	Reducing Agent – $NaBH_4$	Precursor – $AgNO_3$/Na_3citrate
A-Ag-R-S	63.3 mM	0.38/0.38 mM
B-Ag-R-F	63.3 mM	0.38/0.38 mM
C-Ag-P-S	1.36 mM	9.1/9.1 mM
D-Ag-P-F	1.36 mM	9.1/9.1 mM

Figure 6-4 shows TEM images of the synthesized silver NPs with an average diameter of 11.1 ± 3.0 nm, 6.7 ± 1.7 nm, 9.5 ± 1.4 nm and 11.5 ± 2.4 nm for conditions A-Ag-R-S, B-Ag-R-F, C-Ag-P-S and D-Ag-P-F respectively. The average peak absorbance and average wavelength obtained from 3 repeat experiments obtained by analysing the silver NPs using UV-vis spectroscopy can be seen in Figure 6-5 (the percentage of deviation in peak absorbance for each condition was: A-Ag-R-S = 3.2%, B-Ag-R-F = 2.1%, C-Ag-P-S = 2.2% and D-Ag-P-F = 2.7%). The peak wavelength had increased deviation for conditions A and D on repeat experiments. Overall there was little variation in the value of the peak wavelength across all the conditions tested. Since the NPs are less than around 11 nm, it is consistent with the behaviour of little variation in peak wavelength for NPs below 10 nm.[139] Condition B-Ag-R-F produced the smallest NPs followed by condition C-Ag-P-S, while conditions A-Ag-R-S and D-Ag-P-F produced NPs of comparable size. The smallest NPs were produced when a small volume of concentrated sodium borohydride was added quickly into the dilute silver nitrate and trisodium citrate mixture, or when drops of a concentrated mixture of silver nitrate and trisodium citrate were added slowly to a sodium borohydride solution (condition B and C respectively). Conversely, larger NPs were synthesized when drops of concentrated sodium borohydride were added slowly to a dilute mixture of silver nitrate and trisodium citrate or when a concentrated mixture of silver nitrate and trisodium citrate were added quickly into a dilute volume of sodium borohydride. In this synthesis, trisodium citrate is the ligand and since it is mixed with silver nitrate prior to addition of sodium borohydride, it can be assumed that the ligand is available in the vicinity where silver nitrate is reduced by sodium borohydride. However it is known that sodium borohydride also behaves as a stabilizing agent, where the surface charge of the particles is affected by borohydride ion adsorption.[136] The difference in sizes obtained using the different conditions is due to the availability of sodium borohydride in the local region surrounding areas where silver nitrate has been reduced to silver metal. The silver metal subsequently produces small silver clusters which are stabilized by sodium borohydride. Silver NPs catalyse the hydrolysis of sodium borohydride which produces hydrogen and normally this catalysis leads to a switching point where the NPs suddenly increase in size due to aggregation,[68] which occurs because the stabilizing presence of borohydride ions is depleted through the hydrolysis reaction which provides evidence for their stabilizing effect. No switching point is observed in this study due to an elevated pH because of the presence of sodium hydroxide, suppressing the hydrolysis reaction.[137] Another important point to note is that sodium borohydride can reduce more than its own stoichiometric equivalent of silver ions since it can provide multiple electrons in the reduction reaction.[133-135] Therefore a small amount of sodium borohydride ca3en reduce many silver ions (which subsequently form silver NPs), but

there may be a deficient amount of sodium borohydride to provide stabilization of NPs resulting in growth to a larger size. This would occur through coalescence of smaller silver clusters into larger sizes, the reduced surface charge resulting in the possibility of clusters approaching each other close enough for attractive forces to bring them together. Coalescence has been identified in previous studies as a main growth mechanism in the silver NP formation process.[68, 82, 139]

Considering the properties and role of the sodium borohydride in the reaction, as well as the mass transport mechanisms within the batch reactor, can help to explain the results obtained. The size of the NPs obtained under conditions A-Ag-R-S and D-Ag-P-F can explained as follows: the conditions potentially create mixing conditions in which silver nuclei are exposed to deficient amounts of sodium borohydride with an abundance of precursor leading to their growth to a larger size. Condition A-Ag-R-S has concentrated sodium borohydride which is added slowly drop by drop. Since there is enhanced advection within the batch vessel because of the stirring action, each drop will be mixed with the bulk of the silver nitrate/trisodium citrate solution before subsequent drops are added. The first few drops can reduce the much larger mass of silver nitrate in the batch vessel which creates NPs prone to growth because of deficiency in sodium borohydride. Condition D-Ag-P-F has concentrated silver nitrate added quickly to dilute sodium borohydride. Since there is a sudden influx of a large mass of silver nitrate because addition is quick (0.6 ml of fluid takes 0.72 seconds to add at a flow rate of 50 ml/min), the reaction of silver nitrate can occur in localized regions in the microscale where it is highly concentrated. This would again create NPs prone to growth since the reaction and subsequent nucleation occurs in areas where the silver nitrate to sodium borohydride ratio is high, resulting in a larger final size. In this case, rather than the enhanced advection causing growth of the NPs (as is the case for condition A-Ag-R-S), the slow diffusion on the microscale after the influx of a small concentrated volume of silver nitrate would cause reactions in areas that are rich in silver nitrate. This leads to the possibility of large nuclei forming at the very beginning of the reaction because of decreased stability (sodium borohydride deficiency) and would result in fewer nuclei which would subsequently grow into larger NPs. The smallest NPs are obtained under the condition B-Ag-R-F, when a concentrated volume of sodium borohydride is added quickly to a dilute volume of silver nitrate. Compared to the case where sodium borohydride is added slowly, in this case a large mass of sodium borohydride becomes available quickly to the dilute volume of silver nitrate. This would create a condition in which there is initially an abundance of sodium borohydride in localized regions in the microscale before the enhanced advection causes complete mixing in the bulk of the fluid within the vessel, resulting in silver NPs which are very stable and hence not prone to growth. As the mixing proceeds and completes on the macroscale, the sodium borohydride concentration would reduce due to mixing with a larger dilute volume and because of reaction that has occurred during the mixing process. The reaction can be visibly seen as a dark brown plume on addition of sodium borohydride immediately after injection, after which the solution transitions into a bright yellow colour once the mixture has been homogenized through mixing. The dark brown plume could be indicative of aggregated silver NPs and the transition to a bright yellow colour (indicative of non-aggregated silver NPs) may be because of rapid acquisition of stabilising borohydride causing the aggregated NPs to repel each other and separate. As the sodium borohydride concentration

is reduced, reaction may occur in some regions where the sodium borohydride to silver nitrate ratio is lower and hence the possibility of some larger NPs may be produced. In fact, this is what is seen in the particle size distribution for condition B-Ag-R-F. There is a relatively large amount of small NPs (around 6 nm) with relatively small amounts of larger NPs (around 10 nm). Finally, condition C-Ag-P-S produced the most monodispersed NPs and these were of an intermediate size. Concentrated drops of silver nitrate were added to a dilute volume of sodium borohydride. In this case, each silver nitrate drop is exposed to a much higher mass of sodium borohydride so is therefore expected to make stable NPs that are not prone to growth. However, since the micromixing time is slower using this mixing configuration, it is expected that some reaction will take place as the concentrated silver nitrate drop is mixed on addition to the dilute volume of sodium borohydride. This explains the intermediate size obtained, where the localized silver nitrate concentration is high but is subsequently exposed to an abundance of sodium borohydride. The combination of diffusion and advection and how it can offer control over the NP size is demonstrated well in these experiments. Because diffusion is slow, larger nuclei could form in the silver nitrate rich drop as it enters the bulk fluid (where reaction occurs in silver nitrate rich region within the fluid in the immediate vicinity of the drop) but this is quickly suppressed as advection aids in mixing the silver nitrate droplet into the bulk sodium borohydride fluid to stabilise it. In essence, each drop of silver nitrate reacts to form silver NPs which are quickly stabilized as they are mixed into the sodium borohydride solution, and further drops then produce NPs which do not interact with existing NPs in the solution because of their stability which explains the lower dispersity of the resultant NPs. It is the configuration which gives the most uniform sodium borohydride concentration exposure to the silver NPs, and points to the sodium borohydride being crucial in determining the NP size and dispersity in this synthesis. Shirtcliffe *et al*. also compared different orders of reagent addition and found that adding silver nitrate to sodium borohydride produced the narrowest and most reproducible UV-VIS spectra, pointing to lower dispersity.[65] Song et al. also noted that increasing sodium borohydride resulted in decreasing aggregation, again highlighting the importance of sodium borohydride to the stability of the silver NPs.[67]

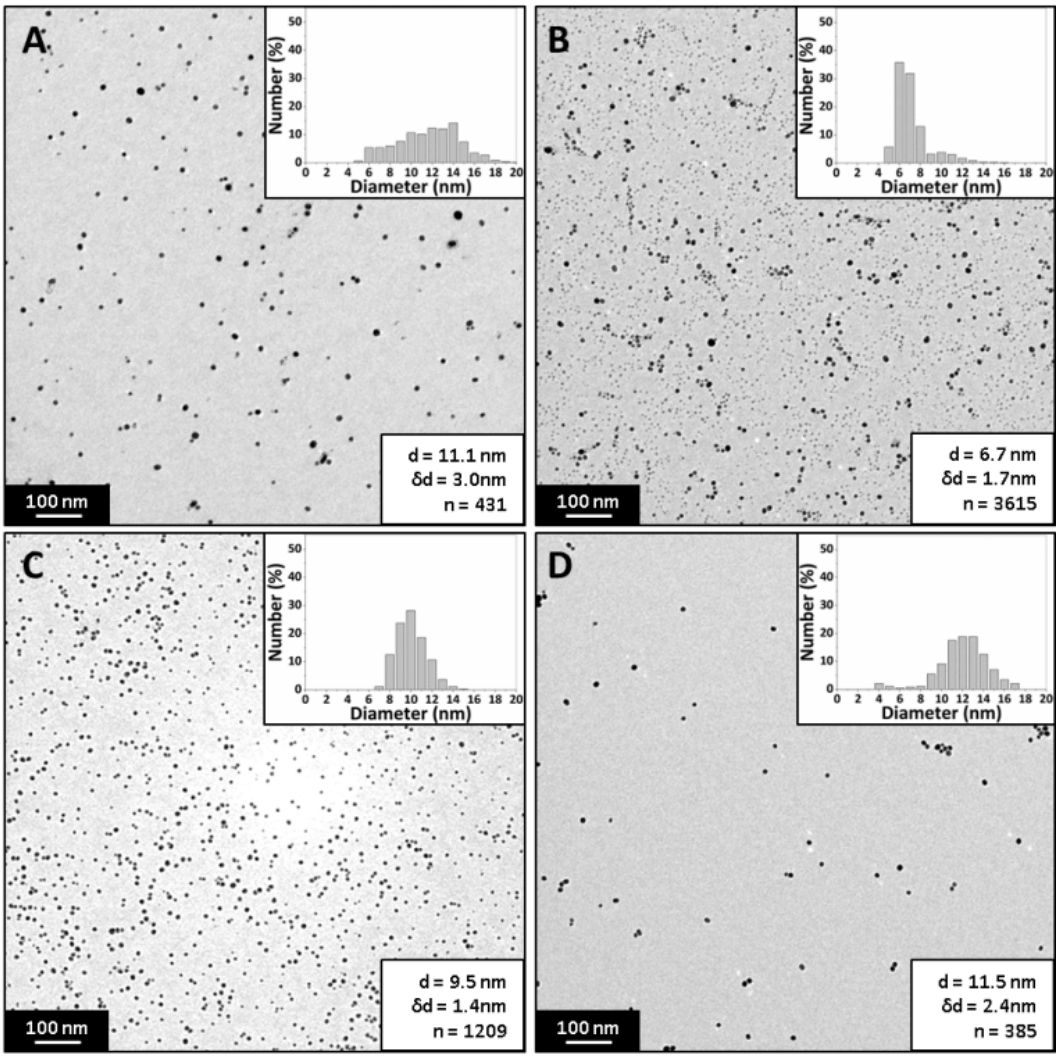

Figure 6-4: TEM images of silver NPs synthesized in a batch vessel under various conditions. A) 0.6 ml sodium borohydride [63.3 mM] added via drops to 20 ml of a mixture of silver nitrate [0.38 mM] and trisodium citrate [0.383 mM] at a flow rate of 0.5 ml/min, B) 0.6 ml sodium borohydride [63.3 mM] added near the stir bar tip to 20 ml of a mixture of silver nitrate [0.38 mM] and trisodium citrate [0.383 mM] at a flow rate of 50 ml/min, C) 0.6 ml of a mixture of silver nitrate [9.1 mM] and trisodium citrate [9.1 mM] added via drops to 20 ml sodium borohydride [1.36 mM] at a flow rate of 0.5 ml/min and D) 0.6 ml of a mixture of silver nitrate [9.1 mM] and trisodium citrate [9.1 mM] added near the stir bar tip to 20 ml sodium borohydride [1.36 mM] at a flow rate of 50 ml/min. Experiments were conducted at room temperature and stirring speed was set at 500 rpm.

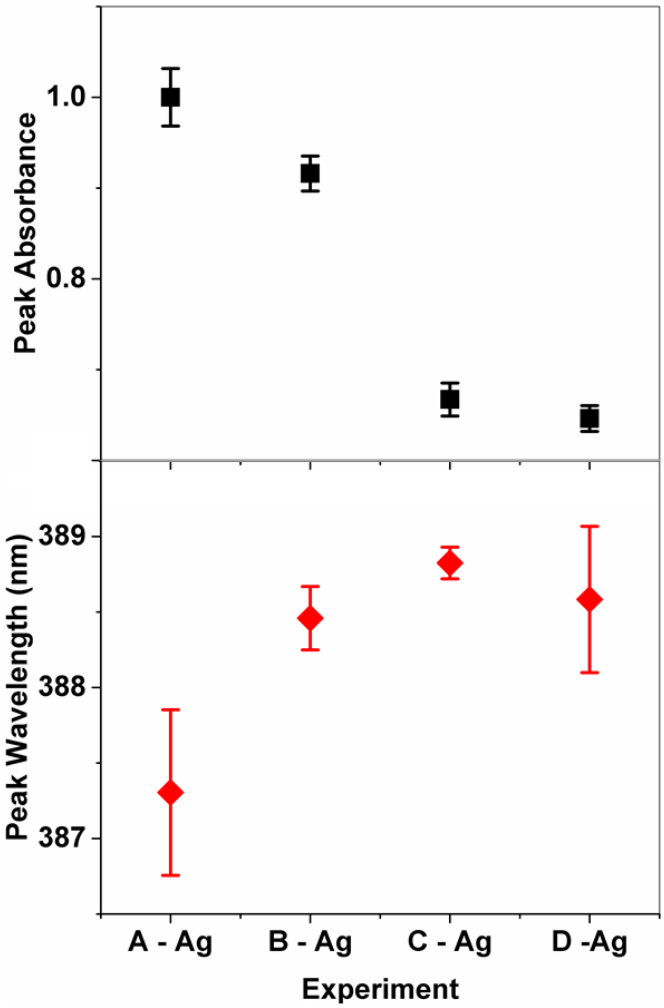

Figure 6-5: Average peak absorbance and average peak wavelength obtained using UV-vis spectroscopy of silver NPs synthesized in batch vessel under various conditions. A) 0.6 ml sodium borohydride [63.3 mM] added via drops to 20 ml of a mixture of silver nitrate [0.38 mM] and trisodium citrate [0.383 mM] at a flow rate of 0.5 ml/min, B) 0.6 ml sodium borohydride [63.3 mM] added near the stir bar tip to 20 ml of a mixture of silver nitrate [0.38 mM] and trisodium citrate [0.383 mM] at a flow rate of 50 ml/min, C) 0.6 ml of a mixture of silver nitrate [9.1 mM] and trisodium citrate [22.7 mM] added via drops to 20 ml sodium borohydride [1.36 mM] at a flow rate of 0.5 ml/min and D) 0.6 ml of a mixture of silver nitrate [9.1 mM] and trisodium citrate [22.7 mM] added near the stir bar tip to 20 ml sodium borohydride [1.36 mM] at a flow rate of 0.5 ml/min. Experiments were conducted at room temperature and stirring speed was set at 500 rpm. Bars represent standard deviation of absorbance and wavelength for 3 repeated experiments.

6.2.3 Gold nanoparticle synthesis

Gold NPs were synthesized in the batch vessel by reduction of tetrachloroauric acid via trisodium citrate at a temperature of 80°C. The effect of changing the mixing configuration and the effect of changing the order of reagent addition on the size and dispersity of the NPs was investigated. The same four conditions to those used for silver NP synthesis were tested and will be described as conditions A-Au-R-S, B-Au-R-F, C-Au-P-S and D-Au-P-F. Table 6-2 summarizes the concentrations for each mixing condition (3 to 1 ratio of citrate to tetrachloroauric was used in all cases).

Table 6-2: Summary of concentrations for each mixing condition used in the gold NP synthesis

Condition	Reducing Agent – Na_3citrate	Precursor – $HauCl_4$
A-Au-R-S	92.7 mM	0.556 mM
B-Au-R-F	92.7 mM	0.556 mM
C-Au-P-S	2.78 mM	18.5 mM
D-Au-P-F	2.78 mM	18.5 mM

Figure 6-6 shows TEM images of the synthesized gold NPs with an average diameter of 18.0 ± 4.8 nm, 13.1 ± 2.2 nm, 16.3 ± 3.3 nm and 16.2 ± 2.1 nm for conditions A-Au-R-S, B-Au-R-F, C-Au-P-S and D-Au-P-F respectively. The average peak absorbance and average wavelength obtained from 3 repeat experiments obtained by analyzing the gold NPs using UV-vis spectroscopy can be seen in Figure 6-7 (the percentage of deviation in peak absorbance for each condition was: A-Au-R-S = 0.8%, B-Au-R-F = 1.6%, C-Au-P-S = 0.5% and D-Au-P-F = 0.2%). The peak wavelength of NPs synthesised using condition B-Au-R-F was slightly lower than the other conditions in line with the average size of the NPs being smaller. Diameter was found to be 14.3 ± 3.3 nm, 13.8 ± 1.7 nm, 14.2 ± 2.8 nm and 14.1 ± 2.1 nm based on a number percentage obtained from DCS measurements for conditions A-Au-R-S, B-Au-R-F, C-Au-P-S and D-Au-P-F respectively. The curves and diameter vs condition can be found in Figure 6-8.

The largest and most polydisperse NPs were observed using condition A-Au-R-S and the smallest NPs were observed using conditions B-Au-R-F. Conditions C-Au-P-S and D-Au-P-F produced NPs of a similar size though D-Au-P-F produced slightly more monodispersed NPs. The reactions in the Turkevich method are complex because of the many different species which can coexist in the solution as it proceeds. The precursor can exist in increasingly hydroxylated form from $AuCl_4^-$ to $AuOH_4^-$,[95] with the hydroxylated form being formed at elevated pH. According to the literature, increasingly hydroxylated forms result in a decrease in reactivity.[104] This would result in a lower nucleation rate and hence larger NPs. The citrate species also changes its speciation dependent on pH. At lower pH it exists in its most protonated form of H_3Cit with increasing deprotonation to Cit^{3-} as pH is elevated while the $HCit^{2-}$ species is suggested to be the most likely form responsible for reduction of the gold precursor.[106] Hence, the mixing of these two reagents becomes important because the combination of the acidic precursor with the buffer reducing agent results in an evolution of pH as mixing proceeds. Ideally, to achieve small monodispersed NPs, the nucleation period should be maintained to produce many nuclei (resulting in a small size) and there should be a good separation between nucleation and growth (resulting in monodispersity). Nucleation occurs when there is high reaction rate, which depends on less hydroxylated forms of precursor and monoprotonated citrate being present. A separation of nucleation and growth is achieved by a transition from high reaction rate to a lower reaction rate. This occurs in the Turkevich method because the buffer capacity of the citrate solution neutralizes the acidic precursor as mixing proceeds while the pH increases as the precursor reacts. Considering the roles of precursor and reducing agent, the results obtained from each condition can be explained. Condition A-Au-R-S produced the largest and most disperse NPs. Concentrated citrate is added drop wise to the dilute precursor. Relatively large NPs are produced in this case because citrate is added slowly (0.6 ml takes 72

s to add at a rate of 0.5 ml/min), resulting in the reduction reaction occurring at a relatively low rate since the citrate concentration will be perpetually low. This is the case because of the enhancements in mass transport through advection because of the stirring motion, which hastens the incorporation of citrate into the bulk fluid which causes dilution of the concentration. A low reduction reaction rate results in a lower nucleation rate and hence larger NPs. The polydisperse nature of the sample arises from the evolving citrate concentration as the rate of addition was quite slow. Initially there is a low citrate to gold ratio, resulting in larger and less spherical shaped NPs. Over time this ratio decreases resulting in smaller and more spherical NPs. Condition B-Au-R-F produced the smallest NPs because the citrate was added at a higher flow rate near the stir bar tip. This resulted in the precursor being exposed quickly to a larger amount of reducing agent in comparison to condition A-Au-R-S, resulting in a higher reaction rate and subsequent amounts of nucleation leading to smaller NPs. In this case, the concentrated nature of the citrate leads to a high reduction rate in the local vicinity, resulting in smaller and more numerous nuclei. As mixing proceeds through the aid of advection, the increased concentration of nuclei would ultimately grow to a smaller size assuming the remaining unreacted precursor is spread equally across each nucleus. Condition C-Au-P-S and condition D-Au-P-F produced NPs of a similar size. The addition of 0.6 ml to a larger volume of 20 ml wouldn't reduce the concentration of the larger volume significantly. In this case, the length of time required to add the precursor is not significant since it is all exposed to approximately the same concentration of reducing agent resulting in similar reaction rates and nucleation rates, which is why conditions C-Au-P-S and D-Au-P-F produce a similar size of NP. Sivaraman *et al*. note that there is no significant reduction in size of gold NPs using the inverse method for citrate to gold molar ratios < 5,[102] and we observe no significant reduction according to this study at a citrate to gold molar ratio of 5. The quick addition of citrate to tetrachloroauric acid did yield smaller NPs, but the manner in which reagents are added has not been the specific focus of other studies of gold NP syntheses in batch reactors. Another point to note is that the faster addition rate near the stir bar tip in general had a lower dispersity than the slow addition via drops. Considering that the citrate behaves as a reducing agent and stabilizing agent the conditions can be compared with respect to this reduction in dispersity. In comparing the conditions, this difference in dispersity can be explained with the evolution of concentrations within the stirred fluid. Fast addition of citrate creates burst nucleation in condition B-Au-R-F, after which the solution pH increases resulting in a transition to growth. Slow addition of citrate in condition A-Au-R-S results in nucleation initially, subsequent addition of citrate then interacts not only with gold precursor but also gold nuclei. This gives the possibility of both nucleation and growth occurring at the same time. In fact, this results in somewhat of an overlap between growth and nucleation. In essence, there is a sharper separation using condition B-Au-R-F than condition A-Au-R-S, resulting in a decrease of dispersity with fast addition of citrate. Similarly, with condition C-Au-P-S and D-Au-P-F, adding tetrachlorauric acid slowly results in the possibility of an overlap of nucleation and growth, whereas the fast addition would result in a sharper separation of nucleation and growth resulting in lower dispersity.

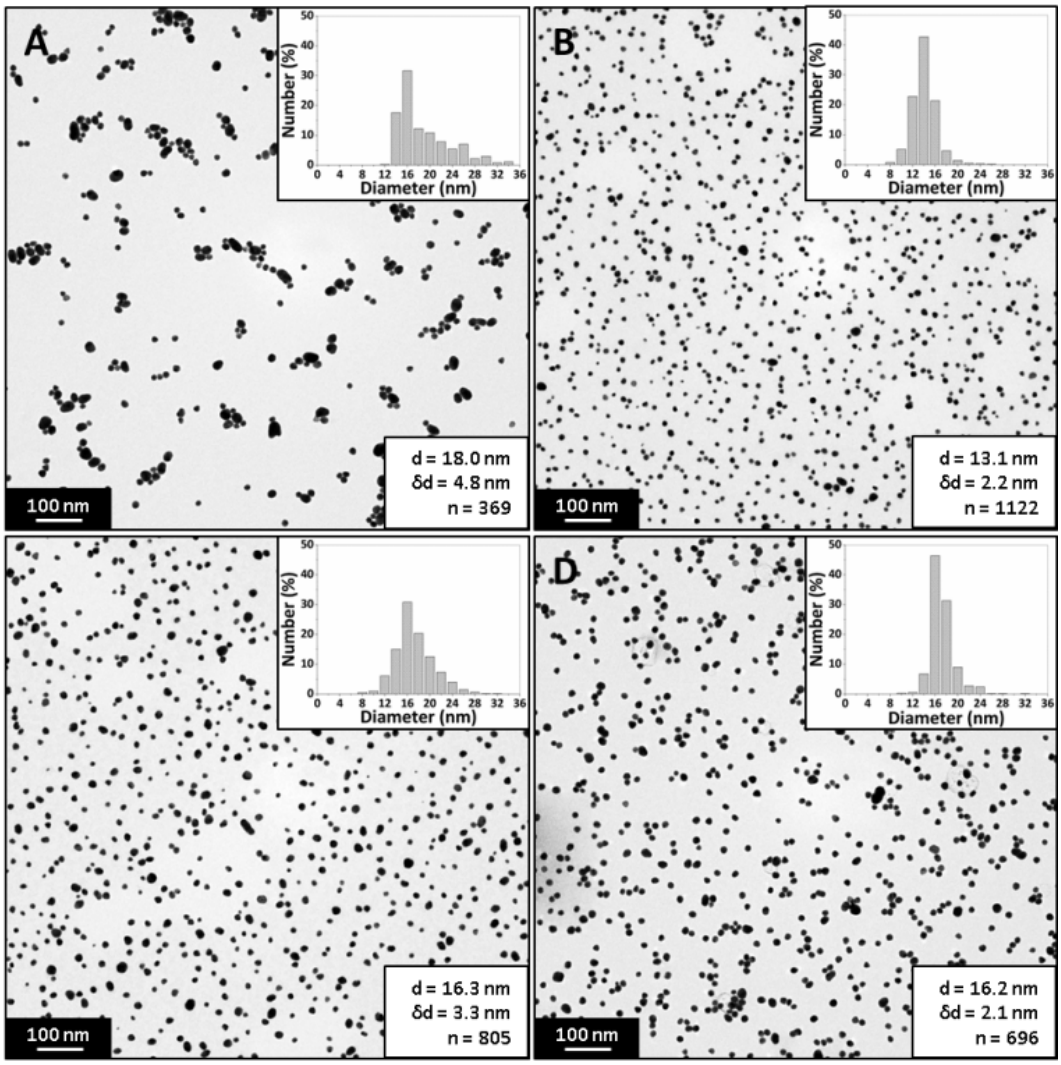

Figure 6-6: TEM images of gold NPs synthesized in a batch vessel under various conditions. A) 0.6 ml trisodium citrate [92.7 mM] added via drops to 20 ml of tetrachloroauric acid [0.556 mM] at a flow rate of 0.5 ml/min, B) 0.6 ml trisodium citrate [92.7 mM] added near the stir bar tip to 20 ml of tetrachloroauric acid [0.556 mM] at a flow rate of 50 ml/min, C) 0.6 ml of tetrachloroauric acid [18.5 mM] added via drops to 20 ml trisodium citrate [2.78 mM] at a flow rate of 0.5 ml/min and D) 0.6 ml of tetrachloroauric acid [18.5 mM] added near the stir bar tip to 20 ml trisodium citrate [2.78 mM] at a flow rate of 50 ml/min. Experiments were conducted at 80°C and stirring speed was set at 500 rpm.

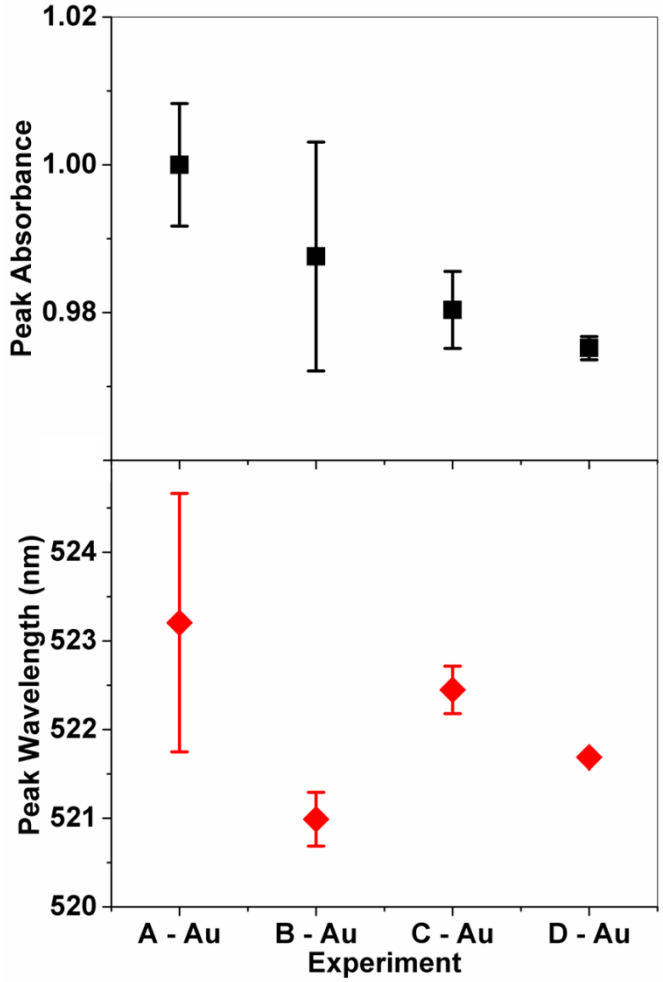

Figure 6-7: Peak absorbance and peak wavelength obtained using UV-vis spectroscopy of gold NPs synthesized in batch vessel under various conditions. A - Au) 0.6 ml trisodium citrate [92.7 mM] added via drops to 20 ml of tetrachloroauric acid [0.556 mM] at a flow rate of 0.5 ml/min, B - Au) 0.6 ml trisodium citrate [92.7 mM] added near the stir bar tip to 20 ml of tetrachloroauric acid [0.556 mM] at a flow rate of 50 ml/min, C - Au) 0.6 ml of tetrachloroauric acid [18.5 mM] added via drops to 20 ml trisodium citrate [2.78 mM] at a flow rate of 0.5 ml/min and D - Au) 0.6 ml of tetrachloroauric acid [18.5 mM] added near the stir bar tip to 20 ml trisodium citrate [2.78 mM] at a flow rate of 0.5 ml/min. Experiments were conducted at 80°C and stirring speed was set at 500 rpm. Bars represent standard deviation of absorbance and wavelength for 3 repeated experiments.

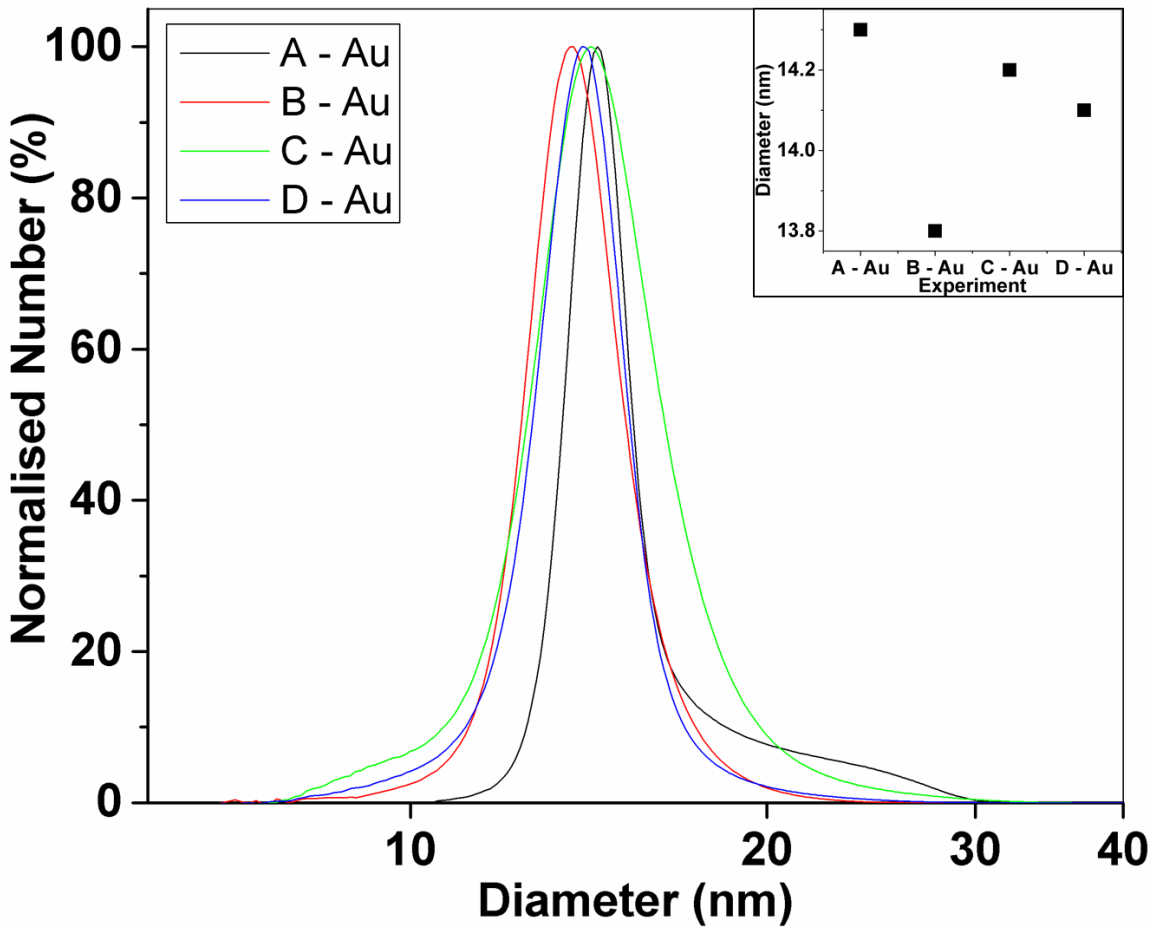

Figure 6-8: Normalized number percentage vs diameter obtained using DCS of gold NPs synthesized in batch vessel under various conditions. A - Au) 0.6 ml trisodium citrate [92.7 mM] added via drops to 20 ml of tetrachloroauric acid [0.556 mM] at a flow rate of 0.5 ml/min, B - Au) 0.6 ml trisodium citrate [92.7 mM] added near the stir bar tip to 20 ml of tetrachloroauric acid [0.556 mM] at a flow rate of 50 ml/min, C - Au) 0.6 ml of tetrachloroauric acid [18.5 mM] added via drops to 20 ml trisodium citrate [2.78 mM] at a flow rate of 0.5 ml/min and D - Au) 0.6 ml of tetrachloroauric acid [18.5 mM] added near the stir bar tip to 20 ml trisodium citrate [2.78 mM] at a flow rate of 0.5 ml/min. Experiments were conducted at 80°C and stirring speed was set at 500 rpm. Inset is an average diameter for each condition obtained from 3 repeat experiments.

6.3 Conclusions

Mixing efficiency in the batch vessel was characterized using the Villermaux-Dushman reaction system for two different mixing configurations: injection of reagent from above the stirred solution in the batch vessel and injection of reagent near the stir bar tip of the stirred solution. It was found that the mixing time was 209 ms when injection was from above and 46 ms when injection was near the stir bar tip.

Silver NPs were synthesized by reducing sodium borohydride in the presence of trisodium citrate. Various mixing configurations were tested and it was found addition of sodium borohydride at a fast rate near the stir bar tip produced the smallest NPs (6.7 ± 1.7 nm). In general, larger more polydispersed NPs were found when the mixing conditions encouraged areas rich in silver nitrate and deficient in sodium borohydride. Gold NPs were synthesized using the Turkevich method, where tetrachloroauric acid is reduced by trisodium citrate at an elevated temperature. Using the same mixing configurations as those for the silver NP synthesis, the smallest NPs (13.1 ± 2.2 nm) were obtained when the reducing

agent (trisodium citrate) was added at a fast rate near the stir bar tip to the precursor (tetrachloroauric acid). These were significantly smaller than if the trisodium citrate was added at a slow rate from above the solution (18 ± 4.8 nm), showing that the mass transfer conditions and how the trisodium citrate is administered to the precursor in the classical Turkevich method is important. The mixing configuration did not significantly affect the size when using the inverse method, similar to what is observed in the literature for similar citrate to gold molar ratios. However, fast addition of reagent produced lower dispersity than slow addition because it produces a sharper separation of nucleation and growth.

The study highlights the importance of mass transfer conditions in determining the size and dispersity of the resultant NPs, even when the molar ratio of reducing agent to precursor is fixed. Often, batch reactor studies state the molar ratio of syntheses, but this may be insufficient to reproduce results since specific information on the manner in which reagents are mixed may also be needed. The results demonstrate that both diffusion and advection mass transport mechanisms are important in determining the resultant size and dispersity of synthesised NPs. Mass transport concepts of advection and diffusion can explain apparent differences in syntheses using similar concentration of reagent but different apparatus.

7 Conclusions and further work

7.1 Conclusions

The work presented in this thesis focuses on the role of mass transfer on the size and dispersity of silver and gold NPs synthesized in microfluidic devices. To achieve this, characterization of the microfluidic devices in terms of mass transfer characteristics was made to understand how concentration profiles would evolve during a reaction. The concentrations at which reaction, nucleation and growth of NP formation takes place are very important in determining their size and dispersity. The objective is to be able to control size and dispersity of synthesized NPs since this controls their properties, and hence their suitability for use in any application. The concentration at which the processes for NP formation occur is controlled by mass transfer. Subsequently, a variety of microfluidic devices were tested with gold and silver NP systems to investigate how changing mass transfer conditions affected the size and dispersity. The gold NP system investigated was the well-known Turkevich method, where tetrachloroauric acid is reduced via citrate at elevated temperatures. The silver NP system was the reduction of silver nitrate via sodium borohydride in the presence of a ligand (trisodium citrate or PVA). The microfluidic devices used were the coaxial flow reactor (CFR), impinging jet reactor (IJR), coiled flow inverter (CFI) and split and recombine (SAR) mixer. A batch reactor study for the synthesis of silver and gold NPs was also performed.

The primary objective of this study was to investigate how a variety of different mass transfer conditions can affect the size and dispersity of synthesised NPs. The overarching conclusion of the study, after investigating a variety of different mass transfer conditions using microfluidic devices and a batch reactor vessel, is that mass transfer is an important property to consider when manipulation of size and dispersity of NPs is desired. The variety of reactors used for the synthesis of NPs in this study each had their own unique mass transport characteristics which can be summarised as follows: the CFR maintained a separation of reagents through the channel because of the laminar flow and lack of geometry manipulation to reduce diffusion distance, the IJR presented an efficient mixing device as demonstrated by the low mixing times found with the conditions tested (<10 ms), the CFI utilised Dean flow to aid the mixing of the reagents while improving RTD, the SAR also presented an efficient mixing device through channel geometry manipulation which reduces the diffusion distance and the batch reactor vessel used external energy through the action of a magnetic stirrer which enhanced mixing through an advection mechanism to speed up the bulk mixing of the fluid.

To manipulate the size of synthesised NPs, controlling reaction and subsequent nucleation and growth is the main consideration. These processes are driven by the concentrations at which they take place, which is ultimately determined by the mass transport. Another important consideration is the stabilisation when achieving small monodispersed NPs is desired. This increases the complexity of the problem of NP size control, particularly when the stabilising agent behaves as a reducing agent (as is the case with the reactions studied in this work). The CFR presents a promising microfluidic device to control size of synthesised NPs because of restriction of reaction at an interface between reagent streams (due

to laminar flow and simple channel geometry). This allows for a reservoir of reagents which are supplied to the reaction interface at a constant concentration at a fixed point along the channel length. The concentration of reagents drops as reaction proceeds along the length of the channel, which results in a natural transition from nucleation to growth. The CFR also suppresses fouling because the synthesis of nanoparticles is primarily taking place away from channel walls. The major drawback of the CFR is that it would require very long channels to allow reagents to fully mix (because mass transport through diffusion only is a slow process), or through the utilisation of smaller channel dimensions. Although it is possible to implement the CFR with long channels, this may be unfeasible because of space limitations within a laboratory, and the use of smaller channel dimensions would present the need for more powerful (and expensive) pumps. The IJR performed extremely well when considering the problem of fouling of channel walls when synthesising NPs. Since there were no channel walls in the IJR, fouling (or cleaning) was eliminated. It demonstrated a good control over NP size and is easily scaled up through numbering up. However, the operation window in terms of flow rates lacks flexibility because a minimum flow rate is required to obtain jets while too high a flow rate would result in a deterioration of mixing quality. On top of this, it is unknown how the flow rate ratio (if the flow rates from each jet are not equal) would affect the mass transport properties. The CFI presents an improved RTD but fouling was observed under certain conditions, and the SAR suffered the most from fouling problem (because of a high surface area to volume ratio) even though it is an efficient mixer. This makes these reactors less suitable for synthesis of NPs since they produce a dynamic condition as fouling evolves within the channel over the course of the reaction. The batch reactor is a simple and effective means of synthesising NPs, which is perhaps the biggest advantage in the sense that it is the easiest to implement within the laboratory setting. It offers a quick and easy way to test a variety of synthesis conditions, which can then be further investigated with a focus on mass transport within the microfluidic devices presented in this work as well as others presented in the literature. The low surface area to volume ratio within the batch reactor vessels used in this work minimises the issue of fouling but nevertheless there was some fouling observed on the PTFE magnetic stirrers used in the syntheses. Of the devices studied in this work, the CFR and IJR present the most promising reactor technologies for controlling the size of NPs using microfluidic devices. It is hoped that this study provides a platform for further work in the area of synthesis of nanomaterials using microfluidic devices.

7.2 Further work

There are some exciting directions in which work on synthesis of NPs in microfluidic devices can take. Ultimately, the goal would be to produce large quantities of NPs in a reliable manner with the ability to tune the size conveniently.

The CFR has shown the potential to control size through variation in residence time using laminar flow. A vortex flow regime at higher Reynolds number was also tested, but didn't produce good results in terms of increasing control over size. Further work using the CFR should include operating it under turbulent conditions to achieve mixing kinetics faster than the reaction. This would in theory allow for reproducible results since mass transfer would no longer play a factor because concentrations within the reactor would be homogenized before reaction occurred. A study on the kinetics of the silver NP

system to discover the reaction rate equation and kinetic rate constant would be beneficial to determine how efficient the mixing needs to be. Theoretically this should increase monodispersity since reaction, nucleation, growth and stabilization can take place at the same concentration across the bulk of the fluid, rather than at various localized concentrations within the reactor. Discovery of the reaction rate equation and rate constant would also enable the simulation of accurate CFD models, enabling the potential to test a variety of reactor designs in a virtual environment rather than having to fabricate and test them experimentally. However, CFD can be computationally expensive for accurate models and would be dependent on designing models which reduce computational expense or the use of very powerful computers.

The IJR offers exceptional continuous flow characteristics for synthesis of NPs, namely the lack of a possibility of blockage through fouling. Because of this there is no need to clean the reactor before runs with aqua regia for instance, meaning that it can produce various samples of NPs at different flow rates quickly. This makes it ideal to rapidly obtain information on new NP systems when the idea is to investigate how mass transfer affects size and dispersity. One limitation of the IJR however is that it has a narrow range of operability in terms of flow rates, because it requires a certain flow rate to actually generate a jet and it has a limit on the maximum flow rate since too high a flow rate will generate a spray that does not mix efficiently. One interesting possibility would be to operate the IJR with unequal volumetric flow rate ratios, to investigate how the mass transfer is affected. Hydrodynamics of the IJR would be affected, with the combined stream being skewed in one direction dependent on which side the jet velocity was higher. By knowing the mass transfer characteristics under these conditions, operation under unequal volumetric flow rates for each input would allow an increase in the conditions that one could test quickly for a new NP system.

Flow reactors in general also afford benefits over batch reactors that would make them ideal candidates for investigating kinetics and mechanisms of various NP systems. This is because of concept of space time in a flow reactor as opposed to reaction time in a batch reactor. More specifically, the length or residence time in a reactor allows the reactions to be studied at any particular moment. By conducting in-line characterization such as UV-Vis or SAXS, one can study the process of NP formation at very small time resolutions (similar to the studies by Polte *et al*. and Takesue *et al*.)[82, 121] This system would also allow for a wide range of conditions to be studied quickly when operated in conjunction with a microfluidic device which can be operated continuously for long periods. This would help obtain information to understand the mechanisms of NP formation in a relatively rapid manner as opposed to using batch reactors.

Synthesis of NPs in the batch reactor also revealed that different results can be obtained by changing the mass transfer conditions. There is a need for more specific information when describing how reagents are mixed when considering batch reactor synthesis studies. Batch reactors still offer a very simple and effective route to synthesize NPs, and are a good tool to inform researchers who want to translate syntheses to flow. It would be interesting to see how the batch reactor results could be reproduced in a flow system, for instance using a distributed feed to mimic the droplet addition of reagent to the bulk in the batch reactor.

Appendix A: Mixing characterization using the Villermaux-Dushman reactions

Triiodide extinction coefficient evaluation

A known concentration of iodine is made by mixing a stoichiometric balance of iodide and iodate ions using the following concentrations:

[KI] = 1.13 mM

[KIO_3] = 0.226 mM

To this we add an excess of sulphuric acid to convert all the iodide and iodate into iodine according to the reaction:

$$IO_3^- + 5I^- + 6H^+ \rightarrow 3I_2 + 3H_2O$$

14.2 mM H_2SO_4 is added to a mixture of 2.26 mM KI and 0.452 mM KIO_3 with equal volumes (i.e. the volume of acid is equal to that of the iodide/iodate mixture). This results in a concentration after mixing of 7.1 mM H_2SO_4, 1.13 mM KI and 0.226 mM of KIO_3. By combining these reagents in the quantities above, one obtains the following iodine concentration:

$$5[IO_3^-] = [I^-] = \frac{5}{3}[I_2] = 1.13\ mM$$

$$[I_2] = 0.68\ mM$$

Diluting the resulting solution to 20%, 40%, 60%, 80% and 100% the original concentration and measuring the absorbance at 460 nm (wavelength at which iodine absorbs light significantly), one can obtain the extinction coefficient for iodine. Figure A1 shows the obtained calibration curve for iodine from which an extinction coefficient of 626 l/mol.cm is obtained (literature value of 758 l/mol.cm is reported for iodine at 460 nm).[189]

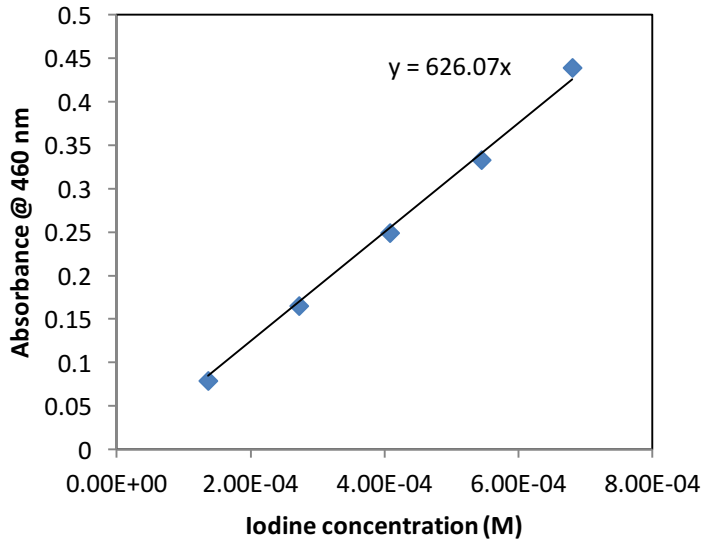

Figure A1: Calibration curve for iodine, absorbance vs. concentration, with straight line used to obtain the extinction coefficient of iodine.

Following this, we prepare solutions with the necessary concentration for triiodide extinction coefficient calculations. To do this the saturation method is used. In this method, we take a known amount of iodine and mix with an excess of iodide as per the following reaction:

$$I^- + I_2 \leftrightarrow I_3^-$$

By using a large excess of iodide ions (saturation), the equilibrium is driven largely in favor of the triiodide ion. Thus, 1ml of 0.321 M KI was added to 1 ml of 92.88 µM iodine. The prepared solution is then diluted to the appropriate concentrations and the absorbance is measured at 353 nm to obtain the calibration curve and extinction coefficient for triiodide. A value of 23209 l/mol.cm is found for the triiodide extinction coefficient shown Figure A2.

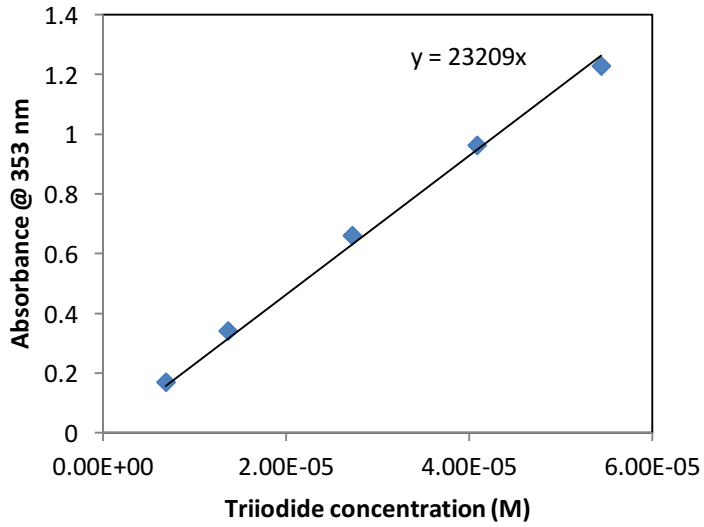

Figure A2: Calibration curve for triiodide, absorbance vs. concentration, with straight line used to obtain the extinction coefficient of triiodide.

gProms model for solution of differential mass balance equations for the Villermaux-Dushman reactions:

Model:

```
PARAMETER

Alpha       AS  REAL                #Volumetric fraction of acid
k1          AS  REAL                #reaction rate constant for reaction 1, l/mol.s
k3          AS  REAL                #forward reaction rate constant for reaction 3, l/mol.s
k3prime     AS  REAL                #backward reaction rate constant for reaction 3, 1/s
k           AS  INTEGER DEFAULT 6   #chemical species (1 = H+, 2 = H2BO3-, 3 = I-, 4 = IO3-, 5 = I2, 6 = I3-)
s           AS  INTEGER DEFAULT 2   #stream number   (1 = acid stream, 2 = reagent stream)
tm          AS  REAL                #mixing time, s

VARIABLE

k2      AS              NoType              #Reaction rate constant for reaction 2, which varies with ionic
strength, l/mol.s
C       AS  ARRAY(k,s)  OF  MolarConcentration   #Concentration of component k in stream s, mol/l
Ca      AS  ARRAY(k)    OF  NoType          #Average concentration of component k, mol/l
r1      AS  ARRAY(s)    OF  ReactionRate    #Reaction rate for reaction 1 in stream s, mol/l.s
r2      AS  ARRAY(s)    OF  ReactionRate    #Reaction rate for reaction 2 in stream s, mol/l.s
r3      AS  ARRAY(s)    OF  ReactionRate    #Reaction rate for reaction 3 in stream s, mol/l.s
I       AS          MolarConcentration  #ionic strength

EQUATION
# Differential Mass balance equations for each species
#chemical species (1 = H+, 2 = H2BO3-, 3 = I-, 4 = IO3-, 5 = I2, 6 = I3-)
FOR m:= 1 TO s DO
   $C(1,m) = (Ca(1) - C(1,m))/tm - r1(m) - 6*r2(m);
   $C(2,m) = (Ca(2) - C(2,m))/tm - r1(m);
   $C(3,m) = (Ca(3) - C(3,m))/tm - 5*r2(m) - r3(m);
   $C(4,m) = (Ca(4) - C(4,m))/tm - r2(m);
   $C(5,m) = (Ca(5) - C(5,m))/tm + 3*r2(m) - r3(m);
   $C(6,m) = (Ca(6) - C(6,m))/tm + r3(m);
END
#average concentration of species
FOR j:= 1 TO k DO
   Ca(j) = (1-alpha)*C(j,2) + alpha*C(j,1);
END
```

```
#reaction rate equations
FOR z:= 1 TO s DO
   r1(z) = k1*C(1,z)*C(2,z);
   r2(z) = k2*C(1,z)^2*C(3,z)^2*C(4,z);
   r3(z) = k3*C(5,z)*C(3,z) - k3prime*C(6,z);
END
```

Process:

```
UNIT
IEM AS IEM_VMD
SET
WITHIN IEM DO
tm     :=  1e-4;   #mixing time, s
k1     :=  1e20;   #reaction rate constant for reaction 1, l/mol.s
k3     :=  5.6e9;  #forward reaction rate constant for reaction 3, l/mol.s
k3prime :=  7.5e6;  #backward reaction rate constant for reaction 3, 1/s
Alpha   :=  0.5;    #Volumetric fraction of acid
END

EQUATION
# Equations
WITHIN IEM DO
I = 0.5*(C(1,1)+C(1,2)+C(2,1)+C(2,2)+C(3,1)+C(3,2)+C(4,1)+C(4,2)+C(6,1)+C(6,2));
k2 = 10^(9.28-3.66*I^0.5);   #Reaction rate constant for reaction 2, which varies with ionic strength, l/mol.s
END

INITIAL
WITHIN IEM DO
C(1,1) = 0.04;                  #acid concentration
FOR a:= 2 TO k DO               #sets all other species concentration to zero
   C(a,1) = 0;
END

#chemical species (1 = H+, 2 = H2BO3-, 3 = I-, 4 = IO3-, 5 = I2, 6 = I3-),
#set concentration for buffer
#conc. mol/l
C(1,2) = 0;
C(2,2) = 0.09/2;
C(3,2) = 0.032;
```

```
C(4,2) = 0.006;
C(5,2) = 0;
C(6,2) = 0;
END

SOLUTIONPARAMETERS
   ReportingInterval   :=  1e-3;

SCHEDULE
# OperationSchedule
Continue for   10;
```

Appendix B: Synthesis of silver nanoparticles in a microfluidic coaxial flow reactor

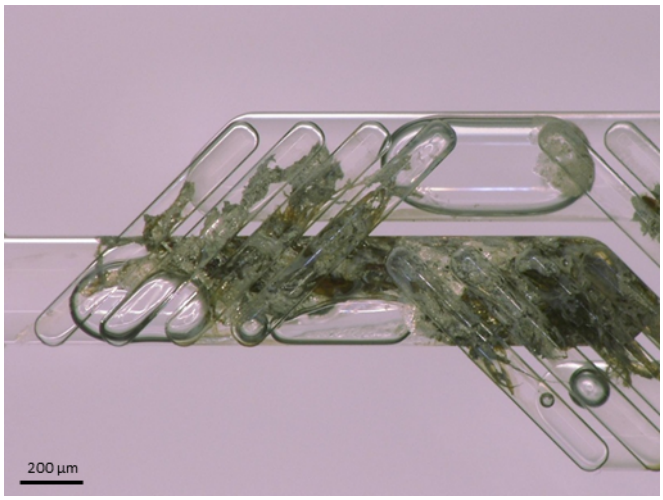

Figure B1: Microscope image showing the fouling of the channel in a split and recombine micromixer after synthesis of silver nanoparticles using silver nitrate, sodium borohydride and trisodium citrate.

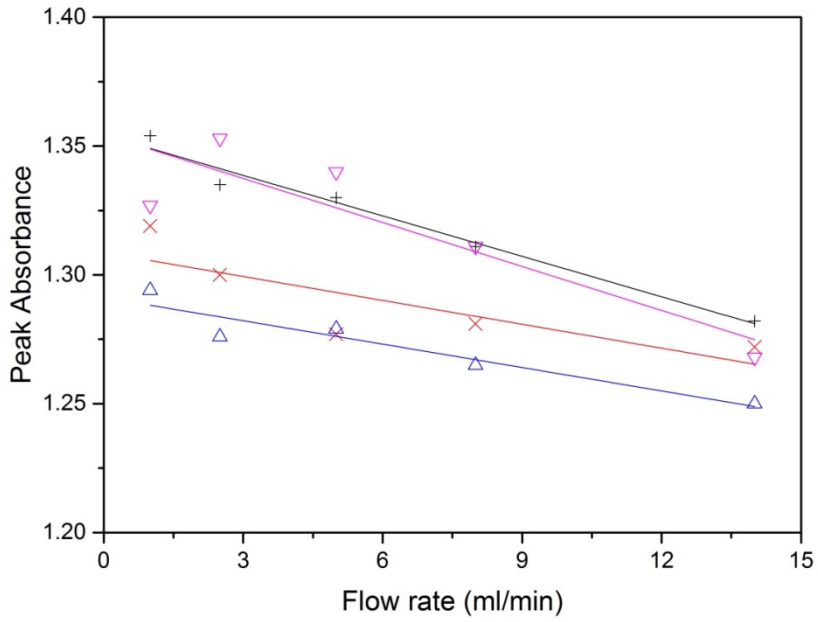

Figure B2: Peak absorbance of silver NPs synthesized at various total flow rates in the range 1-14 ml/min. Synthesis was repeated four times for each flow rate. Concentrations of silver nitrate 0.2 mM, trisodium citrate 0.2 mM, sodium borohydride 0.3 mM. 0.798 mm inner tube I.D.

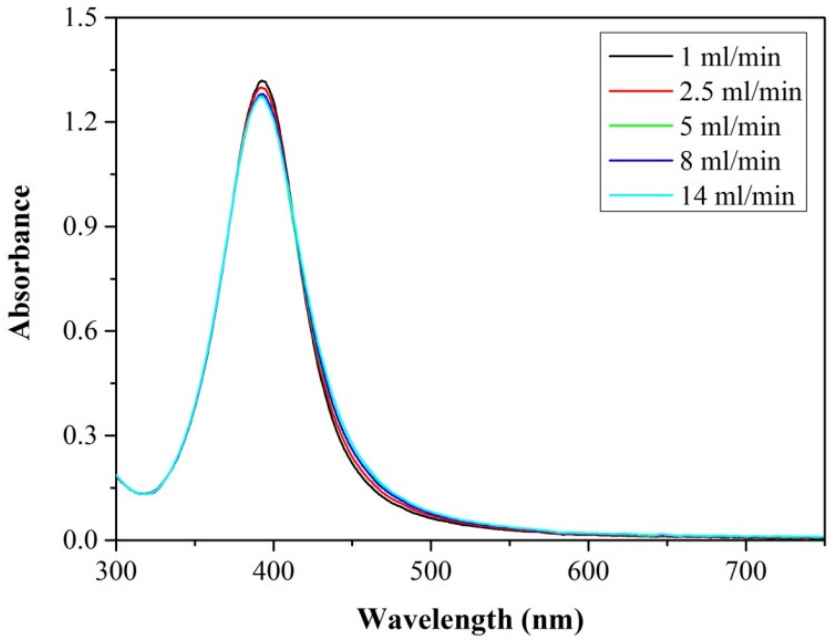

Figure B3: UV-vis spectra of silver NPs synthesized at various total flow rates in the range 1-14 ml/min. Concentrations of silver nitrate 0.2 mM, trisodium citrate 0.2 mM, sodium borohydride 0.3 mM. 0.798 mm inner tube I.D.

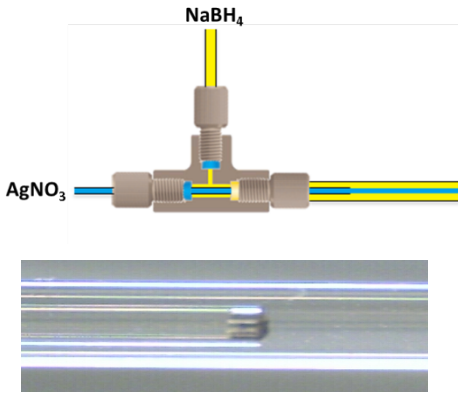

Figure B4: Fouling on the inner wall of the inner tube when silver nitrate solution flowed through the inner tube

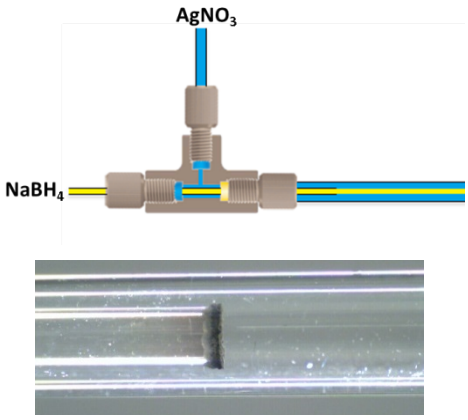

Fig. B5: Fouling on the outer wall of the inner tube when silver nitrate solution flowed through the outer tube

Appendix C: Synthesis of silver nanoparticles using a microfluidic impinging jet reactor

Reproducibility of synthesis

The reproducibility of the syntheses in the IJR was investigated by repeating experiments with citrate and PVA. The peak absorbance obtained from UV-Vis spectroscopy was used as a measure for the reproducibility. Figure C1 shows reproducibility for the synthesis in the 0.5 mm I.D. tubing IJR using citrate as a ligand. Figure C2 shows reproducibility for the synthesis in the 0.25 mm and 0.5 mm I.D. tubing IJR using PVA as a ligand.

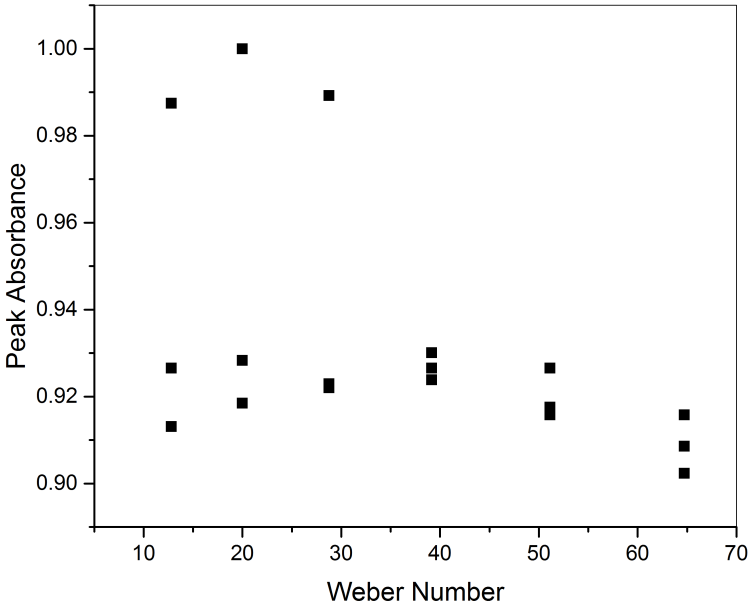

Figure C1: Peak absorbance (peak wavelength varied between 386-389 nm) obtained from UV-Vis spectroscopy vs. Weber number of silver NPs synthesized at different total flow rates using 0.5 mm I.D. tubing IJR. Experiments at each flow rate were repeated three times. Concentration of silver nitrate 0.9 mM, trisodium citrate 6 mM in input 1 and sodium borohydride 1.8 mM in input 2.

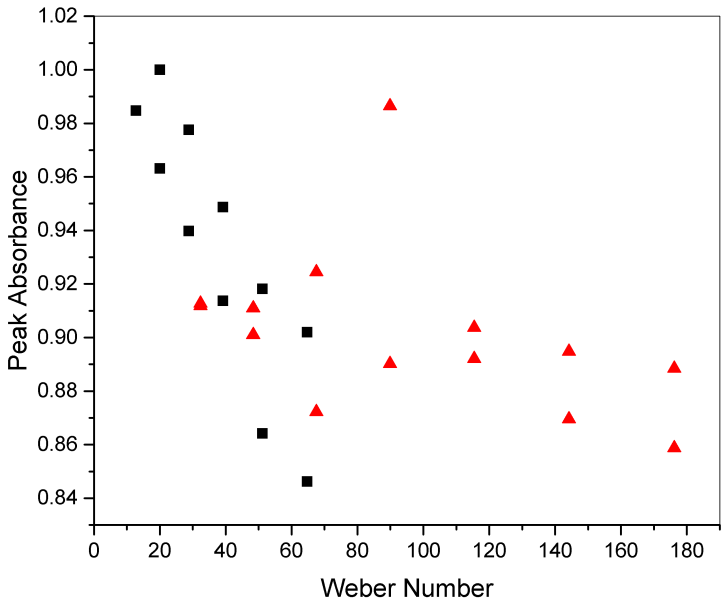

Figure C2: Peak absorbance (peak wavelength varied between 398-401 nm) obtained from UV-Vis spectroscopy vs. Weber number of silver NPs synthesized at different total flow rates using: i) 0.5 mm (black squares) and ii) 0.25 mm (red triangles) I.D. tubing IJR. Each flow rate was repeated twice. Concentration of silver nitrate 0.9 mM, PVA 0.02 wt% in input 1 and sodium borohydride 1.8 mM in input 2.

Comparison of hydrodynamics between water only system and silver NP synthesis using PVA in 0.25 mm IJR

Figure C3 compares the hydrodynamics of the impinging jets in the 0.25 mm I.D. tubing IJR when water is used and for the silver NP synthesis where one of the streams contains PVA.

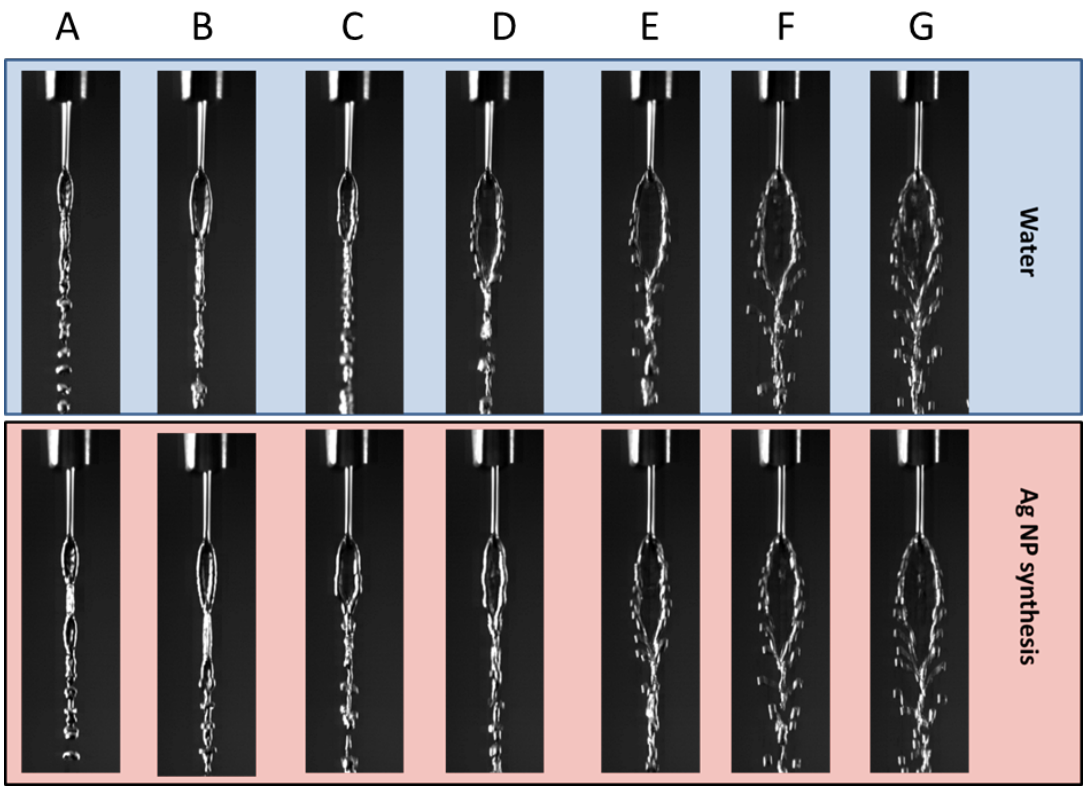

Figure C3: High speed camera images of hydrodynamics in the 0.25 mm I.D. tubing IJR for a system using only water and under silver NP synthesis conditions of concentration of silver nitrate 0.9 mM, PVA 0.02 wt%, sodium borohydride 1.8 mM. Total flow rates were: A: 18 ml/min (We: 32), B: 22 ml/min (We: 48), C: 26 ml/min (We: 68), D: 30 ml/min (We: 90), E: 34 ml/min (We: 115), F: 38 ml/min (We: 144) and G: 42 ml/min (We: 176).

TEM image of silver NPs synthesized using an increased PVA concentration

Figure C4 shows the silver NPs obtained when the PVA concentration was doubled.

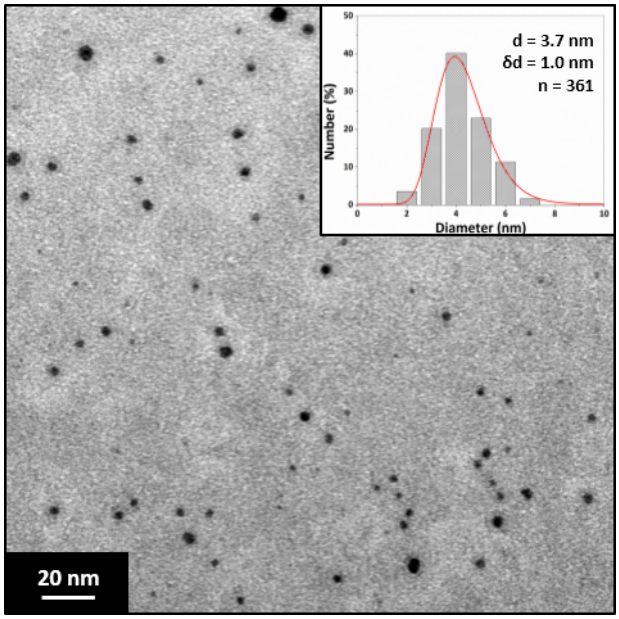

Figure C4: TEM image and particle size distribution of silver NPs synthesized using the 0.5 mm I.D. tubing IJR at a flow rate of 72 ml/min (We: 65). Concentration of silver nitrate 0.9 mM, PVA 0.04 wt%, sodium borohydride 1.8 mM.

Appendix D: Effect of hydrodynamics and mixing conditions on the continuous synthesis of gold and silver nanoparticles in a coaxial flow device

Gold NP synthesis repeatability

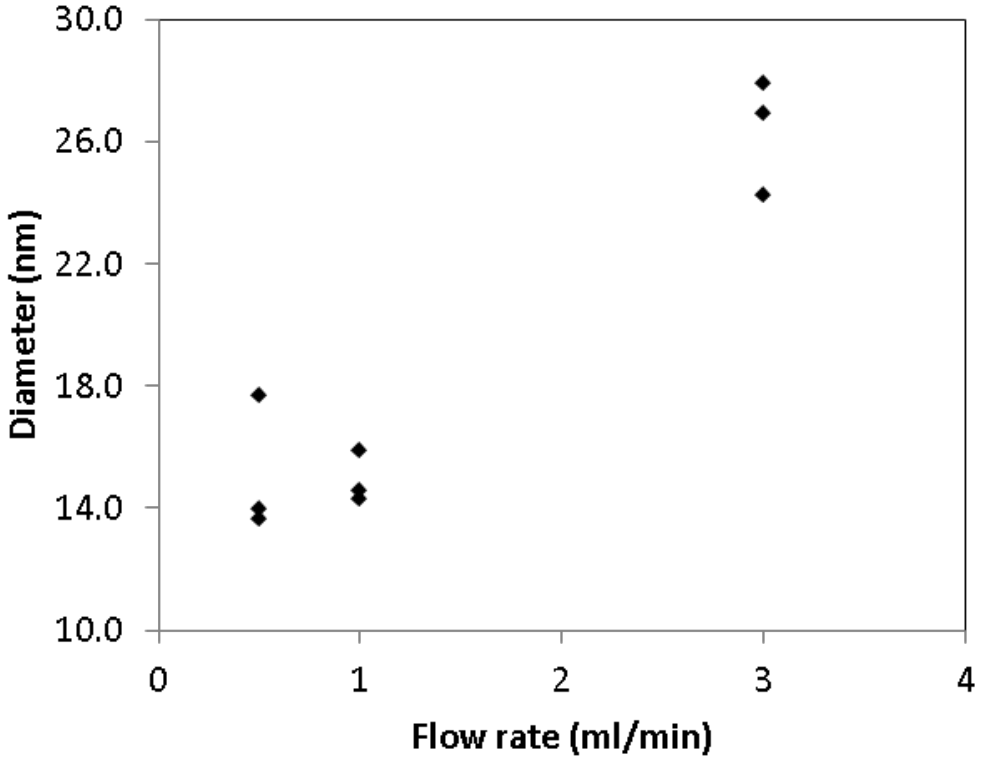

Figure D1: Average diameter of gold NPs synthesized using the CFR with a CFI residence loop at flow rates of 0.5, 1 and 3 ml/min obtained using DCS analysis. Concentration of tetrachloroauric acid, 0.557 mM; concentration of trisodium citrate, 0.09 M; volumetric flow rate ratio, 32.3: 1 (Q_{out}:Q_{in}, $HAuCl_4$: Na_3citrate); molar flow rate ratio, 1:5 ($HAuCl_4$: Na_3citrate); temperature, 80°C.

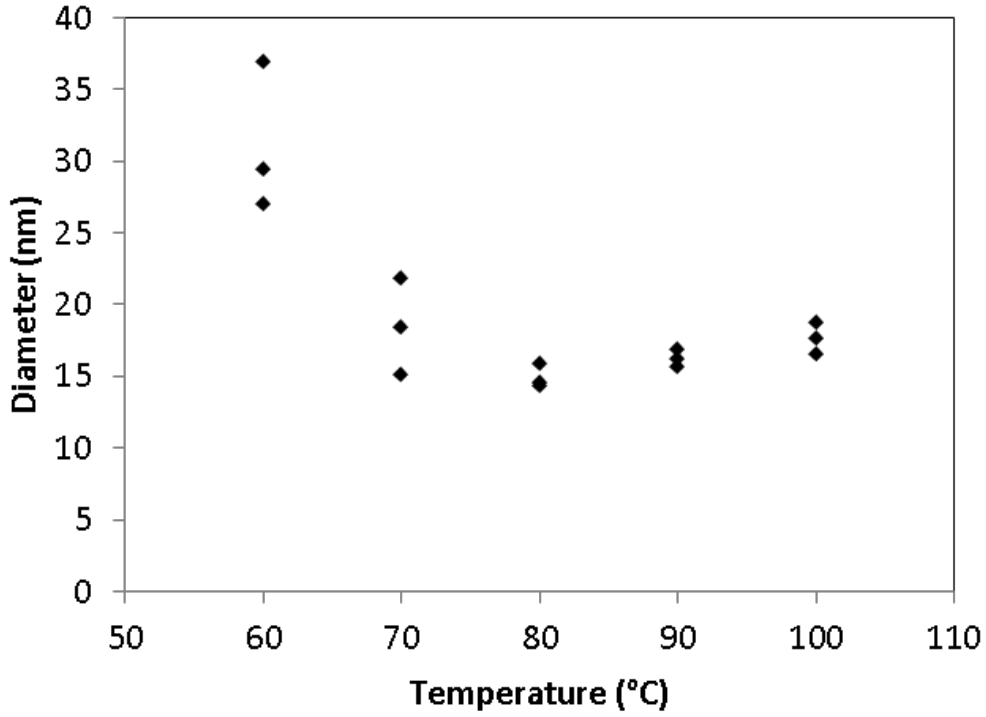

Figure D2: Average diameter of gold NPs synthesized using the CFR with a CFI residence loop at temperatures between 60-100°C obtained using DCS analysis. Concentration of tetrachloroauric acid, 0.557 mM; concentration of trisodium citrate, 0.09 M; volumetric flow rate ratio, 32.3: 1 (Q_{out}:Q_{in}, $HAuCl_4$: Na_3citrate); molar flow rate ratio, 1:5 ($HAuCl_4$: Na_3citrate); flow rate, 1 ml/min.

Visualization of flow in the CFR using turbulent conditions

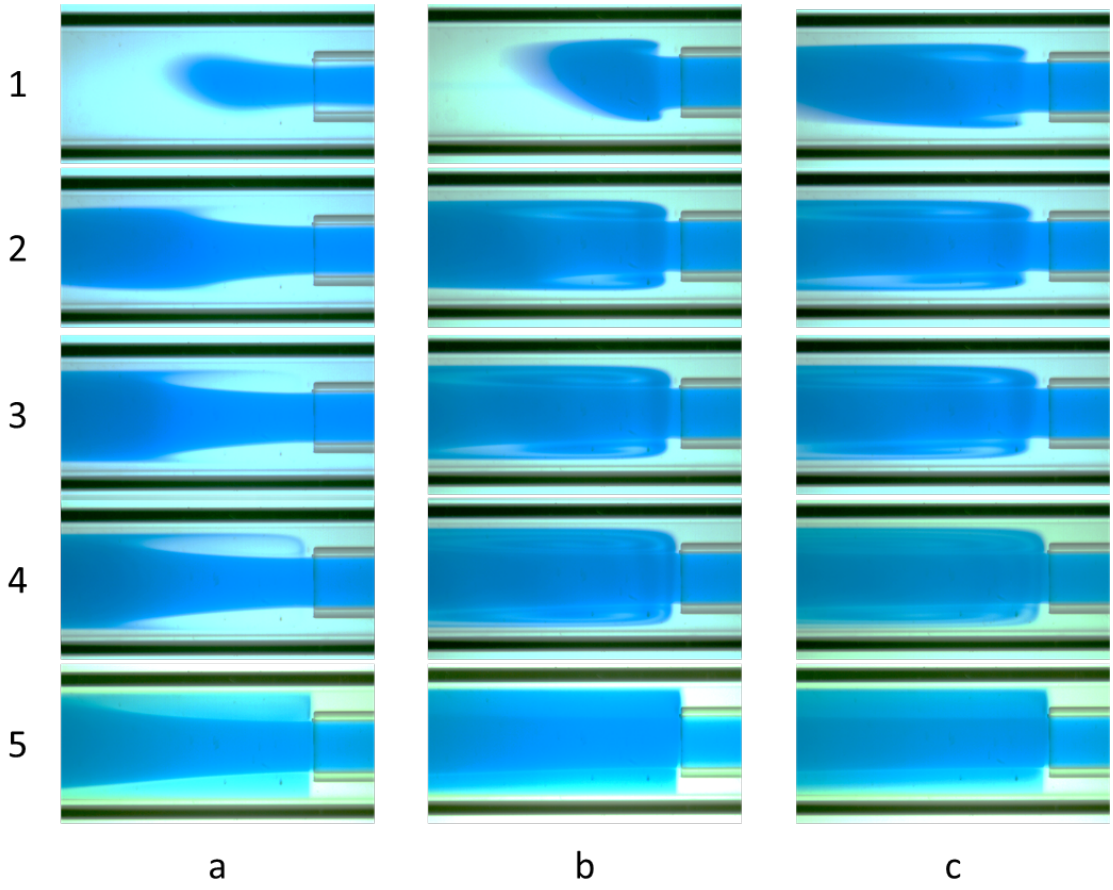

Figure D3: Flow visualization in the CFR with an inner tube I.D. of 0.798 mm at different Reynolds numbers a) 5.1 ml/min (Re inner tube, 133, Re main channel, 54), b) 10.1 ml/min (Re inner tube, 265, Re main channel, 107) and c) 15.1 ml/min (Re inner tube, 397, Re main channel, 160)**.** Basic Blue dye was pumped through the inner tube between 5 and 15 ml/min and water was pumped through the outer tube at a fixed flow rate of 0.1 ml/min. 1 indicates when dye is initially pumped through the inner tube with increasing numbers going up to show the CFR at steady state.

Silver NP synthesis repeatability with inner tube I.D. variation

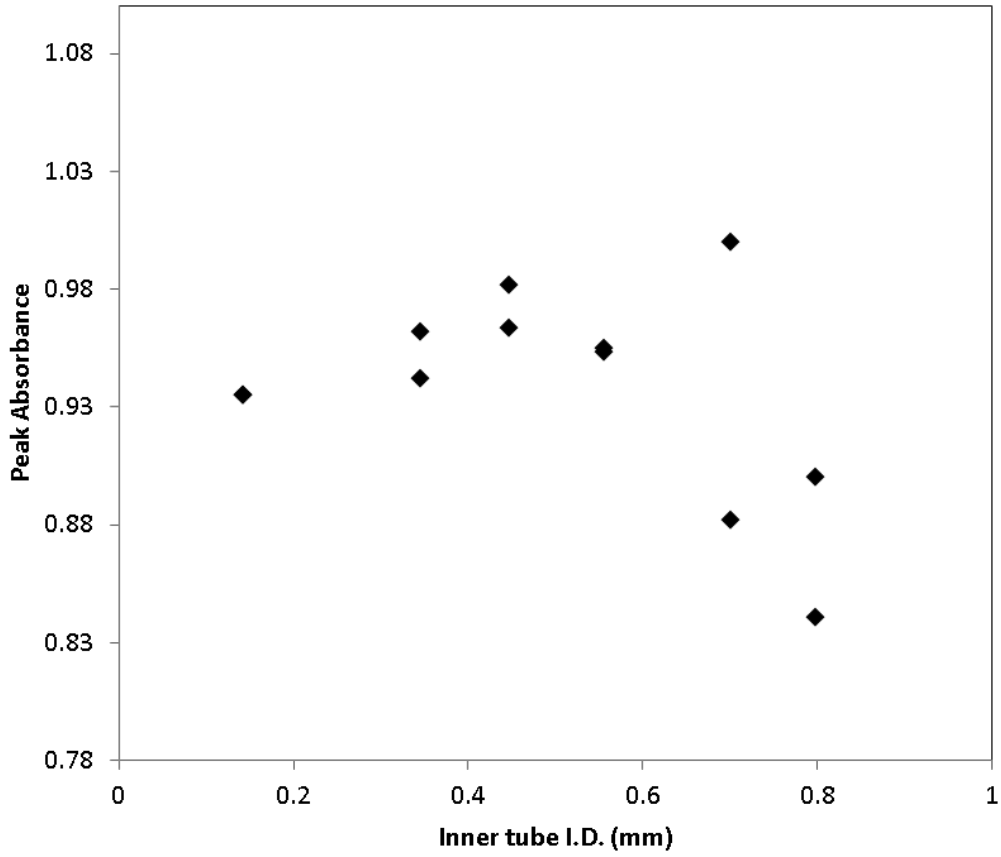

Figure D4: Peak absorbance obtained from UV-Vis spectra vs. inner tube internal diameter of repeat experiments for silver NPs synthesized using the CFR with inner tube internal diameters ranging between 0.142 and 0.798 mm. Concentration of silver nitrate, 0.1 mM; concentration of sodium borohydride, 0.3 mM; concentration of trisodium citrate, 0.5 M; volumetric flow rate ratio, 1: 1 (Q_{out}:Q_{in}, $NaBH_4$: $AgNO_3$); molar flow rate ratio, 1:3:5 ($AgNO_3$:$NaBH_4$:Na_3citrate); flow rate, 1 ml/min, temperature 22-24°C.

The following list are publications which resulted from the work contained in this thesis:

1. R. Baber, L. Mazzei, N. T. K. Thanh and A. Gavriilidis, *RSC Advances*, 2015, **5**, 95585-95591.

2. R. Baber, L. Mazzei, N. T. Thanh and A. Gavriilidis, *Journal of Flow Chemistry*, 2016, 1-11.

1. A. Gavriilidis, P. Angeli, E. Cao, K. K. Yeong and Y. S. S. Wan, *Chemical Engineering Research & Design*, 2002, **80**, 3-30.
2. V. V. Mody, R. Siwale, A. Singh and H. R. Mody, *Journal of Pharmacy and Bioallied Sciences*, 2010, **2**, 282.
3. W. K. Leutwyler, S. L. Bürgi and H. Burgl, *Science*, 1996, **271**, 933.
4. W. C. Chan, D. J. Maxwell, X. Gao, R. E. Bailey, M. Han and S. Nie, *Current opinion in biotechnology*, 2002, **13**, 40-46.
5. S. Agnihotri, S. Mukherji and S. Mukherji, *RSC Advances*, 2014, **4**, 3974-3983.
6. Y. Sun and Y. Xia, *Advanced Materials*, 2003, **15**, 695-699.
7. M. Maillard, S. Giorgio and M.-P. Pileni, *Advanced Materials*, 2002, **14**, 1084.
8. B. D. Busbee, S. O. Obare and C. J. Murphy, *Advanced Materials*, 2003, **15**, 414-416.
9. P. Hugounenq, M. Levy, D. Alloyeau, L. Lartigue, E. Dubois, V. Cabuil, C. Ricolleau, S. Roux, C. Wilhelm, F. Gazeau and R. Bazzi, *The Journal of Physical Chemistry C*, 2012, **116**, 15702-15712.
10. O. M. Bakr, B. H. Wunsch and F. Stellacci, *Chemistry of Materials*, 2006, **18**, 3297-3301.
11. H. Khurshid, S. Chandra, W. Li, M. H. Phan, G. C. Hadjipanayis, P. Mukherjee and H. Srikanth, *J Appl Phys*, 2013, **113**, 17B508.
12. C. J. Murphy and N. R. Jana, *Advanced Materials*, 2002, **14**, 80.
13. E. V. Shevchenko, M. I. Bodnarchuk, M. V. Kovalenko, D. V. Talapin, R. K. Smith, S. Aloni, W. Heiss and A. P. Alivisatos, *Adv. Mater*, 2008, **20**, 4323-4329.
14. A. D. McFarland and R. P. Van Duyne, *Nano letters*, 2003, **3**, 1057-1062.
15. G. Korotcenkov, B. K. Cho, L. B. Gulina and V. P. Tolstoy, *Sensors and Actuators B: Chemical*, 2012, **166–167**, 402-410.
16. N. Bahadur, K. Jain, R. Pasricha, Govind and S. Chand, *Sensors and Actuators B: Chemical*, 2011, **159**, 112-120.
17. D. D. Evanoff and G. Chumanov, *ChemPhysChem*, 2005, **6**, 1221-1231.
18. S. Panigrahi, S. Praharaj, S. Basu, S. K. Ghosh, S. Jana, S. Pande, T. Vo-Dinh, H. Jiang and T. Pal, *The Journal of Physical Chemistry B*, 2006, **110**, 13436-13444.
19. C. J. Murphy, T. K. Sau, A. M. Gole, C. J. Orendorff, J. Gao, L. Gou, S. E. Hunyadi and T. Li, *The Journal of Physical Chemistry B*, 2005, **109**, 13857-13870.
20. D. Chen, X. Qiao, X. Qiu and J. Chen, *J Mater Sci*, 2009, **44**, 1076-1081.
21. Y. Li, Y. Wu and B. S. Ong, *J Am Chem Soc*, 2005, **127**, 3266-3267.
22. Z.-J. Jiang, C.-Y. Liu and L.-W. Sun, *The Journal of Physical Chemistry B*, 2005, **109**, 1730-1735.
23. A. C. Patel, S. Li, C. Wang, W. Zhang and Y. Wei, *Chemistry of materials*, 2007, **19**, 1231-1238.
24. S. Link, Z. L. Wang and M. El-Sayed, *The Journal of Physical Chemistry B*, 1999, **103**, 3529-3533.
25. C. Marambio-Jones and E. M. Hoek, *J Nanopart Res*, 2010, **12**, 1531-1551.
26. G. A. Sotiriou and S. E. Pratsinis, *Current Opinion in Chemical Engineering*, 2011, **1**, 3-10.

27. V. K. Sharma, R. A. Yngard and Y. Lin, *Advances in Colloid and Interface Science*, 2009, **145**, 83-96.
28. Y. Yang, S. Matsubara, L. Xiong, T. Hayakawa and M. Nogami, *The Journal of Physical Chemistry C*, 2007, **111**, 9095-9104.
29. R. A. Sperling, P. Rivera Gil, F. Zhang, M. Zanella and W. J. Parak, *Chem. Soc. Rev.*, 2008, **37**, 1896-1908.
30. L. Dykman and N. Khlebtsov, *Chem. Soc. Rev.*, 2012, **41**, 2256-2282.
31. S. Guo and E. Wang, *Analytica Chimica Acta*, 2007, **598**, 181-192.
32. M.-C. Daniel and D. Astruc, *Chemical Reviews*, 2004, **104**, 293-346.
33. W. Ehrfeld, V. Hessel and H. Lowe, *Microreactors: New Technology for Modern Chemistry*, Wiley-VCH, Weinheim, 2000.
34. N. T. K. Thanh, N. Maclean and S. Mahiddine, *Chemical Reviews*, 2014, **114**, 7610–7630.
35. A. Abou-Hassan, O. Sandre, S. Neveu and V. Cabuil, *Angewandte Chemie International Edition*, 2009, **48**, 2342-2345.
36. A. Abou-Hassan, R. Bazzi and V. Cabuil, *Angewandte Chemie International Edition*, 2009, **48**, 7180-7183.
37. S. A. Khan, A. Günther, M. A. Schmidt and K. F. Jensen, *Langmuir*, 2004, **20**, 8604-8611.
38. X. Shen, Y. Song, S. Li, R. Li, S. Ji, Q. Li, H. Duan, R. Xu, W. Yang and K. Zhao, *RSC Advances*, 2014, **4**, 34179-34188.
39. R. Wang, W. Yang, Y. Song, X. Shen, J. Wang, X. Zhong, S. Li and Y. Song, *Scientific reports*, 2015, **5**, 9189.
40. W. Chen-Hsun, H. Chih-Chia, Y. Chen-Sheng, L. Huan-Yao and L. Gwo-Bin, *J Micromech Microeng*, 2008, **18**, 035019.
41. J. M. Ottino, *Annu Rev Fluid Mech*, 1990, **22**, 207-253.
42. N. T. Nguyen and Z. G. Wu, *J Micromech Microeng*, 2005, **15**, R1-R16.
43. C. J. Campbell and B. A. Grzybowski, *Philosophical Transactions of the Royal Society a-Mathematical Physical and Engineering Sciences*, 2004, **362**, 1069-1086.
44. E. A. Mansur, M. Ye, Y. Wang and Y. Dai, *Chinese Journal of Chemical Engineering*, 2008, **16**, 503-516.
45. D. Bokenkamp, A. Desai, X. Yang, Y. C. Tai, E. M. Marzluff and S. L. Mayo, *Analytical Chemistry*, 1998, **70**, 232-236.
46. N. Kockmann, T. Kiefer, M. Engler and P. Woias, 2005.
47. S. H. Wong, M. C. L. Ward and C. W. Wharton, *Sens. Actuator B-Chem.*, 2004, **100**, 359-379.
48. M. Yi and H. H. Bau, *International Journal of Heat and Fluid Flow*, 2003, **24**, 645-656.
49. F. G. Bessoth, A. J. deMello and A. Manz, *Analytical Communications*, 1999, **36**, 213-215.
50. J. B. Knight, A. Vishwanath, J. P. Brody and R. H. Austin, *Phys Rev Lett*, 1998, **80**, 3863-3866.
51. F. Schonfeld, V. Hessel and C. Hofmann, *Lab on a Chip*, 2004, **4**, 65-69.
52. M. Kashid, A. Renken and L. Kiwi-Minsker, *Chem Eng J*, 2011, **167**, 436-443.
53. W. Buchegger, C. Wagner, B. Lendl, M. Kraft and M. J. Vellekoop, *Microfluid Nanofluid*, 2011, **10**, 889-897.

54. Z. Chen, M. Bown, B. O'Sullivan, J. MacInnes, R. Allen, M. Mulder, M. Blom and R. van't Oever, *Microfluid Nanofluid*, 2009, **6**, 763-774.
55. S. Waelchli and P. Rudolf von Rohr, *International Journal of Multiphase Flow*, 2006, **32**, 791-806.
56. M. N. Kashid, D. F. Rivas, D. W. Agar and S. Turek, *Asia-Pacific Journal of Chemical Engineering*, 2008, **3**, 151-160.
57. W. Tanthapanichakoon, N. Aoki, K. Matsuyama and K. Mae, *Chem Eng Sci*, 2006, **61**, 4220-4232.
58. R. Miyake, T. S. J. Lammerink, M. Elwenspoek and J. H. J. Fluitman, *Micro mixer with fast diffusion*, 1993.
59. R. Miyake, K. Tsuzuki, T. Takagi, K. Imai and Ieee, in *Mems 97, Proceedings - Ieee the Tenth Annual International Workshop on Micro Electro Mechanical Systems: An Investigation of Micro Structures, Sensors, Actuators, Machines and Robots*, 1997, DOI: 10.1109/memsys.1997.581779, pp. 102-107.
60. J. Voldman, M. L. Gray and M. A. Schmidt, *Journal of Microelectromechanical Systems*, 2000, **9**, 295-302.
61. V. Hessel, H. Lowe and F. Schonfeld, *Chem Eng Sci*, 2005, **60**, 2479-2501.
62. A. D. Stroock, S. K. W. Dertinger, A. Ajdari, I. Mezic, H. A. Stone and G. M. Whitesides, *Science*, 2002, **295**, 647-651.
63. T. G. Kang and T. H. Kwon, *J Micromech Microeng*, 2004, **14**, 891-899.
64. J. A. Creighton, C. G. Blatchford and M. G. Albrecht, *Journal of the Chemical Society-Faraday Transactions ii*, 1979, **75**, 790-798.
65. N. Shirtcliffe, U. Nickel and S. Schneider, *J. Colloid Interface Sci.*, 1999, **211**, 122-129.
66. B. H. Ryu, Y. Choi, H. S. Park, J. H. Byun, K. Kong, J. O. Lee and H. Chang, *Colloid Surface A*, 2005, **270**, 345-351.
67. K. Song, S. Lee, T. Park and B. Lee, *Korean J. Chem. Eng.*, 2009, **26**, 153-155.
68. J. Polte, X. Tuaev, M. Wuithschick, A. Fischer, A. F. Thuenemann, K. Rademann, R. Kraehnert and F. Emmerling, *ACS Nano*, 2012, **6**, 5791-5802.
69. V. V. Pinto, M. J. Ferreira, R. Silva, H. A. Santos, F. Silva and C. M. Pereira, *Colloids and Surfaces A: Physicochemical and Engineering Aspects*, 2010, **364**, 19-25.
70. A. Thogersen, J. Bonsak, C. H. Fosli and G. Muntingh, *J Appl Phys*, 2011, **110**.
71. J. Wagner, T. R. Tshikhudo and J. M. Koehler, *Chem Eng J*, 2008, **135**, S104-S109.
72. J. M. Kohler, L. Abahmane, J. Wagner, J. Albert and G. Mayer, *Chem Eng Sci*, 2008, **63**, 5048-5055.
73. X. Z. Lin, A. D. Terepka and H. Yang, *Nano Letters*, 2004, **4**, 2227-2232.
74. C. Sonnichsen, J. Boleininger, A. Kurz and V. Reuss, *Phys Chem Chem Phys*, 2006, **8**, 3824-3827.
75. N. R. Jana, L. Gearheart and C. J. Murphy, *Chem. Commun.*, 2001, DOI: 10.1039/b100521i, 617-618.
76. A. Knauer, A. Thete, S. Li, H. Romanus, A. Csaki, W. Fritzsche and J. M. Koehler, *Chem Eng J*, 2011, **166**, 1164-1169.
77. J. D. Tice, H. Song, A. D. Lyon and R. F. Ismagilov, *Langmuir*, 2003, **19**, 9127-9133.

78. J. M. Koehler, M. Held, U. Huebner and J. Wagner, *Chem Eng Technol*, 2007, **30**, 347-354.
79. H. Liu, J. Huang, D. Sun, L. Lin, W. Lin, J. Li, X. Jiang, W. Wu and Q. Li, *Chem Eng J*, 2012, **209**, 568-576.
80. D. V. R. Kumar, B. L. V. Prasad and A. A. Kulkarni, *Chem Eng J*, 2012, **192**, 357-368.
81. L. L. Lazarus, C. T. Riche, B. C. Marin, M. Gupta, N. Malmstadt and R. L. Brutchey, *ACS Applied Materials & Interfaces*, 2012, **4**, 3077-3083.
82. M. Takesue, T. Tomura, M. Yamada, K. Hata, S. Kuwamoto and T. Yonezawa, *J Am Chem Soc*, 2011, **133**, 14164-14167.
83. A. Henglein and M. Giersig, *ChemInform*, 2000, **31**, 9533-9539.
84. Z. S. Pillai and P. V. Kamat, *The Journal of Physical Chemistry B*, 2003, **108**, 945-951.
85. W. Zhang, X. Qiao, Q. Chen, Y. Cai and H. Chen, *Applied Surface Science*, 2012, **258**, 5909-5913.
86. T. J. Woehl, J. E. Evans, I. Arslan, W. D. Ristenpart and N. D. Browning, *ACS Nano*, 2012, **6**, 8599-8610.
87. X. C. Jiang, C. Y. Chen, W. M. Chen and A. B. Yu, *Langmuir*, 2010, **26**, 4400-4408.
88. J. Turkevich, P. C. Stevenson and J. Hillier, *Discussions of the Faraday Society*, 1951, **11**, 55-75.
89. G. Frens, *Nature*, 1973, **241**, 20-22.
90. S. L. Goodman, G. M. Hodges, L. K. Trejdosiewicz and D. C. Livingston, *Journal of Microscopy*, 1981, **123**, 201-213.
91. M. K. Chow and C. F. Zukoski, *J. Colloid Interface Sci.*, 1994, **165**, 97-109.
92. C.-H. Su, P.-L. Wu and C.-S. Yeh, *The Journal of Physical Chemistry B*, 2003, **107**, 14240-14243.
93. L. Pei, K. Mori and M. Adachi, *Langmuir*, 2004, **20**, 7837-7843.
94. J. Kimling, M. Maier, B. Okenve, V. Kotaidis, H. Ballot and A. Plech, *The Journal of Physical Chemistry B*, 2006, **110**, 15700-15707.
95. X. Ji, X. Song, J. Li, Y. Bai, W. Yang and X. Peng, *J Am Chem Soc*, 2007, **129**, 13939-13948.
96. W. Patungwasa and J. H. Hodak, *Materials Chemistry and Physics*, 2008, **108**, 45-54.
97. I. Ojea-Jiménez, F. M. Romero, N. G. Bastús and V. Puntes, *The Journal of Physical Chemistry C*, 2010, **114**, 1800-1804.
98. M. A. Uppal, A. Kafizas, T. H. Lim and I. P. Parkin, *New Journal of Chemistry*, 2010, **34**, 1401-1407.
99. M. A. Uppal, A. Kafizas, M. B. Ewing and I. P. Parkin, *New Journal of Chemistry*, 2010, **34**, 2906-2914.
100. I. Ojea-Jiménez, N. G. Bastús and V. Puntes, *The Journal of Physical Chemistry C*, 2011, **115**, 15752-15757.
101. I. Ojea-Jiménez and J. M. Campanera, *The Journal of Physical Chemistry C*, 2012, **116**, 23682-23691.
102. S. K. Sivaraman, S. Kumar and V. Santhanam, *J. Colloid Interface Sci.*, 2011, **361**, 543-547.
103. F. Schulz, T. Homolka, N. G. Bastús, V. Puntes, H. Weller and T. Vossmeyer, *Langmuir*, 2014, **30**, 10779-10784.
104. M. Wuithschick, A. Birnbaum, S. Witte, M. Sztucki, U. Vainio, N. Pinna, K. Rademann, F. Emmerling, R. Kraehnert and J. Polte, *ACS Nano*, 2015, **9**, 7052-7071.

105. J. Piella, N. G. Bastús and V. Puntes, *Chemistry of Materials*, 2016, **28**, 1066-1075.
106. F. Kettemann, A. Birnbaum, S. Witte, M. Wuithschick, N. Pinna, R. Kraehnert, K. Rademann and J. Polte, *Chemistry of Materials*, 2016, **28**, 4072-4081.
107. J. Ftouni, M. Penhoat, A. Addad, E. Payen, C. Rolando and J.-S. Girardon, *Nanoscale*, 2012, **4**, 4450-4454.
108. K. Sugano, Y. Uchida, O. Ichihashi, H. Yamada, T. Tsuchiya and O. Tabata, *Microfluid Nanofluid*, 2010, **9**, 1165-1174.
109. J. M. Kohler, J. Wagner and J. Albert, *Journal of Materials Chemistry*, 2005, **15**, 1924-1930.
110. D. Shalom, R. C. R. Wootton, R. F. Winkle, B. F. Cottam, R. Vilar, A. J. deMello and C. P. Wilde, *Materials Letters*, 2007, **61**, 1146-1150.
111. V. Sebastian Cabeza, S. Kuhn, A. A. Kulkarni and K. F. Jensen, *Langmuir*, 2012, **28**, 7007-7013.
112. H. Tsunoyama, N. Ichikuni and T. Tsukuda, *Langmuir*, 2008, **24**, 11327-11330.
113. V. K. LaMer and R. H. Dinegar, *Journal of the American Chemical Society*, 1950, **72**, 4847-4854.
114. J. Turkevich, P. C. Stevenson and J. Hillier, *The Journal of Physical Chemistry*, 1953, **57**, 670-673.
115. S. Biggs, M. K. Chow, C. F. Zukoski and F. Grieser, *J. Colloid Interface Sci.*, 1993, **160**, 511-513.
116. S. Biggs, P. Mulvaney, C. F. Zukoski and F. Grieser, *Journal of the American Chemical Society*, 1994, **116**, 9150-9157.
117. J. F. Wall, F. Grieser and h. F. Zukoski, *Journal of the Chemical Society, Faraday Transactions*, 1997, **93**, 4017-4020.
118. S. Kumar, K. S. Gandhi and R. Kumar, *Industrial & Engineering Chemistry Research*, 2006, **46**, 3128-3136.
119. B.-K. Pong, H. I. Elim, J.-X. Chong, W. Ji, B. L. Trout and J.-Y. Lee, *The Journal of Physical Chemistry C*, 2007, **111**, 6281-6287.
120. J. r. Polte, T. T. Ahner, F. Delissen, S. Sokolov, F. Emmerling, A. Thünemann and R. Kraehnert, *Journal of the American Chemical Society*, 2010, **132**, 1296-1301.
121. J. Polte, R. Erler, A. F. Thunemann, S. Sokolov, T. T. Ahner, K. Rademann, F. Emmerling and R. Kraehnert, *ACS Nano*, 2010, **4**, 1076-1082.
122. D. Goia and E. Matijević, *Colloids and Surfaces A: Physicochemical and Engineering Aspects*, 1999, **146**, 139-152.
123. J. Park, V. Privman and E. Matijević, *The Journal of Physical Chemistry B*, 2001, **105**, 11630-11635.
124. J. Polte, *CrystEngComm*, 2015, **17**, 6809-6830.
125. A. Plech, V. Kotaidis, A. Siems and M. Sztucki, *Phys Chem Chem Phys*, 2008, **10**, 3888-3894.
126. A. Knauer, A. Csáki, F. Möller, C. Hühn, W. Fritzsche and J. M. Köhler, *The Journal of Physical Chemistry C*, 2012, **116**, 9251-9258.
127. J. Wagner and J. M. Kohler, *Nano Letters*, 2005, **5**, 685-691.
128. M. Takagi, T. Maki, M. Miyahara and K. Mae, *Chem Eng J*, 2004, **101**, 269-276.
129. T. Maki, J. I. Kitada and K. Mae, *Chem Eng Technol*, 2013, **36**, 1027-1032.
130. A. Abou Hassan, O. Sandre, V. Cabuil and P. Tabeling, *Chem. Commun.*, 2008, DOI: 10.1039/B719550H, 1783-1785.

131. J.-M. Lim, A. Swami, L. M. Gilson, S. Chopra, S. Choi, J. Wu, R. Langer, R. Karnik and O. C. Farokhzad, *ACS Nano*, 2014, **8**, 6056-6065.
132. J. Schülein, I. Minrath, R. Pommersheim and H. Löwe, *Journal of Flow Chemistry*, 2014, **4**, 44-53.
133. J. Shen, Z. Li, Q. Yan and Y. Chen, *The Journal of Physical Chemistry*, 1993, **97**, 8504-8511.
134. W. M. Haynes, *CRC handbook of chemistry and physics*, CRC Press; Taylor & Francis, Boca Raton, Fla. [u.a.]; London, 95th edn., 2014.
135. J. C. Fanning, B. C. Brooks, A. B. Hoeglund, D. A. Pelletier and J. A. Wadford, *Inorganica Chimica Acta*, 2000, **310**, 115-119.
136. D. L. Van Hyning, W. G. Klemperer and C. F. Zukoski, *Langmuir*, 2001, **17**, 3120-3127.
137. V. R. Fernandes, A. M. F. R. Pinto and C. M. Rangel, *International Journal of Hydrogen Energy*, 2010, **35**, 9862-9868.
138. H. I. Schlesinger, H. C. Brown, A. E. Finholt, J. R. Gilbreath, H. R. Hoekstra and E. K. Hyde, *J Am Chem Soc*, 1953, **75**, 215-219.
139. D. L. Van Hyning and C. F. Zukoski, *Langmuir*, 1998, **14**, 7034-7046.
140. O. Brand, G. K. Fedder, C. Hierold, J. G. Korvink, O. Tabata and N. Kockmann, *Micro process engineering: fundamentals, devices, fabrication, and applications*, John Wiley & Sons, Weinheim, Germany, 2013.
141. H. S. Harned and C. L. Hildreth, *J Am Chem Soc*, 1951, **73**, 3292-3293.
142. M. Chatenet, M. B. Molina-Concha, N. El-Kissi, G. Parrour and J. P. Diard, *Electrochimica Acta*, 2009, **54**, 4426-4435.
143. M. Wuithschick, B. Paul, R. Bienert, A. Sarfraz, U. Vainio, M. Sztucki, R. Kraehnert, P. Strasser, K. Rademann, F. Emmerling and J. Polte, *Chemistry of Materials*, 2013, **25**, 4679-4689.
144. W. L. W. Hau, D. W. Trau, N. J. Sucher, M. Wong and Y. Zohar, *J Micromech Microeng*, 2003, **13**, 272-278.
145. R. Baber, L. Mazzei, N. T. K. Thanh and A. Gavriilidis, *RSC Advances*, 2015, **5**, 95585-95591.
146. C. H. Sohn, W. S. Seol, A. A. Shibanov and V. P. Pikalov, *Journal of Propulsion and Power*, 2007, **23**, 131-139.
147. A. J. Mahajan and D. J. Kirwan, *AIChE Journal*, 1996, **42**, 1801-1814.
148. J. W. Mullin, *Crystallization*, Butterworth-Heinemann, Oxford, 2001.
149. P. Erni and A. Elabbadi, *Langmuir*, 2013, **29**, 7812-7824.
150. D. R. Kumar, B. L. Prasad and A. A. Kulkarni, *Ind. Eng. Chem. Res.*, 2013, **52**, 17376-17382.
151. M. Hosni, S. Farhat, I. Hinkov, M. Ben Amar, A. Kanaev and N. Jouini, *AIChE Journal*, 2015.
152. B. K. Johnson and R. K. Prud'homme, *Australian Journal of Chemistry*, 2003, **56**, 1021-1024.
153. B. K. Johnson and R. K. Prud'homme, *Phys Rev Lett*, 2003, **91**, 118302.
154. D. L. Marchisio, L. Rivautella and A. A. Barresi, *AIChE Journal*, 2006, **52**, 1877-1887.
155. H. C. Schwarzer and W. Peukert, *Chem Eng Technol*, 2002, **25**, 657-661.
156. S. W. Siddiqui, Y. Zhao, A. Kukukova and S. M. Kresta, *Ind. Eng. Chem. Res.*, 2009, **48**, 7945-7958.
157. J. Aubin, M. Ferrando and V. Jiricny, *Chem Eng Sci*, 2010, **65**, 2065-2093.
158. V. Hessel, S. Hardt, H. Löwe and F. Schönfeld, *AIChE Journal*, 2003, **49**, 566-577.

159. P. Guichardon and L. Falk, *Chem Eng Sci*, 2000, **55**, 4233-4243.
160. J.-M. Commenge and L. Falk, *Chemical Engineering and Processing: Process Intensification*, 2011, **50**, 979-990.
161. L. Falk and J. M. Commenge, *Chem Eng Sci*, 2010, **65**, 405-411.
162. J. Villermaux and L. Falk, *Chem Eng Sci*, 1994, **49**, 5127-5140.
163. V. Bergeron, D. Bonn, J. Y. Martin and L. Vovelle, *Nature*, 2000, **405**, 772-775.
164. J. W. Bush and A. E. Hasha, *Journal of fluid mechanics*, 2004, **511**, 285-310.
165. N. Bremond and E. Villermaux, *Journal of Fluid Mechanics*, 2006, **549**, 273-306.
166. N. Ashgriz, W. Brocklehurst and D. Talley, *Journal of Propulsion and Power*, 2001, **17**, 736-749.
167. D. Paramelle, A. Sadovoy, S. Gorelik, P. Free, J. Hobley and D. G. Fernig, *Analyst*, 2014, **139**, 4855-4861.
168. A. Bhattacharya and P. Ray, *Journal of Applied Polymer Science*, 2004, **93**, 122-130.
169. H. L. Chou, C. M. Wu, F. D. Lin and J. Rick, *AIP Advances*, 2014, **4**, 087111.
170. P. K. Khanna, R. Gokhale, V. V. V. S. Subbarao, A. K. Vishwanath, B. K. Das and C. V. V. Satyanarayana, *Materials Chemistry and Physics*, 2005, **92**, 229-233.
171. G. Mpourmpakis and D. G. Vlachos, *Phys Rev Lett*, 2009, **102**, 155505.
172. R. Patakfalvi, Z. Virányi and I. Dékány, *Colloid Polym Sci*, 2004, **283**, 299-305.
173. L. Zhao, D. Jiang, Y. Cai, X. Ji, R. Xie and W. Yang, *Nanoscale*, 2012, **4**, 5071-5076.
174. R. Baber, L. Mazzei, N. T. Thanh and A. Gavriilidis, *Journal of Flow Chemistry*, 2016, 1-11.
175. D. Liu, S. Cito, Y. Zhang, C. F. Wang, T. M. Sikanen and H. A. Santos, *Advanced Materials*, 2015, **27**, 2298-2304.
176. R. Couto, S. Chambon, C. Aymonier, E. Mignard, B. Pavageau, A. Erriguible and S. Marre, *Chem. Commun.*, 2015, **51**, 1008-1011.
177. T. Gendrineau, S. Marre, M. Vaultier, M. Pucheault and C. Aymonier, *Angewandte Chemie International Edition*, 2012, **51**, 8525-8528.
178. B. Giroire, S. Marre, A. Garcia, T. Cardinal and C. Aymonier, *Reaction Chemistry & Engineering*, 2016, DOI: 10.1039/C5RE00039D.
179. N. Acharya, M. Sen and C. Hsueh-Chia, *Int J Heat Mass Tran*, 1992, **35**, 2475-2489.
180. N. Acharya, M. Sen and H.-C. Chang, *Int J Heat Mass Tran*, 2001, **44**, 3189-3199.
181. M. M. Mandal, C. Serra, Y. Hoarau and K. Nigam, *Microfluid Nanofluid*, 2011, **10**, 415-423.
182. A. K. Saxena and K. D. P. Nigam, *AIChE Journal*, 1984, **30**, 363-368.
183. J. Reijenga, G. Aben, T. P. Verheggen and F. Everaerts, *J Chromatogr A*, 1983, **260**, 241-254.
184. P. K. Jain, K. S. Lee, I. H. El-Sayed and M. A. El-Sayed, *The Journal of Physical Chemistry B*, 2006, **110**, 7238-7248.
185. X. Liu, M. Atwater, J. Wang and Q. Huo, *Colloids and Surfaces B: Biointerfaces*, 2007, **58**, 3-7.
186. T. Hendel, M. Wuithschick, F. Kettemann, A. Birnbaum, K. Rademann and J. Polte, *Analytical Chemistry*, 2014, **86**, 11115-11124.
187. M. B. Hariri, A. Dolati and R. S. Moakhar, *Journal of The Electrochemical Society*, 2013, **160**, D279-D288.
188. L. Djenidi and B. Moghtaderi, *Journal of Fluid Mechanics*, 2006, **568**, 223-242.

189. W. G. Burns, M. Matsuda and H. E. Sims, *Journal of the Chemical Society, Faraday Transactions*, 1990, **86**, 1443-1447.